UNIVERSITAT DE BARCELONA

Bioimpedance monitoring system for pervasive biomedical applications

Jaime Punter Villagrasa

UNIVERSITAT DE BARCELONA

BIOIMPEDANCE MONITORING SYSTEM FOR PERVASIVE BIOMEDICAL APPLICATIONS.

Per Jaime Punter Villagrasa

Directors: Pere Lluis Miribel Català i Jordi Colomer Farrarons

Tutor: Pere Lluis Miribel Català

Memòria per optar al títol de doctor per la Universitat de Barcelona en Enginyeria i Tecnologies Avançades.

Departament d'Electrònica, Facultat de Física

Universitat de Barcelona, 2015

Agradecimientos / Acknowledgements

La realización de esta tesis doctoral no habría llegado a buen puerto sin la ayuda de muchas personas e instituciones a las cuales debo agradecer su esfuerzo y su colaboración. Soy una persona de pocas palabras, así que seré escueto.

En primer lugar, quiero agradecer al Dr. Pere Lluis Miribel Català toda su dedicación, entusiasmo y motivación, que ha compartido conmigo, para que esta tesis doctoral se haya hecho realidad. Han sido muchos años de trabajo donde nunca me ha faltado su apoyo y su constancia al confiar en mi trabajo, como tampoco ha faltado nunca su apoyo económico para la realización de publicaciones y congresos.

También quiero agradecer a mi codirector, Dr. Jordi Colomer Farrarons, el dador de motes y peluches decorativos, cuyo apoyo técnico, sus consejos y su vehemencia a la hora de alentar e impulsar han sido parte fundamental para la elaboración de esta tesis.

También quiero mencionar al Dr. Joan Cid Vidal, poro su inmenso apoyo logístico y la oportunidad que me brindó confiando en mi trabajo y compartiendo sus conocimientos. No me quiero tampoco olvidar del Dr. Ginés Escolar Albadalejo y su equipo de trabajo, que me brindaron un espacio de trabajo en su laboratorioy toda la ayuda que pude necesitar.

Agradecer al Dr. Josep Samitier Martí y al Institute for Bioengineering of Catalonia su apoyo económico en las primeras fases de esta tesis.

También me gustaría agradecer a Beatriz del Moral Zamora por tantos días compartiendo las penas y alegrías que suele brindar este tipo de empresas. Así como su mirada de aprobación, o tal vez de desaprobación, casi maternal para con mis felices devenires investigadores y mi personalidad. Gracias también a Joan Canals y Dr. Oscar Alonso, por el agua barata y de calidad, las cervezas y los cigarros, también baratos y de calidad.

Muchísimos agradecimientos para mi familia, a mis padres Laura y Vicente todo el cariño y la buena educación que me han dado, aunque lo más importante para haber llegado hasta aquí ha sido haberme apretado las tuercas cuando ha sido necesario. Mi queridísima hermana Baldesca, la persona que más ha reído y llorado conmigo, compartiendo hasta la parte más infinitesimal de nuestra vida.

A mis abuelas Celia y Matilde por ser las abuelas cariñosas que todo el mundo necesita, a mi abuelo Bernardino que no ha podido ver este trabajo acabado, y mi abuelo Francisco, el cual me ha reconciliado con la vida.

Finalmente quería dedicar un pequeño espacio de agradecimiento a todos mis amigos, aprendices del ejercicio de la vitalidad, compañeros de clase de estética, políticos de barra de bar, y adalides de la música visceral y minoritaria.

Y a Merche, por ser lo mejor que me ha pasado.

Abbreviations

PoC	Point-of-Care
LoC	Lab-on-a-Chip
ASIC	Application Specific Integrated Circuit
BioZ	Biological Electrical Impedance
IA	Impedance Analysis
IM	Impedance Measurement
FPGA	Field Programmable Gate Array
SNR	Signal to Noise Ratio
THD	Total Harmonic Distortion
DEP	Dielectrophoresis
DEPIM	Dielectrophoretic Impedance Measurement
IDE	Interdigitated Electrodes
HCT	Haematocrit

Contents

List of Figures

Chapter 1 Introduction

The Discrete-to-Integrated Electronics group (D2In), at the University of Barcelona, in partnership with the Department of Hemotherapy and Hemostasis, at Hospital Clínic of Barcelona, and the Bioelectronics and Nanobioengineering Group (SICBIO), is researching on PoC solutions for cellular detection, quantification and monitoring relying on label-free sensing. Our interest is focused on the development of custom built electronic and sensing solutions for versatile tools on the field of bio-medical applications, from discrete devices to ASIC solutions.

The integration of biological, medical and electronic technologies allows the development of biomedical devices for cellular monitoring, able to diagnose and/or treat pathologies by detecting, quantifying and monitoring cellular species in different media. The development of such devices enables advances in various areas such as microelectronics, microfluidics, microsensors and bio-compatible materials which open the door to developing human body LoC implantable devices, PoC n vitro devices, protocols for enhanced health and biohazard control, etc.

In today's healthcare landscape, there is a great need for multipurpose and reliable tools that aim to improve patient quality of life while reducing manufacturing costs [1]. Rapid advances are already being achieved at remarkably low cost with modest investments. Accessible prices of final devices represent a significant advantage, particularly in the underdeveloped world, where the health domain is underfunded. Moreover, low investments in improved health have shown a significant return in reduced morbidity and mortality [2, 3]. PoC technologies can be defined as immediately actionable healthcare information outside the clinic laboratory in applications from diagnosis, to monitoring and therapy adjustment. In this context, PoC devices could not only improve the diagnosis and control of high prevalence diseases, but also reach difficult scenarios where clinics are often many miles away from villages, where there is an absence of laboratory facilities and trained staff, or where there are hostile environmental conditions [4]. For example, nowadays, automated haematology counters provide the necessary information about red blood cells with a high degree of precision [5]. However, they are huge, complex and expensive pieces of equipment, making them inappropriate as PoC portable devices [6]. Micro-HCT is the standard method for HCT determination. This technique uses anticoagulants as a prior step before separating red blood cells from the plasma by centrifugal force. The height of the separated red blood cell column is compared to the height of the entire sample column to determine the packed cell fraction (i.e., the HCT). Besides being a method that reduces HCT below its value in-vivo, the HCT can also be altered by the anticoagulant. Furthermore, this technique overcomes some of the complications related to blood extractions used in conventional methods, including haematoma formations, nerve damage, pain, haema-concentration, extra-vasation, iatrogenic anaemia, arterial puncture, petechiaes, allergies, infection, syncope and fainting, excessive bleeding, edema or thrombus [7].

Furthermore, PoC technologies are a useful tool in the environmental field. The air and water pollutants are affecting the health of living beings (humans, animals, and plants), agriculture, fisheries and physical infrastructures [8-10]. Water pollution is present in all these fields, where

bacteriological contamination are contained in the drinking water, oceans, lakes and food. In the past years, it has become a global concern of associations such the U.S. and Scottish Environmental Protection Agency (EPA), American Water Resource Association (AWRA), the World Water Council, the European Environment Commission and others organizations. In response of the actual necessities, the research in systems designed to detect and monitor pollutants is exponentially increased. Devices able to detect in less time, in the point of care, handled by non-qualified personal and with lower cost in the fabrication process are the main aim of these research groups. In this way it is expected for example the detection of contaminated drinking water that could cause health problems and in many cases the dead of living beings.

The requirements of laboratory-based tests are often incompatible with the constraints of resource-limited settings and are difficult to access in developing countries because of their high costs. Generally, tests are clinic-based and trained personnel are often required. Access to electricity to power the instrumentation is also assumed [11]. Therefore, traditional diagnosis for prevention, identification, and treatment of diseases is labour and time consuming as well as expensive; and laboratory methods are currently being replaced by PoC technologies, so PoC testing promotes a shift away from traditional diagnostic tests in the clinical laboratory setting to near-patient settings, providing physicians with timely diagnostic information so as to make informed decisions regarding diagnosis and treatment. As laboratory methods are currently being replaced by PoC technologies, PoC testing has a high growth rate market. It constitutes 31% of the diagnostics market (18% glucose testing, 11% professional PoC products, and 2% over-the-counter) [2]. The total PoC based biochip market was US$2.4 billion in 2009 and was projected to increase to US$5.9 billion in 2014. This should be a powerful incentive for commercial efforts to move toward true global health solutions [4].

The first PoC device was the urine dip-stick to measure urinary protein, developed in 1957 [12, 13]. Nowadays, the most common PoC device is used for glucose monitoring in diabetes management [14]. Since 1962, glucose devices have been significantly improved, from its original design for home self-monitoring [15], to non-invasive glucose monitoring systems [16]. The first generation of glucose biosensors measured either oxygen consumption or hydrogen peroxide production by the enzyme glucose oxidase in the presence of glucose [16, 17]. Second generation biosensors replaced oxygen, the enzyme natural electron acceptor, with non-physiological compounds (called redox mediators) that were able to shuttle electrons from the enzyme to the working electrode in in-vitro sensing [18, 19]. Last, third generation biosensors avoid redox mediators and rely on the direct transfer of electrons between the enzyme and the electrode [20, 21]. These sensors have led to be implantable and needle-type devices [16],[22]. Significant efforts have been made also in non-invasive glucose analysis through optical or transdermal approaches [23]. MEMS-based glucose level measurement techniques include the use of electrochemical, impedance, electrophoretic, thermal, optical, and colorimetric principles [24]. Currently, the accuracy and robustness of glucose monitoring is being improved through the use of algorithms. Approaches in this field include Electrical Impedance, reported as in vivo and ex vivo approaches [25-27], Electrochemical Impedance Spectroscopy (EIS) [28], and color-based diagnostics [29]. Commercially available PoC diagnostic tests have low manufacturing cost and accessible prices. Examples include the microfluidic manipulator devices, such as AnaemiaCheck

(Express Diagnostics), the photometry hemoglobin detection, such as STAT-Site (Stanbio Laboratory), and the HemoPoint H2 (Alere). In most cases these are fast assays, ranging from 60 seconds to 15 minute. Some other analytes such as triglyceride can also be sensed through composite porous silicon/polysilicon micro-cantilevers [23], and cholesterol, which can be detected with microfluidic systems using nanoparticles with cholesterol oxidase immobilized on their surface [30].

1.1. Application of PoC technologies to biomedical cellular detection and monitoring applications: HCT.

HCT is a major control determinant of several diseases, diagnoses and treatments. HCT concentration is an indicator of thrombosis, haemostasis and bleeding time, and an increased HCT level has proven to be an indicator of myocardial infarction, angina pectoris and cerebral infarction. Other diseases, such as colon cancer or gastrointestinal lesions, can cause a decrease in HCT due to internal bleeding or lack of nutrients. Moreover, anaemia is considered a worldwide problem by the World Health Organization, being a widespread disease affecting nearly one-third of the world's population (1620 million people). Therefore, there is a great need for multipurpose and reliable telemetric tools and PoC devices that aim to improve patient quality of life while reducing manufacturing costs.

1.1.1. Anaemia

According the WHO, data collected from 1993 and 2005 shows that the global prevalence of anaemia for the general population is nearly one-third of the world's population and it is estimated that 1620 million people are affected by it. In particular, anaemia has the highest prevalence in the developing world with Africa (67.6%) at the top and South-East Asia (65.5%) ranked in second place. In the Eastern Mediterranean, the prevalence is 46% and around 20% in the other WHO regions, the Americas, Europe and Western Pacific [31, 33]. Anaemia is known to be very extensive, especially in women; half of them are affected in the under-developed countries, especially in Asia and Africa, but even in South America and the Caribbean one-quarter of women are anaemic. This contributes to increased maternal mortality risks, ill health and debilitation. Anaemia in the general (non-pregnant) female population is assessed as haemoglobin less than 12g/dl, and this leads to anaemia in pregnancy, estimated as < 11 g/dl [33,34]. Another population group with high prevalence of anaemia is children, especially in poor countries. In pre-school-age children, the anaemia prevalence is 47.4%, affecting 293 million children globally [34]. In the United States, iron deficiency anaemia (IDA) affects approximately 3% of young children. Globally, approximately half of the world’s children may have IDA, and millions of adults are affected as well [35].

1.1.2. Erythrocytosis

On the other hand, if the increase in the number of red blood cells is higher than normal, then this anomaly is known as erythrocytosis, which is present in Polycythemia Vera (PV), a bone narrow disease. This rare disorder has a prevalence of 44-57 per 100,000 people in the United States, and is often observed in women [36]. In this context, the HCT value has been suggested as a surrogate marker for an increased red cell mass (RCM) for the diagnosis and control of PV [37].

1.1.3. Other HCT related diseases.

Current studies also have associated a positive correlation between high levels of HCT in non-alcoholic steato-hepatitis or fatty liver disease (NAFLD). Moreover, it has been shown that HCT levels increased with the severity of hepatic fibrosis. Therefore, HCT levels may have potential interest as a clinical marker also in NAFLD severity [38]. High levels of HCT are also present in renal cell carcinomas, congenital heart diseases, pulmonary fibrosis, hypoxia and dehydration. Additionally, in some clinical procedures such as cardiac surgery, HCT/haemoglobin measurements are also useful because clinicians need to determine their patient's level of haemo-dilution, as well as their transfusion threshold [39].

Finally, HCT is a main factor in athletic performance in sports. Blood doping is the process of artificially increasing HCT to improve athletic performance. Procedures such as blood transfusion before an athletic competition or drugs like Erythropoietin (EPO) [40], a hormone protein produced by the kidney that stimulates the production of RBCs, have been banned from sports not only due to ethical issues but because of serious health risks for athletes [40,41]. Therefore, HCT detection and monitoring is considered a useful tool with many fields of application. Some of the related complications and diseases are summarized in figure 1.1.

Commercial devices for PoC anaemia detection from quantitative HCT results are: AnaemiaCheck (Express Diagnostics, Blue Earth, Minnesota); HemoPoint H2 (Alere, Waltham, Massachusetts) which is based on photometry; and i-SAT System based on conductometry. These three devices have short ranges of HCT measurement, and also are slow methods. In particular, the i-STAT analyser, despite providing lab-quality results for patient PoC testing, turns out to be less specific, involving a much more expensive and slower device. Harter et al., (2014) have also shown that the fairly basic HCT measurement performed by the i-STAT system was consistently and significantly lower than the values measured with the standard micro-capillary tubes and it was sensitive to the concentration of other non-conductive elements in the plasma, i.e. proteins and lipids [42].

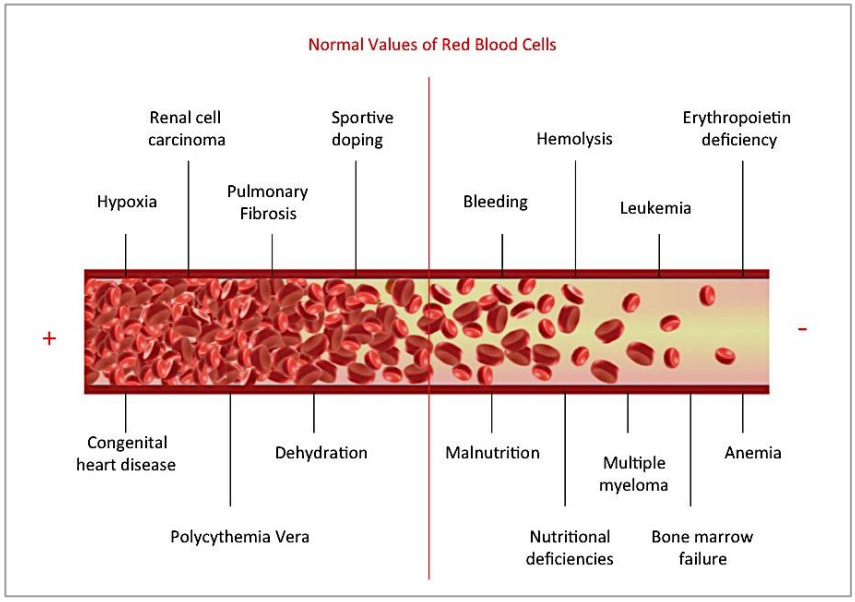

Figure 1.1: General overview of health complications and diseases related to red blood cell concentration.

As seen in the table, the proposed device has the lowest test time compared with the commercial PoC devices for anaemia detection, and is the only one that generates HCT values in a wide range and in a direct way. However, the sample size is still high compared with the rest of the devices, this being a property susceptible to be improved in future works.

The AnemoCheck device uses a colorimetric principle for anaemia detection based on haemoglobin measurement [43]. This could give subjective results because of its visual interpretation by using a colour scale, which probably could not be used by a colour-blind person. Also, numeric values obtained through its optional smartphone app for automated analysis, besides being an additional step, generates values that are predisposed to have errors due to light variations. AnemoCheck and AnaemiaCheck, do not use high-tech instrumentation, which is an advantage regarding manufacturing and maintenance costs. However, they are single-use disposable devices and this could increase the price budget for continuous anaemia control patients.

Device	Sample Size (µL)	Test time (sec.)	Weight (g)	Principle	Range (HCT and Hb)	SD(%)	CV(%)	Status	Manufacturer
AnaemiaCheck™	50	900	---	Filtering	HCT: 12% – 42% Hb: 8–15g/dL	0.74	4.10	Marketed	Express Diagnostics, Blue Earth, Minnesota
STAT-Site	15	120	57	Reflectance photometry	Hb: 5.6 g/dL – 20.6 g/dL	---	4.20	Marketed	EKF Diagnostics
Hemo Point H2/ HemoControl	8	10-60	700	Optical absorption photometry	Hb: 0 g/dL – 25.6 g/dL HCT: 36% – 54%	---	1.5	Marketed	Alere, Waltham, Massachusetts
AnemoCheck	10	45	---	Chemical Colorimetric	Hb: 7.2g/dL - 16.3 g/dL	---	---	Pre-Clinical	Georgia Institute of Technology
HemoCue® Hb 201 DM System	10	60	350	A modified azidomethemoglobin method and photometry light absorption	Hb:0–25.6 g/dL (0–256 g/L, 0–15.9 mmol/L)	---	2.5	Marketed	Hemocue
DiaSpect Hb-system	<10	1-2	500	Photometry	Hb: 0–25.5 g/dl	---	3-3.9	Marketed	DiaSpect Medical GmbH
i-STAT® System	100	>60	---	Conducto-metry	HCT: 10%-75% Hb: 3.4-25.5 g/dL	0.50	1.5	Marketed	Abbott Point of Care Inc.
HemoSmart™	3	20	64	Biosensor based amperometric	Hb:4-20 g/dL haematocrit calculation is based on Hgb	---	---	Marketed	Apex Biotechnology Corp

Table 1.1: Comparison of Point-of-care devices for HCT and haemoglobin detection.

On the market, there are also non-invasive PoC devices. Advantages of these technologies include reduced pain and discomfort for patients and a decrease in exposure to potential bio-hazards. Like haematology analyzers, co-oximeters do not measure HCT directly. A fixed relationship between haemoglobin and HCT is used to calculate HCT through spectrophotometry [44]. The disadvantages of this type of device includes less strong data which is also subject to error due to skin colour and device motion [45-47].

Recently, other PoC anaemia devices have been published, such as a color-based diagnostic test for self-screening/self-monitoring of anaemia presented by Tyburski et al. [29], a novel PoC diagnostic test for self-screening, self-monitoring of anaemia. The device measures hemoglobin (Hgb) levels, which are estimated via visual interpretation by the user using a color scale. This system presents several performance drawbacks. First of all, the readout stage, based on a color scale, relies on the visual interpretation of the user, which could introduce errors on the Hgb levels data interpretation, and reduces considerably the system resolution. Furthermore, the principle of operation of the color-based PoC device is based on biochemical reactions, where the blood comes into contact with a reagent solution initiating a redox reaction, which is a slow and destructive procedure.

1.2. Whole blood multiparametric PoC devices. Diabetes case.

The World Health Organization, WHO, included diabetes mellitus among the top 10 causes of death in 2014. Type-2 diabetes mellitus, which accounts for over 90% of all cases, is the most common form of diabetes. According to the latest national study [48], in Spain alone this disease has a prevalence up to 13.8%, despite the fact that only about half the people who suffer from it have been diagnosed, and therefore are aware of it. Consequently, new screening tools that facilitate its early diagnosis are needed so that the complications related to this disease can be prevented, mitigated, or effectively controlled, with the resulting life quality improvement of those suffering from the disease. Among these complications, cardiovascular diseases are one of the leading causes of morbidity and mortality among patients with type-2 diabetes [49]. Dyslipidemia is characterized by high triglyceride concentration, and high cholesterol levels composed of a low concentration of high-density lipoprotein (HDL) cholesterol and a high concentration of dense low-density lipoprotein (LDL) cholesterol particles. Anaemia is an additional risk factor for cardiovascular disease and other adverse outcomes in diabetic patients, especially when chronic kidney disease is present [50, 51].

More recently, multi-parametric PoC devices are able to detect different pathogens [52] or to target different metabolites such as glucose, cholesterol, triglycerides, creatinine, lactate, ammonia, and urea [53], being the first and the best-known metabolite [54] (Table I). An example is a compact sensor developed for fast and reagent-free PoC determination of glucose, lactate and triglycerides in blood serum based on a tuneable external-cavity quantum cascade laser (EC-QCL) [55]. Additionally, paper-based colorimetric biosensors are highly being suited for blood samples analysis [56] used for of bilirubin or cholesterol detection [57]. Sample volumes range between 10 and 100 µl, and the systems operate on a time scale of minutes, often containing a disposable part with miniaturized elements [58]. Most clinical applications of multiplexing devices include

the diagnosis and prognosis of disorders such as cancer, diabetes, AIDS, tuberculosis, Alzheimer's disease and other communicable diseases cancer detection [59, 60]. Even though multiplexing is becoming increasingly important [61], the number of multi-analyte PoC devices is relatively few [62]. In terms of value, the annual European market related to diabetes is about 3900 million euros, of which personal glucose self-monitoring devices accounted for nearly 80%. It is estimated that by 2018 this market be around 5000 million euros [58].

Although the diagnosis of diabetes involves complex blood analysis in a clinical laboratory, PoCket glucose meters are routinely used for screening and in awareness campaigns. Such glucose meters are easy to use and can work with tiny sample volumes ranging from 0.3 – 1.5µL. However, multi-parametric devices that measure glucose and other parameters such as cholesterol and triglycerides can offer accurate information in less than 5 minutes, but they require larger blood sample volumes to operate (15-20 µL). Besides, some devices pose a major safety issue: the risk of infection if the devices become contaminated and are shared between users without proper cleaning and disinfection [63]. In contrast single use, fully disposable analytical devices would avoid such risks completely. This approach to diabetes screening is challenging due to the comparatively high cost of such devices (ranging in the low tens of euros) compared to the cost of disposable glucose strips (ranging in the cents of euro). However, the technology may have an opportunity in multi-parametric measurements, as the current cost of multi-parameter disposable strips is also in the range of a few euros.

Instrument	Mechanism	Description	Analytes	Sample volume	Analysis time (seconds)	References
i-SAT	Electrode biosensor	Hand-held system that utilizes a single- use disposable Cartridge containing microfabricated biosensors (thin-film electrodes microfabricated on silicon chips).	Sodium, Potassium, Chloride, pH, pCo2, pO2, blood urea nitrogen, Urea, Glucose	60-95 µL	90-120	[64], [65]
Beckman Synchron CX3 Delta	Chemical reaction	Determines sodium ion concentration by measuring electrolyte activity in solution. High molar-strength buffer is employed to establish a constant ionic strength.	Sodium, Potassium, Chloride, Creatinine, Glucose, blood urea nitrogen	10-62 µL	10-26	[59]
Radiometer ABL 705	Gas and electrolyte analyser	In-house laboratory-based bench-top analyzer	Sodium, Potassium, Chloride, Calcium, pH, pCO2, Glucose, Lactate	95 µL	80	[66]
3D µPADs: microfluidic paper-based analytical devices	Biochemical or electrochemical reactions	Quantitative colorimetric detection of analytes using µPADs is possible by reflectance detection when the intensity of the color that develops in the test zones is a function of the concentration of the analyte	Can test four different samples for glucose and protein. Glucose, Rabbit IgG, Transamidase	15-22 µL	120	[67]–[69]
Aptamer-based microfluidic beads array sensor	Dual signal amplification strategy	Simultaneous detection and quantification of multiple analytes using multienzyme-linked nanoparticle amplification and quantum dots labels.	Adenosine and cocaine	10 µL of blood serum	40 minutes	[70]

Table 1.2: Multiparametric Point-of-care devices summary.

1.3. Impedance analysis for cellular detection.

As it has been seen in the previous sections, PoC testing devices for different diseases have long been available and have become common diagnostic tools in such a variety of different income countries [72]. However, the vast majority of PoC testing relies on chemical biomarkers, which often needs of sophisticated microfluidics, microelectronics and optical systems to be functional and reliable. However, this technological complexity, the use of chemical biomarkers, or the PoC output data management are issues that must be addressed. The technological complexity of such devices entails some operational challenges, such as human resources and training, quality assurance, and equipment maintenance. This issue leads sometimes to the inability of patients self-screening and decentralization of testing, increasing the clinic visits to ensure the access to the test and the proper results recording. This fact is exacerbated as high percentage of PoC testing devices outputs visual or colour-based results, which are subject to user interpretation and need of human personnel to record the results on a specific database for follow-up of patients. The PoC devices complexity and the use of chemical biomarkers results on a limited device, sub-optimal cost-effectiveness, and issues related to the product regulation and the supply chain. In addition, samples under analysis are usually destroyed during the process, lacking the versatility to be integrated in other medical equipment and environments for increased functionality as monitoring device or medical actuator.

In that scenario, it is necessary to develop truly PoC devices that addresses the presented issues of current PoC devices and steps forward as a new generation of PoC devices and technology, where it is presented a reliable, sensitive and robust detection, while relying in a much less complex technique that does not require any user interpretation or chemical agent, while enabling different functionalities for data management, such as a monitoring device for real telemedicine applications for patients self-screening and easy database follow-up, or as a controller of other clinical actuators.

Several studies have reported that cellular detection, quantification and monitoring can be accurately monitored by means of its inherent BioZ [26-28, 72-77] in different environments, in-vivo or ex-vivo experiences. One example of such work is the paper presented by Pop et al. (2013) [26], where blood HCT was continuously in-vivo monitored in the human right atrium by a dedicated central venous catheter equipped with an impedance measuring device. Pradhan et al. (2012) [28] studied ex-vivo the electrical properties of blood and its constituents using Electrochemical Impedance Spectroscopy (EIS) and three-electrode sensors. Ramaswamy et al. (2013) [27] performed a blood coagulation test based on a custom microfluidic device and the electrical impedance detection of whole blood samples. Li et al. (2012) [73] monitored Legionella serogroups in clinical and environmental samples by means of EIS. Dweik et al. (2012) [74], where bacterial presence was rapidly detected measuring the antibody/antigen bonding analysing its BioZ between 100 Hz and 10 MHz. Also, in the work developed by Grossi et al. (2010) [75], the quantity of bacteria during a culture process was detected by impedance measured at 200 Hz sinusoidal with a 100mV peak-to-peak signal. Furthermore, other studies have reported the detection of cell-derived microparticles [78] and insulin in blood serum [79] based on an EIS technique.

1.3.1. Biological Electrical Impedance

Typical cellular electrical model for dilute cell suspensions can be described as network of electrical passive components, so the BioZ is the response of applying an electrical stimulus to a biological material through a sensing system and measuring its electrical response defined by the Ohm's law [80]. The analysis of the BioZ is defined as the IA. The electrical response is frequency dependant, and depending on the samples under examination and the sensing system there are different frequency working ranges where an appropriate electric response can be found, so a frequency sweep is needed to evaluate the electrical response of the whole designed system (biological sample along with the sensing system). The response variation of a cell model at various frequencies, and the effect of cell parameters, such as cell membrane resistance and capacitance, made electrical models of cellular species very complex and diverse.

There are different sensing electrodes topologies to be considered depending on the number of electrodes used. A simple and typical cellular electrical model for dilute cell suspensions can be described as network of electrical components [81] (figure 1.2.). Injected current can flow through external media (R_E resistance) or flow through the cell across the membrane ($R_M \| C_M$) and the intracellular medium (R_I resistance). Considering that R_M resistance is nearly negligible a simplified model is considered.

$$Z_{CELL} = \frac{R_E(1+j\omega C_M R_I)}{1+j\omega C_M(R_I+R_E)} \quad (1)$$

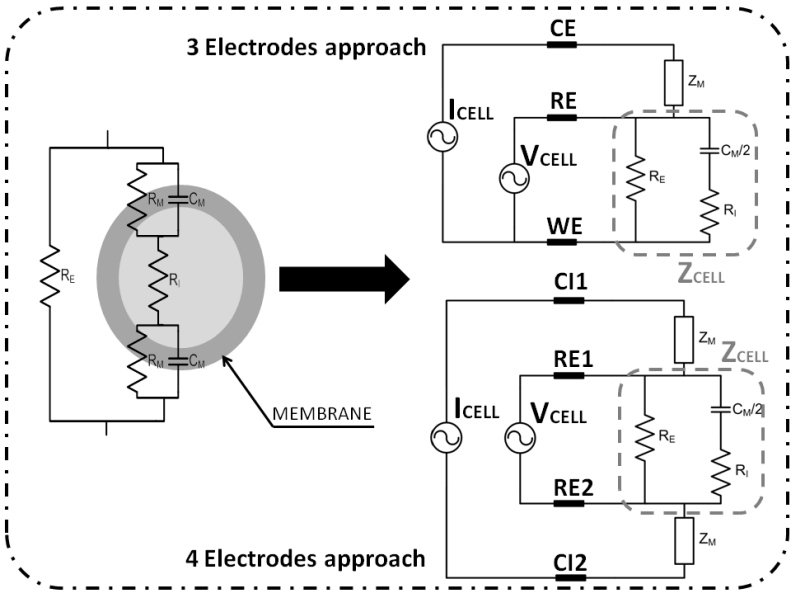

Figure 1.2: Cellular electrical model. Sensing system based on 3 electrodes and 4 electrodes approach.

A two electrodes topology is defined by the working electrode (WE), where the sample is placed and the electrical signal is applied, in addition to the auxiliary electrode (AE), which tracks the solution potential and supplies the current required for experience. This topology brings some kind of problematic behaviour by the AE polarization effects causing a distortion of the applied electrical signal. The three electrodes configuration is defined as follows: the working electrode

(WE), where is the object under investigation, the reference electrode (RE), which tracks the electric signal and the counter or auxiliary electrode (CE), which supplies the required current. This topology avoids the distortion of the applied electrical signal.

Finally, the four electrodes configuration avoids the measurement distortion due to the WE impedance polarization, as in the three electrodes topology, the electric signal is directly applied where the single-ended voltage measurement signal is read. The four electrode topology is composed of two current injection electrodes and two voltage reading electrodes avoiding the electrode polarization distortion in IA due to a complete differential voltage measurement [82].

BioZ technique allows the use of different sensing topologies and systems, making possible the integration of such electrodes in a great variety of devices and environments, such as biosensors and microfluidic devices for increased functionality and performance. Moreover, the simplicity of the technique implementation makes it possible to accomplish the experience objectives with very simple sensing systems. Hernández et al. (2011) [77] obtained the electric impedance spectrum of human blood using reactive strips of the Bayer's portable glucometer. The electronics instrumentation involved on customized PoC devices are implemented as a front-end electronics depending on the sensing topology.

1.3.2. Instrumentation electronics for 3 electrodes configuration sensing system. Potentiostat.

A potentiostat amplifier is a useful tool in many fields of investigation and industry performing electrochemical measurements [83-85], so the quantity and variety of them are very extensive, having different characteristics. However this electronics instrumentation based on a 3 electrodes driving potentiostat amplifier, is a very useful configuration in wide variety of applications, ranging from voltametric electrochemical test, such as amperometry, cyclic voltammetry, chrono-amperometry, pulse voltammetry, etc., to IA ,such as electrochemical impedance spectroscopy. This features establish the potentiostat as a straight-forward electronics instrumentation with a wide variety of applications and huge state-of-the-art technology.

In that way, two different approaches can be followed in the design and implementation of a potentiostat amplifier: a discrete or integrated solution. In order to design a portable system for standard electrochemical assays, a discrete implementation is an extremely good solution in terms of portability, accuracy and economy being a standard on electrochemical experiments. But demand for increased functionality, reduced system size, reduced size of the electrodes, defining complex arrays of sensors, ultra-low current detection and versatility, are introducing a major interest in LoC solutions, to be implemented in advanced CMOS processes. The scaled supply voltages in these processes [86-90], however, seriously limit the chemical analysis range. Driving voltages of amperometric chemical sensors do not scale with electrode size, but are instead defined by the reduction/oxidation (redox) potentials of the analyses being investigated, as stated in [91] many analysis are undetectable using standard potentiostats in a 0.18µm CMOS process due to its maximum supply voltage of 1.8V.

The main tasks of these kind of structures are the measurement and recognition of some kind of particles in a media (or the media itself), through the application of an electric signal and the readout and conditioning of an output signal. The main functionalities envisaged for a potentiostat amplifier are: a) driving the sensor electrodes with the desired electrical signal, ensuring that the electrical signal remains invariable and supplies the current necessary for the experience, and b) be able to extract an output signal. Different approaches are conceived to fulfill this last objective.

One of the main tasks of a potentiostat is the control of voltage difference between working and reference electrodes of the electrochemical cell and supplying the required current from or into the electrochemical cell through the counter electrode. This task can be realized with two different circuit configurations, grounded working electrode and grounded counter electrode, the first being the most popular configuration depicted in figure 1.3 which illustrates the basic implementation of this configuration. As shown, the working electrode is kept at the ground potential and an operational amplifier, called the driving amplifier, controls the cell current I_{CELL}, so the cell potential V_{CELL} is at the desired potential V_{IN}.

The system operation is very simple, but, like other electronic instrumentation circuits, we get potentiostat functionality limitations due to its own driving amplifier limitations. Since current flow in the reference electrode changes the potential of the reference electrode due to polarization effects, driving amplifier input bias current should be small and input resistance should be very large. Depending on the target, you must consider several limitations on the driving amplifier parameters. Voltage gain and input offset voltage of the driving amplifier define the accuracy and linearity of the potential control. Other important parameters to be considered are the output voltage swing, input referred noise, bandwidth and slew rate, considering the stability as a sensitive issue due to the fact that the electrochemical cell is the load and feedback network of the amplifier.

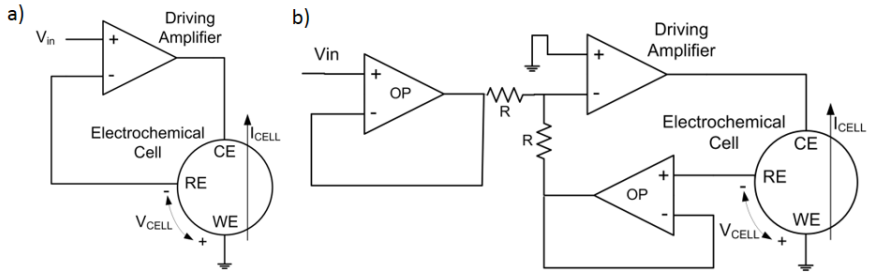

Figure 1.3: a) Potential control. General scheme. b) Usage of voltage buffers to isolate driving amplifier and reference electrode.

In previous section, a typical electrical cell model has been depicted, where frequency dependent impedances like capacitors are present, the frequency and transient simulations of these impedances being quite complex to study. For this reason, it is necessary that the potentiostat provides stability over wide operation ranges, being able to carry out diverse electrochemical experiences for different biochemical species.

Some circuits used to fix the electrochemical cell's driving signal have been reported. The next stage concerns circuits related to the flowing current readout. Different approaches can be adopted and are presented in this section.

1.3.2.1. Transimpedance amplifier stage.

In the present configuration the measurement is based on the direct conversion of the current generated in the electrochemical cell into a voltage signal using a transimpedance configuration, depicted in figure 1.4 dotted rectangle.

In order to read the faradic current generated by the reaction I_{CELL}, a transimpedance ance stage amplifier (TIA), converts it to a voltage signal by means of a single resistor, as is indicated in (2), so the output signal $V_{out,TR}$ is equivalent to the faradic current through working electrode.

$$V_{out,TR} = -I_{CELL} \cdot R_{TIA} (2)$$

The system operation it is simple, but, as is stated in the previous section, we get functionality limitations due to transimpedance amplifier limitations. V_{IN} voltage will be tracked to the electrodes if WE electrode is ground referenced, assuming operational amplifier virtual ground. In that case, input offset voltage and input referred noise must be considered in order to provide a steady virtual ground. Since generated current must flow through trans-impedance amplifier resistor R_{TIA}, trans-impedance amplifier TIA input bias current should be small and input impedance should be very large in order to minimize any current losses through this stage.

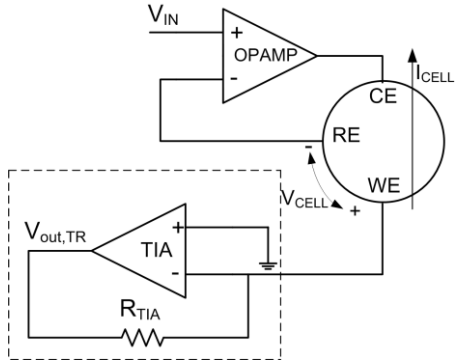

Figure 1.4: Basic grounded working electrode driving control configuration with a transimpedance amplifier readout stage.

As is shown on the operational amplifier equivalent circuit in figure 5, the input impedance is the equivalent impedance between the positive and negative inputs. This impedance is linked to some leakage currents (I_{offset}), which could cause problems both in I_{CELL} current readout and V_{CELL} tracking, especially when extremely low faradic currents are generated on the reaction in which case a very high transimpedance resistor is required. This error in both cases can be minimized by reducing amplifier offset and bias current by means of very high input impedance.

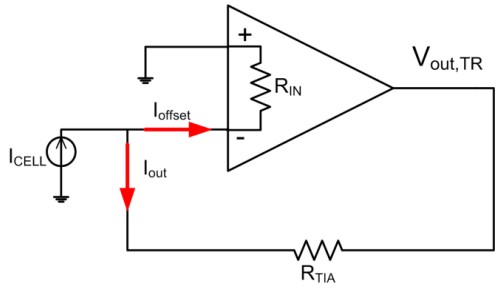

Figure 1.5: Operational amplifier in transimpedance configuration. General Scheme.

Other parameters to be considered are the amplifier's flicker and thermal noise or inherent current and voltage offset. Flicker and thermal noise are inherent to electronics and are characterized as an output voltage (V_{noise}) (3) or as an input current (4) defining the transimpedance amplifier stage resolution, establishing a minimum SNR (5).

$$V_{OUT} = V_{out,TR} + V_{noise} (3)$$

$$I_{noise} = \frac{V_{noise}}{R_{TIA}} (4)$$

$$SNR = \frac{I_{CELL}}{I_{noise}} (5)$$

There are different solutions to maximize resolution of the measurement, increasing the SNR, and sensitivity, reducing thermal and flicker noise. For instance, one of the best solutions is based on chopper modulation, which implies more complexity on the design. A simplest solution is to just place a bandwidth filter. The capacitor on transimpedance amplifier feedback loop should remove the inherent 50 Hz network or any other frequency noise and harmonics but does not permit to avoid flicker noise problems. Depending on the application, if the system is required to work in a limited range of frequencies, like amperometric and voltametric experiences where you apply DC signals, or potential sweeps with an scan-rate of less than 1000 mV/s [83], it is useful to filter low frequencies to remove network powering noise, typically 50Hz and harmonics, and reduce thermal and flicker spectra to improve the SNR.

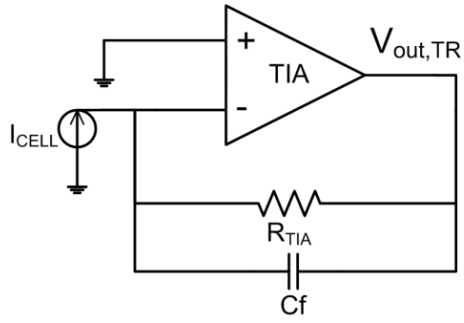

Figure 1.6: Transimpedance amplifier stage. Low-pass noise reduction capacitor configuration.

1.3.2.2. Instrumentation amplifier stage.

This kind of current measurement topology consists in the direct conversion of the current in to a voltage signal by means of a resistor on the counter electrode, and an instrumentation amplifier that measures the voltage difference in the resistance, as it is depicted in figure 1.7.

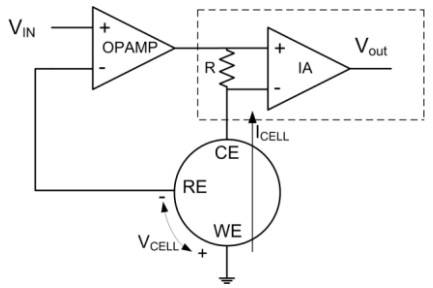

Figure 1.7: Basic grounded working electrode driving control configuration with a instrumentation amplifier readout stage.

We assume that the current through resistor R, is equal to the faradic current developed by the electrochemical reaction (I_{CELL}), and it is considered that voltage between reference and working electrode (V_{CELL}) is more steady than in the transimpedance amplifier stage due to the direct connection of working electrode to ground. An instrumentation amplifier transfer function is theoretically described by this equation:

$$V_{OUT} = A \cdot (V_+ - V_-) (6)$$

Where A is the amplifier's gain and (V+ - V-) is the voltage difference on the amplifier's positive and negative, so we can determine that if the voltage (V+ - V-) is (7) the output signal is equivalent to the faradaic current through working electrode (8).

$$(V_+ - V_-) = I_{CELL} \cdot R (7)$$

$$V_{OUT} = A \cdot I_{CELL} \cdot R (8)$$

There are some parameters to be considered as a source of noise errors; input impedance, offset current, and bias current. Amplifiers are a source of noise and non-idealities that are critical, mainly if very low current resolution, such as nanoamperes or picoamperes is desirable. It will be assumed that all the amplifiers have an input bias current that interferes with the current readout system. In order to minimize these effects we need to use an amplifier with very high input impedance, as is depicted in the previous section. There are other parameters to be considered, such as resistor tolerance and resistor thermal noise. This stage is very dependent on resistors, the conversion of the flowing current to a measurable output voltage it depends on the stability of

three different resistors. There is a very high probability of getting an error source, making impossible to get a very precise measurement, if the system depends on the tolerance and thermal noise of three different resistors, but it's possible to minimize output voltage dependence of this large number of resistors, as it is depicted in figure 1.8.

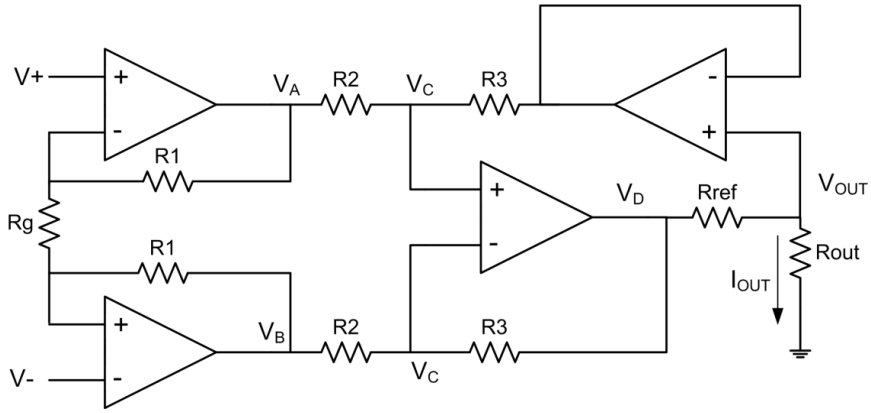

Figure 1.8: Modified instrumentation amplifier.

The modified instrumentation amplifier transfer function is theoretically described by the following equations:

$$\frac{(V_A - V_-)}{R1} = \frac{(V_- - V_+)}{Rg} = \frac{(V_+ - V_B)}{R1} (9)$$

$$\frac{(V_B - V_C)}{R2} = \frac{(V_C - V_{OUT})}{R3} (10)$$

$$\frac{(V_A - V_C)}{R2} = \frac{(V_C - V_D)}{R3} (11)$$

Combining these three equations and considering that R3 = R2

$$V_{OUT} = I_{OUT} \cdot R_{OUT} (12)$$

$$(V_{OUT} - V_D) = (V_A - V_B) = (V_+ - V_-)\left(1 + \frac{2R1}{Rg}\right) = I_{OUT} \cdot Rref (13)$$

And if we consider

$$Rref = R_{OUT}\left(1 + \frac{2R1}{Rg}\right) (14)$$

$$I_{OUT} = \frac{(V_+ - V_-)}{R_{OUT}} (15)$$

We found that the output current signal is the same current as through electrodes and the evaluation only depends on the value of one resistor. Regarding other error sources, the fact that there are no active components in the flowing current path, and being both flowing current and measured

voltage referenced directly to ground, gives the system better stability than in the transimpedance amplifier stage.

1.3.2.3. Switching capacitors solution.

Another feasible solution to current readout is the switching capacitors transimpedance stage avoiding the use of resistors. This topology needs a clock control signal, but, assuming the possibility of using a microcontroller for a later signal processing or data transmission this should not be a problem. The basic circuit approach is depicted in figure 1.9.

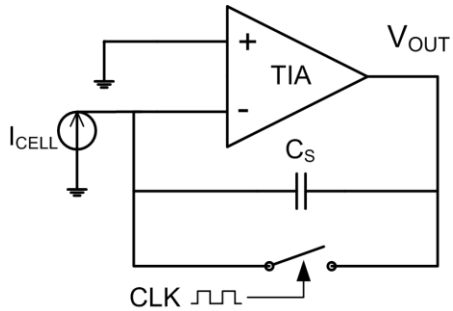

Figure 1.9: Switching capacitors transimpedance stage.

This stage has a very simple operation system, on the first clock semi cycle the switch is closed and electrochemical cell current, I_{CELL}, charges capacitor C_S to a concrete output voltage V_{OUT} as depicted in equation 16, where T_{CLK} is the clock period.

$$V_{OUT} = \frac{I_{CELL} T_{CLK}}{2C_S} (16)$$

On the second clock semi cycle the switch is opened, and V_{OUT} is directly connected to ground and the capacitor is discharged. Depending on the measurement range, the capacitor or the clock cycle can be modified to a larger or smaller value, giving the possibility of a more versatile stage.

The system operation it is simple, but, as stated in the previous section, we get functionality limitations due to transimpedance amplifier limitations. First of all the WE electrode is ground referenced through amplifier virtual ground. In that case, input offset voltage and input referred noise must be considered in order to provide a steady virtual ground. Since generated current must flow through transimpedance stage, TIA amplifier input bias current should be small and input impedance should be very large in order to minimize any current losses through the stage.

Another important consideration is that the capacitance of the flowing current source, that is the electrochemical cell, must be of a few orders of magnitude higher than the capacitor C_S. If not, the errors due to charge injection will be larger than desirable for any designed application.

This kind of topology is widely used in CMOS processes and microelectronics development due to the difficulty of realizing large resistors at small scales. The fact of using small capacitance values provides the possibility of developing multichannel sensor arrays [92-94] on ASIC structures, due to the high degree of integration of small size capacitors.

A more complex development of the switching capacitors technique makes it possible to perform direct A/D conversion by converting the current to variables such as frequency [91,95] or direct current input sigma-delta converter [96,97].

1.4. Back-end electronics data processing for IA.

The electrochemical cell and its theoretical electrical approximation by circuit modeling it is extremely complex and depends on several factors, with just the simpler models, or even complex ones, being a vague approximations to reality [98]. A direct measurement of the impedance in a range of frequencies, usually from 1mHz to 1MHz [99], is fitted afterwards to an electrical model and its IA, with different elements, that are used to fit the data. This process is called Impedance Spectroscopy (IS).

Nowadays, IS, the response of an electrochemical cell to small amplitude sinusoidal electrical signal as a function of frequency, is the most prominent solution to check and test the sensors development in current research in biosensor technology, and has helped to developed better transducers that demonstrate superior sensitivity, portability, accuracy and throughput. IS is an effective method to probe the interfacial properties of the modified electrode, through measuring the change of electron transfer resistance at the electrode surface, caused by the adsorption and desorption of bio-chemical molecules and the antibody-antigen (Ab-Ag) interactions. The measured signal, in this case the signal generated (voltage or current signal) in the experiment, differs in time (phase shift) with respect to the perturbing (voltage or current) wave, and the ratio $V_{CELL}(t)/I_{CELL}(t)$ is defined as the impedance (Z_{CELL}), and accounts for the combined opposition of all the components within the electrochemical cell to the flow of electrons. The key electronic component for these measurements, as it is stated before, is the electronic instrumentation that bias the sensor and read the electrical response produced by the experiment. It is the interface between the biological elements and the post-processing stage.

The key component of a post-processing IS experiment is the Lock-in Amplifier (LIA) which generates the real and imaginary components for the IS solution rejecting undesirable harmonics and noise interferences [100-103] even in the presence of high noise level. The block diagram of a whole system, including the front-end electronics, is depicted in figure 1.10, where a general schematic view of a lock-in amplifier is shown.

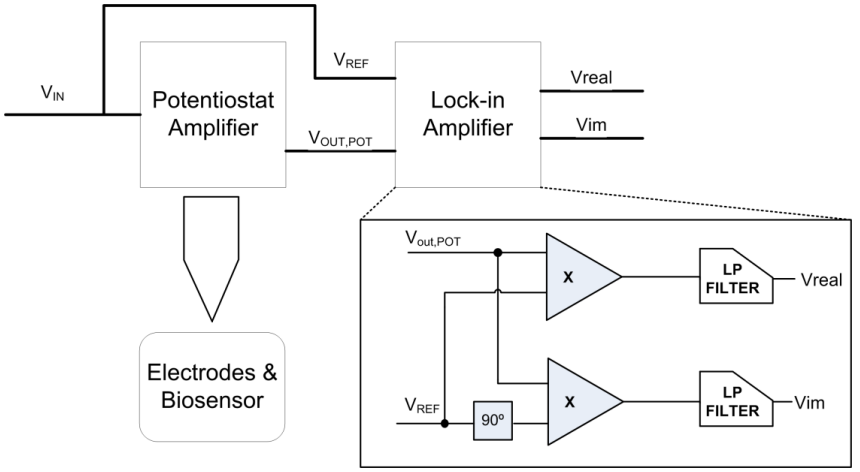

Figure 1.10: Block diagram view of a complete system of a front-end instrumentation (Potentiostat in this case), sensing system and LIA.

The basic operation of the LIA is very simple. $V_{out,POT}$ represents the potentiostat amplifier output signal, so

$$V_{out,POT} = I_{CELL} \cdot R \ (1)$$

where R is the relation in ohms between the current on the cell and the output potentiostat signal (like R_{TIA} on transimpedance amplifier based potentiostats). Considering the $V_{out,POT}$ function as a frequency dependant, we get:

$$\begin{aligned} V_{out,POT}(t) &= V_{OUT}\sin(2\pi ft + \phi_{OUT}) \\ &= V_{OUT}[\sin(2\pi ft)\cos(\phi_{OUT}) + \cos(2\pi ft)\sin(\phi_{OUT})] (2) \end{aligned}$$

So, our functions Vreal and Vim are represented by the following equations.

$$\begin{aligned} Vreal &= V_{out,POT} \cdot V_{IN} \sin(2\pi ft) \\ &= V_{OUT} \cdot V_{IN} \cdot (\sin^2(2\pi ft)\cos(\phi_{OUT}) \\ &+ \frac{1}{2}\sin(2\pi ft)\cos(2\pi ft)\sin(\phi_{OUT}) (3) \end{aligned}$$

$$\begin{aligned} Vim &= V_{out,POT} \cdot V_{IN} \cos(2\pi ft) \\ &= V_{OUT} \cdot V_{IN} \cdot (\cos^2(2\pi ft)\sin(\phi_{OUT}) \\ &+ \frac{1}{2}\sin(2\pi ft)\cos(2\pi ft)\cos(\phi_{OUT}(4) \end{aligned}$$

$$\begin{aligned} Vreal = \frac{1}{2}V_{OUT} \cdot V_{IN} \cdot [\cos(\phi_{OUT}) - \cos(4\pi ft)\cos(\phi_{OUT}) \\ + \sin(4\pi ft)\sin(\phi_{OUT})] (5) \end{aligned}$$

$$\mathrm{Vim} = \frac{1}{2}\mathrm{V_{OUT}} \cdot \mathrm{V_{IN}} \cdot [\cos(\phi_{\mathrm{OUT}}) + \cos(4\pi \mathrm{ft})\sin(\phi_{\mathrm{OUT}}) + \sin(4\pi \mathrm{ft})\cos(\phi_{\mathrm{OUT}})](6)$$

Taking into account only the DC component,

$$\mathrm{Vreal} = \frac{1}{2}\mathrm{V_{OUT}} \cdot \mathrm{V_{IN}} \cdot \cos(\phi_{\mathrm{OUT}})(7)$$

$$\mathrm{Vim} = \frac{1}{2}\mathrm{V_{OUT}} \cdot \mathrm{V_{IN}} \cdot \sin(\phi_{\mathrm{OUT}})(8)$$

The magnitude and phase of $V_{out,POT}$ are

$$\left|\mathrm{V_{out,POT}}\right| = \frac{2}{\mathrm{V_{IN}}}\sqrt{\mathrm{V_{real}}^2 + \mathrm{V_{im}}^2}\ ;\ \Phi_{\mathrm{Vout,POT}} = \mathrm{arctg}(\frac{\mathrm{V_{im}}}{\mathrm{V_{real}}})(9)$$

Being the magnitude and phase of impedance Z_{CELL}:

$$|\mathrm{Z_{CELL}}| = \frac{\mathrm{V_{IN}} \cdot \mathrm{V_{CELL}} \cdot \mathrm{R}}{2\sqrt{\mathrm{V_{real}}^2 + \mathrm{V_{im}}^2}}\ ;\ \Phi_{\mathrm{ZCELL}} = \mathrm{arctg}(\frac{\mathrm{V_{im}}}{\mathrm{V_{real}}})(10)$$

1.4.1. The Lock-in amplifier analog approach.

In the previous section have the idea of a whole system based on a potentiostat and a lock-in amplifier as a complete solution for an electrochemical impedance spectroscopy experiment was introduced. In this section, it is presented the configuration of a lock-in amplifier that generates the real and imaginary components of the impedance (Z_{CELL}) based on an analog instrumentation implementation is presented.

The lock-in amplifier architecture based on an analogue approach [101-103], consists in different modules, which are two Synchronous Demodulated Channels which generates DC voltage signals which are proportional to the real (V_{real}) and imaginary (V_{im}) components of the input signal (front-end instrumentation). The circuit schematic, with the demodulator and the low pass filter, is depicted figure 1.11, where $V_{out,POT}$ represents the potentiostat amplifier output signal (equation 19).

The lock-in amplifier provides real and imaginary components through the DC values Vreal and Vim, respectively, after filtering the rectified signals from the demodulator stage, getting a complete characterization of potentiostat output signal and an accurate estimation of Z_{CELL} (electrochemical reaction characteristics).

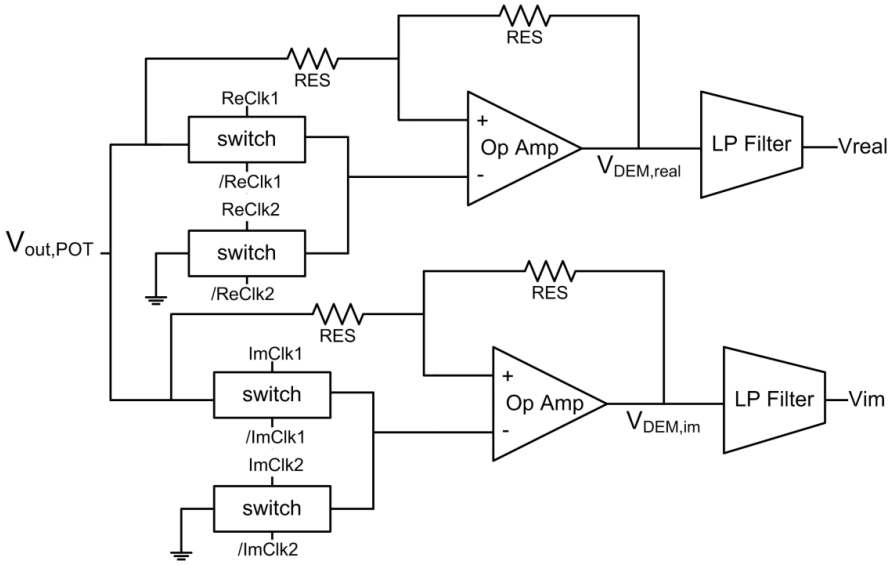

Figure 1.11: Full schematic view of the implemented lock-in module [58].

Special attention is given to the reference signal used by the demodulator channels which is multiplied by the signal to be measured. The reference (V_{REF}) signal is an ac voltage, of the same frequency of the input signal, which can be either generated by an oscillator, locked to the input signal by a phase locked loop or mainly using the same polarization signal of the previous stages (V_{IN}). A phase shifter allows the reference signal to be trimmed at the following phases: phase ReClk1 = 0º, phase ReClk2 = 180º, phase ImClk1 = 90º, phase ImClk1 = 270º. The clock signals generator is depicted on figure 1.12.

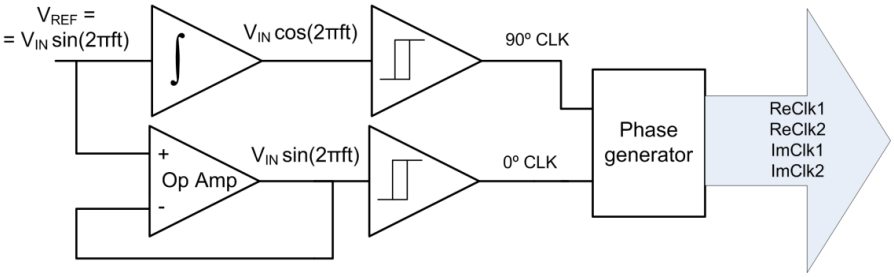

Figure 1.12: Clock generation module.

Clock signals are generated by two hysteretic comparators, one for the 0º phase clock and the other one for 90º phase clock signals, previously generated by an integrator. It's desirable that the different four clock signals be generated with a dead time, DT in figure 1.13, between them for each channel, ReClk1 and ReClk2 for V_{REAL} channel and ImClk1 and ImClk2 for V_{IM} channel. The dead time must be implemented in order to avoid undesired spikes at the generated clocks and harmonic distortion coupling on the demodulator channels. Dead time values must be several orders of magnitude less than the clock period to not interfere with the clocks phase shift.

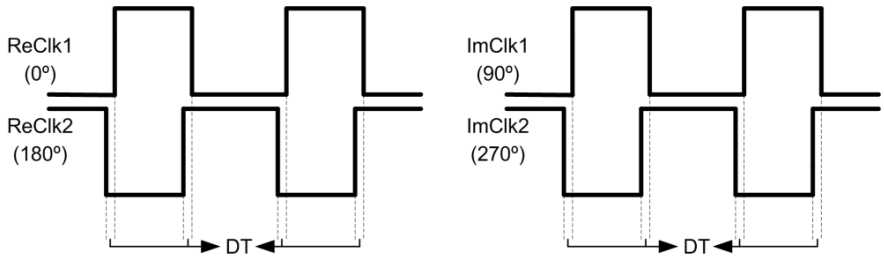

Figure 1.13: Dead time conceptionClock generation module.

Finally, the demodulation stage consists of two simple wave rectifiers. On each rectifier, when the input signal to be measured and the reference signal are of the same frequency, the demodulator output has a dc component proportional to the input signal amplitude. By adjusting the phase of the reference signal using the phase-shifters present in the reference channel, the phase difference between the input signal and the reference can be brought to zero (null shift procedure). If we get all the four phases; 0º, 90º, 180º and 270º; considering the two different channels on demodulation stage, we have a complete data spectrum to evaluate the whole input signal.

A low pass filter characterized by a low cut-off frequency is necessary to reject the noise and harmonics superimposed to the output demodulation stage and acquire the dc component proportional to the signal. A very interesting architecture is based on a trans-conductance amplifier (OTA), due to the very small trans-conductance values, in the order of nano-siemmens, that can be defined [104]. The basic structure is based on a source degenerated trans-conductance amplifier (OTA) to define the filter. The source degeneration increases the input range of the amplifier and also decreases the equivalent trans-conductance of the OTA amplifier. The ratio between the current mirrors decreases the current level at output, which results in an even minor value [105]. These current mirrors are based on composite transistors, used to reach greater copy factors. The typical transfer equation and cut-off frequency are the following

$$|H_{FILTER}| = \frac{\frac{gm1 \cdot gm2}{C1 \cdot C2}}{s^2 + s \cdot \frac{gm2}{C2} + \frac{gm1 \cdot gm2}{C1 \cdot C2}} \quad (11)$$

$$\omega_0 = \sqrt{\frac{gm1 \cdot gm2}{C1 \cdot C2}} \quad (12)$$

Then, integratable capacitors can be implemented, defining cut-off frequencies in the range of 0.1Hz to 30Hz. The LP Filter on Figure 13. is depicted as a Gm-C second-order low pass-filter in figure 1.14.

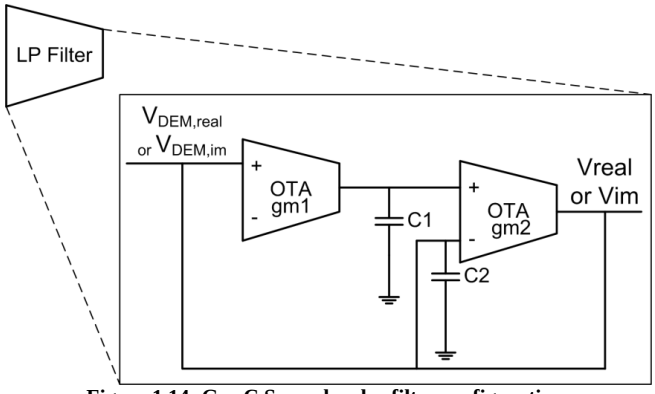

Figure 1.14: Gm-C Second order filter configuration.

Once we get both real and imaginary components of the measured signal from the analogue lock-in amplifier, we need to process these raw dc values to obtain reliable information about our system to perform an EIS experiment with them. In order to develop a complete system for EIS experiments, the dc raw data on lock-in output must be digitalized in order to carry out the mathematical post-processing, equation 31 to 34, on a microcontroller, DSP or computer. The digitalization of the output data is easiest than in other devices due to the acquisition of only DC signals. The theoretical expression of the module and phase of $V_{out,POT}$, in figure 13, using the Randles model, are found in following equations:

$$\left|V_{out,POT}\right| = \frac{\pi}{2}\sqrt{{V_{real}}^2 + {V_{im}}^2} (13)$$

$$\Phi_{Vout,POT} = arctg(\frac{V_{im}}{V_{real}}) (14)$$

$$|Z_{CELL}| = \frac{2}{\pi} \cdot V_{CELL} \cdot R \cdot \frac{1}{\sqrt{{V_{real}}^2 + {V_{im}}^2}} (15)$$

$$\Phi_{ZCELL} = arctg(\frac{V_{im}}{V_{real}}) (16)$$

Where 2/pi is the mean absolute value of the sine function [101].

Obtaining with equation 33 and 34 a direct measurement of both Z_{CELL} module and phase and Z_{CELL} real and imaginary components and obtaining reliable data for Electrochemical Impedance Spectroscopy experience. In figure 1.15 the behavior of the demodulation stage for both channels is shown.

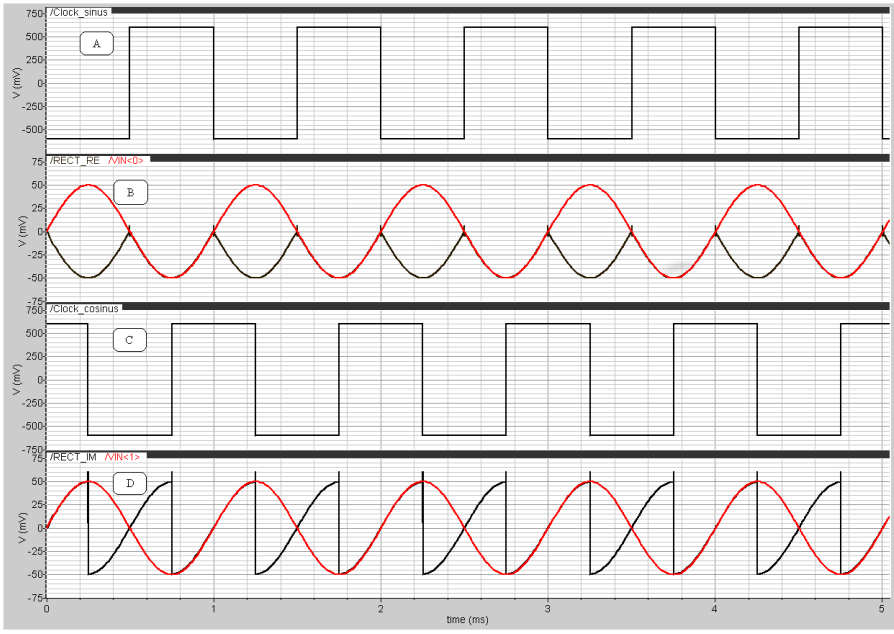

Figure 1.15: Caption of the rectified signals for the real and imaginary channels before the active filters. Upper trace (A) represents the reference clock signal for the synchronous demodulated channel for the real component, before the filter (Vreal); next figure (B) is the rectified signal. The third signal (C) is the reference clock signal for the synchronoys demodulated signal for the imaginary component (Vim), and the last trace (D) at the bottom, is the trace of the rectified signal at the imaginary channel. These traces are obtained for a 180º condition.

1.4.2. The Lock-in Amplifier digital approach.

Some potentiostat solutions employ an output digital signal in order to facilitate the data processing and transmission. Since the use of analogue instrumentation processing usually leads to a final data digitalization, the possibility of a direct embedded processing is an interesting approach to developing a lock-in amplifier. The digital lock-in (DLIA) approach is based on an embedded mathematical processing on a microprocessor or DSP device [106,107]. The block diagram of the lock-in software is depicted in figure 1.16.

In order to proceed with the signal processing there are two main approaches: a) the Fast Fourier Transform (FFT) [108], and b) the Frequency Response Analyser (FRA) [106]. In the case of the FFT, a pulse, or a step, -the approach to be followed is the ideal Dirac function-, is applied to the sample because it contains a wide frequency content. Then, the response of the sample is digitalized and processed in a digital processor, for instance a DSP, and using the FFT algorithm, the different frequency components are obtained for their analysis. Another possibility is the logarithmic sampling in the DFFT calculus, reducing the data required in the process [108]. This appears to be simple, but there are several problems in the implementation. First of all, it is very difficult to generate a fast step function and a very fast electronics capable of driving this step on the electrodes and extracting the resulting current signal. If the sensing system and front-end electronics rising time is too slow, the resulting frequency components will be distorted. Since the important information is contained in a short period of time after the step is applied, in addition to a very fast front-end electronics, very fast ADC with a high precision bit resolution is also required

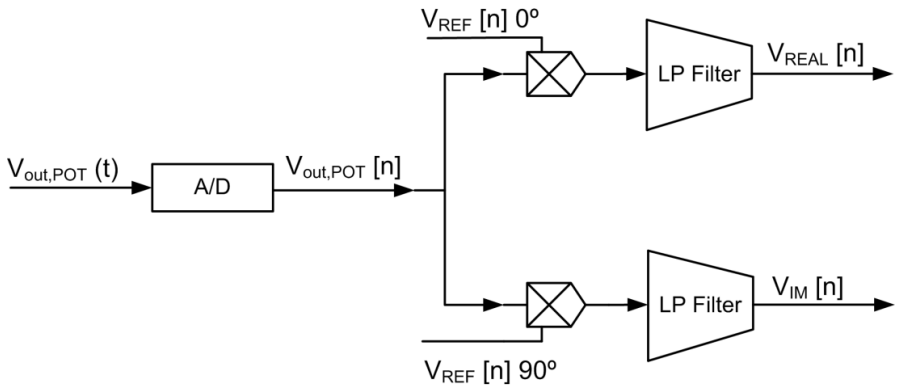

Figure 1.16: Digital lock-in block diagram.

A simpler solution is based on the FRA approach. In this case a sine and cosine signals are adopted and by means of two multipliers and a filter stage the real and imaginary components of the response are obtained. This measurement must be done for each frequency. Working with just one sensor and in terms of the size of the final product, the FFT option could be adopted, although high speed hardware and heavy algorithm implementation is required, because the response for several frequencies is obtained. The FRA solution is more oriented to multi-sensor approaches but is also a good option in the case of single sensors, in terms of the trade-off between complexity and speed, if not too low frequencies are to be measured.

This lock-in approach is more feasible. The digital lock-in FRA approach [107] is based on the principle that there is no correlation between noise and measured signal. In contrast to the analogue approach, an orthogonal arithmetic multiplying between the incoming potentiostat signal and reference signal are used to get the real and imaginary components, coming close to the theoretical behavior of a LIA. A digital lock-in has no low frequency limitations, being capable of working properly at the sub-hertz region. The upper frequency limitation is mainly limited by the ADC conversion time, being able to develop a wide frequency range IS system. On the other hand, the DLIA is limited by area and power consumption. The area and power consumption levels depend on the electronics involved. If a microprocessor is needed, we get typical power consumption, for commercial solutions, of several hundreds of mW, which is far from the desired power waste. But in the recent years a step forward in microprocessors field has been presented in [109, 110]. [109] present a microprocessor, in a 180 nm technology, with a power consumption of 226 nW, and area of 915x915 mm^2. It evolved from [110], where the sub-threshold operating region is explored. In the same way there has been an evolution in microprocessor development, in terms of area and power consumption. [111], present an evolution of the digital lock-in algorithm based on an oversampling solution, simplifying the orthogonal vector arithmetic cutting off all the multiplying operations.

In that way, evolution of both microprocessor hardware and lock-in algorithm software, leads to a whole post-processing embedded system with great throughput, functionality and versatility without involving a high area or power consumption.

1.5. Contribution of this Thesis.

The aim of this research is to design, fabricate and test a novel device / technology for PoC instantaneous screening and monitoring of cellular analytes. The method used is based on direct measurement from samples by means of its inherent electrical IA in order to overcome the operational challenges present on the actual PoC devices on the market.

The state of the art of PoC devices have been analysed (Chapter 1) to study their strengths and weakness, and determine the necessary improvements. This is, the development of instrumentation electronics, sensing systems as well as design protocols for truly PoC devices, relying on straight forward standards for economic, low power consumption, versatile, safe and reliable devices. The development of such technologies and devices is entailed to the evolution of these systems as implantable LOC devices for in vivo continuous monitoring of the patients. In this case, the development of simplified low-power electronics and sensing systems, leads to its miniaturization and integration in a single microchip with multiple functionalities.

A discrete bench-top system for IA have been designed, fabricated and tested. In Chapter 2 it is presented the design and validation of different instrumentation electronics and sensing systems, as well as design protocols for truly PoC devices. The device has been designed to perform an Impedance Spectrometry (IS) experiment in order to validate the whole device electronics as well as to characterize the sensing system and its interface accurately.

In Chapter 3, the first experiments for cellular detection by means of IA are exposed. A first approach to a portable and compact device for PoC early instantaneous detection of anaemia, relying on HCT screening, is described. This device has been designed to work directly with fresh whole blood samples. An experimental set-up and protocol of operation have been defined for instant impedance detection to determine the system detection accuracy, sensitivity and coefficient of variation. As you will notice, the device has been developed using prototyping tools from National Instruments for fast development and validation, as well as application functionalities.

In chapter 4 is validated the possibilities of the integration of this technology within other devices for increased functionalities. The experiments were carried out with different instrumentations front-end as well as different sensing systems typologies, and the same back-end electronics for signal processing and system control. The analysed samples and its environment were dramatically different: laboratory sample formed by *E. coli* 5K strains working as a monitoring functionality of a DEP-enhanced concentrator for automated detection and concentration of bacteriological species.

In chapter 5, the development of a specific PoC device for HCT detection and a clinical test from whole blood samples is presented. The design is based in the previously presented device's electronic instrumentation and sensing system with the addition of an economic and low power back-end solution. A clinical study has been performed and the results obtained during the experimental procedures are shown, analysed and discussed.

Finally, in chapter 6 we summarize the conclusions obtained after this research and recommend future developments that could be done to develop truly last generation PoC devices and integrated LOC single-chip devices.

1.6. References

[1] Juanola-Feliu E, et al. “Design of a customized multipurpose nano-enabled implantable system for in-vivo theranostics” *Sensors*; vol. 14, no. 10, pp. 19275 – 19306, 2014.

[2] Chin CD, Linder V, Sia SK. “Commercialization of microfluidic PoC diagnostic devices”. *Lab Chip*, vol. 12, no. 12, pp. 2118–2134, 2012.

[3] Sachs JD. “Primary Health Care in Low-Income Countries Building on Recent Achievements” *JAMA*, vol. 307, no. 19, pp. 2031–2032, 2014.

[4] Fu BE, Yager P, Floriano PN, Christodoulides N, Mcdevitt JT. “Perspective on Diagnostics for Global Health” *IEEE Pulse*, vol. 2, no. 6, pp. 40–50, 2011.

[5] World Health Organization. Iron Deficiency Anaemia: Assessment, Prevention and Control; A Guide for Programme Managers. Geneva, Switzerland, 2001.

[6] Thompson, R.B. A Short Textbook of Haematology, 4th ed.; Pitman Medical Publishing Co., Kent, 1975.

[7] Brown J, et al. “A hand-powered, portable, low-cost centrifuge for diagnosing anaemia in low-resource settings”. *Am. J. Trop. Med. Hyg*. vol. 85, no. 2, pp. 327–332, 2011.

[8] Cleven R, Nur Y, Krystek P, Van den Berg G. “Monitoring Metal Speciation in the Rivers Meuse and Rhine using DGT” *Water Air Soil Pollut*, vol.165, pp. 249-263, 2005.

[9] Poyatos JM, Muñio MM, Almecija MC, Toress JC, Hontoria E, Osorio F. “Advanced Oxidation Processes for Wastewater Treatment: State of the Art” *Water Air Soil Pollut*, vol. 205, pp. 187-204, 2010.

[10] Terbouche A, Djebbar S, Benali-Baitich O, Hauchard D. “Complexation Study of Humic Acids Extracted from Sahara Soils with Zuinc (II) and Cadmium (II) by Differential Pulse Anodic Stripping Voltammetry (DPASV) and Conductimetric Methods” *Water Air Soil Pollut*, vol. 216, pp. 679-691, 2011.

[11] Buowari O. “Complications of venepuncture” *Adv. Biosci. Biotechnol.*, vol. 4, pp. 126–128, 2013.

[12] Song Y, Huang YY, Liu X, Zhang X, Ferrari M, Qin L. “Point-of-care technologies for molecular diagnostics using a drop of blood.,” *Trends Biotechnol.*, vol. 32, no. 3, pp. 132–139, Mar. 2014.

[13] Hu J, Wang S, Wang L, Li F, Pingguan-Murphy B, Lu TJ, Xu F. “Advances in paper-based PoC diagnostics” *Biosens. Bioelectron.* vol. 54, no. 15, pp. 585–97, Apr. 2014.

[14] Xiong F, Hipszer BR, Joseph J, Kam M. “Improved blood glucose estimation through multi-sensor fusion.,” in Annual International Conference of the IEEE Engineering in Medicine and Biology Society., 2011, pp. 377–380.

[15] Rebel A, Rice MA, Fahy BG, “The Accuracy of PoC Glucose Measurements,” *J. Diabetes Sci. Technol.*, vol. 6, no. 2, pp. 396–411, Mar. 2012.

[16] Yoo EH, Lee SY. “Glucose biosensors: an overview of use in clinical practice” *Sensors*, vol. 10, no. 5, pp. 4558–76, Jan. 2010.

[17] Clark L, Lyons C. “Electrode systems for continuous monitoring in cardiovascular surgery” *Ann. N. Y. Acad. Sci*, vol. 102, no. 1, pp. 29–45, 1962.

[18] Turner APF, Chen B, Piletsky SA. “In Vitro Diagnostics in Diabetes: Meeting the Challenge” *Clin. Chem.*, vol. 45, no. 9, pp. 1596–1601, Sep. 1999.

[19] Pickup J, Shaw G, Claremont D. “Potentially-implantable, amperometric glucose sensors with mediated electron transfer: improving the operating stability” *Biosensors*, vol. 4, no. 2, pp. 109–119, 1989.

[20] Koudelka M, Rohner-Jeanrenaud F. “In-vivo behaviour of hypodermically implanted microfabricated glucose sensors” *Biosens. Bioelectron.*, vol. 6, no. 1, pp. 31–36, 1991.

[21] Albisser AM, Leibel BS, Ewart TG, Davidovac Z, Botz CK, Zingg W, Schipper H, Gander R. “Clinical Control of Diabetes by the Artificial Pancreas” *Diabetes*, vol. 23, no. 5, pp. 397–404, May 1974.

[22] Celia H, “Getting under the skin: Implantable Glucose Sensors” *Anal. Chem.*, vol. 70, no. 17, p. 594A–598A, Jun. 2011.

[23] Khoshnoud F, De Silva CW, “Recent Advances in MEMS Sensor Technology — Biomedical Applications” *Instrumentation & Measurement Magazine, IEEE*, vol.15, no.1, pp.8-14, February 2012.

[24] Sashidar S, European Diabetes Diagnostic Market: Growing Diabetes Prevalence Drives Demand, Frost & Sullivan, 2012.

[25] Chang Z, Pop AGM, Meijer GCM. “A comparison of two- and four-electrode techniques to characterize blood impedance for the frequency range of 100 Hz to 100 MHz” *IEEE Trans. Biomed. Eng.*, no. 3, pp. 1247–1249, Mar. 2008.

[26] Pop GAM, Bisschops LLA, Iliev B, Struijk PC, van der Hoeven JG, Hoedemaekers CWE. “On-line blood viscosity monitoring in vivo with a central venous catheter, using electrical impedance technique” *Biosens. Bioelectron.*, vol. 41, no. 15, pp. 595–601, Mar. 2013.

[27] Ramaswamy B, Yeh TT, Zheng SY. “Microfluidic device and system for PoC blood coagulation measurement based on electrical impedance sensing” *Sensors Actuators B Chem.*, vol. 180, pp. 21–27, Apr. 2013.

[28] Pradhan R, Mitra A, Das S. “Impedimetric characterization of human blood using three-electrode based ECIS devices” *J. Electr. Bioimpedance*, vol. 3, no. 1, pp. 12–19, Jul. 2012.

[29] Tyburski E, Gillespie S. “Disposable platform provides visual and color-based PoC anaemia self-testing” *J. Clin. Invest.*, vol. 124, no. 10, pp. 4387–4394, 2014.

[30] Kumar S, et al. “Microfluidic-integrated biosensors: prospects for PoC diagnostics” *Biotechnol. J.*, vol. 8, no. 11, pp. 1267–79, Nov. 2013.

[31] de Benoist B, McLean E, Egli I, Cogswell ME. Worldwide prevalence of anaemia 1993–2005: WHO global database on anaemia, Geneva, Switzerland, 2008.
[32] Tolentino K, Friedman J. "An update on anaemia in less developed countries" *Am. J. Trop. Med. Hyg*. vol. 1, pp. 44–51, 2007.
[33] Brown J, et al. "A hand-powered, portable, low-cost centrifuge for diagnosing anaemia in low-resource settings" *Am. J. Trop. Med. Hyg.* vol. 85, no. 2, pp. 327–32, 2011.
[34] Mason J, Shrimpton R. 6th Report on the World Nutrition Situation. 2010.
[35] Powers J, Buchanan G. "Diagnosis and Management of Iron Deficiency Anaemia" *Hematol. Oncol. Clin. North Am.* vol. 28, no. 4, pp. 729–745, 2014.
[36] Keohane C, McMullin M, Harrison C. "The diagnosis and management of erythrocytosis" *BMJ Br. Med. J.*, vol. 347, pp. 1–6, 2013.
[37] Silver R, Gjoni S. "The HCT Value in Polycythemia Vera: Caveat Utilitor" *Leuk. Lymphoma*, [Online], pp. 1–8, 2014.
[38] Li Y, Liu L, Wang B, Wang J, Chen D. "HCT is associated with fibrosis in patients with nonalcoholic steatohepatitis" *Eur. J. Gastroenterol. Hepatol.*, vol. 26, no. 3, pp. 332–338, 2014.
[39] Myers GJ, Browne J. "Point of care HCT and hemoglobin in cardiac surgery: a review" *Perfusion*, vol. 22, no. 3, pp. 179–183, 2007.
[40] Eichner ER. "Blood doping: infusions, erythropoietin and artificial blood" *Sports Med.*, vol. 37, pp. 389-391, 2007.
[41] Böning D, Maassen N, Pries A, "The HCT paradox – how does blood doping really work" *Int. J. Sports Med.*, vol. 32, pp. 242-246, 2011.
[42] Harter TS, Shartau RB, Brauner CJ, Farrell AP. "Validation of the i-STAT system for the analysis of blood parameters in fish" *Conserv. Physiol.*, vol. 2, no. 1, pp. 37–38, 2014.
[43] McGann PT, Tyburski E, de Oliveira V, Santos B, Ware RE, Lam WA. "An Accurate and Rapid Color-Based PoC Assay for the Detection of Severe Anaemia in Low Resource Settings" *Blood*, vol. 124, no. 21, pp. 688 – 688, 2014.
[44] Sears D, Charache S, Perlstein M. "Electronic blood cell counters. Faulty calibration due to type and amount of anticoagulant in collection tubes" *Arch. Pathol. Lab. Med.*, vol. 109, no. 3, pp. 247–249, 1985.
[45] Gayat E, et al. "Performance evaluation of a noninvasive hemoglobin monitoring device" *Ann. Emerg. Med.*, vol. 57, no. 4, pp. 330–333, 2011.
[46] Pagliaro P, et al. "A non-invasive strategy for haemoglobin screening of blood donors" *Blood Transfus.*, vol. 12, no. 4, pp. 458–463, 2014.
[47] Singh A, Dubey A, Sonker A, Chaudhary R. "Evaluation of various methods of PoC testing of haemoglobin concentration in blood donors" *Blood Transfus*. pp. 1–7, 2014.
[48] Soriguer F, Goday A, Martínez-Larrad A, Menéndez E, Mora-Peces I, Ortega E, Pascual-Manich F, Rojo-Martínez G, Serrano-Rios M, Valdés G, Vázquez JA, Vendrell J, "Prevalence of diabetes mellitus and impaired glucose regulation in Spain: the Di@bet.es Study" *Diabetologia*, vol. 55, no. 1, pp. 88–93, Oct. 2011.
[49] Taskinen MR, Borén J. "New insights into the pathophysiology of dyslipidemia in type 2 diabetes" *Atherosclerosis*, vol. 239, no. 2, pp. 483–495, Apr. 2015.
[50] Vlagopoulos PT, et al. " Anaemia as a Risk Factor for Cardiovascular Disease and All-Cause Mortality in Diabetes: The Impact of Chronic Kidney Disease." *JASN*, vol. 16, pp. 3403-3410, November 2005.
[51] El-achkar TM, et al. "Anaemia as a Risk Factor for Cardiovascular Disease and All-Cause Mortality in Diabetes: The Impact of Chronic Kidney Disease." *Kidney International*, vol. 67, pp. 1483-1488, October 2004.
[52] Cai D, Xiao M, Xu P, Xu YC, Du W. "An integrated microfluidic device utilizing dielectrophoresis and multiplex array PCR for PoC detection of pathogens" *Lab Chip*, vol. 14, no. 20, pp. 3917–24, Oct. 2014.
[53] Gubala V, Harris LF, Ricco AJ, Tan MX, Williams DE. "Point of care diagnostics: status and future" *Anal. Chem.*, vol. 84, no. 2, pp. 487–515, Jan. 2012.
[54] Vahlsing T, Delbeck S, Budde J, Cocchieri L, Ihrig D, Leonhardt S, Heise HM. "Ex-vivo glucose sensors using micro-dialysis: importance of on-line recovery rate determination by multi-analyte infrared spectrometry" in Proc. SPIE 9332, Optical Diagnostics and Sensing XV: Toward PoC Diagnostics, 2015, p. 933209.
[55] Brandstetter M, Volgger L, Genner A, Jungbauer C, Lendl B. "Direct determination of glucose, lactate and triglycerides in blood serum by a tunable quantum cascade laser-based mid-IR sensor" *Appl. Phys. B*, vol. 110, no. 2, pp. 233–239, Jun. 2012.
[56] Zhang L, Cao X, Wang L, Zhao X, Zhang S, Wang P. "Printed microwells with highly stable thin-film enzyme coatings for PoC multiplex bioassay of blood samples" *Analyst*, p. Accepted Manuscript, Apr. 2015.
[57] Pollock NR, et al. "A paper-based multiplexed transaminase test for low-cost, PoC liver function testing" *Sci. Transl. Med.*, vol. 4, no. 152, p. 152ra129, Sep. 2012.
[58] Sashidar S, European Diabetes Diagnostic Market: Growing Diabetes Prevalence Drives Demand, Frost & Sullivan, 2012.
[59] Shadfan BH, Simmons AR, Simmons GW, Wong AHJ, Lu KH, Bast RC, McDevitt JT. "A multiplexable, microfluidic platform for the rapid quantitation of a biomarker panel for early ovarian cancer detection at the PoC" *Cancer Prev. Res.*, vol. 8, no. 1, pp. 37–48, Jan. 2015.
[60] Kumar S, Ali MA, Anand P, Agrawal VV, John R, Maji S, Malhotra BD. "Microfluidic-integrated biosensors: prospects for PoC diagnostics" *Biotechnol. J.*, vol. 8, no. 11, pp. 1267–1279, Nov. 2013.
[61] Spindel S, Sapsford KE. "Evaluation of optical detection platforms for multiplexed detection of proteins and the need for PoC biosensors for clinical use" *Sensors*, vol. 14, no. 12, pp. 22313–22341, Jan. 2014.

[62] St John A, Price CP. "Existing and Emerging Technologies for PoC Testing" *Clin. Biochem. Rev.*, vol. 35, no. 3, pp. 155–67, Aug. 2014.
[63] Blood glucose monitoring test systems for prescription PoC use, FDA draft guidance, January 2014, https://federalregister.gov/a/2014-00023
[64] Erickson K, Wilding P. "Evaluation of a novel PoC system, the i-STAT portable clinical analyzer" *Clin. Chem.*, vol. 39, no. 2, pp. 283–287, Feb. 1993.
[65] Jacobs E, Vadasdi E, Sarkozi L, Colman N. "Analytical evaluation of i-STAT Portable Clinical Analyzer and use by nonlaboratory health-care professionals" *Clin. Chem.*, vol. 39, no. 6, pp. 1069–1074, Jun. 1993.
[66] Dechant JE, Symm WA, Nieto JE. "Comparison of pH, lactate, and glucose analysis of equine synovial fluid using a portable clinical analyzer with a bench-top blood gas analyzer" *Vet. Surg.*, vol. 40, no. 7, pp. 811–6, Oct. 2011.
[67] Martinez AW, Phillips ST, Whitesides GM, Carrilho E. "Diagnostics for the developing world: Microfluidic paper-based analytical devices" *Anal. Chem.*, vol. 82, no. 1, pp. 3–10, 2010.
[68] Songjaroen T, Dungchai W, Chailapakul O, Henry CS, Laiwattanapaisal W. "Blood separation on microfluidic paper-based analytical devices" *Lab Chip*, vol. 12, no. 18, pp. 3392–3398, Sep. 2012.
[69] Lewis GG, DiTucci MJ, Phillips ST. "Quantifying analytes in paper-based microfluidic devices without using external electronic readers" *Angew. Chem. Int. Ed. Engl.*, vol. 51, no. 51, pp. 12707–10, Dec. 2012.
[70] Jin G, et al. "Multi-nanomaterial electrochemical biosensor based on label-free graphene for detecting cancer biomarkers" *Biosens. Bioelectron.*, vol. 55, pp. 464–469, May 2014.
[71] Jani IV, Peter TF. "How PoC Testing Could Drive Innovation in Global Health" *N Engl J Med*., vol. 368, no.24, pp. 2319-2324, June 2013.
[72] Li N, et al. "Disposable Immunochips for the Detection of Legionella pneumophila Using Electrochemical Impedance Spectroscopy" *Anal. Chem.*, no. 84, pp. 3485–3488, Mar. 2012.
[73] Dweik M, Stringer RC, Dastider SG, Wu Y, Almasri M, Barizuddin S. "Specific and targeted detection of viable Escherichia coli O157:H7 using a sensitive and reusable impedance biosensor with dose and time response studies" *Talanta*, vol. 94, pp. 84–89, May 2012.
[74] Grossi M, Lanzoni M, Pompei A, Lazzarini R, Matteuzzi D, Riccò B. "An embedded portable biosensor system for bacterial concentration detection." Biosens. Bioelectron., vol. 26, pp. 983–990, Nov. 2010.
[75] Ramirez N, Regueiro A, Arias O, Contreras R. "Electrochemical impedance spectroscopy: An effective tool for a fast microbiological diagnosis" *Biotecnologia Aplicada*, vol. 26, pp. 72–78, 2008.
[76] Pop GA, et al. "Blood electrical impedance closely matches whole blood viscosity as parameter of hemorheology and inflammation" *Appl. Rheol.*, vol. 13, no. 6, pp. 305–312, 2003.
[77] Hernández F, Guerrero C, Bernal J. "Determinación de las propiedades eléctricas en tejido sangíneo" *Ciencia UANL*, vol. 8, pp. 7-13, 2011.
[78] Lvovich V, Srikanthan S, Silverstein RL. "A novel broadband impedance method for detection of cell-derived microparticles" *Biosensors and Bioelectronics*, vol. 26, no. 2, pp. 444–451, October 2010.
[79] Xu M, Luo X, Davis JJ. "The label free picomolar detection of insulin in blood serum," *Biosensors and Bioelectronics*, vol. 39, pp. 21–25, January 2013.
[80] Patterson R. Bioelectric Impedance Measurements: The Biomedical Engineering Handbook, J.D. Bronzino, 2nd Edition, Boca Raton, CRC Press, 734-73, 2000.
[81] Grosse C, Schwan HP. "Cellular membrane potentials induced by alternating fields" *Biophys. J.*, vol. 63, pp. 1632–1642, 1992.
[82] Lenaerts B, Puers R. Omnidirectional inductive powering for biomedical implants. Springer, Netherlands, 2009.
[83] Bard A, Faulkner L. Electrochemical Methods, Second Edition. John Wiley & Sons; 2001.
[84] Martin SM, Gebara FH, Larivee BJ, Brown RB. "A CMOS-Integrated Microinstrument for Trace Detection of Heavy Metals" *IEEE Journal of Solid-State Circuits*, vol. 40, no. 12, pp. 2777-2786, 2005.
[85] Colomer-Farrarons J, Miribel-Catala P, Rodriguez-Villareal I, Samitier J. Portable Bio-Devices: Design of Electrochemical Instruments from Miniaturized to Implantable Devices. In: Serra PA. (ed.) New Perpspectives in Biosensors Technology and Applications. Intech; 2011. pp. 373-400.
[86] Kakerow R, Kappert H, Spiegel E, Manoli Y. "Low-power Single-Chip CMOS Potentiostat" *The 8th International Conference on Solid-State Sensors and Actuators*, 25-29 June 1995, Stockholm, Sweden.
[87] Kraver KL, Guthaus MR, Strong TD, Bird PL, Cha GS, Hold W, Brown RB. "A Mixed-signal Sensor Interface Microinstrument" *Journal of Sensors and Actuators A*, vol. 91, pp. 266-277, 2001.
[88] Reay R, Kounaves S, Kovacs G. "An Integrated CMOS Potentiostat for Miniaturized Electroanalytical Instrumentation" Proceedings of the 41st IEEE International Solid-State Circuits Conference, ISSCC1994, 16-18 February 1994.
[89] Martin SM, Gebara FH, Larivee BJ, Strong TD, Brown RB. "A Low-Voltage, Chemical Sensor Interface for Systems-On-Chip: The Fully-Differential Potentiostat" Proceedings of the International Symposium on Circuits and Systems, ISCAS2004, 23-26 May 2004, Vancouver, Canada.
[90] Stanacevic M, Murari K, Cauwenberghs G, Thakor N. "16-Channel Wide-range VLSI Potentiostat Array" IEEE International Workshop on Biomedical Circuits and Systems, BioCAS2004, 1-3 December 2004, Singapore.
[91] Qisong W, Haigang Y, Tao Y, Chong Z. "A High Precission CMOS Weak Current Readout Circuit" *Journal of Semiconductors*, vol. 30, no. 7, pp. 075011-075016, July 2009.
[92] Gore A, Chakrabartty S, Pal S, Alocilja EC. "A Multichannel Femtoampere-Sensitivity Potentiostat Array for Biosensing Applications" *IEEE Transactions on Circuits and Systems*, vol. 53, no. 11, pp. 2357-2363, 2006.

[93] Aziz JNY, Abdelhalim K, Shulyzki R, Genov R, Bardakjian BL, Derchansky M, Serletis D, Carlen PL. "256-channel Neural Recording and Delta Compression Microsystem With 3D electrodes" *IEEE Journal of Solid-State Circuits*, vol. 44, no. 3, pp. 995-1005, 2009.
[94] Jichun Z, Trombly N, Mason A. "A Low Noise Readout Circuit for Integrated Electrochemical Biosensors Array" Proceedings of 3th IEEE Conference on Sensors, IEEE Sensors 2004, 24-27 October 2004, Vienna, Austria.
[95] Calvo B, Medrano N, Celma S. "A Low-Power High-Sensitivity CMOS Voltage-to-Frequency Converter" Proceedings of 52nd IEEE International Midwest Symposium on Circuits and Systems, MWASCAS2009, 2-5 August 2009, Cancun, Mexico.
[96] Ma LY, Khan S, Nordin AN, Alam AZ, Omar J, Al-Khateeb KAS, Islam MR, Naji AW. "A Low-Cost First-Order Sigma-Delta Converter Design and Analysis" Proceedings of IEEE Instrumentation and Measurement Technology Conference, I2MTC2011, 10-12 May 2011, Hangzhou, China.
[97] Chun-Yueh H. "Design of a Voltammetry Potentiostat for Biochemical Sensors" *Analog Integrated Circuits and Signal Processing*, vol. 67, no. 3, pp. 375-381, 2011.
[98] Scully JR, Silverman DC, Kendig MW. Electrochemical Impedance: Analysis and Interpretation. ASTM Special Technical Publication, 1993.
[99] Barsoukov E, Macdonald JR. Impedance Spectroscopy: Theory, Experiment, and Applications. Wiley, 2005.
[100] Min M, Märtens O, Parve T. "Lock-In Measurement of Bio-Impedance Variations" *Journal of the International Measurement Confederation*, vol. 27, no. 1, pp. 21-28, 2000.
[101] Gabal M, Medrano N, Calvo B, Celma S, Martinez PA, Azcona C. "A Single Supply Analog Phase Sensitive Detection Amplifier for Embedded Applications" Proceedings of 25th Conference on Design of Circuits and Integrated Systems, DCIS2010, 17-19 November 2010, Lanzarote, Spain.
[102] Ferri G, De Laurentis P, D'Amico A, De Natalem C. "A Low-Voltage Integrated CMOS Analog Lock-In Amplifier Prototype for LAPS Applications" *Journal of Sensors and Actuators A: Physical*, vol. 92, no. 1-3, pp. 263-272, 2001.
[103] Azzolini C, Magnanini A, Tonelli M, Chiorboli G, Morandi C. "A CMOS Vector Lock-In Amplifier for Sensor Applications" *Microelectronics Journal*, vol. 41, no. 8, pp. 449–457, 2010.
[104] Veeravalli A, Sánchez-Sinencio E, Silva-Martínez J. "Transconductance Amplifier Structures with Very Small Transconductances: A Comparative Design Approach" *IEEE Journal of Solid-State Circuits*, vol. 37, no. 6, pp. 770-775, 2002.
[105] Arnaud A, Fiorelli R, Galup-Montoro C. "Nanowatt, Sub-nS OTAs, With Sub-10-mV Input Offset, Using Series-Parallel Current Mirrors" *IEEE Journal of Solid-State Circuits*, vol. 41, no. 9, pp. 2009-2018, 2006.
[106] Li G, Zhou M, He F, Lin L. "A Novel Algorithm Combining Oversampling and Digital Lock-In Amplifier of High Speed and Precision." *Review of Scientific Instruments*, vol. 82, no. 9, 2011. http://link.aip.org/link/doi/10.1063/1.3633943.html.
[107] Gaspara J, Chen SF, Gordillo A, Hepp M, Ferreyra P, Marqués C. "Digital Lock-In Amplifier: Study, Design and Development with a Digital Signal Processor" *Microprocessors and Microsystems: Embedded Hardware Design*, vol. 28, no. 4, pp. 157–162, 2004.
[108] Park S, Yoo J, Chang B, Ahn E. "Novel Instrumentation in Electrochemical Impedance Spectroscopy and a Full Description of an Electrochemical System" *Journal of Pure and Applied Chemistry*, vol. 78, no. 5, pp. 1069–1080, 2006.
[109] Hanson S, Seok M, Lin Y, Foo Z, Kim D, Lee Y, Liu N, Sylvester D, Blaauw D. "A Low-Voltage Processor for Sensing Applications With Picowatt Standby Mode" *IEEE Journal of Solid-State Circuits*, vol. 44, no. 4, pp. 1145-1155, 2009.
[110] Bo Z, Pant S, Nazhandali L, Hanson S, Olson J, Reeves A, Minuth M, Helfand R, Austin T, Sylvester D, Blaauw D. "Energy-Efficient Subthreshold Processor Design" *VLSI*, vol. 17, no. 8, pp. 1127-1137, 2009.
[111] Strong TD, Martin SM, Franklin RF, Brown RB. "Integrated Electrochemical Neurosensors" Proceedings of the IEEE International Symposium on Circuits and Systems ISCAS'06, pp.4110-4113, 21-24 May 2006.

Chapter 2

Design, test and validation of PoC device instrumentation.

This chapter presents in detail the design and validation of instrumentation electronics and sensing systems, as well as design protocols for truly PoC devices. The device has been designed to perform an Impedance Spectrometry (IS) technique in order to validate the whole device electronics as well as to characterize the sensing system and its interface accurately. It is focused on the development of such devices relying on straight forward standards for economic, low power consumption, versatility, safety and reliability. The first section presents different sensing topologies regarding the actual state-of-the-art. Subsequently, the following section presents the different designs of an electronic instrumentation prototype to address the different sensing typologies previously described. Finally, the back-end for system control and signal processing will be presented, and its very functionalities described.

2.1. Front-end electronics depending on the sensing topology.

As it has been stated in the introduction, there are different electrodes topologies for the sensing system implementation, depending on the system and applications requirements. Different configurations must be designed for the front-end electronics architecture depending on the sensing topology.

In case of a three electrodes sensing topology, the potentiostat is the key electronic component for these sensing configuration, which is the interface between the biological elements and the instrumentation electronics. The potentiostat can be implemented in different ways, especially in terms of electrodes current, which can be designed as an instrumentation amplifier current readout stage or a trans-impedance amplifier readout stage.

In figure 2.1.A it is depicted a simple potentiostat with an instrumentation amplifier readout stage. It consists on an operational amplifier (OA), which tracks the input signal (V_{IN}) on to electrodes, and an instrumentation amplifier that senses the current through the electrodes (1).

$$I_{CELL} = \frac{V_{IN}}{Z_{CELL}} \quad (1)$$

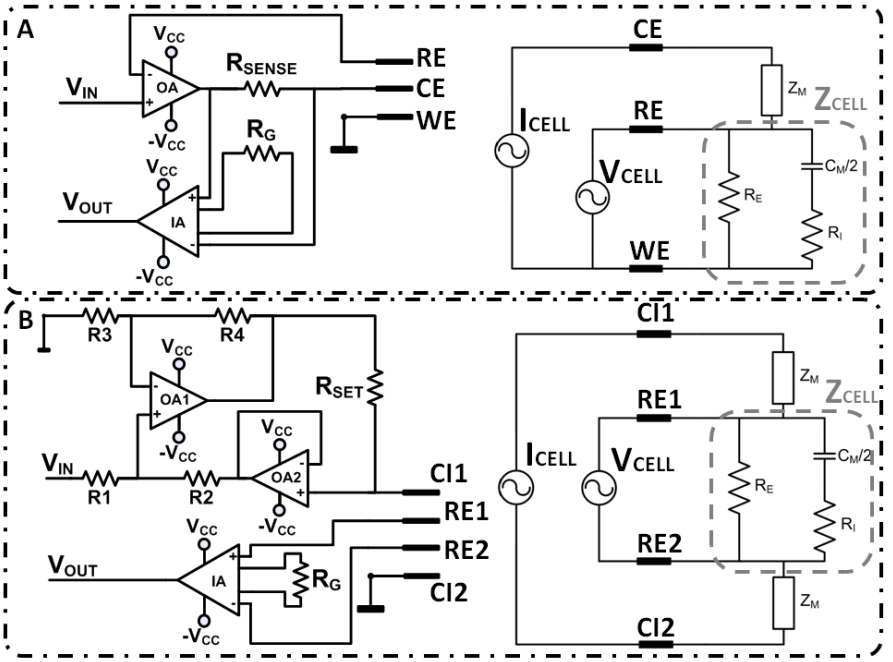

Figure 2.1: Cellular model, sensing system and front-end electronics. A: 3 electrodes approach. B: 4 electrodes approach.

The current measurement consists on the direct conversion of the current through the biological specie (I_{CELL}) into a voltage signal by means of a resistor on the counter electrode (R_{SENSE}), and an instrumentation amplifier that measures the voltage difference in the resistance. We assume that the current through resistor R_{SENSE}, is equal to the current through the electrodes, and it is considered that the voltage between reference (RE) and working electrodes (WE) is more steady due to the direct connection of working electrode to ground. Instrumentation amplifier transfer function is described by equation 2, where (V+ - V-) is the voltage difference on the amplifier's input voltage pins and G is the amplifier's gain which has been set to 1 to optimize the amplifier's Total Harmonic Distortion.

$$V_{OUT} = G \cdot (V_+ - V_-) = R_{SENSE} \cdot I_{CELL} \quad (2)$$

$$Z_{CELL} = R_{SENSE} \cdot \left(\frac{V_{IN}}{V_{OUT}}\right) \quad (3)$$

In case of a four electrode configuration, a voltage to current converter is implemented. In figure 2.1.b, the voltage to current converter is a modified Howland cell based on operational amplifiers (OA1 and OA2), which must guarantee a wide bandwidth and a high slew-rate while maintaining a low spectral noise and a low offset performance. The Howland cell uses R_{SET} and the input signal (V_{IN}) amplitude to define a stable current signal (I_{OUT}) at the output of the circuit regardless the connected load related to the biological specie.

$$I_{CELL} = \left(\frac{1}{R_{SET}}\right) V_{IN} \quad (4)$$

The differential voltage between ER1 and ER2 electrodes is acquired by means of the instrumentation amplifier (IA in figure 2.1). The measured voltage (signal V_{IS}) is related to the differential voltage between the reading electrodes (ER1 and ER2), G being the instrumentation amplifier gain.

$$V_{OUT} = G \cdot (V_{ER1} - V_{ER2}) = G \cdot (Z_{CELL} \cdot I_{CELL}) \quad (5)$$

$$Z_{CELL} = R_{SET} \cdot \left(\frac{V_{OUT}}{G \cdot V_{IN}}\right) \quad (6)$$

2.2. Back-end electronics for data Impedance Spectrometry post-processing and user interface.

The sensing topology and front-end electronics chosen for the implementation of the PoC device outputs a voltage signal related to the biological impedance, which is a complex magnitude. The purpose of the back-end electronics, independently of the front-end electronics and sensing system, is to supply the proper voltage signal to bias the instrumentation electronics, depending on the biological sample, sensor, and experimental set-up; process de output data, and present a proper user interface.

Two different approaches can be considered for the Impedance Spectrometry method; the Fast Fourier Transform (FFT) [1] method and the Frequency Response Analyzer (FRA) [2]. In the case of the FFT method, a pulse is applied, ideally a Dirac function, to the sample, and considering that it contains a wide frequency content, the response provides a full spectrum data of the analysed sample impedance. The front-end electronics response is analysed with a Fourier Transform algorithm in order to extract the frequency components of the impedance spectra [1]. This method is simple and fast solution for the IS, but there are several drawbacks in the implementation. It is very difficult to generate a fast step function and a very fast electronic instrumentation capable of driving this step on the electrodes and extracting the resulting signal, producing a distortion in the measurement. Moreover, the important impedance information is contained in a short period of time after the step is applied so, in addition to a very fast electronic instrumentation, a very fast analog-to-digital converter (ADC) with a high precision bit resolution is also required, resulting in a high speed hardware and heavy algorithm implementation device. Considering the PoC characteristics of the device, the FRA approach is a simpler and more efficient solution based on a Lock-in Amplifier (LIA). This method is much slower, as every frequency component is analysed separately, to obtain the Bode plot of the measured impedance. The FRA solution is a good solution in terms of the trade-off between speed and complexity, particularly if not too low frequencies need to be measured, as it actually happens on biological cellular samples [3-6]. Moreover, the implementation of a LIA is useful to reject undesirable harmonics and noise interferences [7-9], which are predominant on biological environments, such as bacteria culture, saline solution buffers, blood plasma, etc.

Taking into account these considerations, a first approach for Impedance Spectroscopy (IS) analysis, has been a complete back-end electronics designed to perform the Frequency Response Analyzer (FRA) solution based on a real-time mathematical processing Digital Lock-in Amplifier (DLIA) [1,2]. It has been embedded on a real-time platform sbRIO9632 (National Instruments, Austin, TX, USA), which has been used for fast software prototype development and versatility. To perform the FRA analysis based on a DLIA, the biasing signal of the front-end electronics (V_{IN}) is adopted as a reference signal to analyze the response of the sensing system (V_{OUT}). A sine and cosine signals are derived from V_{IN}, and by means of two multipliers and a filter stage the real and imaginary components of V_{OUT} are obtained. This measurement must be done for each frequency and front-end electronics output signal bode plot is composed of its magnitude $|V_{OUT}|$ and phase φ_{OUT}, where V_{REAL} and V_{IM} are the real part and imaginary part of the output signal.

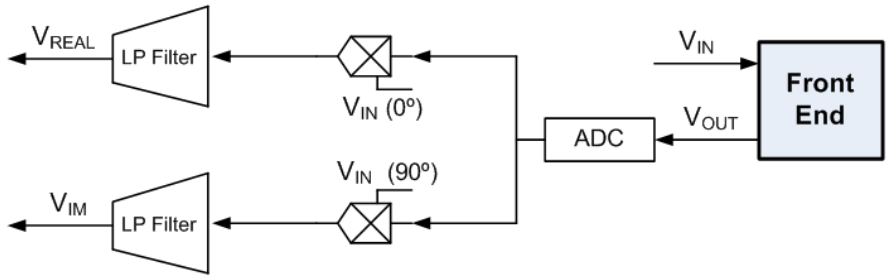

Figure 2.2: Lock-in software diagram. V_{OUT} is the input signal coming from the front-end electronics, V_{IN} is the reference signal and V_{REAL}, V_{IM} are the real and the imaginary part of the sensing system response.

$$|V_{OUT}| = \frac{\sqrt[4]{(V_{REAL}^2+V_{IM}^2)}}{|V_{IN}|} \quad (7)$$

$$\varphi_{OUT} = \arctan\left(\frac{V_{IM}}{V_{REAL}}\right) \quad (8)$$

$$V_{REAL} = \frac{1}{2}V_{OUT} \cdot V_{IN} \cdot \cos(\varphi_{OUT}) \quad (9)$$

$$V_{IM} = \frac{1}{2}V_{OUT} \cdot V_{IN} \cdot \sin(\varphi_{OUT}) \quad (10)$$

In figure 2.3 is depicted the back-end electronics architecture for the IA device. It is composed by the the sbRIO 9632 real time platform that allows us to develop different back-end functionalities, an oscillator (OSC in figure 2.3) that provides the desired biasing signal (V_{IN}) for the front-end electronics, and the signal conditioning for dual analog to digital conversion of both V_{IN} and V_{OUT} signals needed for the FRA approach. The oscillator is based on a signal generator AD9833 (Analog Devices, Norwood, MA, USA) that provides a stable voltage signal with a wide variable frequency range, 0 MHz to 12.5 MHz, which is controlled by an SPI communication protocol. The signal conditioning consists in a 12-bit dual, low power ADC (ADC in figure 2.3) ADC12D040 (Texas Instruments, Dallas, TX, USA), capable of converting both analog input signals at 40 MSPS simultaneously. The analogic inputs are converted from single ended to differential with a differential amplifier (DA in figure 2.3) AD8138 (Analog Devices, Norwood,

MA, USA). Finally, a software for system control, data processing and user interface is embedded on the real-time platform, which offers several functionalities.

First of all, it provides steady clock signals as needed that can be automatically real-time adjusted, allowing complete parallel signal acquisition for all the frequency ranges and more precise control of the oscillator, enabling the development of a signal generator automatic frequency sweep for an automated and complete FRA.

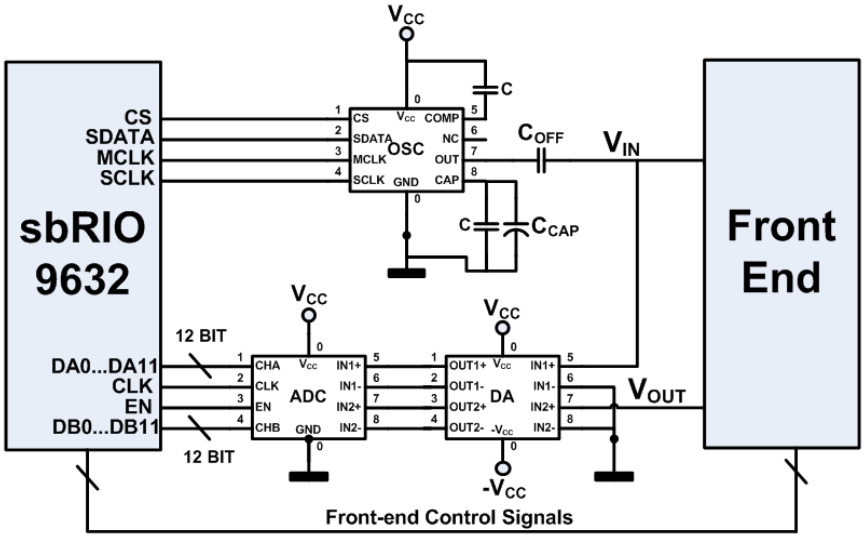

Figure 2.3: Back-end electronics based on a real time platform sbRIO9632.

Furthermore, some functionalities on the front-end electronics, like R_{SENSE} or R_{SET} multiplexed auto-scale, are basic features for a precise FRA method and can be implemented by means of additional digital control as it is depicted in figure 2.3 (Front-end Control Signals). The real-time platform allows the system configuration and data display, with a user-friendly front-end user panel using Labview (National Instruments, Austin, TX, USA), by means of an external computer connected to the platform with a standard Ethernet connection.

2.3. Back-end electronics test.

Digital lock-in (DLIA) is the key component of the whole back-end electronics system, and must be capable to extract information from high contaminated signals provided by the sensing system, usually electrical signals buried in noise.

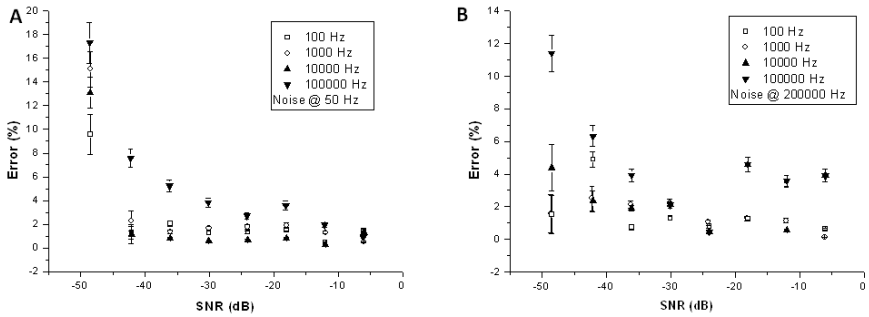

Figure 2.4: System response to a resistor IA. A: 50Hz low frequency noise signal. B: 200kHz high frequency noise signal.

To estimate the SNR of the DLIA; the parameter that quantifies the ability of the DLIA to extract information of highly contaminated signals; a signal of 10 mV amplitude had been injected at the back-end electronics input V_{OUT}, as the information signal to be processed, for different frequencies ranging from 10 Hz to 100 kHz. Different noise signals representing different noise amplitude values had been added to the information signal for two different frequencies, 50 Hz and 200 kHz. Figure 2.4 shows the error and standard deviation when recovering the information from the different noise contaminated 10mV electrical signal. Measurement errors are below 10% for SNR up to -45 dB, noise levels 200 times higher than the signal amplitude, which means a great environmental noise rejection for both lower (50Hz) and higher frequencies (200 kHz).

2.4. Combined front-end and back-end electronics test using passive components.

The complete PoC device combining both front-end instrumentation for sensing system driving, and back-end electronics for data processing and device control, have been tested using passive components (figure 2.5). The 3 electrode front-end architecture, based on a potentiostat, has been selected for these studies, as three electrodes commercial sensors will be used later. Moreover, the passive components used on the study are in the ranges of typical blood impedance values [4, 10-13], as the PoC device will be later applied to particular blood analysis.

The operational amplifier to bias the sensor is the AD825 (Analog Devices, Norwood, MA, USA), a dual supply high speed Junction Gate Field Effect Transistor (JFET) amplifier with low leakage current and low distortion capable of high output driving. The instrumentation amplifier, is the AD8421 (Analog Devices, Norwood, MA, USA), a dual supply high speed instrumentation amplifier with low noise and ultralow bias current. The amplifier's gain has been set to 1 in order to optimize the amplifier's THD. This stage has been designed with 4 different multiplexed sensing resistors (R_{SENSE}) taking into account the expected impedance values shown in the literature between 100Ω and 100kΩ [4, 10-13], as was subsequently confirmed in the system validation experiments. These resistors are automatically multiplexed with an auto-scale function controlled by the embedded software.

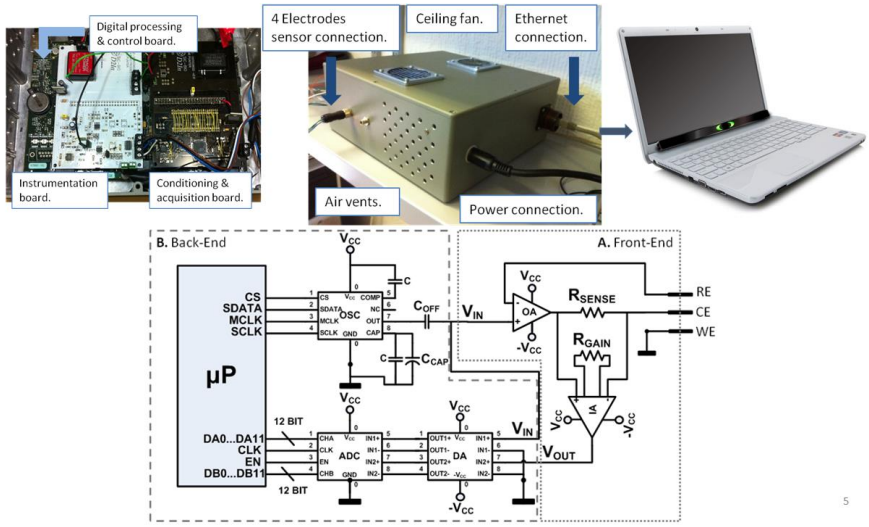

Figure 2.5: PoC IA device. Schematic view. A: Front-End Electronics. B: Back-End Electronics.

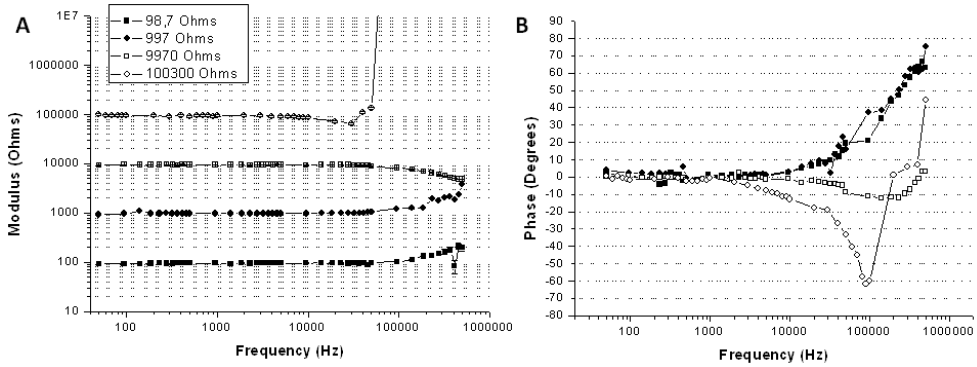

Figure 2.6: System response for a different resistor values. A: Impedance magnitude. B: Impedance phase.

First of all, we analyse a single resistor of different values as an electrode load in both impedance magnitude, figure 2.6.A, and phase, figure 2.6.B. Results demonstrate a great performance and reliability with an impedance magnitude standard deviation of 1%, maximum error of 12.3% in a 100kHz bandwidth for loads inferior to 10 kΩ. For loads greater than 10kΩ the system performance declines with an impedance magnitude standard deviation of 3% and maximum error of 14% and bandwidth less than 10 kHz. In terms of impedance phase, figure 2.6.B, the system performance shows a standard deviation of 3.7º in a 10 kHz bandwidth except for higher load values. The potentiostat topology causes a bandwidth limitation, as the instrumentation amplifier current readout system introduces an extra load (R_{SENSE}) on the main amplifier feedback loop, especially when the load increases.

A transimpedance amplifier topology, may solve this problem, as the current readout system, as well as the sensing resistor (R_{SENSE}) are placed outside the feedback loop of the main amplifier. However, the generation of a voltage reference on the electrodes is based on a virtual ground

provided by the transimpedance amplifier (TIA on figure 2.7.B), leading to possible errors on electrodes biasing.

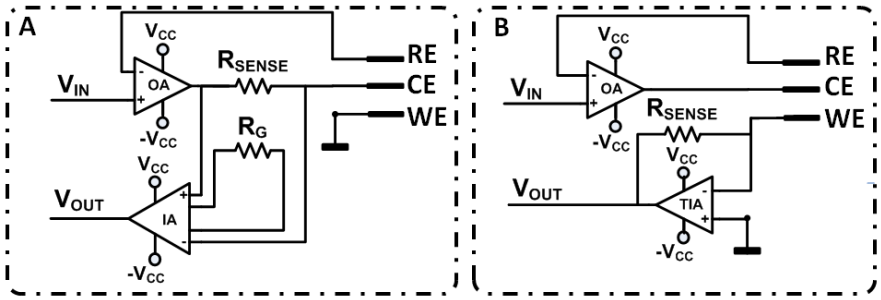

Figure 2.7: Potentiostat topologies. A: Instrumentation amplifier current readout topology. B: Transimpedance amplifier current readout topology.

Moreover, presence of stray capacitances creates a high frequency measurement deviation called "Hook Effect". It is caused by leaking currents on the instrumentation [14], producing an IA error that can be observed above the 100kHz. This error is frequency and load dependant, as leaking current paths through parasitic capacitances is more conductive at high frequencies and loads. Even though these limitations, it is not a major drawback to the PoC device application, because the typical impedance and working frequency values for HCT analysis found in literature are below the described limitations.

Finally, the whole PoC device has been tested adopting a parallel resistor and capacitor as a load configuration. In figure 2.8 it is shown the impedance magnitude and phase, compared with the theoretical load behavior. Three different resistor and capacitor values have been tested:

	Resistor Value.	Capacitor Value.
Test 1	597Ω	9.98nF
Test 2	994Ω	3.86nF
Test 3	9940Ω	9.98nF

Table 2.1: Parallel resistor and capacitor values.

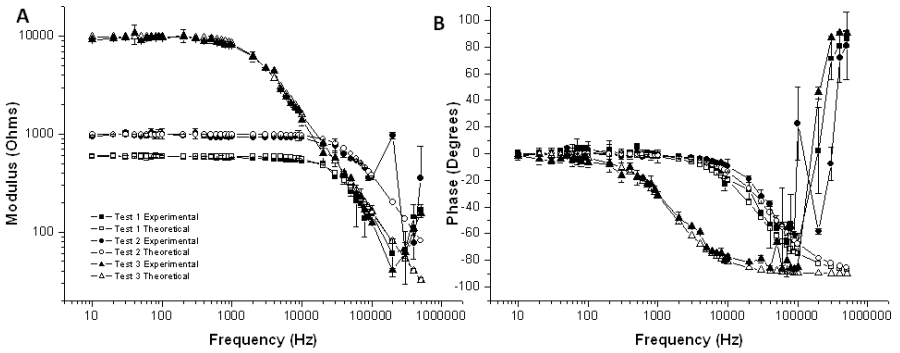

Figure 2.8: System response for a different parallel resistor and capacitor values. A: Impedance magnitude. B: Impedance phase.

Results shows a great performance with an impedance magnitude standard deviation of 1.5%, a mean error of 3.5% with a defined 100 kHz bandwidth.

2.5. Combined front-end and back-end electronics test using a ferrocyanide/ferricyanide solution.

Finally, the whole PoC device have been validated for different sensors topology and compared the device measurements with a commercial equipment SP-150 (BioLogic Science Instruments, Grenoble, France) using a ferrocyanide/ferricyanide solution, a commonly used substance on sensor and equipment characterization [15-17].

Two different sensors have been used: a disposable commercial three screen printed electrode C223AT (DropSens, Llaneras, Spain); and a standard three electrodes laboratory sensor composed by three different probes. Figure 2.9.A and 2.9.B shows the impedance magnitude and phase comparison between the developed device and the commercial equipment SP-150, using the same disposable three screen-printed electrodes (C223AT sensor).

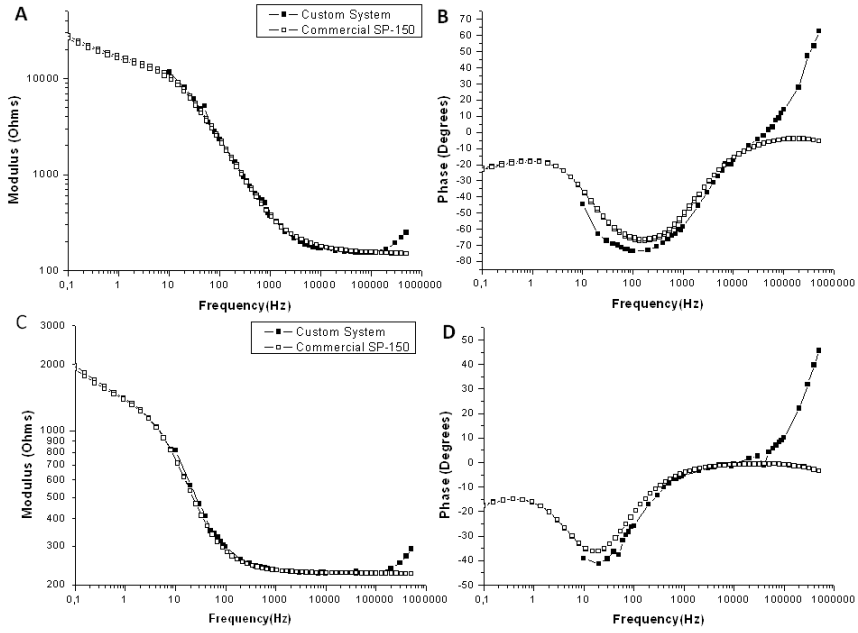

Figure 2.9: Comparative results with commercial equipment SP-150. A: Commercial sensor C223AT impedance magnitude. B: Commercial sensor C223AT impedance phase. C: Standard laboratory probe impedance magnitude. D: Standard laboratory probe impedance phase.

Figure 2.9.C and 2.9.D shows the impedance magnitude and phase comparison between the developed device and the commercial equipment SP-150 using the same standard laboratory three probe electrodes sensor for all the experiments. The system has a proper IA response in the

frequency operating range from 10 to 100 kHz, working within the ranges described before, with an impedance magnitude standard deviation of 1% and a maximum error of 1.5%. In terms of phase, maximum error is under 12.1º and the electrodes electrical pole positions represented are at accurate position. A final system characteristics summary is reported in Table 2.2:

	Conditions (T = 25ºC)	Value
Power Consumption		24 VDC 0.35 A
Applied Voltage Signal Amplitude		10 Vrms
Frequency Working Range	Load < 10 kΩ	< 100 kHz
	Load > 10 kΩ	< 10 kHz
Magnitude Maximum Error	In Frequency Working Range	< 12.3%
Phase Maximum Error	In Frequency Working Range	< 12.1º
Lock-In Average SNR Rejected		-43 dB

Table 2.2: System characteristics summary.

2.6. Conclusions.

In this chapter it is described a first-approach device based on a full-custom electronics composed by a front-end sensing interface instrumentation, and a back-end electronics for IA composed by a digital lock-in. The different electronics have been developed and evaluated for portable, low cost, PoC analysis device. The apparatus is validated by means of several IA, using different passive electrical elements and well-known state-of-the-art chemical compounds used for equipment characterization, in the typical whole blood impedance and frequency detection ranges.

Experimental results show a reliable performance for biomedical PoC experiences, resulting in a cheap, fast and portable equipment electronics for biochemical and cell concentration analysis relying on IAs.

Next steps will be focused on the study of different whole blood samples, system capability for HCT detection and other cellular species.

2.7. References.

[1] Park S, Yoo J, Chang B, Ahn E. "Novel Instrumentation in Electrochemical Impedance Spectroscopy and a Full Description of an Electrochemical System" *Journal of Pure and Applied Chemistry*, vol. 78, no. 5, pp. 1069–1080, 2006.

[2] Li G, Zhou M, He F, Lin L. "A Novel Algorithm Combining Oversampling and Digital Lock-In Amplifier of High Speed and Precision." *Review of Scientific Instruments*, vol. 82, no. 9, 2011. http://link.aip.org/link/doi/10.1063/1.3633943.html.G.A.

[3] Pop GA, et al. "Blood electrical impedance closely matches whole blood viscosity as parameter of hemorheology and inflammation" *Appl. Rheol.*, vol. 13, no. 6, pp. 305–312, 2003.

[4] Pradhan R, Mitra A, Das S. "Impedimetric characterization of human blood using three-electrode based ECIS devices" *J. Electr. Bioimpedance*, vol. 3, no. 1, pp. 12–19, Jul. 2012.

[5] Cheng MS, Ho JS, Lau SH, Chow VTK, Toh CS. "Impedimetric microbial sensor for real-time monitoring of phage infection of Escherichia coli." *Biosens. Bioelectron.*, vol. 47, pp. 340–344, 2013.

[6] Yang L. "Electrical impedance spectroscopy for detection of bacterial cells in suspensions using interdigitated microelectrodes" *Talanta*, vol. 74, pp. 1621–1629, 2008.

[7] Min M, Märtens O, Parve T. "Lock-in measurement of bio-impedance variations," *Journal of the International Measurement Confederation*, vol. 27, no. 1, pp. 21–28, 2000.

[8] Gabal M, Medrano N, Calvo B, Celma S, Martinez PA, Azcona C. "A Single Supply Analog Phase Sensitive Detection Amplifier for Embedded Applications" Proceedings of 25th Conference on Design of Circuits and Integrated Systems, DCIS2010, 17-19 November 2010, Lanzarote, Spain.

[9] Azzolini C, Magnanini A, Tonelli M, Chiorboli G, Morandi C. "A CMOS Vector Lock-In Amplifier for Sensor Applications" *Microelectronics Journal*, vol. 41, no. 8, pp. 449–457, 2010.

[10] Hernández F, Guerrero C, Bernal J. "Determinación de las propiedades eléctricas en tejido sangíneo" *Ciencia UANL*, vol. 8, pp. 7-13, 2011.

[11] Li N, Brahmendra A, Veloso AJ, Prashar A, Cheng XR, Hung VWS, Guyard C, Terebiznik M, Kerman K. "Disposable Immunochips for the Detection of Legionella pneumophila Using Electrochemical Impedance Spectroscopy." *Anal. Chem.*, no. 84, pp. 3485–3488, Mar. 2012.

[12] Xu M, Luo X, Davis JJ. "The label free picomolar detection of insulin in blood serum," *Biosensors and Bioelectronics*, vol. 39, pp. 21–25, January 2013.

[13] Ribaut C, et al. "Electrochemical impedance spectroscopy to study physiological changes affecting the red blood cell after invasion by malaria parasites," *Biosensors and Bioelectrincs*, vol. 24, no. 8, pp. 2721–2725, April 2009.

[14] Buendia R, Seoane F, Gil-Pita R. "A Novel Approach for Removing the Hook Effect Artefact from Electrical Bioimpedance Spectroscopy Measurements," Journal of Physics, Conference on Electrical Bioimpedance, ICEBI2010, 4-8 April 2010, Gainesville, Florida.

[15] Taliene VR, Ruzgas T, Razumas V, Kulys J. "Chronoamperometric and cyclic voltammetric study of carbon paste electrodes using ferricyanide and ferrocenemonocarboxylic acid," *Journal of Electroanalytical Chemistry*, vol. 372, pp. 85-89, 1994.

[16] Beriet C, Pletcher D. "A microelectrode study of the mechanism and kinetics of the ferro/ferricyanide couple in aqueous media: The influence of the electrolyte and its concentration," *Journal of Electroanalytical Chemistry*, vol. 361, pp. 93–101, 1993.

[17] Petrovic S. "Cyclic voltammetry of hexachloroiridate(IV): an alternative to the electrochemical study of the ferricyanide ion," *The Chemical Educator Journal*, vol. 5 (5), pp. 231–235, 2000.

References.

Chapter 3

A study of IA for cellular detection. HCT detection approach.

This chapter describes the experimental analysis performed in order to validate the IA for detection, quantification and monitoring of diluted cells suspensions. A compact, portable and user-friendly solution, for early detection of anaemia through whole blood HCT monitoring is studied, as a first approach for a PoC device relying on cellular detection. The experiments were carried out with a three electrode sensor and a potentiostat instrumentation front-end with a digital lock-in post-processing and Ethernet data transmission back-end. The element under analysis was HCT from different whole blood samples.

The purpose of this study and its relevancy are framed on the following points:

1. Once the system has been validated for different passive electrical elements and well-known chemical compounds, study the feasibility of detecting **a cellular specie such as HCT**.

2. Study the **influence in the IA technique and the whole device performance of different sensors sensors** using laboratory modified blood samples.

3. Study the impact of the **buffer of the cellular cell suspensions on the IA technique** using laboratory modified blood samples.

4. Validate the system using non-modified whole blood samples and **calibrate the device for whole blood HCT screening**.

5. Define a protocol for **HCT detection.**

3.1. HCT screening. Focus on Anaemia disease and PoC screening devices.

The World Health Organization (WHO) defines anaemia as the stage at which the amount of haemoglobin in blood drops below a certain WHO threshold for specified population groups, being considered a worldwide problem associated with many factors [1]. According to the WHO, 1.62 billion people, which correspond to 24.8% of the global population, are affected by anaemia [2]. Measurement of Hb concentration is considered the most reliable anaemia indicator and it is widely utilized in national demographic health surveys and by national governments surveying populations [1]. Also, evaluation of the Hb concentration in possible blood donors is a required condition in most countries to prevent blood collection from a donor with significant anaemia being, generally, the only laboratory control test performed before donation [3]. Blood donation

is the only source of support to patients who require blood transfusion but, on the other hand, frequent donations may lead to iron deficiency in blood donors, especially females [4]. Hb is an iron-containing protein responsible for transporting oxygen in the blood and it is the main component of red blood cells (RBCs). HCT is the proportion of blood volume occupied by RBCs and is determined by cell number and size, so HCT numbers below a certain reference range may indicate anaemia or abnormal cell development [5, 6].

New non-invasive methods are being studied and developed for Hb screening but have been demonstrated to have lower precision and sensitivity level [3]. These different factors are drivers for the development of PoC anaemia equipment providing an easy to use, reliable and sensitive test with a short response time in a portable device relying on 50 µL blood sample, which can be capillary collected by standard medical procedures [7], providing reduced disposition decision time [8] and replacing current venipuncture based laboratory test and improving patient satisfaction [9]. Moreover, low volume blood samples analysis represents a means of avoiding inducing anaemia or making it worse, as phlebotomy is reported to induce anaemia in hospitalized patients [10].

Currently, commercial bench top and non-specific huge laboratory devices are utilized for EIS based applications, involving complex experimental setups and significant expenditure of time. Furthermore, whole blood PoC specific sensing systems also rely on complex microfluidic devices [11], [12] entailing a low environmental integration-level to develop autonomous PoC applications [13].

In the present study, we evaluated the feasibility of HCT detection, as well as the sensing system and cells buffer influence on the analysis, applied as an early anaemia detection PoC device.

3.2. Biological Electrical Impedance applied to HCT, electrodes and IA.

As it has been stated before, the electrical model of a diluted cellular specie can be very complex; however, it can be defined as very simple one, for device development purposes, as a biological impedance (Z_{CELL}) defined by simple Ohm's law [14], being the current response (I_{CELL}) to applying an alternating voltage signal (V_{CELL}) to a biological material by its corresponding sensing system (1).

$$Z_{CELL} = \frac{V_{CELL}}{C_{CELL})} \quad (1)$$

Although a two electrodes configuration is the basic sensor topology; defined by the working electrode (WE), where V_{CELL} is applied, and the auxiliary electrode (AE), which tracks V_{CELL} and supplies $I_{CELL,}$ this topology entails some problematic behaviour related to V_{CELL} signal distortion due to the AE polarization effects. In order to avoid this effect, the current is supplied using an extra, third, electrode (figure 3.1.a). A three electrode sensor is also a commonly used configuration on blood characterization [15], [16] and is defined as: a) the working electrode (WE), where V_{CELL} is applied, b) the reference electrode (RE), which tracks V_{CELL} and c) the counter or auxiliary electrode (CE), which supplies I_{CELL}.

In figure 3.1.a is depicted the typical electrical model for dilute cell suspensions in a three electrode sensor, which can be described as an electrical components network [17]. I_{CELL} can flow through an external cellular path (R_E resistance) or across the cell membrane ($R_M \| C_M$) and go through the intra-cellular medium (R_I resistance). Since R_M resistance is nearly negligible [18] the electrical model of the whole system can be extremely simplified as noted before.

Considering this electrical cell model, the close relation between HCT and impedance at low frequencies (up to 100 kHz) has been confirmed [19]. At this frequency range the response current I_{CELL} flow outside the RBCs across R_E impedance. HCT increment makes the current flow path larger between the reference and working electrodes, becoming an increment on Z_{CELL} impedance due to an increment of R_E impedance (figure 3.1.b). This phenomenon occurs at the 10 Hz to 100 kHz frequency range [20]. As the IA depends on the quantity of RBCs in the sample, we used the IA of whole blood plasma as a reference value, so as to be able to determine the HCT according to the impedance increment to that reference value. This relationship between impedance and RBCs will be studied in section III.

IA measurements were performed at alternating biasing voltage of 10 mVrms, in order to prevent undesired effects like electroporation or irreversible electrical breakdown, which will damage blood cells membranes [21], so unlike actual clinical equipments for blood analysis, whole blood samples are not destroyed on the measurement process.

3.3. Sensing system

To develop a PoC device, the sensing system must be a low-cost disposable commercial sensor, it must be easy to manipulate by clinical laboratory technicians using standard clinical laboratory tools. Additionally, the sensing system must work with 50 µL blood samples, the standard volume for a whole blood drop and easily collected by capillarity [7], and must be made of gold, an acknowledged bio-compatible material. Different commercial sensors have been evaluated, such as AC1 sensor (BVT Technologies, Brno, Czech Republic) or the G-AUG sensor series (Bio-Logic SAS, Claix, France), and the commercial sensor that best meets the defined specifications is the C223AT and 220AT (Dropsens, Llaneras, Spain). These sensors have screen-printed electrodes based on gold and are specifically designed to work with 50 µl samples (figure 3.1.c). Since they have two different working areas; 1.6mm diameter for C223AT and 4mm diameter for 220AT, both of them will be studied to evaluate how much impact have the electrode size on the IA, and the ability of the device ability to work with different sized electrodes. To ensure that the 50 µl blood samples remains stable on the electrodes during the experimental procedure, the electrodes are covered with a polydimethylsiloxane (PDMS) reservoir placed on top of the sensor to retain the sample (figure 3.1.c). PDMS is a widely used polymer in industry and is an inert and non-toxic material, resulting in a good bio-compatible material for our sensing system. The PDMS polymer is a result of mixing Sylgard® silicone base and curing agent in a 10:1 ratio by weight. The mixture is degassed under vacuum to remove air bubbles, poured into a petri dish and remains at room temperature until cured. Afterwards, the PDMS polymer was peeled off and cut into small

squares (about 1 cm^2). A through-hole was punched in each PDMS square to get the biocompatible reservoir. The clean PDMS surface is sticky enough to adhere to the sensor surface by itself; therefore, it is important to keep the surface clean by soaking and washing the polymer in ethanol and/or removing any fibre with adhesive tape. The device has a plug-and-play sensor system inside a Faraday cage and it is connected to the electronics with a custom made three wire coaxial insulated cable in order to provide an easy to use set-up and reliable performance. Blood samples were put on top of the sensor with an automatic pipette (Labopette Manual 10 - 100 µL; Hirschmann Laborgeräte, Eberstadt, Germany).

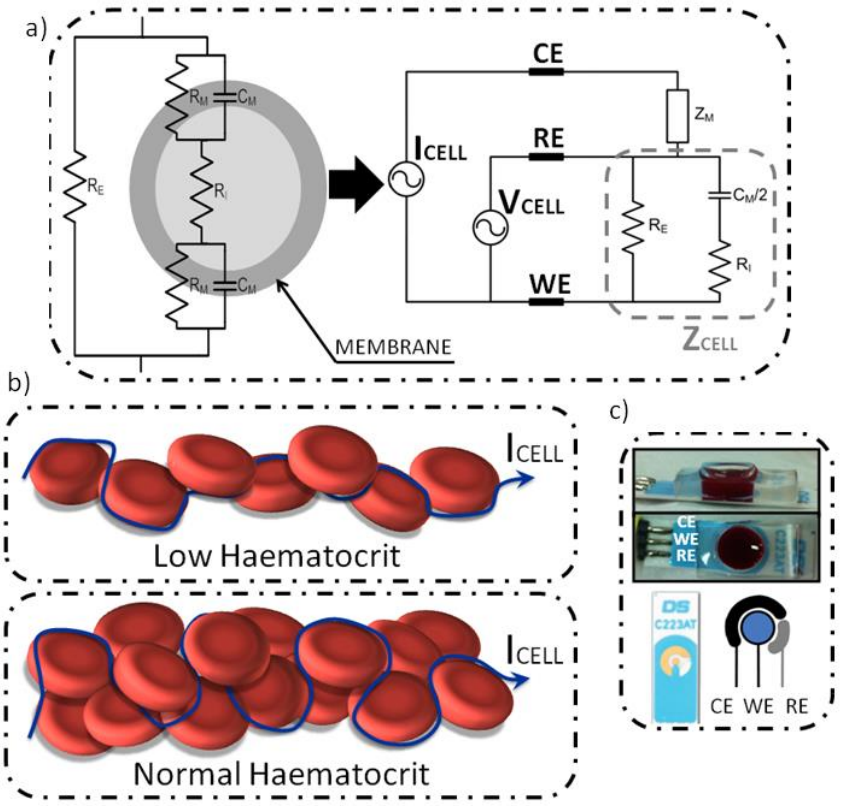

Figure 3.1: Sensor and RBC electrical model. a) Red Blood Cell electrical model. Three electrodes model for RBC sample. b) Current flow path through different blood samples with different HCT. c) Sensing system: commercial disposable sensor with PDMS reservoir wit with a 50 µL whole blood drop sample.

3.4. PoC device Front-end and Back-end electronics description.

A full custom electronic circuit was specifically designed to carry out the FRA approach with a 3 electrode sensor topology. The device architecture has two modules: a) an Electrodes Biasing and Instrumentation module (EBI in figure 3.2.a) which provides a frequency configurable voltage signal and an instrumentation amplifier based potentiostat; and b) a Signal Digitalization and Post-

Processing module (SDPP in figure 3.2.a), which adapts both signals needed for the FRA analysis, Reference Signal (V_{RS} in figure 3.2.a) and Impedance Signal (V_{IS} in figure 3.2.a), from a bi-polar single-ended to an uni-polar differential signal to be processed by a 12-bit parallel output analog-to-digital converter. Finally, a digital lock-in amplifier (DLIA) carries out the FRA approach that provides the Bode diagrams for both impedance magnitude and phase.

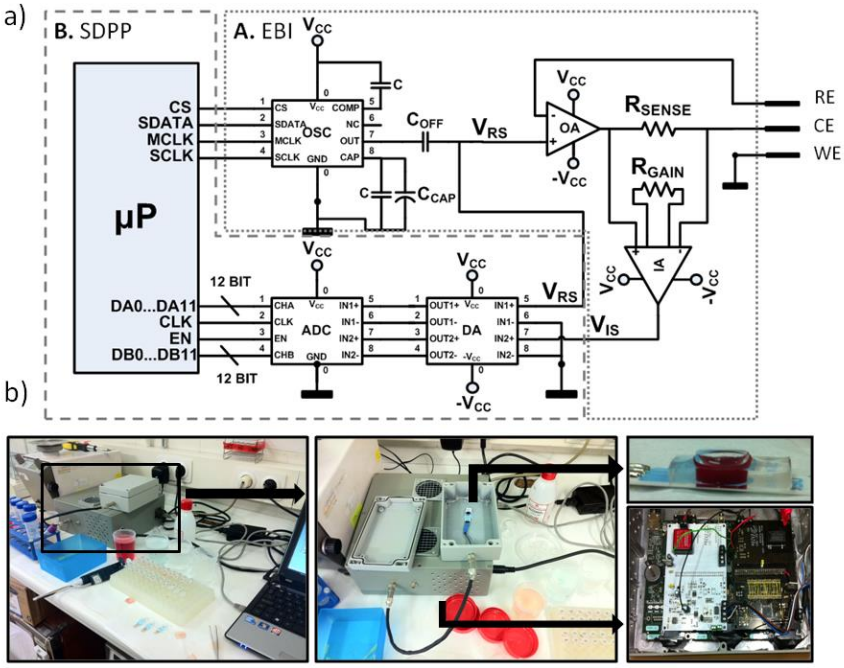

Figure 3.2: PoC device prototype and set-up. (a) Prototype electronics schematic, A: Electrodes Biasing Module; B: Signal Digitalization and Post-Processing. (b) Device prototype electronics: Two custom PCB and a sbRIO 9632 board (National Instruments) on a faraday cage. Experimental set-up: Disposable sensor; Electronic instrumentation; External computer with control and data displaying software.

The first module (EBI), Electrodes Biasing and Instrumentation, is based on a signal generator, OSC in figure 3.2.a (AD9833; Analog Devices, Norwood, USA), and an instrumentation amplifier based potentiostat. The signal generator provides a stable voltage signal with a wide variable frequency range, 0 MHz to 12.5 MHz, which is controlled by an SPI communication protocol. The instrumentation is based on a potentiostat with an instrumentation amplifier current readout stage [22], which consists of an operational amplifier to bias the sensor and an instrumentation amplifier as an electrode current readout. The operational amplifier, OA in figure 3.2.a (AD825; Analog Devices, Norwood, USA), is a dual supply high speed JFET amplifier with low leakage current and low distortion capable of high output driving, which tracks the signal on to the electrodes. The instrumentation amplifier, IA in figure 3.2.a (AD8421; Analog Devices, Norwood, USA), is a dual supply high speed instrumentation amplifier with low noise and ultralow bias current. The instrumentation amplifier converts the current through the electrodes into a voltage signal (V_{IS}) by means of a sensing resistor on the counter electrode (R_{SENSE} in figure 3.2.a) between

the amplifier's non-inverting and inverting inputs. The amplifier's gain has been set to 1 in order to optimize the amplifier's THD.

This stage has been designed with 4 different multiplexed sensing resistors (R_{SENSE}) taking into account the expected impedance values shown in the literature between 100Ω and 100kΩ [15, 16, 23-25] as was subsequently confirmed in the system validation experiments. These resistors are automatically multiplexed with an auto-scale function that will be explained below.

The second module (SDPP), Signal Digitalization and Post-Processing, consists in a 12-bit dual, low power ADC, ADC in figure 3.2.a (ADC12D040; Texas Instruments, Dallas, USA), capable of converting both analogue input signals at 40 MSPS simultaneously. 12-bit resolution does not represent a significant drawback in the final system resolution, as V_{RS} is scaled to the full range ADC analogue input and the system provides a real time gain auto scale for the R_{SENSE} gain factor. The analogue inputs are converted from single ended to differential with a differential amplifier, DA in figure 3.2.a (AD8138; Analog Devices, Norwood, USA), with a high slew rate with low distortion and input noise. Finally, a DLIA based on real-time mathematical processing is embedded on a 400 MHz microprocessor from a real-time platform, sbRIO 9632 in figure 3.2.a (sbRIO9632; National Instruments, Austin, USA). Final impedance bode plot is composed of sample impedance magnitude $|Z_{CELL}|$ (6) and impedance phase φ_{CELL}, where V_{REAL} and V_{IM} stand for real part and imaginary part of the measured impedance. In addition, real-time platform sbRIO9632 has a FPGA (Xilinx Spartan-3; Xilinx, San Jose, USA), which allows us to provide steady clock signals as needed on the instrumentation that can be automatically real-time adjusted, allowing complete parallel signal acquisition for all the frequency ranges. Furthermore, embedded hardware control, like R_{SENSE} multiplexed auto-scale and signal generator automatic frequency sweep can be developed. This real-time embedded hardware control represents the basic features for an automated and complete FRA approach.

The real-time platform allows the system configuration and data display, with a user-friendly front-end user panel, by means of an external computer connected to the platform with a standard Ethernet connection. The user panel, depicted in figure 3.3, has two different configurations that can be selected from a menu (A label). Each option allows the system to perform different experiments when the start button (D label) key is pressed. The first one is a complete EIS that provides the Bode diagrams for both impedance magnitude (F label) and phase (G label), where the user could choose the number of points per decade (C label). EIS frequency ranges are fixed to the defined bandwidth on previous section and R_{SENSE} values are auto-scaled. The second is an automatic HCT analyzer, where the blood sample HCT is displayed with four significant numbers (B label).

Moreover, the front panel has several displays for user control and error monitoring. The two signals needed for the FRA analysis, Reference Signal (V_{RS} in figure 3.2.a) and Impedance Signal (V_{IS} in figure 3.2.a), are real-time monitored and shown on a graph (E label). Errors in electronics connection with the remote computer are displayed (H label) and generic Labview errors are explained (J label).

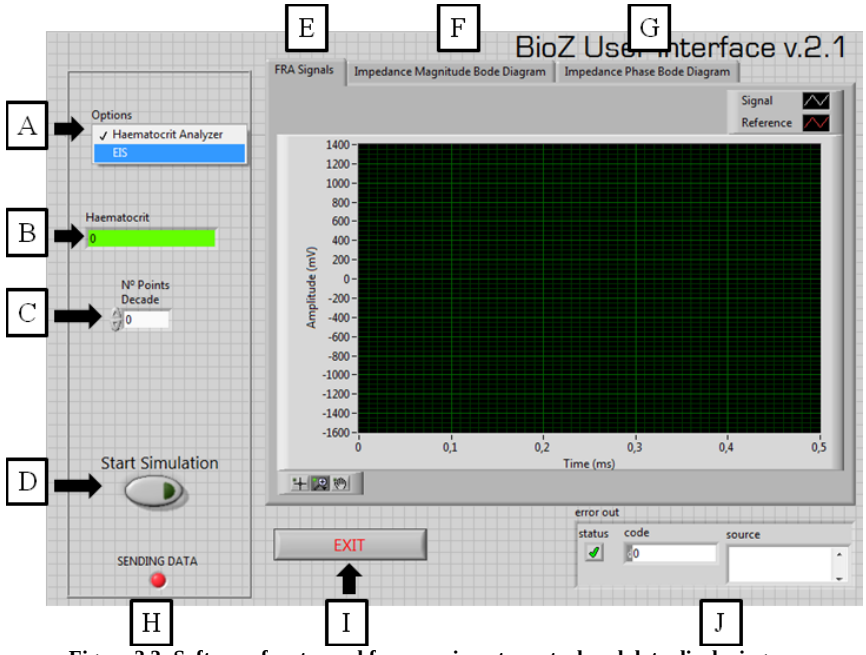

Figure 3.3: Software front-panel for experiments control and data displaying.

3.5. HCT screening studies. First study.

3.5.1. Objectives

This first test will validate the system capabilities to detect a diluted cellular specie, in particular HCT. Moreover, the influence of different sensors and the impact of cellular buffer in the IA technique and the whole device performance will be studied. A complete impedance spectrometry experiment have been performed in order to get a full impedance spectrum analysis of 4 different blood samples, means to represent different degrees of anaemia. These samples came from the manipulation and dilution of a single whole blood sample extracted from a healthy donor. The 4 blood samples have the following HCT: 14.8%, 19.6%, 30.1% and 40.4%.

3.5.2. Blood samples

Blood samples were obtained in 4-mL tubes containing ethylenediaminetetraacetic acid (EDTA 7.2 mg; BD Vacutainer®; BD, Madrid, Spain) from a healthy donor. The whole blood sample was centrifuged (Jouan CR412; DJBlabcare, Buckinghamshire, England) at 2200 rpm for 15 min in order to separate blood plasma from red blood cells (RBC). To obtain 4 different samples with different anaemia degree (Table I), whole blood samples where diluted in different volumes of a saline solution, as a well-known clinical biocompatible material, using an automatic pipette

(Labopette Manual 10 - 100 µL; Hirschmann Laborgeräte, Eberstadt, Germany). Blood plasma was used as a reference value in order to correlate the results and study the influence of different buffers for the RBCs on the IA. We performed a complete blood count (CBC) of the resulting blood samples with a haematology analyzer (ABX Micros 60; Horiba, Madrid, Spain), which reported the haemoglobin and HCT results as g/dL and percentage (%), respectively. This analyzer used electrical impedance technology to perform the CBC. With this methodology, whole blood is aspirated into the system, the sample stream is split, one portion is used for haemoglobinometry and one portion is used for RBC counting and size. Haemoglobinometry is based on RBC lysis and measurement of haemoglobin concentration by absorbance of spectrophotometry. RBC counting and size analyses are performed by passing the RBCs singly through a small direct current. The temporary increase in impedance caused by the passage of the cell provides information about RBC number and RBC volume. HCT is calculated from the measured haemoglobin, RBC number and RBC volume [25].

Therefore, the obtained HCT, haemoglobin and anaemia diagnose for the different blood samples was (Table I): Sample 1 had a 14.8% HCT with 5.7 g/dL haemoglobin, critical anaemia; sample 2 had a 19.6% HCT with 6.8 g/dL haemoglobin, severe anaemia; sample 3 had a 30.1% HCT with 10.5 g/dL haemoglobin, moderate anaemia; and sample 4, had a 40.4% HCT with 14.0 g/dL haemoglobin, absence of anaemia.

	Haematocrit (%)	Haemoglobin (g/dL)	Anaemia diagnose
Sample 1	14.8	5.7	Critical
Sample 2	19.6	6.8	Severe
Sample 3	30.1	10.5	Moderate
Sample 4	40.4	14.0	Absence

Table 3.1. Blood samples description.

3.5.3. First study results

The designed device was validated through EIS experiences with the specified sensors described in section II.B for each sample described in section II.C. Experimental set-up is depicted in figure 3.2.b. All the measurements have been performed at clinical laboratory room temperature. First of all, we measured a complete impedance spectrum with both sensors. As an example, in figure 3.4 is depicted the obtained impedance magnitude (figure 3.4.a) and phase (figure 3.4.b) bode diagram for whole blood plasma, sample 2 (19.6%) and sample 4 (40.4%) blood samples for both sensors.

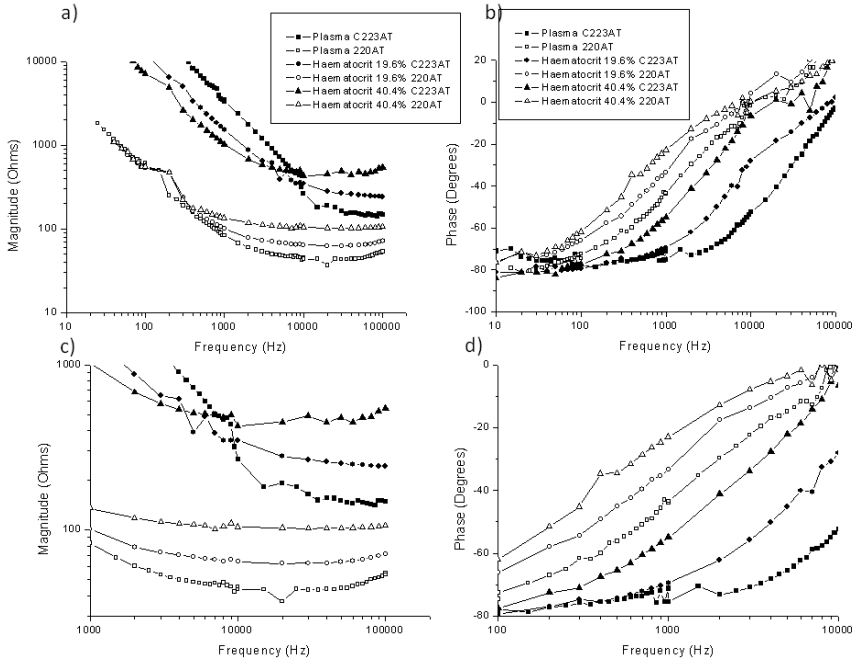

Figure 3.4: Whole blood impedance magnitude and phase comparison between sensor C223AT and sensor 220AT. a) Impedance magnitude over full frequency spectra. b) Impedance phase over full frequency spectra. c) Impedance magnitude over frequency working range. d) I Impedance phase over frequency working range.

We observed that, both in impedance magnitude and phase, there exists a clear difference between impedance results for different samples in specific frequency ranges. Furthermore, these differences must be related to whole blood HCT, as the response current I_{CELL} flow outside the RBCs. When HCT is higher, the current flow path becomes larger between the reference and working electrodes, which represents an increment on measured Z_{CELL} impedance. Therefore, measured impedance differences must be defined as impedance increments related to HCT increments. However, this phenomenon is not present on the whole frequency range defined previously, 10 Hz to 100 kHz, but on a more specific one depending on the sensor. So, we have defined working ranges, depending on the sensor and the correlation between IA and HCT, as shown in figure 3.4.

In terms of impedance magnitude (figure 3.4.c) the frequency working range is on the 10 kHz to 100 kHz range for sensor C223AT and on the 1 kHz to 100 kHz range for sensor 220AT; for impedance phase (figure 5.d) it is on the 1 kHz to 10 kHz range for sensor C223AT and on the 100 Hz to 10 kHz range for sensor 220AT. It is interesting to be able to determine impedance magnitude and phase differences for different HCT samples on a wide frequency working range. It gives flexibility and data redundancy to the system as long as it is not single frequency response dependant, which makes simple statistical data analysis techniques, like linear fit, feasible, turning out to be a more robust and reliable device.

Hence, once we have assumed that measured impedance increments, on the defined frequency working range, are related to blood samples HCT increment, we must determine the system ability for HCT detection, resolution and sensitivity. For a simpler analysis, we have defined this relation to be approached by a linear dependence between measured impedance and blood samples HCT. Linear fit technique has been used to study the relation between impedance data collected with the EIS experiments and blood samples. With this study we want to determine the system HCT detection resolution and sensitivity, on the defined frequency range, in both terms of impedance magnitude (|Z|) and phase (Δφ).

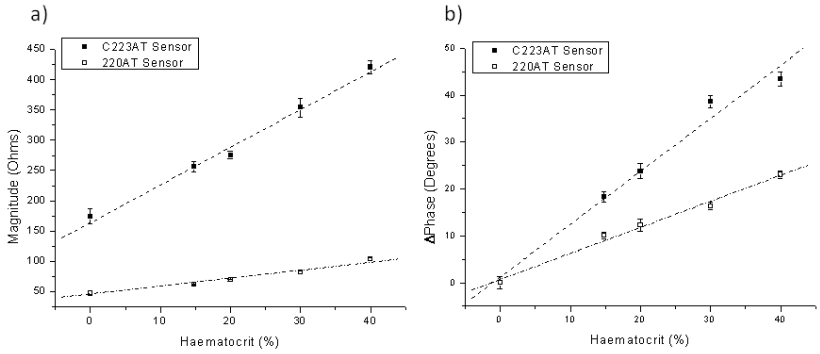

Figure 3.5: Whole blood impedance magnitude and phase comparison between sensor C223AT and sensor 220AT. a) Impedance magnitude as a function of HCT. b) Impedance phase as a function of HCT. Error bars represent the standard deviations across ten repeats.

The measured impedance data, collected with the IS experiments, and the blood samples HCT have been analysed with a linear regression, as we have assumed a linear dependence between them, and highlight the system detection abilities in terms of resolution and sensitivity. First of all, we have calculated the mean value and standard deviation of |Z| for every blood and blood plasma sample for all the measurements on the frequency working range. The defined frequency working range for impedance magnitude (|Z|) is on the 10 kHz to 100 kHz range for sensor C223AT and on the 1 kHz to 100 kHz range for sensor 220AT. The mean value and standard deviation of |Z| are shown on Table III for the C223AT sensor and Table IV for the 220AT sensor. 220AT sensor provides a wide working frequency range with low frequency dependence, as relative standard deviation percentage is smaller than sensor C223AT, which frequency working range must be more bounded as standard deviation percentages are relatively high.

Finally, the relation of |Z| mean value and blood samples HCT had been analysed as a linear dependence approach (10), where the slope (β_Z) defines the sensitivity, in terms of ohms per HCT percentage (Ω/%), meanwhile the HCT detection resolution (%) is the relation between the linear fit standard deviation and β_Z. In figure 3.5.a the |Z| for the different HCT percentages is depicted.

$$|Z_{CELL}|(\Omega) = \alpha_Z + \beta_Z \cdot HCT(\%) \quad (2)$$

220AT sensor has a 1.36 Ω/% sensitivity and a 3.21 % accuracy error with a linear correlation of 0.984; meanwhile the C223AT sensor gives us a 6.19 Ω/% sensitivity and a 1.66 % accuracy error with a linear correlation of 0.995. In summary, 220AT sensor, with a working electrode diameter of 4mm, gives a wider working frequency range. On the other hand, C223AT sensor, with a

working electrode diameter of 1.6mm, provides better sensitivity, accuracy and correlation. Both sensors provide low frequency dependence as the standard deviation is below 5%. High correlation values, for both sensors, support the evidence that impedance magnitude measurement have a strong dependence on HCT.

Sample	Haematocrit (%)	Mean (Ω)	Standard Deviation (Ω)
Plasma	0	173.88	12.45 (7.2%)
Sample 1	14.8	246.43	8.66 (3.5%)
Sample 2	19.6	275.55	6.01 (2.2%)
Sample 3	30.1	353.71	16.01 (4.5%)
Sample 4	40.4	420.33	10.74 (2.5%)

Table 3.2. |Z| mean value and standard deviation. sensor C223AT

Sample	Haematocrit (%)	Mean (Ω)	Standard Deviation (Ω)
Plasma	0	48.03	3.70 (7.7%)
Sample 1	14.8	61.93	1.15 (1.9%)
Sample 2	19.6	69.05	1.35 (2.0%)
Sample 3	30.1	82.39	1.94 (2.4%)
Sample 4	40.4	103.59	2.40 (2%)

Table 3.3. |Z| mean value and standard deviation. sensor 220AT

The same study for impedance magnitude had been done for impedance phase. As impedance phase values have great frequency dependence through the frequency working range, the impedance phase had been normalized. It had been defined as an increment (Δφ) between blood samples and blood plasma measurements to remove the frequency dependence from the data. We have calculated the mean value and standard deviation of Δφ for every blood and blood plasma sample for all the measurements on the frequency working range. The defined frequency working range for impedance phase increment (Δφ) is on the 1 kHz to 10 kHz range for sensor C223AT and on the 100 Hz to 10 kHz range for sensor 220AT.

The mean value and standard deviation of Δφ are shown on Table V for the C223AT sensor and Table VI for the 220AT sensor. In this case, C223AT sensor provides impedance phase measurements with less frequency dependence, although 220AT sensor has a wide frequency working range. The relation of Δφ mean value and blood samples HCT had been analysed as a linear dependence approach (11), where the slope (β_φ) defines the sensitivity, in terms of degrees per HCT percentage (º/%), meanwhile the resolution is the relation between the linear fit standard deviation and β_φ. In figure 3.5 the Δφ for the different HCT values is depicted.

$$\Delta\varphi(\text{deg}) = \alpha_\varphi + \beta_\varphi \cdot HCT(\%) \quad (3)$$

220AT sensor has a 0.55 º/% sensitivity and a 1.87 % accuracy error with a linear correlation of 0.994, while C223AT sensor has a 1.12 º/% sensitivity and a 2.59 % accuracy error with a linear correlation of 0.989.

So, 220AT sensor, with a working electrode diameter of 4mm, gives a wider working frequency range with better accuracy and correlation. On the other hand, C223AT sensor, with a working electrode diameter of 1.6mm, provides better sensitivity. Despite high correlation values for both sensors, impedance phase measurements are more frequency dependant than impedance magnitude measurements, as the standard deviation is much higher, regardless of being normalized to a blood plasma measurement. Even so, it must be considered as a reliable measurement parameter to develop a post-processing system with redundant data to provide more flexibility, effectiveness and robustness to the system.

3.5.4. First study conclusions

The device has been proved to exhibit reliable, robust and effective results using label-free disposable commercial sensors using 50µL whole blood samples. Blood samples, collected from a single healthy donor, were used to demonstrate the IA technique feasibility to perform an easy, fast and sensitive HCT study using two different label-free commercial sensors with low voltage biasing. Although only 4 whole blood samples, collected from 4 different donors with different degrees of anaemia, were analysed, it must be considered as an initial approach data of low population analysis, but with promising results for a significant HCT difference between whole blood samples. The device has a linearity of 1.07 and an accuracy error of 1.83% with a correlation of 0.988. Coefficient of variation is below 5%, with a worst case resolution of 1.22%. Deformation in linearity is caused by deviation in donor 1 whole blood sample HCT measurement and the absence of a higher sample population.

As it was supposed, differences have been found on the impedance results when different sensors, with different sizes, are used. Sensor C223AT, with a working electrode diameter of 1.6mm, shows better sensitivity and accuracy, meanwhile sensor 220AT, with a working electrode diameter of 4mm, provides a wider frequency range and less IA dependence on frequency. As it proved to deliver better sensitivity and accuracy, sensor C223AT will be used on the following studies.

Finally, the use of saline solution as a buffer for the RBCs dilution has no influence on the measurement, as it proved when compared with the blood plasma. This fact indicates that, as the state-of-the-art indicates, the current flow (I_{CELL}) path across the blood sample is through the cells membrane. This is a very important fact, as the different elements found on blood plasma; such as proteins, glucose, etc., can be very different in quantity from one patient to another, and therefore, distorting the measurements performed.

3.6. HCT screening studies. Second study.

3.6.1. Objectives

To validate the anaemia early detection system based on HCT screening, 48 different blood samples have been studied. These samples were randomly obtained from hospitalized patients in Hospital Clínic. First of all, whole blood samples were distributed in two different groups, the first one (group I), has been used for system calibration; and the second one (group II) has been used for system validation. With the group I whole blood samples, we measured a complete impedance spectrum to define a frequency working range, where measured impedance values are well differentiated and related to the blood sample HCT. Afterwards, we defined a protocol for instant impedance detection on the defined working range, and we studied the relation between IAs and whole blood samples HCT. With these studies we have found the detection resolution and system sensitivity and we have calibrated the system for an instantaneous HCT detection. Finally, the HCT detection algorithm, based on previous calibration, has been implemented and validated through the group II whole blood samples randomly obtained. The different studies will be done with sensor C223AT as it delivers better sensitivity and accuracy.

3.6.2. Blood Samples

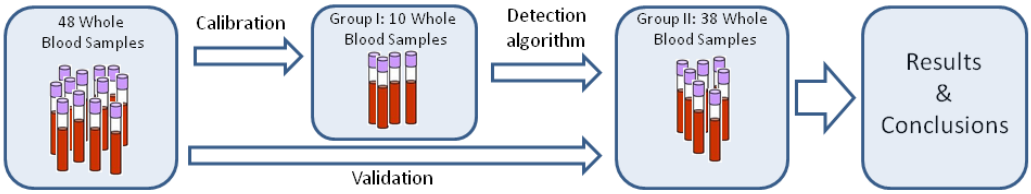

Figure 3.6: hole blood samples groups and experimental procedure.

We used 48 whole blood samples obtained from hospitalized patients in Hospital Clínic. However, personal data of the patients was not available to the investigators and samples were randomly selected. Whole blood samples were obtained in 4-mL tubes containing ethylenediaminetetraacetic acid (EDTA 7.2 mg; BD Vacutainer®; BD, Madrid, Spain). We performed a complete blood count (CBC) of the blood samples with a haematology analyser (Advia 2120, Siemens AG, Madrid, Spain), which reported the haemoglobin and HCT results as g/dL and percentage (%), respectively. These 48 whole blood samples were distributed in two different groups (figure 3.6). The first one (group I), composed of 10 samples, was used to calibrate the system, whereas the second one (group II), composed of the other randomly collected 38 whole blood samples, was used to validate the whole system performance. The samples in group I have been selected to cover the entire possible HCT range present in human blood. Therefore, the obtained HCT (HCT(%)), haemoglobin (Hb (g/dL)) and anaemia diagnosis for the different blood samples in group I was as shown in table 3.4:

Sample	HCT (%)	Hb (g/dL)	Anaemia diagnose
Sample 1	21	6.6	Critical
Sample 2	23	7.4	Critical
Sample 3	25	8.2	Severe
Sample 4	27	9.0	Severe
Sample 5	29	9.2	Severe
Sample 6	33	10.1	Moderate
Sample 7	36	11.9	Very Moderate
Sample 8	40	12.7	Absence
Sample 9	45	14.5	Absence
Sample 10	51	16.1	Absence

Table 3.4. Group I Whole blood samples for system calibration.

Obtained HCT and haemoglobin for the remaining 38 whole blood samples defined as a validation group (group II) are shown in table 3.5:

Sample	HCT (%)	Hb (g/dL)	Sample	HCT (%)	Hb (g/dL)
1	25	8,2	20	34	11
2	26	8,3	21	34	11,1
3	26	8,5	22	34	11,4
4	27	8,9	23	35	11,5
5	28	9	24	35	11,5
6	28	9	25	36	11,6
7	28	9,1	26	39	12,5
8	29	9,2	27	40	12,7
9	29	9,2	28	41	12,7
10	29	9,3	29	42	13,3
11	30	9,4	30	42	13,3
12	31	9,5	31	43	14,5
13	31	9,6	32	44	14,5
14	31	10,1	33	45	14,5
15	32	10,4	34	45	14,5
16	32	10,5	35	46	14,8
17	33	10,5	36	46	15,5
18	33	10,5	37	47	15,9
19	34	10,8	38	49	16,1

Table 3.5. Group II Whole blood samples for system validation.

3.6.3. System calibration: Impedance spectrometry HCT analysis

The designed device was validated through impedance spectrometry experiences for each whole blood sample described. Experimental set-up is depicted in figure 3.2.b. All the measurements have been performed at clinical laboratory room temperature.

First of all, we measured a complete impedance spectrum for the group I whole blood samples. In figure 3.7 shows the obtained impedance magnitude (figure 3.7.a) and phase (figure 3.7.b) bode

diagram for whole blood samples. We observed that, both in impedance magnitude and phase, there exists a difference between impedance results for different samples in specific frequency ranges, as the previously study, with manipulated samples, already highlighted, as well as the differences for different buffers has no influence in it.

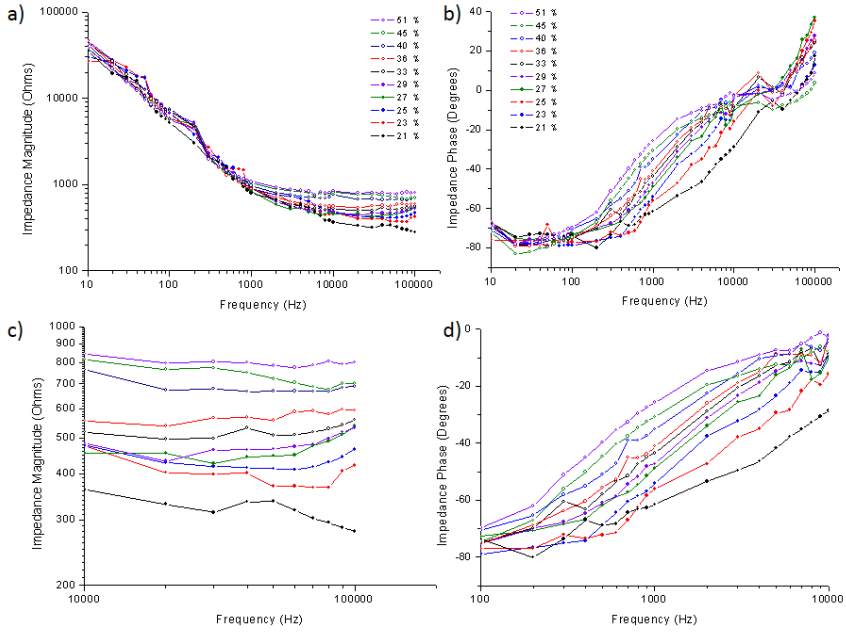

Figure 3.7: Whole blood impedance magnitude and phase measurement for group I whole blood samples. a) Impedance magnitude and b) impedance phase over full frequency spectra. c) Impedance magnitude and d) impedance phase over frequency working range.

Therefore, measured impedance differences must be defined as impedance increments related to HCT increments. However, this phenomenon is not present on the whole frequency range defined on the literature, 10 Hz to 100 kHz, but on a more specific one. So, we have defined working ranges depending on the correlation between IA and HCT. In terms of impedance magnitude (figure 3.7.c) the frequency working range is in the 10 kHz to 100 kHz range and for impedance phase (figure 3.7.d) it is in the 1 kHz to 10 kHz range. Despite being working with whole blood samples, the frequency ranges are invariably the same found on the previous study.

It is interesting to be able to determine impedance magnitude and phase differences for different HCT samples on a wide frequency working range. It gives flexibility and data redundancy to the system as long as it is not single frequency response dependant, which makes simple statistical data analysis techniques, such as linear fit, feasible, turning out to be a more robust and reliable device.

Hence, once we have assumed that measured impedance increments, on the defined frequency working range, are related to blood samples HCT increment, we must determine the system's capacity for HCT detection, resolution and sensitivity.

3.6.4. System calibration: automatic HCT detection.

In this section, linear fit technique has been used to study the relation between impedance data collected and whole blood samples HCT, as we have assumed a linear dependence between them. With this study we want to determine the system HCT detection accuracy, sensitivity and coefficient of variation. We have implemented a software, embedded on the microprocessor from the real-time platform sbRIO 9632, to instantly measure impedance on the previously defined frequency working range. As a first approach to the detection system, only the impedance magnitude measurements will be evaluated. Although impedance phase measurements may be related to HCT, as it is shown in figure 3.7.d, these values, unlike the impedance magnitude, are strongly frequency dependant, so more complex data analysis is needed, resulting in a more complex and slower system. To calibrate the system, the impedance magnitude measurements of the whole blood samples from group I will be compared with the HCT values (HCT (%)). 5 repetitions have been done for each whole blood sample using different sensors and sub-samples from the original sample. Table 3.6 shows the impedance magnitude values, the standard deviation and coefficient of variation for each whole blood sample.

HCT (%)	Mean Impedance Magnitude (Ω)	Standard Deviation (Ω)	Coefficient of Variation (%)
21	343,08	11,13	3,24
23	382,24	21,82	5,71
25	396,77	10,76	2,71
27	421,08	7,11	1,69
29	453,37	12,97	2,86
33	511,42	15,26	2,98
36	536,82	18,09	3,37
40	566,05	16,94	2,99
45	606,49	27,28	4,50
51	645,99	16,05	2,49

Table 3.6. System calibration measurements

$$|Z_{CELL}|(\Omega) = \alpha_Z + \beta_Z \cdot HCT(\%) \quad (4)$$

The relation of impedance magnitude (|Z|) mean value and whole blood samples HCT had been analysed as a linear dependence approach (4), where the slope (β_Z) defines the sensitivity, in terms of ohms per HCT percentage (Ω/%). Meanwhile the HCT detection accuracy (%) is the relation between the linear fit standard deviation and β_Z. Precision can be evaluated with the coefficient of variation: that is, the standard deviation divided by the mean value of the 5 repetitions measurements. In figure 3.8 the impedance magnitude for the different HCT (HCT (%)) is depicted.

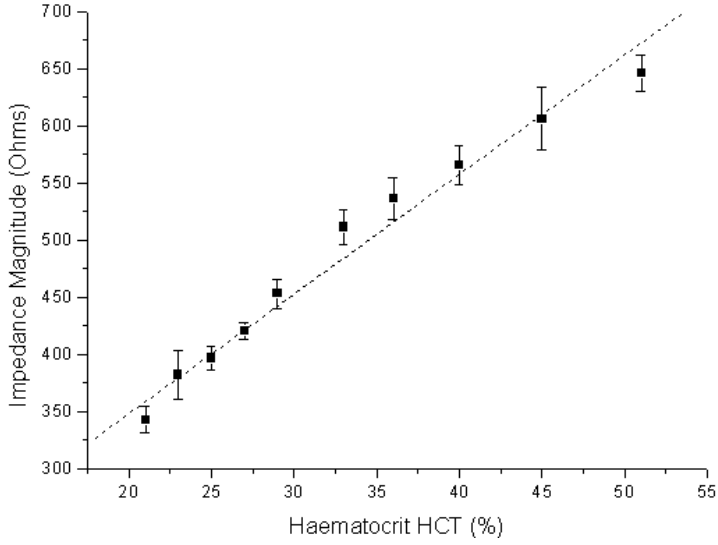

Figure 3.8: Measured impedance magnitude as a function of whole blood samples Haematocrit (HCT (%)). Calibration curve.

The HCT detection system has a 10.46 Ω/% sensitivity and a 1.13 % accuracy error with a linear correlation of 0.987. Precision can be evaluated with the coefficient of variation (CV), which is the standard deviation (SD) divided by the mean value of the 5 repetitions. Acceptable values in quality control procedures in clinical haematology measurements show a coefficient of variation less than 5% [30]

3.6.5. Whole blood HCT detection

In previous sections, we have analysed the HCT (HCT (%)) relation with IA, in both magnitude and phase, defining the frequency working range. An embedded software has been developed to instantly measure impedance magnitude on the defined working range, and we have studied the sensitivity, accuracy and coefficient of variation of the device. With the data from these previous studies, we have implemented an automatic real-time anaemia detection device that provides instantaneous HCT (HCT (%)) measurement. An HCT (%) evaluation algorithm, based on impedance magnitude measurement, has been embedded on the microprocessor from the real-time platform sbRIO 9632. The accuracy, precision and repeatability of the detection device will be evaluated using 38 whole blood samples from the validation group, described in section II.C (group II), which were randomly collected. 5 repetitions have been done for each whole blood sample, using different sensors and sub-samples, to evaluate the precision of the device. The predicted HCT from the detection device (DHCT (%) in Table IV) is the mean value of the 5 measurements performed with each whole blood sample, and it was compared with the HCT measurement (CHCT (%) in Table IV) of the complete blood count (CBC) performed with the haematology analyser (Advia 2120, Siemens AG, Madrid, Spain). HCT measurement and its standard deviation (SD) results are depicted in table 3.7.

CHCT (%)	DHCT (%)	SD (%)	CHCT (%)	DHCT (%)	SD (%)
35	33,82	1,47	34	33,05	1,19
36	32,96	1,28	33	30,08	1,11
33	33,93	1,15	34	35,50	0,62
39	38,71	0,83	42	40,21	1,39
34	35,61	1,64	45	41,14	1,77
49	48,26	1,04	43	40,28	0,94
45	44,40	0,80	31	29,61	1,42
28	27,57	0,77	29	27,90	0,44
32	31,61	1,85	29	28,26	0,41
46	46,72	1,78	41	38,41	1,17
29	28,14	1,27	26	25,42	0,40
31	33,59	1,30	46	42,90	1,21
28	30,33	1,46	42	39,84	1,30
42	39,29	0,84	26	26,39	0,40
28	28,40	1,17	28	26,57	0,54
32	32,48	0,92	47	41,17	1,35
30	32,26	1,04	35	34,35	1,05
34	32,50	1,52	25	24,06	0,30
44	40,44	1,64	31	34,06	1,18

Table 3.7. Device validation with group II whole blood samples.

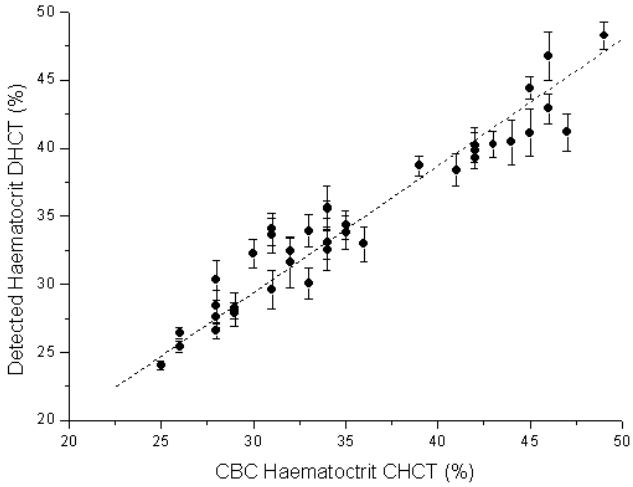

Figure 3.9: Whole blood HCT measurement (DHCT (%)) compared with HCT measurements obtained with a CBC performed by a haematology analyzer (CHCT (%)). Error bars represent the standard deviations across five repetitions.

In figure 3.9 a comparison between detected HCT and HCT calculated with a clinical haematology analyser is shown. The proposed device presented great accuracy in detecting HCT, with a linearity of 0.93 and an accuracy error of 1.75% with a correlation of 0.98. The coefficient of variation has a mean value of 3.27% for the whole samples, without any particular case above 5%. In quality control procedures in clinical haematology measurements, coefficient of variation of less than 5% for a test is considered acceptable [19].

As a first approach, which only contemplates impedance magnitude to a HCT analysis algorithm for anaemia detection, as previously stated, it would be interesting to develop a more complex algorithm involving both impedance magnitude and phase on a wide frequency working range, for more precision and better performance on detection.

3.6.6. Second study conclusions.

As a first approach for cellular detection and monitoring, a PoC device for anaemia detection, based on HCT screening, has been designed, fabricated and tested for instantaneous anaemia detection based on custom instrumentation electronics, IA technique and disposable sensing systems. The system performs real time instrumentation control, data acquisition and results display by means of an external computer and user-friendly software. The device has been proved to exhibit reliable, robust and effective results using label-free disposable commercial sensors using 50µL whole blood samples. Furthermore, unlike actual clinical equipment for blood analysis, whole blood samples are not destroyed in the measurement process.

48 whole blood samples, randomly collected from hospitalized patients in Hospital Clínic, were used to demonstrate the feasibility of the IA technique to perform an easy, fast and sensitive HCT study using disposable label-free commercial sensors with low voltage biasing. A first approach for a HCT evaluation algorithm for anaemia detection, based on whole blood IA, is presented and validated. The system has been evaluated through comparison with complete blood count (CBC) using a clinical haematology analyser (Advia 2120, Siemens AG, Madrid, Spain). The anaemia detection device has a linearity of 0.93 and an accuracy error of 1.75% with a correlation of 0.98. Coefficient of variation is below 5%, with a worst case resolution of 1.63%. Considering this as a first approach algorithm for anaemia detection, the development of a more complex algorithm and a more accurate clinical assay with higher testing population will lead to more accurate results to assess the device performance. Additionally, as the system is based on straightforward standards on instrumentation electronics and sensing, it represents an economic, portable, safe and reliable system of anaemia detection with a high degree of integration for the clinical environment.

Further development must be considered for future stages: real-time platform sbRIO9632 (National Instruments) has been used for fast software prototype development and versatility, but it is a major drawback in terms of power consumption, size and price. It must be replaced by a low-cost microcontroller for instrumentation control, data acquisition and post-processing.

Commercial devices for PoC anaemia detection, based on microfluidics devices, such as AnaemiaCheck (Express Diagnostics, Blue Earth, Minnesota), or on photometry haemoglobin detection, such as STAT-Site (Stanbio Laboratory, Boerne, Texas) or HemoPoint H2 (Alere, Waltham, Massachusetts), are much slower presenting similar detection performance results (table 3.8). Moreover, getting digitalised information provides the possibility of remote care, monitoring and implementation of other clinical actuators. Other commercial PoC devices, like the i-STAT analyzer (Abbott Point of Care, Princeton, New Jersey), despite providing lab-quality results for

patient PoC testing, turn out to be less specific involving a much more expensive and slower device.

In summary, the feasibility of cellular monitoring by means of IA is proved, and an instantaneous PoC device for anaemia detection has been designed, developed and tested. The device presents instantaneous, reliable, sensitive and robust HCT detection, relying on low-cost straightforward electronic equipment and sensing systems.

Device	Test time (sec.)	Range (HCT and Hb)	SD (%)	CV (%)
Proposed Device	< 2	HCT: 0% – 100%	1.17	3.27
Anaemia Check	900	HCT: 12% – 42%	0.74	4.10
STAT-Site	120	Hb: 5.6 g/dL – 20.6 g/dL	---	4.20
Hemo Point H2	60	Hb: 0 g/dL – 25.6 g/dL HCT: 36% – 54%	---	1.5

Table 3.8. Commercial devices comparison

3.7. References.

[1] Northrop-Clewes CA, Thurnham DI. "Biomarkers for the differentiation of anaemia and their clinical usefulness" *J. Blood Medicine*, vol. 4, pp. 11–22, Mar. 2013.

[2] de Benoist B, McLean E, Egli I, Cogswell ME. Worldwide prevalence of anaemia 1993–2005: WHO global database on anaemia, Geneva, Switzerland, 2008.

[3] Belardinelli A, Benni M, Tazzari PL, Pagliari P. "Noninvasive methods for haemoglobin screening in prospective blood donrs." *Vox Sang*. vol.105, pp. 116–120, Apr. 2013.

[4] Pinto D, Barjas-Castro ML, Nascimento S, Falconi MA, Zulli R, Castro V. "The new noninvasive occlusion spectroscopy hemoglobin measurement method: a reliable and easy anaemia screening test for blood donors." *Transfusion*. vol. 53, pp. 766–769, Apr. 2013.

[5] World Health Organization, "Iron Deficiency Anaemia: Assessment, Prevention and Control; A Guide for Programme Managers." Geneva, Switzerland, 2001.

[6] Thompson RB, A Short Textbook of Haematology, fourth ed., Pitman Medical Publishing Co., Kent, 1975.

[7] Ernst DJ, Balance LO, Calam RR, McCall R, Szamosi DI, Tyndall L. Procedures and Devices for the Collection of Diagnostic Capillary Blood Specimens; Approved Standard, sixth ed. CLSI, Wayne, Pennsylvania, 2008.

[8] Asha SD, et al. "Impact from PoC devices on emergency department patient processing times compared with central laboratory testing of blood samples: a randomised controlled trial and cost-effectiveness analysis" *J. Emerg. Med*., vol. 0, pp. 1–6, Jun. 2013.

[9] Jones CDH, et al. "Primary care clinicians' attitudes towards PoC blood testing: a systematic review of qualitative studies" *BMC Family Practice*. vol. 14, pp. 117, Aug. 2013.

[10] Thavendiranathan P, Bagai A, Ebidia A, Detsky AS, Choudhry NK. "Do blood tests cause anaemia in hospitalized patients? The effect of diagnostic phlebotomy on hemoglobin and HCT levels" *J Gen Intern Med*., vol. 20, pp. 520–524, Jun. 2005.

[11] Zheng Y, Shojaei-Baghini E, Azad A, Wang C, Sun Y. "High-throughput biophysical measurement of human red blood cells." *Lab. Chip*. vol. 12, pp. 2560–2567, Jul. 2012.

[12] Ramaswamy B, Yeh TT, Zheng SY. "Microfluidic device and system for PoC blood coagulation measurement based on electrical impedance sensing" *Sensors Actuators B Chem*., vol. 180, pp. 21–27, Apr. 2013.

[13] Esquivel JP, Colomer-Farrarons J, Castellarnau M, Salleras M, del Campo FJ, Samitier J, Miribel-Català P, Sabaté N. "Fuel cell-powered microfluidic platform for LoC applications: Integration into an autonomous amperometric sensing device." *Lab. Chip*. vol. 12, pp. 4232–4235, Nov. 2012.

[14] Patterson R. "Bioelectric Impedance Measurements3" in The Biomedical Engineering Handbook, 2nd Edition, J.D. Bronzino (Ed.), CRC Press, Boca Raton, 2000, pp. 734–773.

[15] Hernández F, Guerrero C, Bernal J. "Determinación de las propiedades eléctricas en tejido sangíneo" *Ciencia UANL*, vol. 8, pp. 7-13, 2011.

[16] Pradhan R, Mitra A, Das S. "Impedimetric characterization of human blood using three-electrode based ECIS devices" *J. Electr. Bioimpedance*, vol. 3, no. 1, pp. 12–19, Jul. 2012.

[17] Beriet C, Pletcher D. "A microelectrode study of the mechanism and kinetics of the ferro/ferricyanide couple in aqueous media: The influence of the electrolyte and its concentration," *Journal of Electroanalytical Chemistry*, vol. 361, pp. 93–101, 1993.

[18] Grosse C, Schwan HP. "Cellular membrane potentials induced by alternating fields" *Biophys. J.*, vol. 63, pp. 1632–1642, 1992.

[19] Hill DW, Thompson FD. "The effect of HCT on the resistivity of human blood at 37ºC and 100 kHz." *J. Medical and Biological Engineering*. vol. 13, pp. 182–186, Mar. 1975.

[20] Pop GAM, Bisschops LL, Iliev B, Struijk PC, van der Hoeven JG, Hoedemaekers CW. "On-line blood viscosity monitoring in vivo with a central venous catheter, using electrical impedance technique." *Biosensors and Bioelectronics*. vol. 41, pp. 595–601, Oct. 2012.

[21] Chernomordik LV, Chizmadzhev YA. "Electrical breakdown of lipid bilayer membranes." In Electroporation and Electrofusion in Cell Biology E. Neumann, A.E. Sowers, and C.A. Jordan (Eds.), SpringerLink, 1989, pp. 83–95.

[22] Brokaw AP, Timko MP. "An improved monolithic instrumentation amplifier." *J. Solid-State Circuits*. vol. 10, no. 6, pp. 417-423.

[23] Li N, Brahmendra A, Veloso AJ, Prashar A, Cheng XR, Hung VWS, Guyard C, Terebiznik M, Kerman K. "Disposable Immunochips for the Detection of Legionella pneumophila Using Electrochemical Impedance Spectroscopy." *Anal. Chem.*, no. 84, pp. 3485–3488, Mar. 2012.

[24] Xu M, Luo X, Davis JJ. "The label free picomolar detection of insulin in blood serum." *Biosensors and Bioelectronics*. vol. 39, pp. 21–25, Jan. 2013.

[25] Corash L. "Laboratory Hematology: Methods for the Analysis of Blood," in Blood, Principles and Practice of Hematology, R.I. Handin, S.E. Lux and T.P. Stossel, Eds. 1st ed. Philadelphia, J.B. Lippincott & Co., 1995, ch. 2, pp. 23–61.

Chapter 4

A study of IA for cellular detection on LoC devices. Increased functionalities for an Escherichia Coli concentrator and detector.

This chapter describes the experimental analysis performed to validate the IA, for detection and monitoring of diluted cells suspensions, with a different cellular specie, Escherichia Coli, other than the HCT used on the previous chapter. Moreover, the experiments were carried out as a complementary part of a LoC device for cellular microfluidic manipulation along with dielectrophoresis technique. The purpose of this study and its relevancy are framed on the following points:

1. Analyse the versatility of the whole electronic system, aiming for the screening of **another diluted cellular specie in different buffer,** as well as its applications and possibilities of **integration on other LoC devices to add new functionalities**.

2. Highlight the problems of using **laboratory modified samples as a model for actual cellular samples** when testing biomedical devices.

3. Present a miniaturized and compact **LoC solution to concentrate bacteria** in a controlled manner, using a fully automated instrument **combining dielectrophoresis and IA**.

4. Address the **issues associated with the combination of these techniques by simplifying the equipment** but also by trying to **solving some issues generally avoided**, to the best of the knowledge in the actual state-of-the-art.

5. Provide the scientific community with a **rapid tool for bacteria presence detection**, by avoiding previous slow preparations in pre-concentration and culture processes, **reducing procedure times for a faster diagnosis and treatment**.

4.1. LoC devices: combination of dielectrophoresis and IA for cellular manipulation.

Beside the aforementioned IA, the electrical properties of cells and pathogens have been used to explore new methods of manipulation and characterization, such as DEP [1]. DEP has been recently used to control stem cells to form embryonic bodies in shorter time [2] and H.O. Fatoyinbo *et al.* [3] have measured biophysical parameters of cells (cytoplasmic conductivity, membrane conductivity and cell wall conductivity) by analysing its cells DEP behaviour.

Bacteria concentration is a time consuming procedure in regular microbiology laboratory practices that involves cell culturing processes [4,5] to obtain a significant sample. This could be improved by using DEP as a mean of concentration in tiny fluidic spaces. DEP, refers to the force experienced by a particle inside a non-uniform electric field [6, 7] and is a convenient, rather selective, handling method that has been applied in many biological fields and in LoC devices [8–10]. An example of this is the work reported by Lapizco-Encinas *et al.* (2004) [11], where several types of bacteria in water were concentrated and separated by DEP induced by insulator-based structures (iDEP), or in the paper presented by Braff *et al.* (2012) [12], where bacteria were successfully DEP trapped in poly(methyl methacrylate) PMMA constructs. DEP selectivity has also been repeatedly reported as a benefit for sample preparation, since it allows isolatation of the desired cell or pathogen based on their electric and geometric properties [13–15]. As an example, Moon *et al.* (2011) [15] used DEP to separate and detect circulating tumour cells (CTCs), whose size and resistance to filtering shear stress presented significant differentiating properties, from regular blood cells. This also becomes an advantage in the case of environmental samples, where soil particles with the same bacteria size are also present and couldn't be eliminated by filtration or centrifugation. This has also been solved by using DEP [16], taking advantage of its selectivity by cell electrical properties. Hence, we used DEP here for concentration purposes.

On the other hand, current bacteria detection protocols are expensive in terms of equipment and time, typically requiring several days to obtain results [17,18]. Techniques like pathogenic-specific antibody coated magnetic beads [19,20] or hybridization of DNA fragments of bacteria [21], have shown to improve the analysis time down to several hours, but they still need complex equipment. This could be improved by using IA technique.

The combination of DEP and IA [22, 23] in a single equipment based on LoC and micro-fluidic technologies allow to develop a practical bench-top device. In recent years several biosensors and applications aiming for the successful combination of both technique have been presented. Hamada *et al.* (2013) [22] presented a bacterial detection device combining both positive and negative DEP with DEPIM. The biosensor relied on a pair of interdigitated electrodes (IDE) for separate DEP concentration and DEPIM measurement, while using commercial devices to operate the application. The cellular solution conductivity varies through time, which affects the IA, which has not been considered, and measurement instability produced by the magnitude of DEP voltage has been reported. Dastider *et al.* (2013) [23] have designed an impedance biosensor for the specific detection of *E. coli* O157:H7 combining DEP and IA techniques at 2µL/min flow rate, which is relatively low. This work used different IDE for cellular separation and detection purposes. The detection IDE was functionalized with polyclonal anti-*E. coli* antibodies for specific detection of *E. coli* O150:H7, removing versatility of the device. Moreover, the presented results for cells concentration detection, based on IAs, did not consider the solution conductivity variations, as well as the influence of DEP voltages on the IA.

In that context, it is very interesting to develop a completely customized LoC equipment for a quick and easy way to concentrate bacteria with DEP technique at relatively high flow rates [24, 25], while monitoring its concentration by means of IA technique in a real-time scenario. The device, with its main components, is presented in Fig. 1. It is composed of a customized electronic module and a LoC. The flowing bacteria sample is pre-concentrated through the generated DEP generation and concentration is measured through IA monitoring, with a four-electrode sensor

topology, embedded on a single micro-fluidic chamber. The electronic module is supported by a real-time platform for continuous concentration monitoring, connected to a remote computer through a standard Ethernet connection, which enables the system configuration and data display. First, it allows automated functionalities, such as multiplexing signals between the DEP generator and the IA analyzer in the micro-fluidic chip, in order to avoid DEP voltages disturbance of IA measurement, and auto-scale of the electronic instrumentation gains when necessary, for better signal acquisition. Second, it is connected to a remote computer with a user-friendly front-end user panel, where the system user can configure the experiment variables, such as measurement time for signal multiplexing, signal operation frequency and output gain, while displaying the IAs related to actual bacteria concentration level.

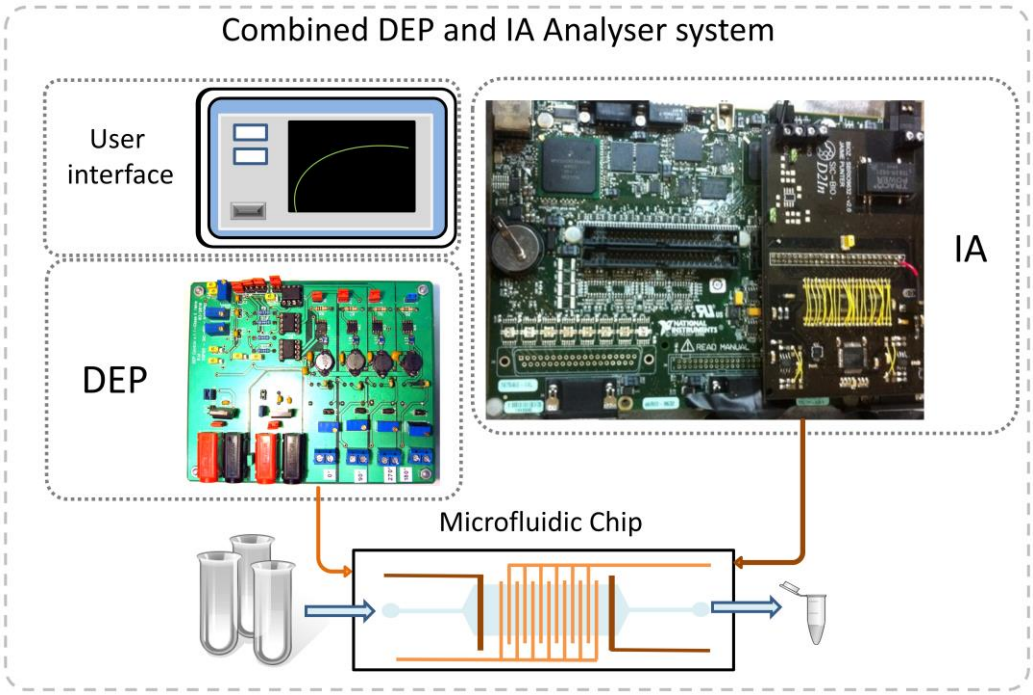

Figure 4.1: Combined system overview

The solution presented controls, in an automated way, the bacteria concentration and monitoring process, and has been validated for *E. coli*, which presents pathogenic variants that cause morbidity and mortality worldwide [26] being therefore a topic of interest. *E. coli* is one of the main antimicrobials resistant pathogens for healthcare-associated infections reported to the National Healthcare Safety Network [27], being the primary cause of widespread pathologies such as significant diarrheal and extra-intestinal diseases [26] or urinary tract infections [28]. Furthermore, *E. coli* can be found as a bacterial food contamination [17] and causes avian coli-bacillosis, one of the major bacterial diseases in the poultry industry and the most common avian disease communicable to humans [29].

4.1.1. The dielectrophoretic effect

Dielectrophoresis [7] defines the movement of an electrically neutral particle when a non-uniform electric field is applied. If the particle is considered homogeneous and isotropic and is polarized linearly, then the dielectrophoretic force is defined by (1) [30, 31], where V is the volume of the particle, E is the electric field, and α is the effective polarizability, which is defined by the expression (2):

$$\langle F_{\mathrm{DEP}} \rangle = \frac{1}{2} V \cdot Re[\alpha^*(\omega) \nabla \left|\vec{E}\right|^2] \quad (1)$$

$$\alpha = 3\varepsilon_0 \varepsilon_m \mathrm{F_{CM}} \quad (2)$$

where ε_0 and ε_m are the vacuum permittivity and the medium permittivity respectively and F_{CM} is the Clausius-Mosotti Factor. The F_{CM} sign describes the force direction: if F_{CM} is positive, the particle is attracted to an electrical field maximum (which is called positive DEP or p-DEP) and if negative, to an electrical field minimum (negative DEP or n-DEP). Hence, the DEP force allows control of the movement of a particle by varying the applied signal, by changing the electrode shape, by placing dielectric structures or by modifying media properties. In the specific case of this LoC, we used a pair of interdigitated gold electrodes to pre-concentrate *E. coli* cells. In order to define the suitable trapping frequency, an *E. coli* geometry model is considered. This bacterium is approximated to an ellipsoid shape with two dielectric layers [6], which modifies the Clausius – Mosotti factor expression:

$$F_{CM_i}(\omega) = \frac{1}{2} \left(\frac{\varepsilon_p^* - \varepsilon_m^*}{\varepsilon_m^* + A_i(\varepsilon_p^* - \varepsilon_m^*)} \right) \quad (3)$$

where ε_m is the medium permittivity, ε_p is the particle permittivity and Ai is the depolarization factor of an individual ellipsoid axe ($i = x,y,z$), where e is the eccentricity that involves the ellipsoid dimensions (where 'b' is the height and 'a' the width):

$$\mathrm{A_x} = \frac{(1-\mathrm{e}^2)}{(2\mathrm{e}^3)} \log\left(1 + \frac{\mathrm{e}}{(1-\mathrm{e}) - 2\mathrm{e}}\right) \quad (4)$$

$$\mathrm{A_z} = \mathrm{A_y} = \frac{(1-\mathrm{A_x})}{2} \quad (5)$$

$$\mathrm{e} = \sqrt{1 - \left(\frac{\mathrm{b}}{\mathrm{a}}\right)^2} \quad (6)$$

The representation of expression (3) showed that the optimal frequency to manipulate *E. coli* cells by p-DEP is at 1 MHz as we know from previous studies of the group [32, 33]. This frequency was therefore chosen for the pre-concentrating stage.

4.1.2. Micro-fluidic chip design and fabrication

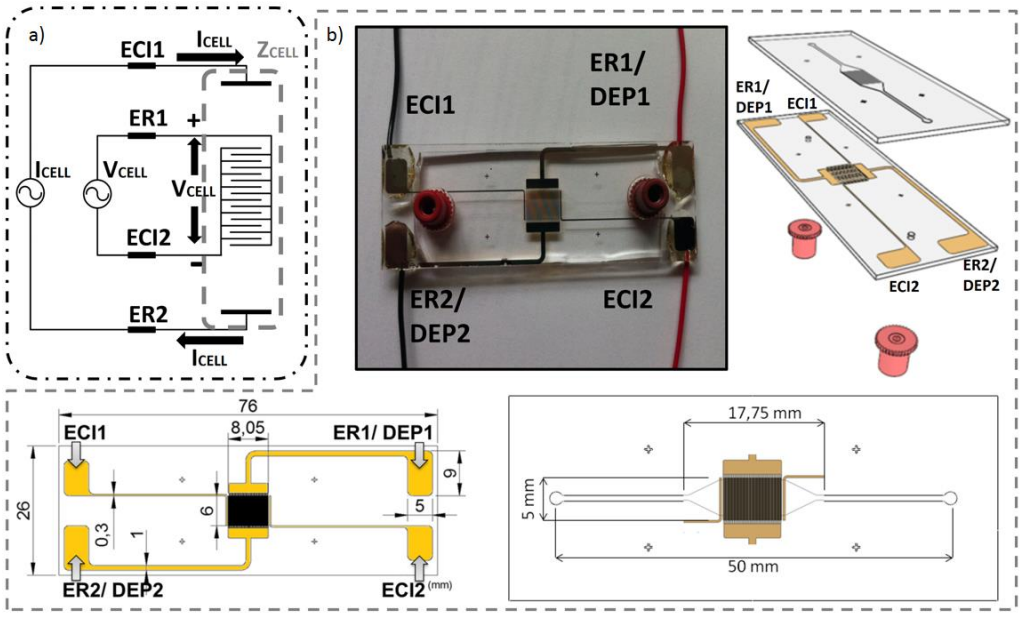

Figure 4.2: A: 4 electrode IA method. B: Designed micro-fluidic chip. ECI1-ECI2 are the current injection electrodes, ER1-ER2 are the reading electrodes and DEP1-DEP2 are referred to electrodes where DEP is applied.

The 3 electrodes topology used in the previous chapter, although is a perfectly viable electrode architecture, can distort the IA if the electrodes are not well geometrically designed, due to the working electrode impedance polarization, as the current bias signal is directly applied where the single-ended voltage measurement signal is read. As the microfluidic device must include a pair of interdigitated electrodes for DEP technique, the geometry of the electrodes for a 3 electrodes solution IA cannot be optimized. So, in order to include the IA as part of the device, the micro-fluidic chip was designed with an extra pair of electrodes (ECI1 and ECI2), in order to use a 4 electrode topology (figure 4.2.a, electrodes ER1, ER2, ECI1, ECI2). This configuration is composed of two current injection electrodes (ECI1 and ECI2) and two voltage reading electrodes (ER1 and ER2), avoiding electrode polarization distortion in IA due to a complete differential voltage measurement [34].

The designed micro-fluidic chip design is showed in figure 4.2.b. This had two interdigitated electrodes, which were shared between the dielectrophoresis generator and impedance analyzer readout electronics, and 2 lateral electrodes, which were used to inject the necessary current so as to obtain the impedance measure. The interdigitated electrodes were formed by 40 pairs of 6 mm x 50 µm electrodes separated by 50 µm. The lateral electrodes (6 mm x 300 µm) were separated by 200 µm from the interdigitated ones. These electrodes were attached to a PDMS micro-fluidic chamber with a volume of 4.8 µl. The fabrication of the micro-fluidic chips followed a protocol

based on three main steps: micro-channel moulding, electrode fabrication, and micro-fluidic chip bonding.

First, SU8 50 (MicroChem™) masters were fabricated over glass slides (Deltalab™) and Polydimethylsiloxane (PDMS) replicas were created. In order to do this, the glass slide was cleaned and activated by Piranha attack for 15 minutes. Then a 50 μm high SU-8 50 (MicroChem™) was spun over the slides. They were later exposed and developed so as to obtain the desired micro-channels. Afterwards, a 10:1 ratio of PDMS pre-polymeric solution (Dow Corning™ Sylgard®184) was mixed, degassed and poured into the mould to replicate the microchannels. Finally, the PDMS was cured at 70ºC for 1 h and peeled from the master.

Secondly, in order to fabricate the microelectrodes over a set of the LoC sealing glass slides (Deltalab™), a lift-off soft lithographic process was used. AZ 1512 (AZ Electronic Materials™) photoresist was chosen as a sacrificial layer in this process. First, a Piranha cleaning procedure was performed over the glass slides. Later, AZ 1512 was spun on these slides, exposed and developed. Then, two metal layers, 20 nm of Ti and 80 nm of gold, were vapour-deposited sequentially. The electrode structures were finally obtained by removing the AZ photo-resist.

As a final micro-fluidic chip fabrication step, once the PDMS replica and the microelectrodes were finished, both parts were assembled to create a sealed structure. First, the surfaces were cleaned using an oxygen plasma process. Hereinafter, the PDMS channels were aligned and attached to the glass substrate. Later, cables were welded to each electrode pad using conductive silver paint and mechanically strengthened using an epoxy glue mix, later cured at room temperature for 60 minutes. Finally, two NanoPort Assemblies were attached in order to set the inlet and outlet fluidic connections.

4.2. Impedance analysis front-end and back-end electronics.

A fully customized electronic circuit was specifically designed to carry out the IA experiments. As previously stated, the micro-fluidic device IA is based on the 4 electrode topology. A 4 electrode method is composed of two Current Injection (ECI1 and ECI2) electrodes and two voltage Reading (ER1 and ER2) electrodes. The main advantage of this system is that electrode impedances are cancelled, obtaining a more reliable measure. The circuit specifications were defined taking into account the sample media impedance, and considering the micro-fluidic device characteristics and the frequency ranges where bacterium could be discriminated [35, 36].

The impedance analyser architecture consists of two modules: the front-end electronics Current Injection module (CI in figure 4.3.b) that provides a frequency configurable voltage sinus signal (V_{RS}) that is converted to a current signal (voltage-to-current converter circuit) to bias/drive the Current Injection electrodes ECI1 and ECI2. An Instrumentation Amplifier senses the differential voltage between the Reading electrodes ER1 and ER2 (V_{IS}). The second module for back-end electronics, Signal Digitalization and Post-Processing (SDPP in figure 4.3.a), calculates the IA through the voltage signals provided by the previous stage, and automatically controls the hardware configuration.

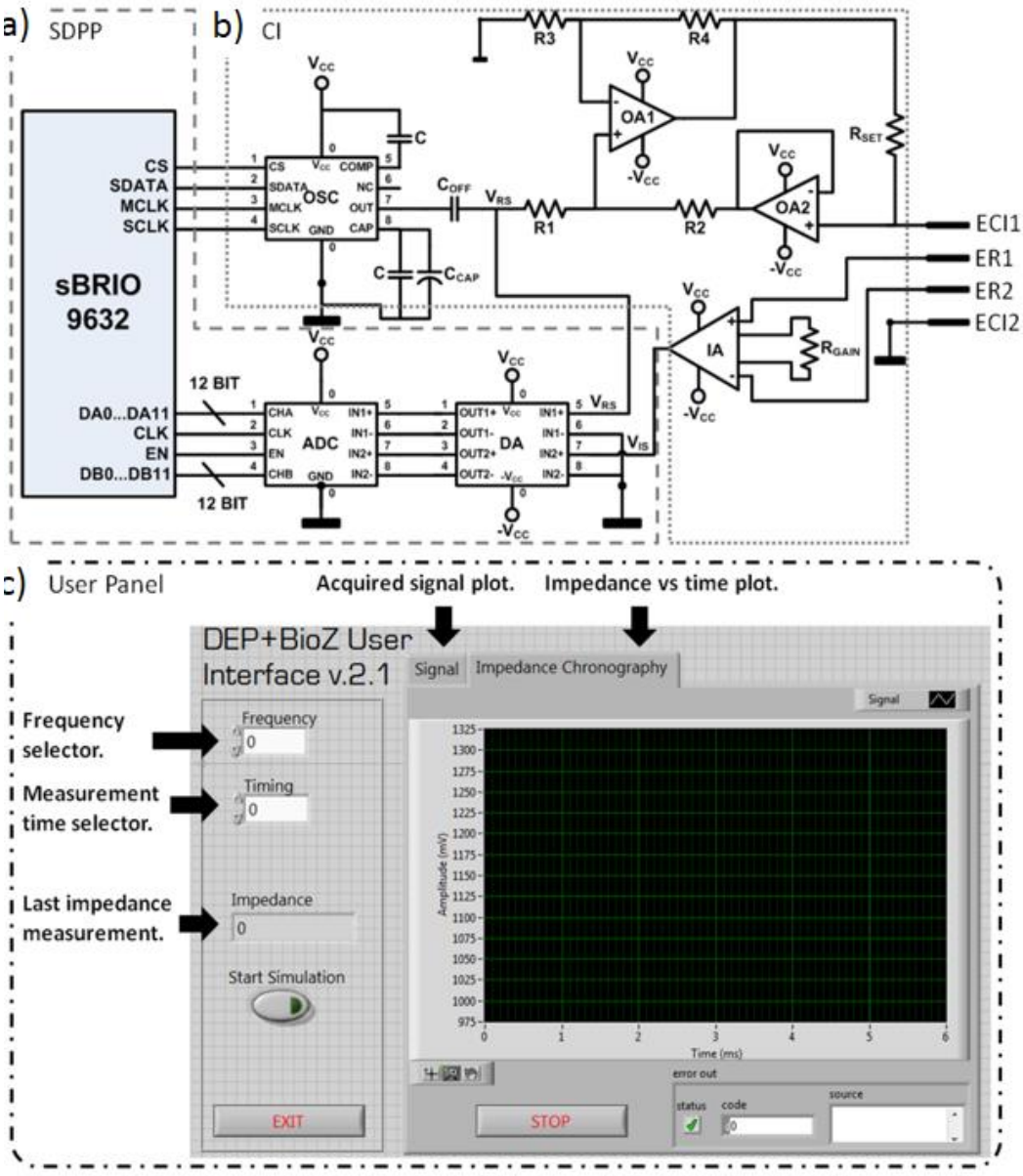

Figure 4.3: chematic of the IA module. a) Signal Digitalization and Post-Processing module (SDPP). b) Current Injection Module (CI). c) Front-end user panel for experiments control and data displaying.

This module is composed of a real time platform sbRIO9632 (National Instruments) with an embedded software for data processing and hardware control. A signal conditioning stage converts voltage signals from a bi-polar single-ended to a unipolar differential signal to be processed by an analog-to-digital converter (ADC).

The first module (CI), Current Injection, is based on a signal generator AD9833 (Analog Devices) and a voltage to current converter. The signal generator AD9833 provides a stable voltage signal with a wide variable frequency range, 0 MHz to 12.5 MHz, which is controlled by an SPI communication protocol. The voltage to current converter is a modified Howland cell based on AD8066 (Analog Devices) operational amplifiers (OA1 and OA2) which guarantee a wide bandwidth and a high slew-rate while maintaining a low spectral noise and a low offset performance. The Howland cell uses R_{SET} and the Reference Signal (V_{RS}) amplitude to define a stable current signal (I_{OUT}) at the output of the circuit (7) regardless the connected load.

$$I_{OUT} = \left(\frac{1}{R_{SET}}\right) V_{RS} \quad (7)$$

The differential voltage between ER1 and ER2 electrodes is acquired by means of the instrumentation amplifier INA163 (Texas Instruments) which allows a wide bandwidth with a low spectral noise and low Total Harmonic Distortion. The measured voltage (signal V_{IS}) is related to the differential voltage between the reading electrodes (ER1 and ER2), G being the instrumentation amplifier gain. This V_{IS} signal is then adapted and processed by the SDPPM module in order to extract the impedance of the media.

$$V_{IS} = G \cdot (V_{ER1} - V_{ER2}) \quad (8)$$

The second module (SDPP), Signal Digitalization and Post-Processing, consists in a 12 bit, dual, low power analogue to digital converter ADC12D040 (ADC) (Texas Instruments), capable of converting both analogue input signals at 40 MSPS simultaneously. 12 bit resolution does not represent a significant drawback in the final system resolution, as V_{RS} is scaled to the full range ADC analogue input and the system provides a real time gain auto-scale for the instrumentation amplifier gain G. The analogue inputs are converted from single ended to differential with a differential amplifier (DA) AD8138 (Analog Devices), with a high slew rate with low distortion and input noise. The IA is carried out with a digital lock-in (DLIA) based on the Frequency Response Analyzer (FRA) approach. The FRA is a real-time mathematical processing system, embedded in the 400 MHz microprocessor from the real time platform sbRIO9632, which adopts sine and cosine signals related to V_{RS}, and by means of two multipliers and a filter stage, the real (V_{REAL}) and imaginary (V_{IM}) components values (9) of the measured signal V_{IS} are obtained (figure 4.3.c.). The key measurement in our work is the impedance magnitude ($|Z_{CELL}|$) (10). This value is calculated based on the V_{REAL} and V_{IM} components.

$$V_{REAL} = \frac{1}{2V_{RS}} \cdot V_{IS} \cdot \cos(\varphi_{IS}) \; ; \; V_{IM} = \frac{1}{2V_{RS}} \cdot V_{IS} \cdot \sin(\varphi_{IS}) \quad (9)$$

$$|Z_{CELL}| = \left(\frac{2\sqrt{{V_{REAL}}^2 + {V_{IM}}^2}}{|V_{RS}|^2}\right) \cdot R_{SET} \quad (10)$$

For accurate hardware control, the real time platform sbRIO9632 has a FPGA Spartan-3 (Xilinx), which allows us to provide steady clock signals, needed on the instrumentation, which can be automatically adjusted, allowing complete real-time control of the chip electrodes multiplexing. As stated in section 2.1, the micro-fluidic chip had two interdigitated electrodes, which were shared between the DEP generator and the IA readout electronics. When an IA measurement was

done the DEP generator was disconnected, suspending the trapping process. If this process was not properly timed, bacteria already trapped would be lost in the process, so the real-time control allowed an optimized timing process minimizing the bacteria loss. Moreover, the disconnection of DEP voltage signals contributes to a better bacterial concentration monitoring avoiding distortion and instability on the IA measurement. The IA process had been programmed and tested to last for a period of the applied current signal, plus 1 ms for multiplexor switching times and stabilization. In addition, real-time platform allows complete parallel signal acquisition for all the frequency ranges, and the development of an embedded hardware control, such as R_{SET} multiplexed auto-scale, instrumentation amplifier gain G auto-scale and signal generator automatic frequency sweep. This real-time embedded hardware control represents the basic features of an automated and complete FRA approach. The real-time platform allows the system configuration and data display, with a user-friendly front-end user panel (figure 4.3.c), by means of an external computer connected to the platform with a standard Ethernet connection.

4.3. Experimental setup

The micro-fluidic chip was placed over an inverted microscope stage (Olympus™ IX71) connected to a digital camera (Hamamatsu™ Orca R2). Moreover, the micro-fluidic chip was connected to a 6-port manual valve (Valco™). This valve was also connected to a 5 mL syringe filled with de-ionized water ($8.2 \cdot 10^{-5}$ S/m) and placed on an infusion micro-pump (Cetoni™ NEMESYS) so as to obtain a continuous flow rate. The micro-fluidic chip's gold electrodes were connected to the custom combined DEP and IA device.

4.3.1. Bacteria culture

A laboratory sample formed by *E. coli* 5K strains (Genotypes: F^-, hdsR, hdsM,thr, thi, leu, lacZ) was grown overnight in 10 mL of Luria–Bertani (LB) broth at 37 °C. The achieved cell concentration (estimated by performing viable cell counts in LB agar) was 10^9 cells/mL. Then, the *E. coli* culture was pelleted by centrifugation at 5000 rpm for 5 minutes. Bacteria were then re-suspended in 10 mL of deionized water. Finally, the samples were diluted (final concentration of $2 \cdot 10^7$ cells/mL) and frozen in 1 mL collecting tubes for storage purposes.

4.3.2. Conductivity measurements

As *E. coli* concentration was measured by means of IA, bacteria samples' conductivity was monitored while in vitro a major factor in IA reliability, using a commercial bench top conductivity meter Corning 441. Prior to the experiments, bacteria samples were diluted in de-ionized water with a conductivity of $8.2 \cdot 10^{-5}$ S/m, but the conductivity of the samples at the time of the experiment, after the process of storage and thawing, was subject to variations. A sample conductivity analysis had to be done at the beginning of the experiment. The conductivity meter

probe was calibrated and introduced into the 1 mL collecting tubes until it was totally covered by the bacteria sample.

4.4. Results and discussion.

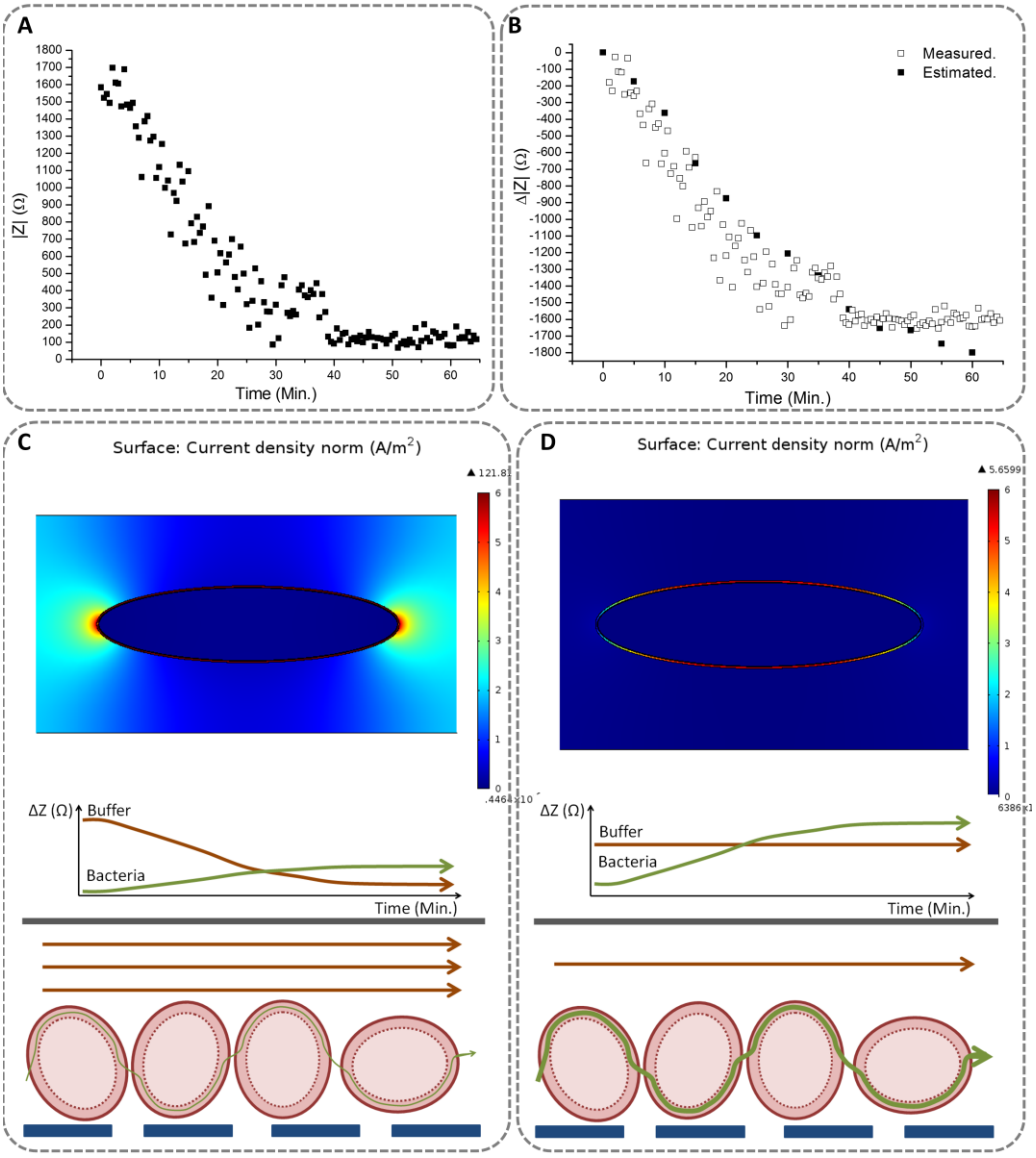

Figure 4.4: a) Impedance magnitude measured during the trapping operation. b) Experimental versus estimated impedance magnitude relative incremental changes. c) Comsol Multiphysics simulation of a single diluted cell on high conductivity buffer (0.5 •10-3 S/m to 2.5 ·10-3 S/m). Schematic modelization of current flow path and contribution to IA of both buffer and trapped bacteria. d) Comsol Multiphysics simulation of a single diluted cell on low conductivity steady buffer (Milli-Q water; 8.2 ·10-5 S/m). Schematic modelization of current flow path and contribution to IA of both buffer conductivity and trapped bacteria.

The designed combined device was validated by a series of *E. coli* concentration and IA tests. First of all, so as to validate the system as an autonomous bacteria concentrator, and study the effect of real-time monitoring by means of IA measurement, *E. coli* was continuously injected through the valve to the micro-fluidic chip at a 5 µL/min flow rate, and pre-concentrated by DEP by two counter-phased signals of 15Vpp. In addition, the impedance module was programmed to proceed with a 3 milliseconds IA every 30 seconds meanwhile DEP module was continuously trapping bacteria. As a first approach, the conductivity of the solution has not been corrected to study the effect its variations over time on the IA measurement. Different tests for different applied current signal frequencies were done. Taking into consideration the electronics and micro-fluidic chip design, IA was performed at continuous alternating current of 10 µA in the 500 Hz to 5 kHz frequency range, where bacterium could be discriminated [35, 36] and evaluated using 100 Hz spaced sampling intervals.

The measured bioimpedance (|Z|), depicted in figure 4.4.a, clearly shows a decreased impedance as the trapped bacteria concentration increases, regardless of the frequency. This behaviour was clearly explained by the conductivity changes taking place in bacteria samples over time. Measured conductivity was recorded periodically in-tube during the experiments showing a rise from $0.5 \cdot 10^{-3}$ S/m to $2.5 \cdot 10^{-3}$ S/m until it stabilized. This conductivity change, related to the original sample prior to the trapping process, may be translated into a theoretical variation in impedance. This estimated impedance, related to measured bacteria sample in-tube conductivity, was calculated considering the micro-fluidic chip electrodes' geometric characteristics. In figure 4.4.b, impedance variation ($\Delta|Z|$) through time for the measured on-chip impedance, during the trapping process, and for the estimated on-tube impedance are shown.

Results show a very similar behaviour through time of both measurements. Acquired data variations through time for the first 40 minutes, before conductivity stabilization, were -52.41 Ω/min for measured impedance and -54.79 Ω/min for conductivity related impedance, which confirms that the first IAs are related to bacteria sample conductivity rather than trapped bacteria concentration, underlining the need for a media conductivity correcting protocol.

A 2-D finite element method (FEM)-based study with Multiphysics software (Comsol) further shows the dominating effect of sample conductivity changes on the bioIAs when left uncontrolled. *E. coli* 5K physical and electrical properties were defined for the different model layers (σ_{wall}= 0.68 S/m, ε_{r_wall}=74, $\sigma_{membrane}$= 5 x 10^{-8} S/m, $\varepsilon_{r\_membrane}$=9.5, $\sigma_{cytoplasm}$= 0.19 S/m, $\varepsilon_{r\_cytoplam}$=49.8). Then different medium conductivities were defined, as well as the applied potential to the external lateral electrodes. Current conservation and an initial state of potential 0 were applied for all the layers. After, an adaptive physical controlled and extra fine mesh was applied. Finally, a frequency domain analysis at 1.7 kHz was performed. Thus, surface current density (ec.normJ) of bacteria was obtained (figure 4.4.c and figure 4.4.d). From the analysis of the obtained simulations we could assure that in case of a single bacteria diluted on a buffer with a conductivity which varies from $0.5 \cdot 10^{-3}$ S/m to $2.5 \cdot 10^{-3}$ S/m, current density is 99.9% located outside the bacteria. Hence, measured impedance is totally related to sample buffer conductivity rather than bacteria concentration (figure 4.4.c).

Controlling buffer conductivity to be stable and at the levels of Milli-Q water, around $8.2 \cdot 10^{-5}$ S/m, current density is mainly located in the cell membrane (figure 4.4.d) and impedance variation related to the quantity of trapped bacteria.

Hence, when the cells' media is not controlled by cleaning processes, impedance variations are strongly related to changes in the conductivity of the media due to bacteria [37, 38]. To solve this issue, which is not confronted in other works to the best of our knowledge, an automated periodic cleaning process was implemented as part of the device working protocol assuring a reliable IA.

In the resulting protocol the micro-fluidic chip was first filled with Milli-Q water media to obtain the threshold IA. Afterwards, a 50 µL sample of *E. coli* were injected through a controlled valve to the micro-fluidic chip and trapped by DEP forces while flowing continuously at 10uL/min, higher flow rate compared with other solutions for DEP and IA combination, such as 2-4 uL/min [23]. After each 50 µL sample of bacteria was injected into the channel, 50 µL of Milli-Q water, with a specified conductivity of $8.2 \cdot 10^{-5}$ S/m, was automatically injected at 10 µL/min to ensure a steady media conductivity for the IA. Once the Milli-Q water was injected, the impedance electronic module was activated and the DEP generator deactivated by means of multiplexor. 4 contiguous IAs were performed each time in order to evaluate precision. Afterwards, another 50 µL sample of *E. coli* was injected and the process repeated until all the samples were injected. So, the IA is always performed after each 50 µL bacteria sample was injected, trapped and cleaned. The whole process were performed to scan the 500 Hz to 5 kHz IA frequency range each 100 Hz. The DEP was generated by applying two 15 Vpp counter phased signals through the interdigitated electrodes. The results of the experimental IAs for three frequencies (500, 1700 and 5000 Hz) are depicted in figure 4.5.

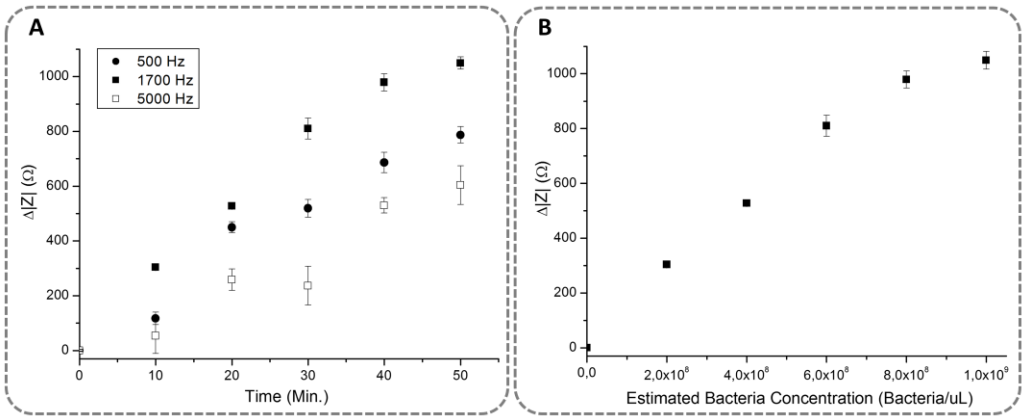

Figure 4.5: a) Impedance magnitude measured changes during bacterial sample on-chip concentration at several given times. Medium cleaning procedure was performed before each measurement. b) Impedance magnitude measurements at 1700 Hz related to estimated bacteria concentrations.

Results are depicted as the increment ($\Delta|Z|=|Z|-|Z_0|$) between the different impedance magnitude measurements for every bacteria sample injected ($|Z|$) and the initial media impedance magnitude measurement ($|Z_0|$). Figure 4.5.a depicts $\Delta|Z|$ measurements through time for the initial and final frequency value, 500 Hz and 5 kHz respectively, as well as the 1.7 kHz frequency $\Delta|Z|$

measurements, which seems to be more sensitive and reliable with an accuracy error of less than 2% of bacteria concentration with a correlation of 0.988 are represented. Precision can be evaluated with the coefficient of variation, which is the standard deviation of the 4 experiment repetitions divided by the mean value of the 4 repetitions measurement. The mean value of the coefficient of variation is 3.1% on the whole range, although the device is more precise for lower bacteria concentration levels where the coefficient of variation is below 3%.

Thus, steady and sensitive $\Delta|Z|$ measurement at different frequencies, which is bacteria dependent, was observed. Furthermore, bioimpedance control of the achieved sample concentration showed a reliable sensitivity for the protocol including a bacteria cleaning step. The controlled and steady low media conductivity microenvironment solves issues regarding overall system viability.

The DEP module had a proven trapping efficiency of 85.65 ± 1.07 %, for a single 50 µl bacteria sample injected at continuous flow of 10 µL/min, by measuring the escaped and the collected bacteria of a single load by cytometric analysis [33]. Although the whole process trapping efficiency had not been tested, each sample load was estimated to increment the bacteria concentration $2 \cdot 10^8$ bacteria/mL inside the micro-fluidic chip. Figure 4.5. B depicts the $\Delta|Z|$ measurements for each bacteria concentration increment (bacteria/µL) when 1.7 kHz frequency is applied. However, our main goal was to verify that the process of bacterial concentration while monitoring the concentration is feasible, as it has been proved. The measured impedance values were related to the quantity of bacteria concentrated with a correlation of 0.988 and a coefficient of variation of 3.1%, avoiding distortion and instability related to undesired effects like media conductivity variations and DEP voltage interferences.

4.5. Conclusions

Here we have designed a novel LoC device and automated protocol, based on DEP and IA, to concentrate bacteria in a controlled manner. The system consists of a microfluidic chip, with integrated electrodes, and its associated custom instrumentation electronics. It performs bacteria injection, trapping, cleaning, and continuous short-time impedance measuring while achieving the desired levels of concentration. As a proof of concept, it has been applied to concentrate *E. coli* and to automatically monitor its concentration. The electronic apparatus was validated using a micro-fluidic chip with 4 integrated gold electrodes specifically designed for the application. The automated system was tested by trapping and measuring samples of *E. coli* 5K at a concentration of $2 \cdot 10^7$ cells/mL. Concentration and real-time detection of the trapped bacteria inside the micro-fluidic chip was proven, working a high flow injection rate, up to 10 µL/min, for different buffer conductivities [24, 25]. Bacteria media conductivity, and its variability, was demonstrated to be a challenging issue when a there is a continuous monitoring by means of IA, and it must be addressed for the correct performance of the technique. An automated protocol integrated in the overall system was proposed to solve this problem, strengthening the system versatility and robustness. Before each measurement, the designed system cleans the bacteria samples

periodically, while trapped on the micro-fluidic chip, with Milli-Q water at a controlled conductivity of $8.2 \cdot 10^{-5}$ S/m. To our best knowledge this proposed system is a useful tool to solve some current microbiology laboratories shortcomings. Bacteria can be concentrated to given specifications while performing analytical procedures. The development of LoC-based equipment, removing the need of huge and expensive devices, is an important research field aiming for smaller systems with better functionalities, such as the integrated application specific integrated system (ASIC) stimulator for electrokinetically-driven micro-fluidic devices presented by Gomez-Quiñones *et al.* (2011) [39]. Nowadays, electronic technology allows further miniaturization of devices such as our concentrator. A SOI technology such as XTO18 from XFAB would be suitable to combine digital instrumentation and class E amplifiers inside a unique chip. However, some drawbacks must be considered when integrating the full system into the LoC device, as it would either increase disposable cost or reduce applicability due to possible contaminations. Still, the simplicity of the presented micro-fluidic device and the development of the custom electronics on a single ASIC, along with an automated procedure protocol, pushes towards the development of robust and reliable LoC automated bacterial concentrator relying on DEP concentration and IA monitoring.

In summary, the technique provides the versatility to be applied in a wide variety of situations and applications, and it is extremely promising to increase LoC devices functionalities. However, it has been noticed, and it is important to remark, that there are still some issues to be addressed, as some conditions can dramatically alter the proper performance of the technique, so the functioning protocol for every specific device for every specific specie sample must be specifically designed.

4.6. References

[1] Pethig R., Biomicrofluidics 2010, 4, 22811.
[2] Agarwal, S., Sebastian, A., Forrester, L. M., Markx, G. H., Biomicrofluidics 2012, 6, 24101–2410111.
[3] Fatoyinbo, H. O., Hoettges, K. F., Hughes, M. P., Electrophoresis 2008, 29, 3–10.
[4] Feldsine, P. T., Falbo-Nelson, M. T., Hustead, D. L., J. AOAC Int. 1994, 77, 58–63.
[5] Pouch Downes, F., Ito, K., Compendium of Methods for the Microbiological Examination of Foods, 4th ed., American Public Health Association, 2001, p. 676.
[6] Morgan, H., Green, N. G., AC electrokinetics: colloids and nanoparticles, Research Studies Press, 2003.
[7] Pohl, H. A., J. Appl. Phys. 1951, 22, 869.
[8] Chin, C. D., Linder, V., Sia, S. K., Lab Chip 2007, 7, 41–57.
[9] Figeys, D., Pinto, D., Anal. Chem. 2000, 72, 330 A–335 A.
[10] Stone, H. A., Stroock, A. D., Ajdari, A., Annu. Mech. 2004, 36, 381–411.
[11] Lapizco-Encinas, B. H., Simmons, B. A., Cummings, E. B., Fintschenko, Y., Anal. Chem. 2004, 76, 1571–1579.
[12] Braff, W. A., Pignier, A., Buie, C. R., Lab Chip 2012, 12, 1327–1331.
[13] Gascoyne, P. R. C., Noshari, J., Anderson, T. J., Becker, F. F., Electrophoresis 2009, 30, 1388–1398.
[14] Gascoyne, P., Mahidol, C., Ruchirawat, M., Satayavivad, J., Watcharasit, P., Becker, F. F., Lab Chip 2002, 2, 70–5.
[15] Moon, H. S., Kwon, K., Kim, S. I., Han, H., Sohn, J., Lee, S., Jung, H. I., Lab Chip 2011, 11, 1118–1125.
[16] Fatoyinbo, H. O., McDonnell, M. C., Hughes, M. P., Biomicrofluidics 2014, 8, 044115.
[17] Zordan, M. D., Grafton, M. M. G., Acharya, G., Reece, L. M., Cooper, C. L., Aronson, A. I., Park, K., Leary, J. F., Cytom. A 2009, 75, 155–162.
[18] Deisingh, A. K., Thompson, M., Analyst 2002, 127, 567–581.
[19] Hahm, B.-K., Bhunia, A. K., J Appl Microbiol 2006, 100, 1017–1027.
[20] Bohaychuk, V. M., Gensler, G. E., King, R. K., Wu, J. T., McMullen, L. M., J Food Prot 2005, 68, 2637–2647.
[21] Hong, B.-X., Jiang, L.-F., Hu, Y.-S., Fang, D.-Y., Guo, H.-Y., J Microbiol Methods 2004, 58, 403–411.
[22] Hamada, R., Takayama, H., Shonishi, Y., Mao, L., Nakano, M., Suehiro, J., Sensors Actuators B Chem. 2013.
[23] Dastider, S.G., Barizuddin, S., Dweik, M., Almasri, M., RSC Advances 2013, 3, 26297–26306.
[24] Park, S., Zhang, Y., Wang, T.-H., Yang, S., Lab Chip 2011, 11, 2893–2900.
[25] Rozitsky, L., Fine, A., Dado, D., Nussbaum-Ben-Shaul, S., Levenberg, S., Yossifon, G., Biomed. Microdevices 2013, 15, 859–65.
[26] Croxen, M. A., Law, R. J., Scholz, R., Keeney, K. M., Wlodarska, M., Finlay, B. B., Clin Microbiol Rev 2013, 26, 822–880.
[27] Sievert, D. M., Ricks, P., Edwards, J. R., Schneider, A., Patel, J., Srinivasan, A., Kallen, A., Limbago, B., Fridkin, S., Infect. Control Hosp. Epidemiol. 2013, 34, 1–14.
[28] Ulett, G. C., Totsika, M., Schaale, K., Carey, A. J., Sweet, M. J., Schembri, M. A., Curr Opin Microbiol 2013, 16, 100–107.
[29] Dhama, K., Chakraborty, S., Tiwari, R., Verma, A. K., Saminathan, M., Amarpal, Y. S. M., Nikousefat, Z., Javdani, M., Khan, R. U., .
[30] Sabounchi, P., Morales, A. M., Ponce, P., Lee, L. P., Simmons, B. A., Davalos, R. V, Biomed. Microdevices 2008, 10, 661–70.
[31] Jones, T. B., Electromechanics of particles, Cambridge Univ Pr, 2005.
[32] Castellarnau, M., Errachid, A., Madrid, C., Juárez, A., Samitier, J., Biophys. J. 2006, 91, 3937–3945.
[33] Moral Zamora, B. del, Micro Nanosyst. 2014, 6.
[34] Martinson, O. G., Grimnes, S., Bioimpedance & Bioelectricity Basics 2008.
[35] Cheng, M. S., Ho, J. S., Lau, S. H., Chow, V. T. K., Toh, C.-S., Biosens Bioelectron 2013, 47, 340–344.
[36] Yang, L., Talanta 2008, 74, 1621–1629.
[37] Varshney, M., Li, Y., Biosens Bioelectron 2009, 24, 2951–2960.
[38] Li, M., Li, S., Cao, W., Li, W., Wen, W., Alici, G., Microfluid. Nanofluidics 2013, 14, 527–539.
[39] Gomez-Quiñones, J., Moncada-Hernández, H., Rossetto, O., Martinez-Duarte, R., Lapizco-Encinas, B.H., Madou, M., Martinez-Chapa, S.O. New Circuits and Systems Conference (NEWCAS), 2011, 350–353.

Chapter 5

New generation of PoC devices: an HCT detection case.

In this chapter it will be presented an instantaneous, reliable, and cost-effective new generation PoC electronic device for HCT detection and screening that correlates HCT levels with a voltage output level, for easy front-end user screening, telemedicine applications and versatile functionalities for medical applications. Its operational principle is related to the inherent electrical impedance properties of blood cells, avoiding the use of chemical biomarkers, making it more cost-effective, easy to operate, and resulting on a non-destructive sample device, enhancing its performance and functionalities. This study compared this new device and its principle of operation with actual HCT screening devices on the market, and discusses the main advantages and addressed issues of actual commercial devices.

A clinical study has been performed and the results obtained during the experimental procedures are shown, analysed and discussed. We tested consecutive whole blood samples from 83 adult patients with the new HCT detection device. Accuracy, precision and correlation for the HCT screening results were analysed by comparing obtained results with haematology analyzer CBC analysis. Collected data were analysed by means of Linear Regression (LR) analysis and Bland-Altman (BA) statistical methodology.

5.1. A review on actual PoC devices.

PoC devices have become common diagnostic tools in such a variety of different income countries [1]. The vast majority of PoC testing often needs of sophisticated microfluidics, microelectronics and optical systems to be functional and reliable. However, this technological complexity and the use of chemical biomarkers, or the PoC output data entails some operational challenges that must be addressed. This fact is exacerbated as high percentage of PoC testing devices outputs visual or colour-based results, which are subject to user interpretation and need of human personnel to record the results on a specific database for follow-up of patients. The PoC devices complexity and the use of chemical biomarkers results on a limited device, increasing the cost-effectiveness, the product regulation and the supply chain. In addition, the sample under analysis is destroyed during the process, lacking the versatility to be integrated in other medical equipment and environments for increased functionality as monitoring device or medical actuator.

Commercialization of biosensors technology is still delayed compared with research in academia. This reduced technology transfer activity could be attributed to technical barriers or cost considerations. Therefore, devices must be versatile to allow automation at a competitive cost [2]. Additionally, to ensure success in the development, innovation and technology transfer, it is

necessary to foster a particular scenario typified by the convergence of technologies and disciplines [3]. In this context, one of the main characteristics of the proposed device is its multidisciplinarity: in an effort to integrate knowledge from various dimensions, main actors and activities. The cross-disciplinary interaction must be examined in the way scientific knowledge flows between engineers, researchers and physicians. Currently, there are huge opportunities to be exploited by researchers and innovation managers in the development of high-tech products, above all in the field of medical devices. As such, the University–Hospital–Industry–Administration (plus Citizens) system should emerge as an essential five-helix leading to a successful technology transfer and commercialization of public-funded medical devices [4].

This chapter presents an improvement on the previously reported device for anaemia detection, as a compact, economic and portable PoC solution, for instantaneous detection of HCT through whole blood samples. The previously developed device relied on full spectrum analysis of blood samples by means of a Digital Lock-In Amplifier (DLIA) based on a Frequency Response Analyzer (FRA) approach. Full spectrum analysis involved a microprocessor for system control and data processing, and further electronics for signal conditioning, such as an SPI controlled oscillator AD9833 from Analog Devices (Norwood, MA, USA), and a 12-bit dual ADC ADC12D040 from Texas Instruments (Dallas, TX, USA) capable of converting simultaneously two analogue input signals at 40 MSPS. Moreover, a real-time platform sbRIO9632 from National Instruments (Austin, TX, USA) was used for fast software prototype development and versatility. All these electronics were a major drawback in terms of power consumption, size and price, when aiming for a specific PoC device.

The system is composed of an economic and reusable low-cost electronic device and a plug-and-play disposable commercial sensor. This sensor is based on three screen-printed electrodes for an envisaged sample of 50 µL. In order to validate the instantaneous HCT detection system, different blood samples, which came from the manipulation and dilution of whole blood samples extracted from 4 healthy donors, have been studied. These samples were randomly obtained from hospitalized patients of Hospital Clínic located in Barcelona, Spain.

5.2. Whole system conception.

A full custom electronic circuit was specifically designed to carry out IAs using a disposable three-electrode sensor. Regarding the previous studies, and the specifications needed, the commercial sensor that best meets the defined specifications is the C223AT (Dropsens, Llaneras, Spain), as it have shown better sensitivity and accuracy.

The electronic system was designed based on the specifications found in the study previously reported. Furthermore, the front-end electronics were redesigned. The previously PoC device for HCT monitoring was designed using a front-end electronics based on an instrumentation amplifier readout potentiostat. This configuration proved to be reliable and robust, but with the cost of increased power consumption, area and complexity. To reduce these factors, the new front-end electronics were designed using a potentiostat with a transimpedance amplifier readout configuration. Moreover, as the real-time platform sbRIO9632 must be removed, there are some

additional electronics to be considered. The architecture of the device is divided in three parts: an oscillator that provides the ac voltage signal (V_{CELL}), a sensor driving instrumentation (potentiostat) and a rms-to-dc converter (figure 5.1.a).

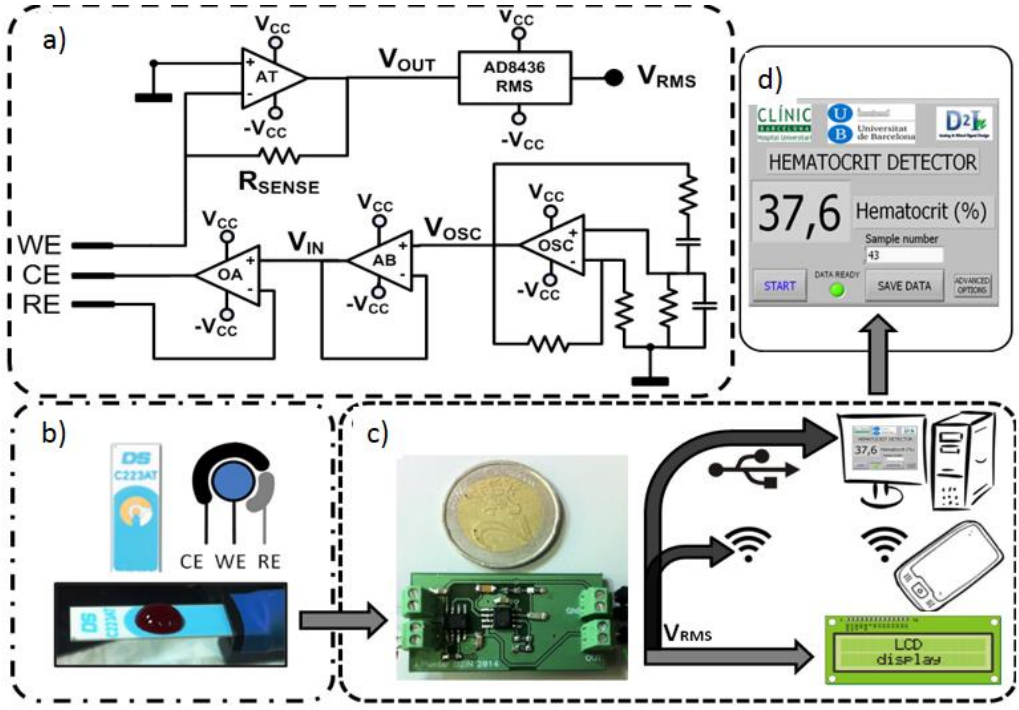

Figure 5.1: a) Custom electronic instrumentation; b) Commercial C223AT disposable sensor with a 50 µL whole blood drop; c) Device prototype electronics and different suitable and functional user readout interfaces (the reference coin has a diameter of 25.75 mm); d) Actual user-friendly front-end user interface develop with Labview.

The oscillator is a Wien bridge oscillator, a stable output amplitude with low distortion. The operational amplifier (OSC in figure 5.1.a) is the AD8066 from Analog Devices, which is a low-cost, high speed Junction Gate Field Effect Transistor (JFET) amplifier dual supply with low leakage current and distortion, in order to provide a stable sinus voltage signal with low offset (V_{OSC}). The oscillator has been configured to provide a voltage sinus signal of 33 kHz, a well-suited frequency for HCT detection using the C223AT sensor. Moreover, as the AD8066 commercial integrated circuit provides two isolated amplifiers, the second amplifier has been used as a voltage follower (AB in figure 5.1.a), due to its high speed and low distortion specifications for isolating the oscillator from the potentiostat. The sensor driving instrumentation is based on a potentiostat with a transimpedance amplifier current readout stage, composed of an operational amplifier to bias the sensor and an operational amplifier in transimpedance configuration as a sensing system current readout. The operational amplifier (OA in figure 5.1.a) is the AD8066 from Analog Devices, which is perfectly designed for singly driving the electrodes and track the voltage-biasing signal (V_{IN}) to the electrodes (1).

$$Z_{CELL} = \frac{V_{IN}}{I_{CELL}} \quad (1)$$

$$V_{OUT} = -R_{SENSE} \cdot I_{CELL} = -R_{SENSE} \frac{V_{IN}}{Z_{CELL}} \quad (2)$$

The JFET high input impedance avoids RE electrode voltage distortion, considering the low load impedance on the sensing system, and the high bandwidth and slew-rate provides stability to the system. The second amplifier included on the integrated circuit package has been configured as the transimpedance amplifier (AT in figure 5.1.a). The transimpedance amplifier converts the current through the electrodes (2) into a voltage signal (V_{OUT}) by means of a sensing resistor (R_{SENSE} in figure 5.1.a). The main drawback of this configuration, an amplifier with low input impedance, is avoided with the JFET input of the AD8066:

Finally, the rms-to-dc converter is the AD8436 from Analog Devices, which computes a precise dc equivalent (V_{RMS}) of the transimpedance amplifier ac signal (V_{OUT}). It is a low cost, low power device, with wide dynamic input range and wide bandwidth that provides low distortion with a Zero sub-threshold swing Field Effect Transistor (ZFET) input buffer for electronic isolation from the instrumentation stage. Considering that the electrodes voltage biasing signal (V_{IN}) and the sensing resistor (R_{SENSE}) are stable and well known, the rms dc variations of V_{OUT} are only related to the variations of Z_{CELL}. The device dc output voltage (V_{RMS}) is inverse compared to the HCT values, so as the HCT increases, V_{RMS} decreases. The device usage is very simple not requiring any qualified users. A blood sample is placed on top of the sensor electrodes and, once the power supply is connected, the device dc output voltage (V_{RMS}) is ready for reading on the output pin. On the presented manuscript, a software interface on an external computer with Labview©, from National Instruments, controlled an electric switch to enable the power supply (an external source at ±5 V), and presents the resultant data on a user-friendly user interface (figure 5.1.d). The electronics and the computer were connected by means of a NI USB-6361 data acquisition (DAQ) device from National Instruments. However, the presented device readout stage can be greatly improved to address different applications and user skills (figure 5.1.c), such as an integrated Liquid Crystal Display (LCD) for an untrained user self-screening, a remote computer connected to the electronics by means of an standardized protocol (USB, ethernet, *etc*…), or a wireless communication protocol for self-monitoring device in telemedicine applications. Additionally, the presence of an electrical signal directly correlated to HCT allows the device implementation as a controller of other clinical actuators in different environments and situations increasing functionality.

The overall low cost and low power system composed of optimized straightforward standards for instrumentation electronics, results in a reusable, robust and low consumption device (300 mWh) making it completely mobile with a long battery life time. Moreover, it is important to highlight that it is an easy to manipulate and economic electronics (less than 10 € per device), providing an instantaneous IA.

5.3. PoC device performance. First study.

5.3.1. Objectives

This first test will validate the designed PoC device capabilities to HCT. In order to validate it, different blood samples, which came from the manipulation and dilution of whole blood samples extracted from 4 healthy donors, have been studied. These samples were randomly obtained from hospitalized patients of Hospital Clínic located in Barcelona, Spain.

5.3.2. Blood samples

Four blood samples were obtained in 4-mL tubes containing ethylenediaminetetraacetic acid (EDTA 7.2 mg from BD Vacutainer, (Franklin Lakes, NJ, USA) from four random hospitalized patients in Hospital Clinic. To obtain a larger sample collection, the initial four whole blood samples were centrifuged (Jouan CR412 from DJB Labcare, Newport Pagnell, UK) at 2200 rpm for 15 min in order to separate blood plasma from RBCs. Finally, 24 blood samples were obtained diluting obtained RBCs in different volumes of blood plasma using a Labopette Manual 10–100 µL automatic pipette from Hirschmann Laborgeräte (Louisville, KY, USA). We performed a complete blood count (CBC) of the 24 blood samples with an ABX Micros 60 haematology analyzer (Horiba, Kyoto, Japan) which reported the hemoglobin and HCT results as g/dL and percentage (%), respectively. Therefore, the obtained HCT (HCT (%)) and hemoglobin (Hb (g/dL)) for the different blood samples are shown in table 5.1.

Sample	HCT (%)	Hb (g/dL)	Sample	HCT (%)	Hb (g/dL)
1	14.2	5.0	13	30.0	10.5
2	18.5	6.7	14	33.7	11.5
3	18.9	6.6	15	33.9	11.8
4	19.3	7.0	16	34.5	11.5
5	20.4	6.9	17	34.7	12.4
6	23.2	7.8	18	37.8	12.5
7	23.4	8.1	19	40.0	12.8
8	24.0	8.1	20	40.4	14.0
9	25.5	9.0	21	40.8	14.0
10	28.4	9.7	22	44.5	14.9
11	29.0	9.8	23	45.0	15.2
12	29.2	9.7	24	50.6	18.0

Table 5.1. Twenty four blood samples obtained in Hospital Clínic from four random hospitalized patients. Blood samples were obtained diluting RBCs in different volumes of blood plasma. HCT (HCT (%)) and hemoglobin (Hb (g/dL)) values for the different blood samples were obtained by means of a complete blood count (CBC).

5.3.3. First study results

A small, compact and portable device for PoC early instantaneous detection of anaemia was prototyped. For its validation, we analysed 24 consecutive blood samples from patients hospitalized at Hospital Clínic in Barcelona. We performed a complete blood count (CBC) of the blood samples with a haematology analyser, the Advia 2120 from Siemens AG, which reported the hemoglobin and HCT results as g/dL and percentage (%), respectively. We tested all samples with the prototype within 2 h of blood collection and CBC. As it is an instantaneous detector with a time response of several milliseconds, to evaluate system precision and accuracy, every whole blood sample was tested 5 times consecutively using fresh sensors and fresh sub-samples. Figure 5.2 depicts the output dc voltage (V_{RMS}) of the device and compares it with the different whole blood samples HCT (HCT (%)).

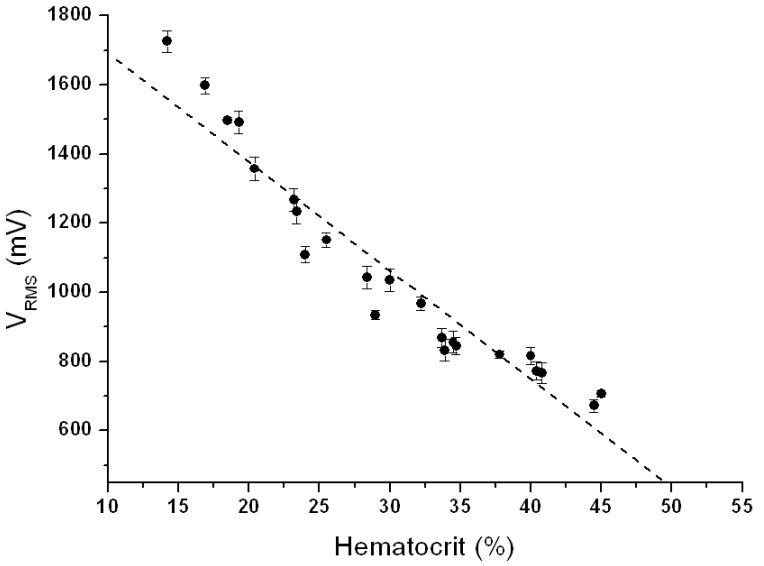

Figure 5.2: Measured output dc voltage (VRMS (mV)) mean value (n = 5) as a function of blood samples HCT (HCT (%)).

We used the Linear Regression (LR) analysis to measure the Pearson's correlation coefficient (r) and coefficient of determination (r^2) between the reference method (CBC method) and the custom electronic device method, where the output voltage (V_{RMS}) mean value (n = 5) has been compared with whole blood samples CBC HCT. The LR slope (β) defines the sensitivity, in terms of mV per HCT percentage (mV/%). Meanwhile the HCT detection accuracy (%) is the relation (3) between r^2 and β:

$$V_{RMS}(mV) = \alpha + \beta \cdot Hematocrit(\%) \quad (3)$$

In table 5.2 the experimental results of whole blood samples HCT (HCT (%)), the output voltage mean value (V_{RMS} (mV)) of the five measurements performed with each whole blood sample and its standard deviation (SD (mV)) are shown. Precision was evaluated with the coefficient of variation: the standard deviation (SD (mV)) divided by the mean value (V_{RMS} (mV).

The proposed anaemia detector device presented great accuracy at detecting HCT, with a Pearson's correlation coefficient of −0.96, an accuracy error of 2.83% HCT, and a coefficient of determination of 92.72%. The mean coefficient of variation is 2.57% without any particular case above 5%. Acceptable values in quality control procedures in clinical haematology measurements show a coefficient of variation less than 5% [5].

HCT (%)	V_{RMS} (mV)	SD (mV)	HCT (%)	V_{RMS} (mV)	SD (mV)	HCT (%)	V_{RMS} (mV)	SD (mV)
14.2	1725.92	31.28	25.5	1152.10	21.24	34.7	845.70	25.20
16.9	1598.31	24.08	28.4	1043.23	32.28	37.8	820.04	10.32
18.5	1498.75	8.12	29.0	934.82	13.08	40.0	816.04	25.08
19.3	1491.64	32.4	30.0	1035.43	33.88	40.4	773.16	25.20
20.4	1358.14	34.56	32.2	968.69	20.04	40.8	766.09	30.36
23.2	1268.13	33.00	33.7	869.14	26.44	44.5	671.69	18.52
23.4	1233.56	34.16	33.9	832.33	31.32	45.0	707.49	8.76
24.0	1109.21	23.28	34.5	856.91	30.12	50.6	490.12	6.32

Table 5.2. Device validation with whole blood samples.

The device presents reliable, sensitive and robust anaemia detection compared with other commercial PoC devices for anaemia detection, such as AnaemiaCheck from Express Diagnostics (Blue Earth, MN, USA), STAT-Site from Stanbio Laboratory (Boerne, TX, USA), or HemoPoint H2 from Alere (Waltham, MA, USA), where its detection performance is similar to the proposed prototype but with much slower response.

Recently, other PoC anaemia devices have been published, such as a color-based diagnostic test for self-screening/self-monitoring of anaemia presented by Tyburski et al., [6], a novel PoC diagnostic test for self-screening, self-monitoring of anaemia. The device measures hemoglobin (Hgb) levels, which are estimated via visual interpretation by the user using a color scale. This system presents several performance drawbacks when compared with our device. First of all, the readout stage, based on a color scale, relies on the visual interpretation of the user, which could introduce errors on the Hgb levels data interpretation, and reduces considerably the system resolution. Furthermore, the principle of operation of the color-based PoC device is based on biochemical reactions, where the blood comes into contact with a reagent solution initiating a redox reaction, which is a slow and destructive procedure.

5.3.4. First study conclusions

Twenty four blood samples, obtained from four patients hospitalized at Hospital Clínic, were used to demonstrate the feasibility of the IA technique to perform an easy, fast and low-cost HCT study using disposable commercial sensors. The system has been evaluated through comparison with complete blood count (CBC) using a clinical haematology analyser. The anaemia detection device has a Pearson's correlation coefficient of −0.96 and a coefficient of determination of 92.72% HCT. Coefficient of variation is below 5%, with a worst-case accuracy error of 2.83%. In summary, this study proves that the developed PoC device for HCT screening, presents reliable, sensitive and

robust detection, relying on low power straightforward electronic equipment and sensing systems. The next study will evaluate the device with a more complete clinical assessment.

5.4. HCT screening studies. Clinical assessment.

5.4.1. Objectives

In this section is described a complete clinical assay performed with the PoC device, and a more complete data analysis of the results. We tested consecutive whole blood samples from 83 adult patients with the new HCT detection device. Accuracy, precision and correlation for the HCT screening results were analysed by comparing obtained results with haematology analyzer CBC analysis. Collected data were analysed by means of Linear Regression (LR) analysis and Bland-Altman (BA) statistical methodology.

5.4.2. Clinical assessment results.

A clinical assessment comparing our PoC HCT quantifying device with a standard haematology analyzer was performed using whole blood samples collected from hospitalized patients in Hospital Clínic. However, personal data of the patients was not available to the investigators and samples were randomly selected. We collected 83 whole blood samples and obtained results were compared with haematology analyzer (Advia 2120, Siemens AG, Madrid, Spain) CBC analysis, which reported the haemoglobin and HCT results as g/L and percentage (%), respectively. Whole blood samples were collected in 4-mL tubes containing ethylenediaminetetraacetic acid (EDTA 7.2 mg; BD Vacutainer®; BD, Madrid, Spain). We tested all samples with the proposed device within 2 hours of blood collection and CBC.

Collected data were analysed by means of Linear Regression (LR) analysis and Bland-Altman (BA) statistical methodology. Our reference for statistical analysis was the CBC count measured by the haematology analyzer (Advia 2120, Siemens AG, Madrid, Spain).

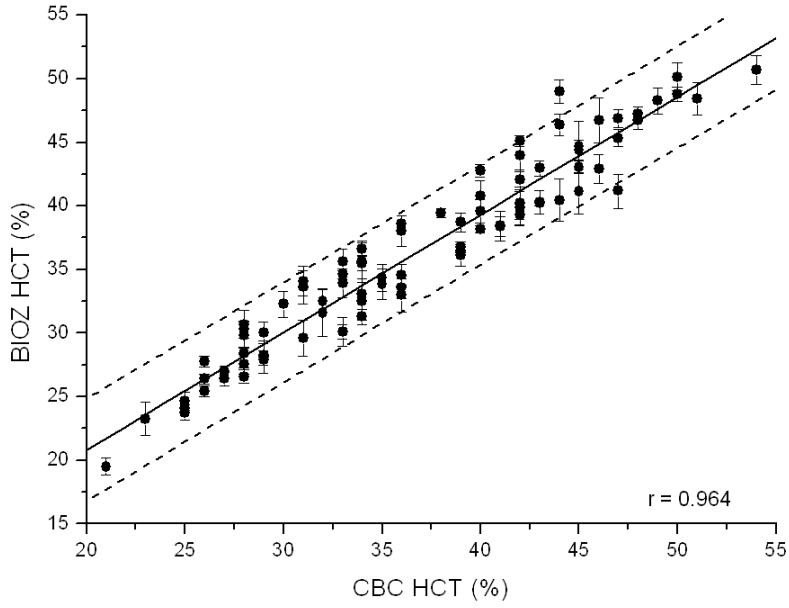

Figure 5.3: Clinical assessment of electrical impedance based HTC test results. Measured electrical HCT value (BIOZ HCT (%)) average value (n=10) plotted against clinical HCT levels obtained via a haematology analyzer CBC technique (CBC HCT (%)) for all 83 patient samples, showing strong correlation (r=0.964). Additionally, 95% prediction limits for the individual values were calculated (dashed lines).

We used the LR analysis to measure the Pearson's correlation coefficient (r) and coefficient of determination (r^2) between the reference method (CBC method) and the proposed device method (electrical impedance method), and every whole blood sample was tested 10 times consecutively using fresh sensors and sub-samples. We also performed a BA analysis and calculated the mean, SDD, and 95% confidence interval (CI) of the differences determined between the electrical impedance method and the CBC method to estimate the bias. Statistical analysis was performed using the remote computer software (Statistical Package for the Social Sciences [SPSS], Version 15.0, SPSS, Chicago IL). The obtained HCT measurement (BIOZ HCT (%) in figure 5.3) is high correlated to the clinical haematology analyzer measurement (CBC HCT (%) in figure 5.3). LR analysis shows that the new HCT quantification device has a linearity of 0.982, a Pearson's correlation coefficient of 0.964 and a coefficient of determination of 92.15% HCT. Coefficient of variation is 2.48±1.26% for the whole samples, with a worst-case scenario of 4.82%. In the bias analysis (figure 5.4) using BA statistical methodology, the electrical impedance method showed a higher HCT count when compared with CBC method. Results showed a very low bias of -0.45%, 2.46% SDD and 95% CI from -4.51% to 3.61%.

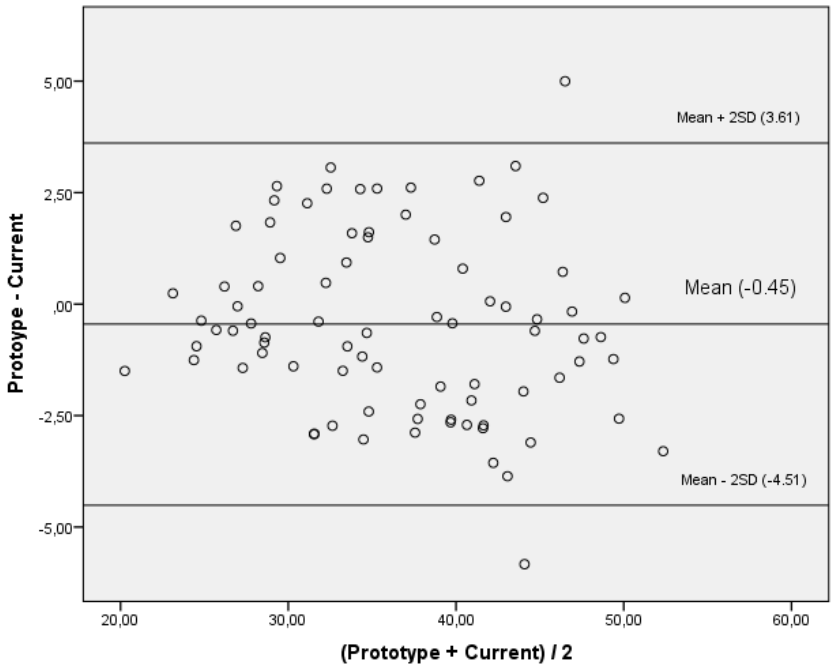

Figure 5.4: Bland Altman plot showing concordance of the tested methods with the reference method. Each dot represents the mean of difference in HCT values between the reference method and the test method with the x axis showing the HCT values of donors measured with the reference method and y-axis showing the variation of the mean difference with standard deviation. The two extreme lines mark two standard deviations from the central line adjacent to the 0 line, which represents the mean of difference in HCT values.

According to CBC results, 49 blood samples indicated low HCT levels (<40%); of these, 20 samples indicated the presence of critical HCT levels (<30%). Considering these limits for the detection of low (<40%) and very low (<30%) HCT levels, the device sensitivity and specificity values were of 90.0% and 98.4%, respectively, when detecting very low HCT levels (<30%), and 100% and 82.4%, respectively, when detecting low HCT levels (<40%).

5.4.3. Clinical assessment conclusions. Market survey.

The device exhibit reliable, robust and effective results using disposable commercial unlabeled sensors. Main advantages of the proposed device include; the facility of use; compactness and portability; rapidity and accuracy of results; and low-cost accessibility. The presented device outputs instantaneous reliable results based on electric voltage data directly correlated to HCT, and unlike actual clinical equipment for blood analysis, whole blood samples are not destroyed in the measurement process.

These system characteristics increase the versatility, functionality and applications, such as a PoC detector, a monitoring device for telemedicine applications, or as a controller of other clinical actuators. So, considering the increased system functionalities, and HCT being a major control determinant in different diseases and conditions, the device presents an increased versatility that makes it a very useful tool for different patients and applications, addressing some of the issues

related to the principle of operation of actual PoC devices for HCT detection, such as AnaemiaCheck (Express Diagnostics, Blue Earth, Minnesota); HemoPoint H2 (Alere, Waltham, Massachusetts) which is based on photometry; and i-SAT System based on conductometry. These three devices have shorter ranges of haematorcrit (%) measurement when compared with the proposed device (figure 5.5), and also are much slower methods of presenting similar detection performance results. In particular, the i-STAT analyser, despite providing lab-quality results for patient PoC testing, turns out to be less specific, involving a much more expensive and slower device. Harter et al., (2014) have also shown that the fairly basic HCT measurement performed by the i-STAT system was consistently and significantly lower than the values measured with the standard micro-capillary tubes and it was sensitive to the concentration of other non-conductive elements in the plasma, i.e. proteins and lipids [7].

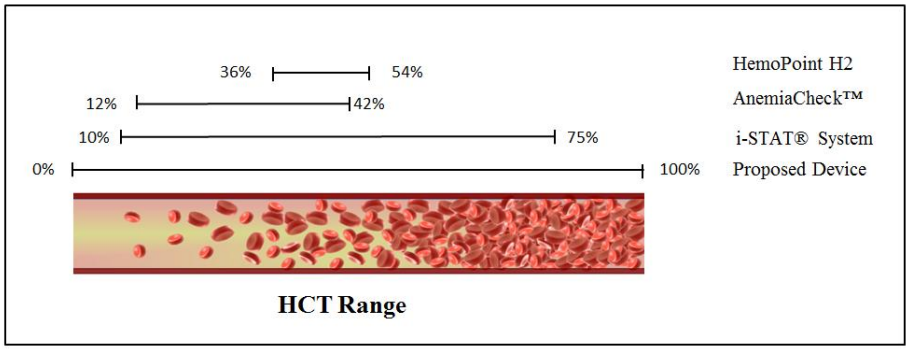

Figure 5.5: Comparison of commercial devices and their range of HCT detection.

Device	Sample Size (µL)	Test time (sec.)	Weight (g)	Principle	Range (HCT and Hb)	SD(%)	CV(%)	Status	Manufacturer
Proposed Device	50	<1	---	Impedance variations	HCT: 0% – 100%	1.17	3.27	Prototype	University of Barcelona
AnaemiaCheck™	50	900	---	Filtering	HCT: 12% – 42% Hb: 8-15g/dL	0.74	4.10	Marketed	Express Diagnostics, Blue Earth, Minnesota
STAT-Site	15	120	57	Reflectance photometry	Hb: 5.6 g/dL – 20.6 g/dL	---	4.20	Marketed	EKF Diagnostics
Hemo Point H2/ HemoControl	8	10-60	700	Optical absorption photometry	Hb: 0 g/dL – 25.6 g/dL HCT: 36% – 54%	---	1.5	Marketed	Alere, Waltham, Massachusetts
AnemoCheck	10	45	---	Chemical Colorimetric	Hb: 7.2g/dL - 16.3 g/dL	---	---	Pre-Clinical	Georgia Institute of Technology
HemoCue® Hb 201 DM System	10	60	350	A modified azidomethemoglobin method and photometry light absorption	Hb:0–25.6 g/dL (0–256 g/L, 0–15.9 mmol/L)	---	2.5	Marketed	Hemocue
DiaSpect Hb-system	<10	1-2	500	Photometry	Hb: 0–25,5 g/dl	---	3-3.9	Marketed	DiaSpect Medical GmbH
i-STAT® System	100	>60	---	Conducto-metry	HCT: 10%-75% Hb: 3.4-25.5 g/dL	0.50	1.5	Marketed	Abbott Point of Care Inc.
HemoSmart™	3	20	64	Biosensor based asperometric	Hb:4-20 g/dL haematocrit calculation is based on Hgb	---	---	Marketed	Apex Biotechnology Corp

Table 5.3: Comparison of Point-of-care devices for HCT and Hb detection

Other commercial or prototype stage devices such as STAT-Site (Stanbio Laboratory, Boerne, Texas), HemoPoint H2 (Alere, Waltham, Massachusetts), AnemoCheck (University of Georgia Tech), HemoCue® Hb 201 DM System (HemoCue), DiaSpect Hb-system (DiaSpect Medical GmbH) and HemoSmart™ (Apex Biotechnology Corp) are also used, but they are heavy, slower and based on haemoglobin detection (table 5.3). The proposed device has the lowest test time compared with the commercial PoC devices for anaemia detection, and is the only one that generates HCT values in a wide range and in a direct way. However, the sample size is still high compared with the rest of the devices, this being a property susceptible to be improved in future works, as the IA technique has been successfully carried out using Bayer glucometer reactive strips for 2 µL blood samples [8].

In summary, a PoC device for instantaneous HCT detection based on custom instrumentation electronics, IA technique and a disposable low-cost sensor has been designed, fabricated and tested. The device has been proved to exhibit reliable, robust and effective results using 50 µL whole blood samples.

Advantages of the proposed device include: (i) the facility of use; (ii) compactness and small size; (iii) portability; (iv) less invasive and less quantity of blood; (v) rapidity and accuracy of results; and (vi) low-cost accessibility. These characteristics are valuable for anaemia-risk patients, especially for pregnant women, neo-nates, pediatric patients and elderly, but also for chronically anemic patients, such as cancer patients receiving chemotherapy, patients with renal failure, patients with chronic inflammatory/immunologic disorders, or patients with primary hematologic disorders. The use of an ultra-low-cost disposable sensor, implies low manufacturing cost, and the accessible price are important advantages, especially in disadvantaged regions where the health domain is undervalued. Furthermore, unlike actual clinical equipment for blood analysis, whole blood samples are not destroyed in the measurement process and the adverse effects for patients and blood samples are being mitigated.

In summary, the presented device and its principle of operation based on electrical impedance show reliable results, while has been proved to address some of the issues of actual HCT PoC devices and introduces a new generation of medical PoC devices.

5.5. References

[1] Jani IV, Peter TF. “How PoC Testing Could Drive Innovation in Global Health” *N Engl J Med.*, vol. 368, no.24, pp. 2319-2324, June 2013.

[2] Luong JHT, Male KB, Glennon JD. “Biosensor technology: technology push versus market pull” *Biotechnol. Adv.*, vol. 26, pp. 492–500, 2008.

[3] Juanola-Feliu E, et al. “Design of a customized multipurpose nano-enabled implantable system for in-vivo theranostics” *Sensors*; vol. 14, no. 10, pp. 19275 – 19306, 2014.

[4] Juanola-Feliu E. et al. “Market challenges facing academic research in commercializing nano-enabled implantable devices for in-vivo biomedical analysis” *Technovation*, vol. 32, pp. 193–204, 2012.

[5] Corash L. Laboratory Hematology: Methods for the Analysis of Blood. In Blood: Principles and Practice of Hematology, 1st ed.; Handin, R.I., Lux, S.E., Stossel, T.P., Eds.; Lippincott Williams & Wilkins: Philadelphia, PA, USA, 1995; pp. 23–61.

[6] Tyburski E, Gillespie S. “Disposable platform provides visual and color-based PoC anaemia self-testing” *J. Clin. Invest.*, vol. 124, no. 10, pp. 4387–4394, 2014.

[7] Harter TS, Shartau RB, Brauner CJ, Farrell AP. “Validation of the i-STAT system for the analysis of blood parameters in fish” *Conserv. Physiol.*, vol. 2, no. 1, pp. 37–38, 2014.

[8] Hernández F, Guerrero C, Bernal J. “Determinación de las propiedades eléctricas en tejido sangíneo” *Ciencia UANL*, vol. 8, pp. 7-13, 2011.

Chapter 6

Discussion and Conclusions.

In this chapter, the results given in previous chapters are used to evaluate the feasibility of IA for cellular detection for PoC applications. These results will highlight the developed technology advantages as a biomedical device and how it could address the issues present on the actual PoC devices on the market, as well as its potential as a very interesting and functional application on LoC devices and bench-top biomedical apparatus.

6.1. Portable bioimpedance HCT monitoring PoC device.

The principle of impedance analyisis for diluted cell suspension monitoring has been proved using HCT as the target under consideration. The device has been proved to exhibit reliable, robust and effective results using label-free disposable commercial sensors using 50µL whole blood samples. Blood samples, collected from a single healthy donor, were used to demonstrate the IA technique feasibility to perform an easy, fast and sensitive HCT study using two different label-free commercial sensors. Furthermore, this technique overcomes some of the complications related to blood extractions used in conventional methods: haematoma formations, nerve damage, pain, haema-concentration, extra-vasation, iatrogenic anaemia, arterial puncture, petechiaes, allergies, infection, syncope and fainting, excessive bleeding, edema or thrombus.

Differences have been found on the impedance results when using different sensors with different sizes. However, these differences are minimal, and only related to the sensor size, involving different working frequency ranges and sensibilities, but pointing out that the sensing system could be very wide shaped, with minimal modifications regarding voltage output and working frequency needed for a proper monitoring.

Finally, the use of saline solution as a buffer for the RBCs dilution has no influence on the measurement, as it proved when compared with the blood plasma. This fact indicates that, as the state-of-the-art indicates, the current flow path across the blood sample is through the cells membrane. This is a very important fact, as the different elements found on blood plasma; such as proteins, glucose, etc., can be very different in quantity from one patient to another, and therefore, distorting the measurements performed.

Moreover, the digital lock-in performance, with measurement errors are below 10% for SNR up to -45 dB, noise levels 200 times higher than the signal amplitude, which means a great environmental noise rejection, as the whole blood samples are regarded as a very electrically noisy environment.

Finally, as a proof of concept, the device have been calibrated and validated with 48 whole blood samples, randomly collected from hospitalized patients in Hospital Clínic, as an instantaneous non-destructive anaemia detector device, using disposable label-free commercial sensors with low voltage biasing. The system has been evaluated through comparison with complete blood count (CBC) using a clinical haematology analyser (Advia 2120, Siemens AG, Madrid, Spain). The anaemia detection device has a linearity of 0.93 and an accuracy error of 1.75% with a correlation of 0.98. Coefficient of variation is below 5%, with a worst case resolution of 1.63%. When compared with actual commercial devices for PoC anaemia detection, it presented similar detection performance while being a much faster device, not destroying the whole blood samples. Moreover, it presents output data directly correlated to HCT on an external computer, for an easy and robust data management as a telemetric tool for patient monitoring both in self-screening and hospitalized patient environments.

6.2. Application on LoC devices. Escherichia coli detector / concentrator device.

The IA have been proved as a very adaptable technique for cellular screening. It has been validated through whole blood samples for HCT detection on a standalone monitoring device, but the results obtained pointed out the high degree of versatility of the technique, regarding different sensors, environments and functionalities. So, the IA technique and the back-end processing electronics have been applied to a LoC device for Escherichia coli concentration for real-time monitoring and control of the process, while outputting the concentration data for user operation. The IA technique and custom electronic were validated using a micro-fluidic chip with 4 integrated gold electrodes, specifically designed for the application, and an dielectrophoretic force generator to concentrate the samples on the chip, and the concentration and while real-time detection and control of the trapped bacteria inside the micro-fluidic chip have been proven, working a high flow injection rate, up to 10 µL/min. Moreover, the inclusion of an embedded software on a real-time platform, allow to overcome the issues regarding bacteria media conductivity variations, creating an automated protocol, integrated in the overall system, strengthening the system versatility and robustness.

These results obtained indicated the ability of the technique to reliably work with two very different cellular species in two very different environments; non manipulated whole blood samples, and laboratory processed cellular culture. The system's feasibility to interact with a microfluidic device and other supporting electronic devices for increased functionalities, pushing towards the development of automated LoC devices for cellular monitoring and manipulation.

6.3. HCT PoC device.

The proposed PoC device represents a novel device / technology for instantaneous screening of HCT, relying on straightforward instrumentation electronics and disposable label-free sensor. The method used is based on direct measurement from whole blood samples by means of its inherent

electrical bioimpedance and addresses some of the issues present on the actual PoC devices on the market, as well as the lack of devices for real HCT screening, as the majority of the available devices on the market make an indirect calculation regarding haemoglobin measurement.

The instantaneous HCT screening device has been studied through consecutive whole blood samples from 83 adult patients, and its impact on medical applications has been discussed. Accuracy, precision and correlation for the HCT screening results were analysed by comparing obtained results with haematology analyser (Advia 2120, Siemens AG, Madrid, Spain) CBC analysis. Collected data were analysed by means of Linear Regression (LR) analysis and Bland-Altman (BA) statistical methodology. As a result, the response, effectiveness and robustness of the portable PoC device has been proved, with a Pearson's correlation coefficient of 0.964 and a coefficient of determination of 92.15% HCT. Mean coefficient of variation is 2.48±1.26% for the whole samples, with a worst case scenario of 4.82%. Using BA statistical methodology, results showed a bias of -0.45%, a standard deviation of the differences (SDD) of 2.46%, and 95% limits of agreement from -4.51% to 3.61%.

On the market of PoC devices for HCT screening, the main principle of operation technique is based on biochemical reactions and biomarkers outputting visual based results or indirect estimated values. The proposed device outputs reliable results based on electric voltage data directly correlated to HCT, which entails several advantages. First of all, results are not open to user interpretation, as it is when the readout stages are optically represented, which addresses the subjective results due to visual interpretation by using a colour scale, making the device also unusable for colour-blind person. This issue leads sometimes to the inability of patients self-screening and decentralization of testing, increasing the clinic visits to ensure a proper results recording. The proposed device provide an easy straight-forward electronics for telemedicine applications, as the results could be easily and reliably processed with no interpretation error, in a general data base of patient self-screening results, as there is a great need for multipurpose and reliable telemetric tools that aim to improve patient quality of life while reducing manufacturing costs.

Moreover, the electrical voltage data can also be very valuable as a part of LoC devices, enabling increased functionalities on other biomedical devices as a controller for other biomedical actuators, or as a main part of whole blood multi-target detection, as the sample is not destroyed in the process, and the measurement is instantaneous, making it much faster than actual PoC biomedical devices on the market.

The use of chemical biomarkers and biochemical reactions, which often needs of sophisticated microfluidics, microelectronics and optical systems to be functional and reliable, involve some operational challenges due to its technological complexity, such as human resources and training, quality assurance, and equipment maintenance. The proposed device is not disposable, only the ultra-low-cost sensor is, and its label-free condition make it making it really cost-effective when used with chronically ill patients. In this context, the proposed device could not only improve the diagnosis and control of high prevalence diseases, but also reach difficult scenarios where clinics

are often many miles away from villages, where there is an absence of laboratory facilities and trained staff, or where there are hostile environmental conditions.

6.4. Future steps towards truly PoC devices and health monitoring applications.

The development of a PoC device, relying on IA, for cellular monitoring that uses straightforward electronics and ultra-low-cost disposable sensors, has been shown to be a feasible option after the obtained results, addressing some of the operational challenges of actual PoC devices, and the use of this type of technology make the next generation of devices for healthcare self-testing a step closer to a real implementation.

However, it must be contemplated the fulfilling of the standards for patient electrical safety (International Electrotechnical Commission 2010) or the Medical Devices Directives (European Comision 2007), while other types of requirements, such as usability, trustworthiness, system maintenance or interoperability must be studied.

The use of Information and Communication Technologies (ICT) as a tool for enhancing the quality, accessibility and efficiency of health care systems has been supported extensively by the European Commission since the launch of the action plan eEurope 2002 (European Commission 2000). As has been described before, in spite of the substantial progress in the field of PoC health devices, issues still exist, and they must be addressed to foster the opportunities for healthcare that the research contributions offer. The proposed technology envision the use of ICT and other technologies to enable a paradigm shift from the traditional hospital-centred healthcare delivery model toward a preventive and person-centred model, while addressing the present operational challenges of actual commercial PoC devices, conforming the basis of the next generation of healthcare devices, defined by:

a) Portable or implantable devices, which acquire, monitor and communicate physiological parameters and other health related context of an individual (e.g., vital body signs, biochemical markers, activity, emotional and social state, environment).

b) Intelligent processing of the acquired information and coupling of it with expert biomedical knowledge to derive important new insights about individual's health status.

c) Active feedback based on such new insights, either from health professionals or directly from the devices to the individuals, assisting in diagnosis, treatment and rehabilitation as well as in disease prevention and lifestyle management.

These defined characteristics are a good approach to identify the different elements that must be present in this type of technology. The underlying concept is to empower the individual's health responsibility while reducing the costs of the current healthcare system.

Appendix 1

Resum

Resum

L’objectiu de la tesi és la realització d’equipaments electrònics per aplicacions biomèdiques de caràcter Point-of-Care (PoC) en entorns d’investigació, control i tractament clínic. Aquest projecte es troba en el marc de les activitats de recerca del grup, on el desenvolupament d’electròniques d’interface amb el mon biomèdic i la recerca de noves tecnologies i aplicacions d’instrumentació són unes de les principals tasques que porten a terme. Donades aquestes consideracions, s’ha definit un camí dintre dels sistemes d’instrumentació PoC orientats al control d’agents biològics cel·lulars amb tècniques d’anàlisi d’impedància (IA). Aquests dispositius estan basats en dos conceptes claus: el disseny d’instrumentació electrònica senzilla, econòmica i de baix consum, així com sistemes de sensat versàtils i d’un sol us. D’aquesta manera, és possible desenvolupar equipaments versàtils, portables i de baix cost que poden aportar gran rendiment en diferents camps de la biomedicina.

Un dels principals objectius d’aquesta tesis es abordar els diferents problemes i desavantatges que presenten els dispositius biomèdics PoC que existeixen actualment al mercat, així com desenvolupar les tecnologies necessàries per adreçar aquestes problemàtiques a la vegada que s’estableixen una sèrie de tecnologies y protocols encaminats cap al desenvolupament d’un nou estàndard de dispositius per al control d’espècies cel·lulars.

Aquests estàndards venen marcats per dos vessants molt concretes, les quals agrupem de la següent manera; millora de l’assistència medicosanitària, i establiment de tecnologies per a la integració en futures aplicacions.

a) Millora de l’assistència medicosanitària.

Dintre d’aquest primer grup s’inclouen l’anàlisi i millora dels procediments y dispositius actualment en us. En el escenari actual, les tecnologies de diagnòstic clàssiques no són molt adequades per satisfer les necessitats de monitorització sanitària. Les proves de laboratori requereixen una infraestructura complexa, tècnics especialitzats, i un subministrament estable d'electricitat, tots els quals són escassos, especialment a les zones no urbanes. A més a més, un anàlisi tradicional es realitza generalment en laboratoris remots, el que augmenta el cost i la inconveniència de tenir accés a l'atenció de salut i condueix a un elevat nombre de pacients que abandonen el sistema abans d'establir un diagnòstic.

Aquestes limitacions han de ser solucionades amb la introducció de dispositius PoC cada cop més fiables, tot i que encara es necessitaran proves de laboratori convencional i microscòpia, els quals tenen un paper cada vegada més gran en l'atenció sanitària de molts països, especialment en aquells amb ingressos baixos i mitjans.

Tot i això, encara hi ha moltes àrees de millora dintre d'aquest camp, on hi ha quatre àrees clau a millorar en els sistemes de salut mitjançant noves generacions de dispositius; sistemes operatius millorats, serveis clínics simplificats i estandarditzats, gestió centralitzada de dades per monitorització de pacients y millora dels protocols d'assistència i les iniciatives de descentralització i promoció de l'autodiagnosi. La millora en aquestes àrees implicaria una millora molt important en la qualitat de l'assistència sanitària, la millora de les eines de diagnosi, tractaments i controls més freqüents i exhaustius, així com una important reducció en els costos de l'assistència mèdica.

Aquestes àrees de millora clau, son motivades tant per factors administratius, com per les pròpies limitacions dels dispositius presents actualment al mercat. En aquesta tesis volem investigar els efectes d'aquestes limitacions dels dispositius PoC actuals i a la vegada definir una tecnologia que ajudi al desenvolupament d'uns dispositius que ajudin a desenvolupar eines dintre del marc de millora que hem descrit abans.

b) Establiment de tecnologies per a la integració en futures aplicacions.

Avui en dia, una gran diversitat de camps de treball i investigació convergeixen a la integració de les tecnologies mèdiques amb altres disciplines com la microfluídica, la bioquímica, la electroquímica, la nanotecnologia, així com la pròpia electrònica, el que permet el desenvolupament de dispositius biomèdics capaç de diagnosticar i / o tractar agents patológics mitjançant la detecció, quantificació i seguiment d'espècies mòbils en diferents mitjans conductors. Aquests avenços en àrees tan diverses obren les portes a una sèrie de dispositius diferents, amb aplicacions molt específiques, com son els dispositius point-of-car (PoC), lab-on-a-chip (LoC), òrgan-on-a-chip (OaC), dispositius d'implantació en el propi cos humà, etc.

Un objectiu molt important d'aquesta tesi es estudiar noves tecnologies i procediments que convergeixin amb els camps d'investigació més importants per tal d'aportar funcionalitats avançades als dispositius abans esmenats. Aquestes funcionalitats poden ser molt diverses, però es poden dividir de dues maneres, quantitatives i qualitatives.

Actualment, els dispositius LoC ens permeten realitzar assajos clínics d'una manera molt més ràpida i estandarditzada, el qual permet al personal biomèdic realitzar proves i assajos d'una manera senzilla i de baix cost, ja sigui per l'estudi d'infermetats, el desenvolupament de fàrmacs i tractaments, el control mediambiental d'espècies contaminants, etc. A més a més, la implementació de dispositius OaC ens permet emular el comportament biològic y físic de diferents òrgans, i poder estudiar d'una manera molt més senzilla econòmica el comportament i influencia de certes malalties, així com la eficiència dels medicaments i tractaments dissenyats per la seva cura.

Tot i les grans avantatges que ens aporten aquestes noves tecnologies i dispositius, encara hi han grans desavantatges a tenir en compte. Primer de tot, la visualització i monitorització de resultats obtinguts de la utilització d'aquest tipus de dispositius, així com la seva validació i manteniment, s'han de fer mitjançant eines de laboratori clàssic com microscopis, equips de compte cel·lular, equips de citometria, etc. El fet de no tenir un sistema de sortida de dades en temps real, y de manera automàtica, implica un desconeixement de l'estat de l'experiment durant la realització del

mateix, el que comporta una manca d'informació necessària per a l'estudi complert del experiment i una manca funcionalitats automatitzades que aportaria una major autonomia i diversitat d'aplicacions al dispositiu, com poden ser la inclusió d'un sistema actuador, com alarmes, el control de les bombes per la injecció dels diferents analits i elements necessaris per el test, la comunicació de totes les dades necessàries per un anàlisi in situ en un dispositiu intel·ligent extern, com un ordinador o una tablet, etc.

Finalment, s'ha de considerar una tecnologia que sigui fàcilment integrable dintre d'un ASIC el que permetria desenvolupar dispositius integrables en el cos humà.

Per assolir aquests objectius s'han de considerar diversos factors molt importants. Per començar, es necessari una tecnologia amb versatilitat per a la detecció de diferents especies cel·lulars, tenint en compte, quan integrem diferents tecnologies, la versatilitat en les condicions de treball per detectar la espècie cel·lular; hi han diferents ambients i espais sensorials molt petits (de l'ordre de nanòmetres), interaccions amb les tecnologies associades, etc. Un altre factor d'extrema importància es la no interacció del sistema de mesura, monitorització i control amb la mostra sota anàlisi. Finalment, les electròniques i els protocols desenvolupats han de ser senzills, robustos i fiables, així com rendibles per a la integració dintre d'aquesta gran varietat de dispositius i aplicacions.

Amb aquestes premisses, s'ha desenvolupat un equipament d'anàlisi d'impedància independent del sistema de sensat, el que comporta la possibilitat d'utilitzar multitud de tipus de sistemes de sensat així com l'anàlisi de diferents especies cel·lulars. Aquest equipament, consta d'una senzilla instrumentació electrònica basada en un sistema de sensat preparat per diferents tipus de sensors, tot controlat per un microprocessador encarregat del control automatitzat del hardware, post-processat de dades i comunicació amb un ordinador remot. El sistema és capaç de treballar en un rang de freqüències molt ampli, amb diferent tipus de potència de senyal i diferent tipus d'anàlisi i representació, com ara diagrames de Bode i Nyquist, o la selecció de punts de freqüencials concrets per un tipus d'anàlisi més específic per a un experiment biomèdic més concret, senzill i ràpid. Es tracta d'un equipament econòmic, fiable i senzill, que aporta avenços com la gran capacitat d'integració en ambients clínics, la possibilitat de fer un control medico sanitari instantani i reportar telemàticament els resultats o la possibilitat d'implementar un sistema de control mèdic integrat i automatitzat. També hem considerat diferents sistemes d'instrumentació i sistemes de sensat, per així estudiar la tecnologia electrònica, la tècnica de anàlisi d'impedància i la capacitat de millorar les diferent limitacions en l'actual assistència medicosanitària.

D'aquesta manera, s'han obert dos camps d'experimentació i aplicació:

1.1 Control i sensat d'hematòcrit per detecció d'anèmia.

Amb el dispositiu descrit anteriorment preparat per a la detecció, mitjançant impedància, d'agents biològics cel·lulars, es va utilitzar en una sèrie d'experiències per a la detecció d'anèmia. L'Organització Mundial de la Salut (OMS) defineix l'anèmia com l'etapa en què la quantitat d'hematòcrit a la sang cau per sota de cert llindar definit per a determinats grups de població, sent considerat un problema mundial associat amb molts factors. Segons l'OMS, 1620 milions de persones, el 24,8% de la població mundial, es veuen afectats per l'anèmia. Els comptadors

hematològics automatitzats proporcionen, amb un alt grau de precisió, la informació necessària per a la detecció d'anèmia, el que representa una eina molt útil per avaluar els donants tant com a rutina com amb situacions complexes de laboratori. No obstant això, l'accés a aquest equipament és un problema en els països en desenvolupament, on els equips i tècniques d'avaluació menys fiables estan disponibles. D'aquesta manera, l'aplicació d'un equipament Point-of-Care senzill amb sensors d'un sol ús i econòmics suposaria un avenç en el control de l'anèmia, una malaltia molt estesa i fàcil de contraure. Com l'hematòcrit és el percentatge del volum de la sang que fa referència a la fracció dels glòbuls rojos, la quantitat d'hematòcrit es pot discernir a partir de l'anàlisi d'impedància. S'ha desenvolupat un equip autònom que consta d'un sensor d'un sol us, una instrumentació electrònica senzilla i de baix consum i un software embebit per al processament i transmissió de les dades a un ordinador extern.

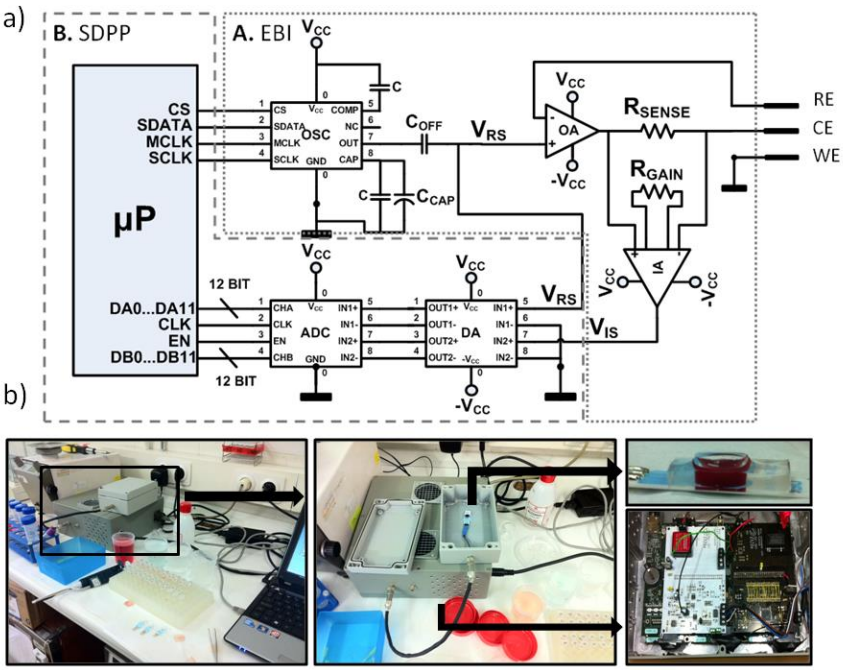

Figura 1: Prototip del dispositiu i tecnologia de detecció d'impedància i el set-up de mesura. (a) Esquemàtic electrònica, A: Electrodes Biasing Module; B: Signal Digitalization and Post-Processing. (b) Prototip dispositiu: Dos PCBs i una tarja sbRIO 9632 (National Instruments), tot en una caixa de faraday. Set-up experimental: Sensor d'un sol us; instrumentació electrònica i ordinador extern.

D'aquesta manera, s'han fet una sèrie d'experiències de validació amb l'equipament d'anàlisi d'impedància i sensors comercials de 3 elèctrodes i capacitat de 50 µL de mostra de sang (l'equivalent a una gota de sang) per evitar grans volums de mostra que puguin agreujar o induir l'anèmia. Aquestes experiències s'han dut a terme a l'Hospital Clínic de Barcelona on hem comptat amb la col·laboració del personal de recerca de l'hospital que ens ha proporcionat mostres de sang de pacients reals.

El dispositiu dissenyat va ser validat a través d'experiències d' espectrometria d'impedància per a cada mostra de sang sencera descrit . Muntatge experimental es representa a la figura 1. Totes les mesures s'han realitzat a temperatura ambient de laboratori clínic.

En primer lloc , es va mesurar un espectre d'impedància completa per a un grup de 10 mostres de sang sencera. A la figura 2 mostra la magnitud obtinguda impedància (figura 2.a) i la fase (figura 2.b) en un diagrama de bode. Hem observat que, tant en la magnitud de la impedància com la fase, hi ha una diferència entre els resultats d'impedància per a diferents mostres en intervals de freqüència específics.

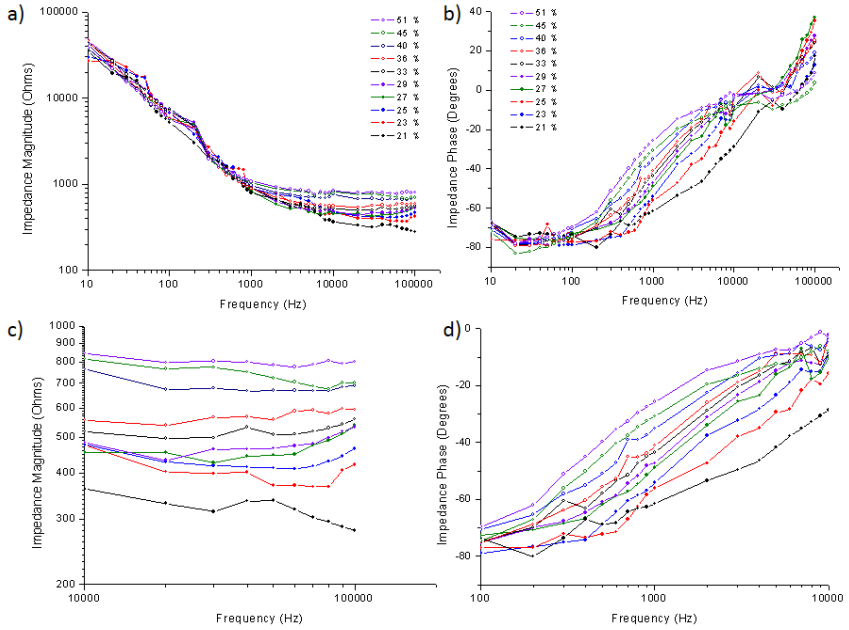

Figura 2: Mesura del mòdul i la fase de la impedància. a) Mòdul de impedància i b) fase de la impedància en tot l'espectre mesurat. c) Mòdul de impedància i d) fase impedància al rang de les freqüències de treball.

Per tant, les diferències d'impedància mesurats han de ser definits com increments de impedància relacionats amb increments d'HCT. No obstant això, aquest fenomen no està present en tota la gamma de freqüència definit en la literatura, 10 Hz a 100 kHz, però en una més específica. Així, hem definit rangs de treball en funció de la correlació entre la IA i HCT. En termes de magnitud de la impedància (figura 2c) el rang de treball de freqüència està en el rang de 10 kHz a 100 kHz i per a la fase d'impedància (figura 2.d) és en el rang d'1 kHz a 10 kHz. Tot i ser treballar amb mostres de sang sencera, els rangs de freqüència són invariablement el mateix es troba en l'estudi anterior.

És interessant poder determinar magnitud de la impedància i de fase per a diferents mostres de diferències HCT sobre una àmplia gamma de treball de freqüència. Es dóna la flexibilitat i la redundància de dades al sistema, sempre que no és única resposta depenent de la freqüència, el que fa que les tècniques d'anàlisi de dades estadístiques simples, com ara ajust lineal, factible, resultant ser un dispositiu més robust i fiable.

Per tant, una vegada que ha suposat que mesura increments de impedància, en el rang de freqüència de treball definit, estan relacionats amb la subhasta mostres de sang HCT, hem de determinar la capacitat del sistema per a la detecció d'HCT, resolució i sensibilitat.

Per tal de calibrar l'equip i la tecnologia s'han estudiat les mostres de sang mitjançant una regressió lineal de la mesura d'impedància enfront del percentatge d'hematòcrit present a les mostres com es pot veure a la figura 3.

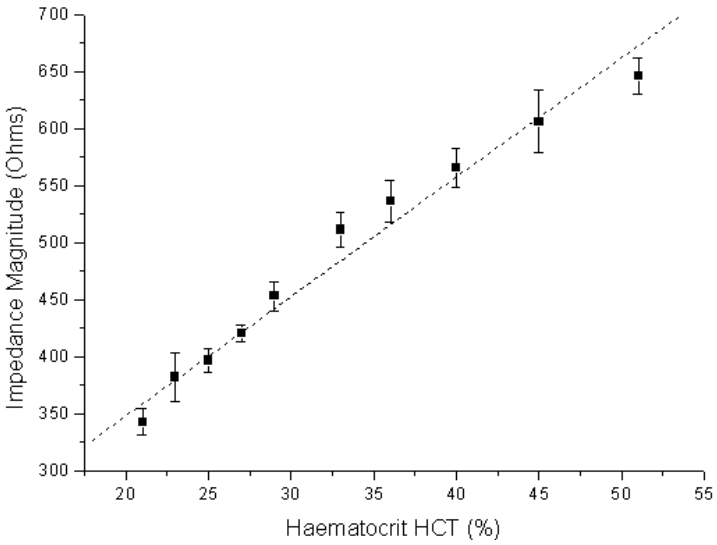

Figura 3: Mòdul d'impedància mesturat respecte al hematòcrit (HCT (%)) de les mostres de sang recollides. Corba de calibratge.

El sistema de detecció d'hematòcrit, amb el sistema de sensat corresponent, presenta una sensibilitat de 10.46 Ω/% i un error de 1.13 % amb una correlació de 0.987. El coeficient de variació es inferior al 5% en tots els casos. Amb aquestes dades de la regressió lineal, hem calibrat el sistema i hem fet un software embebit que calcula l'hematòcrit detectat i el mostra per pantalla de manera instantània.

Hem validat aquest sistema mitjançant 38 mostres de sang recollides de manera aleatòria i hem valorat el valor d'hematòcrit donat per el nostre equip considerant com a referència un equip hematològic homologat de l'hospital clínic (Advia 2120, Siemens AG, Madrid, Spain).

A la figura 4 podem veure la comparativa de resultats entre el valor d'hematòcrit calculat per el nostre equip (DHCT(%)) i el valor donat per l'equip homologat (CHCT (%)). El nostre equip presenta gran precisió al detectar hematòcrit, amb una linealitat de de 0.93, un error relatiu del 1.75% i una correlació de 0.98. El valor mitjà del coeficient de variació es de 3.27%.

Els resultats han estat satisfactoris, aconseguint un sistema econòmic, portable, acurat i robust per la detecció d'anèmia dintre dels estàndards de calibratge dels equipaments mèdics per anàlisi de sang, que a més a més es un assaig instantani, no destructiu i amb aplicacions telemàtiques

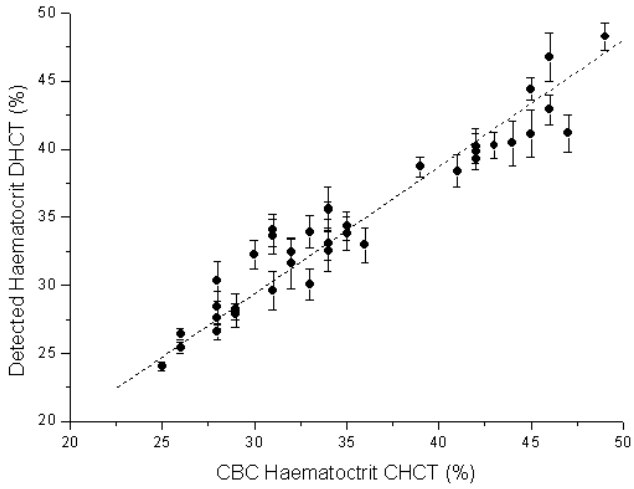

Figura 4: Mesura d'hematòcrit del nostre equip (DHCT (%)) comparada amb la mesura d'hematòcrit obtinguda mitjançant un anàlisi CBC d'un comptador hematològic (CHCT (%)). Les barres d'error representen la desviació estàndard de cinc repeticions.

1.2 Sistema autònom Lab-on-a-Chip per concentració bacteriana.

Considerant les característiques portables i versàtils del equipament i la seva capacitat d'adaptació a multitud de sistemes de sensat diferents, s'han dut a terme unes experiències en sistemes microfluidics Lab-on-a-Chip (LoC) amb diverses funcionalitats integrades per al control de l'aplicació i la monitorització de resultats en temps real. Aquest sistema global, consta d'un dispositiu microfluídic d'atrapament i concentració de bactèries i un mòdul electrònic d'aplicació dielectroforètica que combinat amb la lectura de concentració bacteriana i etapa de software embebit proporciona un equipament capaç de concentrar i controlar un cultiu bacterià de manera autònoma i en temps real, així com detectar de manera autònoma el valor de les concentracions bacterianes en suspensió en un medi controlat.

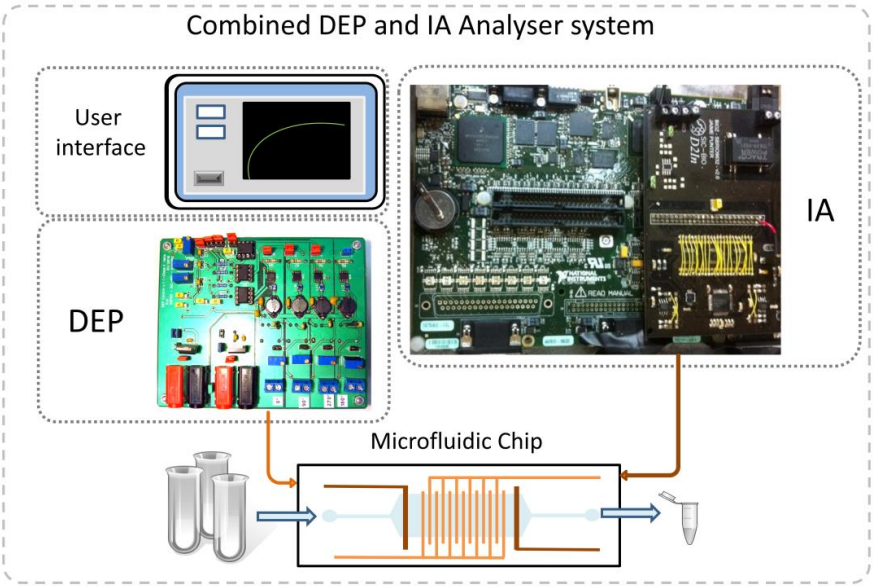

Figura 5: Sistema LoC combinat.

D'aquesta manera, s'ha creat un protocol automatitzat per a la mesura i concentració de poblacions de Escherichia coli. En el dispositiu LoC resultant, el dispositiu electrònic controla de manera automatitzada la acció del sistema de concentració i el sistema de injecció de mostra en el chip microfluídic, mentrestant controla la població dintre del chip mitjançant la lectura de impedància, mesura que es reportada mitjançant la pantalla d'un ordinador a l'usuari. Aquest procés de detecció i concentració ha demostrat ser viable a diferents freqüències de treball, com es pot veure a la figura 6, amb una precisió del 2%, un coeficient de variació de 3.1% i una correlació de 0.988.

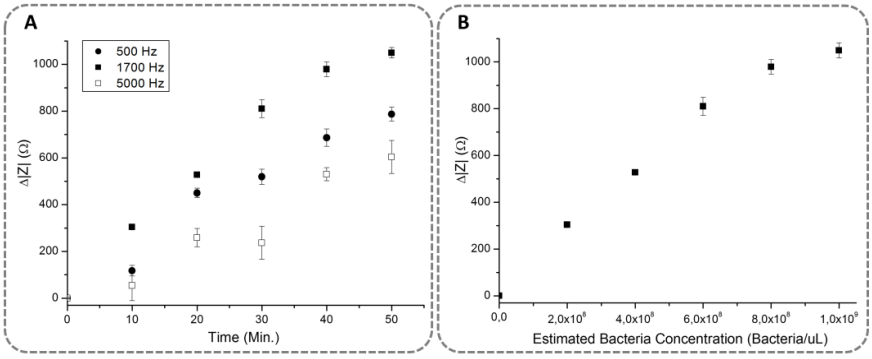

Figura 6: a) La magnitud d'impedància mesura els canvis durant la concentració de la mostra bacteriana en el xip. b) Mesures de magnitud d'impedància en 1.700 Hz en relació amb les concentracions de bactèries.

1.3 Sistema de detecció PoC d'hematòcrit.

S'ha dissenyat un dispositiu electrònic instantani, fiable i rendible com a principi per una nova generació de dispositius PoC per a la detecció i monitorització d'hematòcrit que correlaciona directament una senyal de sortida de tensió amb els nivells d'hematòcrit, el qual té una gran versatilitat. Pot ser utilitzat com a sistema de control rutinari per pacients a casa, aplicacions telemàtiques per estudis clínics y controls centralitzats de seguiment de pacients i una sèrie de funcionalitats per a integració en altres dispositius biomèdics i LoC. El seu principi de funcionament està relacionat amb les propietats d'impedància elèctrica inherents de cèl·lules de la sang, evitant l'ús de biomarcadors químics, pel que és més rendible, fàcil d'operar, i resulta en un dispositiu de mesura no destructiu, millorant el seu rendiment i funcionalitats. Aquest dispositiu, i el seu principi de funcionament, ha estat comparat amb altres dispositius de detecció hematòcrit en el mercat, per tal d'adreçar els problemes que es troben amb la seva utilització.

Al mercat dels dispositius PoC per a la detecció de l'hematòcrit, el principi fonamental de funcionament es basa en les reaccions bioquímiques i biomarcadors, donant els resultats obtinguts amb senyals visuals o valors de estimació indirecte. Una sortida amb un valor de voltatge directament correlacionat amb hematòcrit proporciona diversos avantatges, com ara que els resultats no son oberts a la interpretació de l'usuari, com quan les dades obtingudes són representades òpticament, i a més a més obtenim una major versatilitat en termes d'aplicacions, quan es compara amb altres dispositius comercials, com ara un detector PoC de hematòcrit, un dispositiu de vigilància per a aplicacions de telemedicina, o com un controlador d'altres actuadors clínics. A més, a diferència dels equips clínics al mercat i els dispositius PoC relacionat amb l'anàlisi de sang, les mostres de sang no són destruides en el procés de mesurament, i aquest procés de mesura basat en la detecció d'impedància es realitza de manera instantànea, fent d'aquesta tecnologia una solució adequada per a la integració en altres dispositius com dispositius LoC o equips clínics de sobretaula per a una major funcionalitat. A més, el dispositiu no és totalment rebutjable, només el sistema de sensat d'ultra baix cost, que consisteix en elèctrodes impresos sense cap tipus de de biomarcador o microfluídica; pel que és un dels dispositius econòmics disponibles.

Hem testejat el dispositiu de detecció d'hematòcrit amb mostres de sang consecutives de 83 pacients adults. La exactitud, precisió i correlació dels resultats de la detecció d'hematòcrit s'han analitzat mitjançant la comparació dels resultats obtinguts amb un analitzador de hematologia que utilitza la técnica CBC (ADVIA 2120, Siemens AG, Madrid, Espanya). Les dades recollides van ser analitzades amb la metodologia estadística de la regressió linial (LR) i de l'anàlisi de Bland-Altman (BA). Cada mostra de sang es va testejar 10 vegades a fi d'analitzar l'exactitud i precisió. L'anàlisi LR mostra que el nou dispositiu detector d'anèmia té una linealitat de 0,982, coeficient de correlació de Pearson de 0,964 i un coeficient de determinació de 92,15% d'hematòcrit. El coeficient de variació és de 2.48 ± 1.26% per al conjunt de les mostres, amb el pitjor dels casos de 4,82%. Utilitzant la metodologia estadística BA, els resultats van mostrar un bias de -0.45%, una desviació estàndard de les diferències (SDD) de 2,46%, i 95% els límits d'acord de -4.51% a 3.61%.

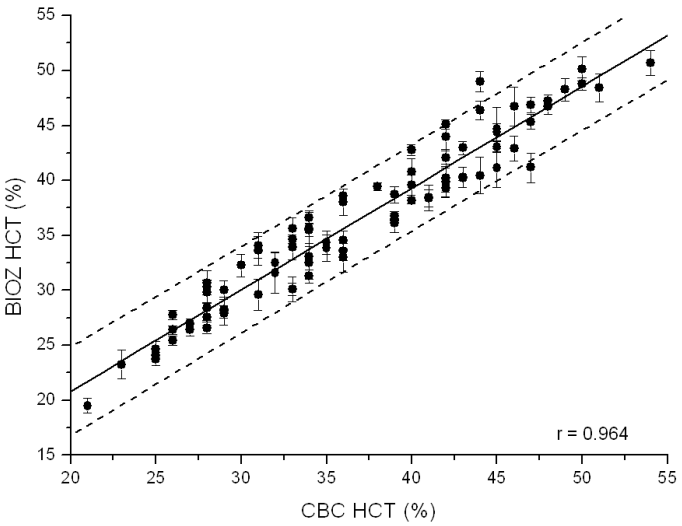

Figura 7: Estudi clínic del dispositiu de mesura de hematòcrit (BIOZ HCT (%)) respecte als valors d'hematòcrit proporcionats per un comptador hematològic (CBC HCT (%)) per un conjunt de mostres de sang de 83 pacients (n=10).

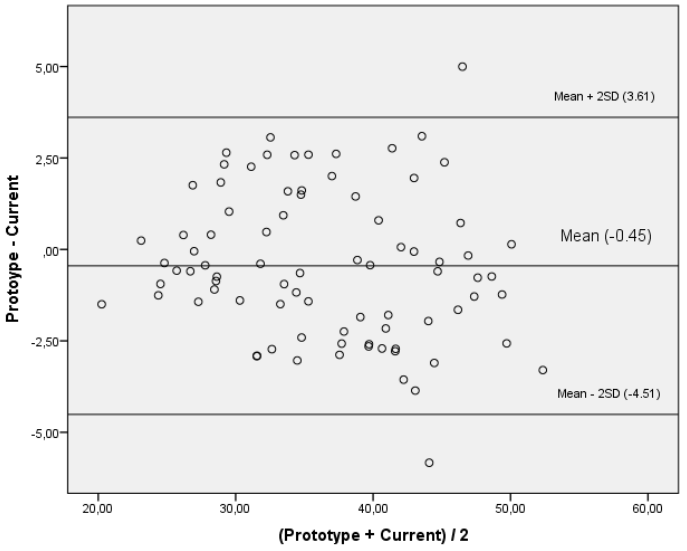

Figura 8: Diagrama de Bland Altman mostrant la concordança dels mètodes provats amb el mètode de referència . Cada punt representa la mitjana de diferència en els valors HCT entre el mètode de referència i el mètode d'assaig amb l'eix x mostra els valors de HCT de donants mesurats amb el mètode de referència i l'eix i mostra la variació de la diferència mitjana amb desviació estàndard. Les dues línies extremes marquen dues desviacions estàndard de la línia central adjacent a la línia 0, el que representa la mitjana de diferència en els valors d'HCT.

.

El dispositiu PoC de detecció d'hematòcrit es mostra com una solució econòmica, fiable, sensible i robusta. El dispositiu presentat ens permet fer mesures d'hematòcrit instantanis, emetre resultats fiables en base a dades de tensió elèctrica, fàcilment representables i fiables per enviar mitjançant eines telemètriques; millorant el rendiment dels dispositius actuals per a l'autodiagnosi de pacients, la detecció multi-objectiu degut a la no destrucció de les mostres, i les aplicacions de telemedicina per al seguiment de pacients amb malalties cròniques, el que representa un avenç significatiu cap a una nova generació de dispositius PoC.

List of Publications

JOURNALS

Authors: Punter-Villagrasa, J. ; Cid, J. ; Colomer-Farrarons, J. ; Rodriguez-Villarreal, I. ; Miribel-Catala, P.L.
Title: Toward an Anemia Early Detection Device Based on 50 µL Whole Blood Sample
Journal: IEEE Transactions on Biomedical Engineering
Volume: 62 **Number:** 2 **Pages:** 708-716 **Year:** 2015 **ISSN:** 0018-9294

Authors: Jaime Punter-Villagrasa, Joan Cid, Cristina Páez-Avilés, Ivón Rodríguez-Villarreal, Esteve Juanola-Feliu, Jordi Colomer-Farrarons and Pere Ll. Miribel-Català
Title: An Instantaneous low-cost point-of-care anemia detection device
Journal: Sensors
Volume: 15 **Number:** 2 **Pages:** 4564-4577 **Year:** 2015 **ISSN:** 1424-8220

Authors: Del Moral-Zamora, Beatriz; Punter-Villagrassa, Jaime; Oliva-Brañas, Ana M.; Álvarez-Azpeitia, Juan Manuel; Colomer-Farrarons, Jordi; Samitier, Josep; Homs-Corbera, Antoni; Miribel-Català, Pere Ll.
Title: Combined dielectrophoretic and impedance system for on-chip controlled bacteria concentration: Application to *Escherichia coli*
Journal: Electrophoresis
Volume: 36 **Number:** 9-10 **Pages:** 1130-1141 **Year:** 2015 **ISSN:** 0173-0835

BOOKS

Authors: Punter-Villagrasa, J.; Colomer-Farrarons, J.; Miribel-Català, P.; Puig-Vidal, M.; Samitier, J.
Title: Discrete to full custom ASIC solutions for bioelectronic applications
Book: VLSI Circuits and System V (Proceedings Volume)
Editorial: Proc. SPIE **Editors:** Teresa Riesgo; Eduardo de la Torre-Arnanz
Volume: 8027 **Year:** 2011 **ISBN:** 978-0-8194-8656-1

Authors: Punter-Villagrasa, J.; Colomer-Farraronsa, J.; Miribel-Català, P.Ll.
Title: Chapter 10. Bioelectronics for Amperometric Biosensors
Book: State of the Art in Biosensors - General Aspects
Editorial: InTech Open Access Publisher **Editor:** Toonika Rinken
Pages: 241-274 **Year:** 2013 **ISBN:** 978-953-51-1004-0

Authors: Punter-Villagrasa, J.;del Moral-Zamora, B.; Colomer-Farrarons, J.; Miribel-Català, P.; Cid.J.; Rodríguez-Villareal, I.; Prieto-Simón, B.
Title: Towards a portable point-of-use blood analysis with EIS technique device.
Book: Proc. Multi-Conference on Systems, Signals & Devices (SSD), 2014 11th International
Editorial: IEEE
Pages: 1-6 **Year:** 2014 **ISBN:** 978-1-4799-3865-0

Authors: Punter-Villagrasa, J. ; del Moral-Zamora, B. ; Colomer-Farrarons, J. ; Miribel-Catala, P. ; Cid, J. ; Rodriguez-Villarreal, I. ; Prieto-Simon, B.
Title: A portable point-of-use EIS device for in-vivo biomedical applications.
Book: Design of Circuits and Integrated Circuits (DCIS), 2014 Conference on
Editorial: IEEE
Pages: 1-6 **Year:** 2014 **DOI:** 10.1109/DCIS.2014.7035532

Authors: Punter-Villagrasa, J.; Cid, J.; Colomer-Farraronsa, J.; Rodríguez-Villarreal, I.; Miribel-Català, P.Ll.
Title: Chapter 10. Bioimpedance Technique for Point-of-Care Devices Relying on Disposable Label-Free Sensors - An Anemia Detection Case
Book: Biosensors - Micro and Nanoscale Applications
Editorial: InTech Open Access Publisher **Editor:** Toonika Rinken
Pages: 290-319 **Year:** 2015 **ISBN:** 978-953-51-2173-2

CONFERENCES

Authors: Punter-Villagrasa, J.; Colomer-Farrarons, J.; Miribel-Català, P.; Samitier, J.
Title: A low-voltage low-power CMOS analog Bio-Impedance Analyzer for implantable devices
Conference: DCIS 2010: 25th Conference on Design of Circuits and Integrated Systems.
Place: Lanzarote, Spain.
Date: 17-19 November 2010.

Authors: Punter-Villagrasa, J.; Colomer-Farrarons, J.; Miribel-Català, P.; Puig-Vidal, M.; Samitier, J.
Title: Discrete to Full Custom ASIC solutions for Bioelectronics Applications
Conference: SPIE 2011.
Place: Prague, Czech Republic.
Date: 18-20 April 2011.

Authors: Punter-Villagrasa, J. ; del Moral-Zamora, B. ; Colomer-Farrarons, J. ; Miribel-Catala, P. ; Cid, J. ; Rodriguez-Villarreal, I. ; Prieto-Simon, B.
Title: Towards a portable point-of-use blood analysis with EIS technique device.
Conference: SSD 2014. 11th International Multi-Conference on Systems, Signals & Devices.
Place: Castelldefels, Spain.
Date: 11-14 February 2014.

Authors: Punter-Villagrasa, J. ; del Moral-Zamora, B. ; Colomer-Farrarons, J. ; Miribel-Catala, P. ; Cid, J. ; Rodriguez-Villarreal, I. ; Prieto-Simon, B.
Title: A portable point-of-use EIS device for in-vivo biomedical applications.
Conference: DCIS 2014: 29th Conference on Design of Circuits and Integrated Systems.
Place: Madrid, Spain.
Date: 26-28 November 2014.

Authors: Punter-Villagrasa, J. ; Paez-Avilés, C. ; Colomer-Farrarons, J. ; Lopez-Sanchez, J. ;Miribel-Catala, P. ; Cid, J. ; Juanola-Feliu, E. ; Rodriguez-Villarreal, I. ; Prieto-Simon, B. ; Kitsara, M. ; Aller-Pellitero, M. ; Sabaté, N. ; del Campo, F. J.
Title: A Portable Point-of-Care Device for Multi-Parametric Diabetes Mellitus Analysis.
Conference: IECON 2015: 29th Conference on Design of Circuits and Integrated Systems.
Place: Yokohama, Japan.
Date: 9-12 November 2015

Appendix 2: Journal Publications.

Publication 1.

Toward an Anemia Early Detection Device Based on 50 µL Whole Blood Sample.

Punter-Villagrasa, J.; Cid, J.; Colomer-Farrarons, J.; Rodriguez-Villarreal, I.; Miribel-Catala, P.L.

IEEE Transactions on Biomedical Engineering, vol. 62, no. 2, pp. 708-716, February 2015.

Towards an Anaemia Early Detection Device Based on 50µl Whole Blood Sample.

Jaime Punter-Villagrasa, Joan Cid, Jordi Colomer-Farrarons, Ivón Rodríguez-Villarreal, and Pere Ll. Miribel-Català.

***Abstract*— A first approach to a portable and compact device for point-of-care early instantaneous detection of anaemia is described. This device works directly with whole blood samples relying on haematocrit analysis by means of impedance analysis. This device consists of a custom electronic instrumentation, post processing software and plug-and-play disposable sensor. The designed electronics are connected to a remote computer, which allows control of the instrumentation and results displaying with a user friendly software panel. The disposable sensor is based on a low-cost label-free three gold electrode commercial sensor for 50µL volume samples. 48 whole blood samples, randomly collected from hospitalized patients in Hospital Clínic, were used to validate the device capability for anaemia detection. Whole blood samples were distributed in two groups; 10 samples for system calibration, and 38 samples for system validation. To calibrate the device, a complete EIS experiment has been performed to get a full impedance spectrum analysis, defining an accurate frequency working range for haematocrit detection. Afterwards, we developed a protocol for instant impedance detection to determine the system detection accuracy, sensitivity and coefficient of variation. As a result, impedance variations between different samples have been detected with less than 2% accuracy error for both impedance magnitude and phase. A haematocrit detection algorithm, relying on impedance analysis, has been developed based on the previous studies. The response, effectiveness and robustness of the portable point-of-care device to detect anaemia have been proved with an accuracy error of 1.75% and a coefficient of variation of less than 5%.**

***Index Terms*—Whole Blood, Haematocrit, Anaemia, Impedance Analysis, Electronics, Point-of-Care.**

I. Introduction

THE World Health Organization (WHO) defines anaemia as the stage at which the amount of haemoglobin in blood drops below a certain WHO threshold for specified population groups, being considered a worldwide problem associated with many factors [1]. According to the WHO, 1.62 billion people, which correspond to 24.8% of the global population, are affected by anaemia [2]. Measurement of Hb concentration is considered the most reliable anaemia indicator and it is widely utilized in national demographic health surveys and by national governments surveying populations [1]. Also, evaluation of the Hb concentration in possible blood donors is a required condition in most countries to prevent blood collection from a donor with significant anaemia being, generally, the only laboratory control test performed before donation [3]. Blood donation is the only source of support to patients who require blood transfusion but, on the other hand, frequent donations may lead to iron deficiency in blood donors, especially females [4]. Hb is an iron-containing protein responsible for transporting oxygen in the blood and it is the main component of red blood cells (RBCs). Haematocrit is the proportion of blood volume occupied by RBCs and is determined by cell number and size, so haematocrit numbers below a certain reference range may indicate anaemia or abnormal cell development.

New non-invasive methods are being studied and developed for Hb screening but have been demonstrated to have lower precision and sensitivity level [3]. These different factors are drivers for the development of point-of-care (PoC) anaemia equipment providing an easy to use, reliable and sensitive test with a short response time in a portable device relying on 50 µL blood sample, which can be capillary collected by standard medical procedures [7], providing reduced disposition decision time [8] and replacing current venipuncture based laboratory test and improving patient satisfaction [9]. Moreover, low volume blood samples analysis represents a means of avoiding inducing anaemia or making it worse, as phlebotomy is reported to induce anaemia in hospitalized patients [10].

Electrochemical Impedance Spectroscopy (EIS) technique is reported as an effective solution to characterize the electrical properties of cells and their behaviour, as well as the sensing systems and the buffer media being used to explore new methods of monitoring and characterization [11], [12]. Considering that EIS technique is related to electrical properties of all kinds of particles, it is applied in many biological fields and is especially useful in lab-on-a-chip (LoC) and point-of-care (PoC) devices. Since one major anaemia indicator, haematocrit, consists of RBC suspended in plasma, it can be accurately monitored by means of its electrical impedance or bioimpedance [11], [13]–[16]. Other studies, involving blood impedance analysis, are reported, as [17] where two- and four-electrode topologies are compared to characterize blood impedance on the frequency range of 100 Hz to 100 MHz. Or [18] where the impedance variations associated to laminar blood flow are studied.

In order to proceed with EIS method, two different approaches have been considered; the Fast Fourier Transform (FFT) [19] method and the Frequency Response Analyzer (FRA) [20]. In the case of the FFT a pulse, ideally a Dirac

Manuscript received June 3, 2014; revised September 8, 2014; accepted October 5, 2014. *(Corresponding Author: Jaime Punter-Villagrasa).*

Jaime Punter-Villagrasa, Jordi Colomer-Farrarons, and Pere Ll. Miribel-Català are with the Department of Electronics, University of Barcelona, Martí i Franquès 1, 08028, Barcelona, Spain (email: jpunter@el.ub.es; jcolomer@el.ub.es; pmiribel@el.ub.edu).

Joan Cid is with the Department of Hemotherapy and Hemostasis, CDB, IDIBAPS, Hospital Clínic, Villarroel 170, 08036 Barcelona, Spain (email: jcid@clinic.ub.es).

Ivón Rodríguez-Villarreal is with the Centre de Recerca Matemàtica, Campus Bellaterra, UAB, Edifici C, 08193, Barcelona, Spain (email: irodvill@crm.cat).

function, is applied to the sample providing that it contains a wide enough frequency content to get a full spectrum response. Then, the sensor system response is digitalized and processed in a digital processor and, using the FFT algorithm, the different frequency components are obtained for their analysis [19]. Although this method appears to be simple there are several problems in the implementation. First and foremost it is very difficult to generate a fast step function and a very fast electronic instrumentation capable of driving this step on the electrodes and extracting the resulting signal and, in addition, being sensitive without the resulting frequency components being distorted. Since the important information is contained in a short period of time after the step is applied, in addition to a very fast electronic instrumentation, a very fast analog-to-digital converter (ADC) with a high precision bit resolution is also required, resulting in a high speed hardware and heavy algorithm implementation device. Considering the PoC characteristics of the device, the FRA approach seems to be the simpler and more efficient solution. In this case a Reference Signal is adopted and by means of a lock-in amplifier (LIA) the Bode plot of the sensor Measurement Signal is obtained. The FRA solution is a good solution in terms of the trade-off between speed and complexity, particularly if not too low frequencies need to be measured: above 10 Hz in whole blood haematocrit EIS experiments [14], [16].

Currently, commercial bench top and non-specific huge laboratory devices are utilized for EIS based applications, involving complex experimental setups and significant expenditure of time. Furthermore, whole blood PoC specific sensing systems also rely on complex microfluidic devices [21], [22] entailing a low environmental integration-level to develop autonomous PoC applications [23].

In the present work, a compact and portable PoC solution, for early detection of anaemia through whole blood haematocrit monitoring is studied. The system is composed of a portable electronic device, which allows real-time data acquisition and control by means of an external computer, and a plug and play low-cost disposable commercial sensor. This sensor is based on three screen printed electrodes for an envisaged sample of 50 µL without involving any microfluidic implementation.

To validate the anaemia early detection system, 48 different blood samples have been studied. These samples were randomly obtained from hospitalized patients in Hospital Clínic. First of all, whole blood samples were distributed in two different groups, the first one (group I), has been used for system calibration; and the second one (group II) has been used for system validation. With the group I whole blood samples, we measured a complete impedance spectrum to define a frequency working range, where measured impedance values are well differentiated and related to the blood sample haematocrit. Afterwards, we defined a protocol for instant impedance detection on the defined working range, and we studied the relation between impedance measurements and whole blood samples haematocrit. With these studies we have found the detection resolution and system sensitivity and we have calibrated the system for an instantaneous haematocrit detection. Finally, the haematocrit detection algorithm, based on previous calibration, has been implemented and validated through the group II whole blood samples randomly obtained. Impedance analysis measurements were performed at alternating biasing voltage of 10 mVrms, in order to prevent undesired effects like electroporation or irreversible electrical breakdown, which will damage blood cells membranes [24].

II. Materials and Methods

A. Haematocrit, Electrodes and Impedance Measurement

Biological impedance (Z_{CELL}) is defined by Ohm's law [25], being the current response (I_{CELL}) to applying an alternating voltage signal (V_{CELL}) to a biological material by its corresponding sensing system (1).

$$Z_{CELL} = V_{CELL} / I_{CELL} \tag{1}$$

Two electrodes is the basic sensor topology defined by the working electrode (WE), where V_{CELL} is applied, and the auxiliary electrode (AE), which tracks V_{CELL} and supplies I_{CELL}. However, this topology entails some problematic behaviour related to V_{CELL} signal distortion due to the AE polarization effects. In order to avoid this effect, the current is supplied using an extra, third, electrode (Fig. 1.a). A three electrode sensor is also a commonly used configuration on blood characterization [15], [16] and is defined as: a) the working electrode (WE), where V_{CELL} is applied, b) the reference electrode (RE), which tracks V_{CELL} and c) the counter or auxiliary electrode (CE), which supplies I_{CELL}.

In Fig. 1.a the electrical model for dilute cell suspensions in a three electrode sensor is shown, which can be described as an electrical components network [26]. I_{CELL} can flow through an external cellular path (R_E resistance) or across the cell membrane ($R_M \| C_M$) and go through the intra-cellular medium (R_I resistance). Since R_M resistance is nearly negligible [27], a simplified model for the sample impedance (Z_{CELL}) is considered in (2).

$$Z_{CELL} = R_E(1 + j\omega C_M R_I)/(1 + j\omega C_M (R_E + R_I)) \tag{2}$$

Considering this electrical cell model, the close relation between haematocrit and impedance at low frequencies (up to 100 kHz) has been confirmed [28], as will be shown in section III. At this frequency range the response current I_{CELL} flow outside the RBCs across R_E impedance. Haematocrit increment makes the current flow path larger between the reference and working electrodes, becoming an increment on Z_{CELL} impedance due to an increment of R_E impedance (Fig. 1.b). This phenomenon occurs at the 10 Hz to 100 kHz frequency range [14]. As the impedance measurement depends on the quantity of RBCs in the sample, we used the impedance measurement of whole blood plasma as a reference value, so as to be able to determine the haematocrit according to the impedance increment to that reference value. This relationship between impedance and RBCs will be studied in section III.

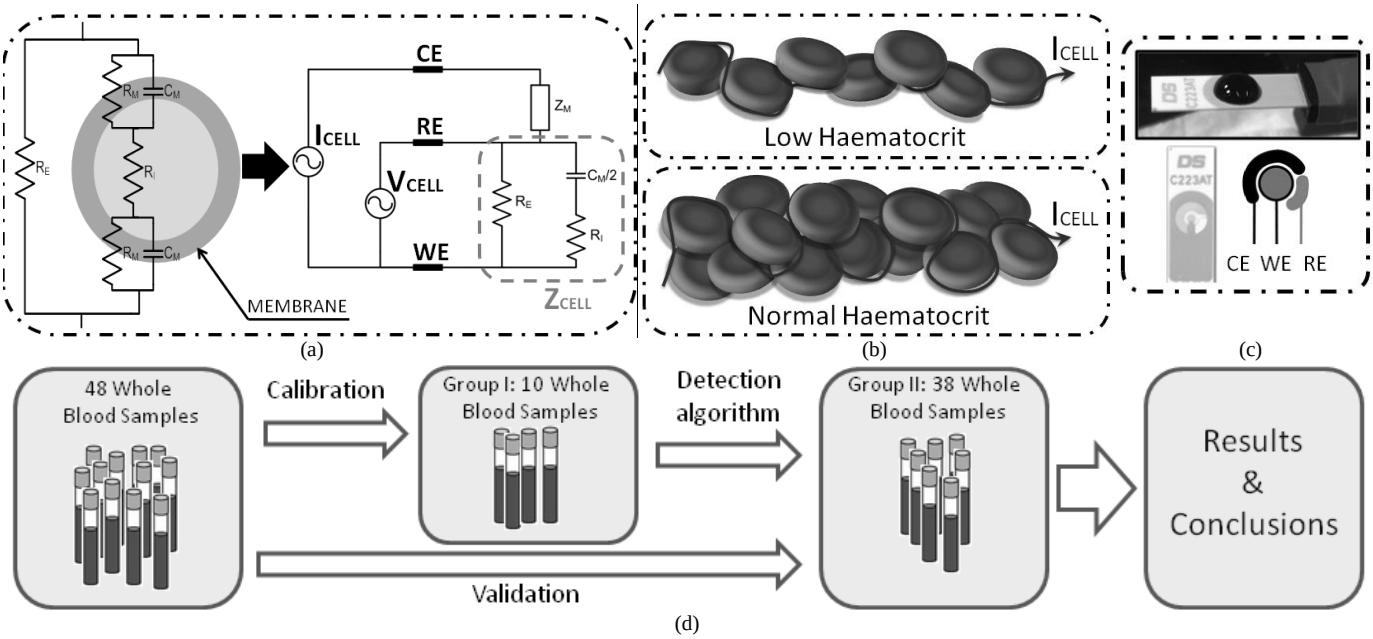

Fig. 1. Sensor and RBC electrical model. (a) Red Blood Cell electrical model. Three electrodes model for RBC sample. (b) Current flow path through different blood samples with different haematocrit. (c) Sensing system: commercial disposable sensor with a 50 µL whole blood drop. (d) Whole blood samples groups and experimental procedure.

B. Sensor

As previously stated, the sensing system is based on a low-cost disposable commercial sensor without involving any micro-fluidic implementation. Moreover, it must be easy to manipulate by clinical laboratory technicians using standard clinical laboratory tools. Additionally, the sensing system must work with 50 µL blood samples, the standard volume for a whole blood drop and easily collected by capillarity [7], and must be made of gold, an acknowledged bio-compatible material. Different commercial sensors have been evaluated, such as AC1 sensor (BVT Technologies, Brno, Czech Republic) or the G-AUG sensor series (Bio-Logic SAS, Claix, France), and the commercial sensor that best meets the defined specifications is the C223AT. This sensor has screen-printed electrodes of 1.6 mm diameter based on gold and is specifically designed to work with 50 µl samples (Fig. 1.c).

The device has a plug-and-play sensor system inside a Faraday cage and it is connected to the electronics with a custom made three wire coaxial insulated cable in order to provide an easy to use set-up and reliable performance. Blood samples were put on top of the sensor with an automatic pipette (Labopette Manual 10 - 100 µL; Hirschmann Laborgeräte, Eberstadt, Germany).

C. Blood Samples

We used 48 whole blood samples obtained from hospitalized patients in Hospital Clínic. However, personal data of the patients was not available to the investigators and samples were randomly selected. Whole blood samples were obtained in 4-mL tubes containing ethylenediaminetetraacetic acid (EDTA 7.2 mg; BD Vacutainer®; BD, Madrid, Spain). We performed a complete blood count (CBC) of the blood samples with a haematology analyser (Advia 2120, Siemens AG, Madrid, Spain), which reported the haemoglobin and haematocrit results as g/dL and percentage (%), respectively. With this methodology, whole blood is aspirated into the system, the sample stream is split, one portion is used for haemoglobinometry and one portion is used for RBC counting and size. Haemoglobinometry is based on RBC lysis and measurement of haemoglobin concentration by absorbance of spectrophotometry. RBC counting and size analyses are performed by passing the RBCs singly through a small direct current. The temporary increase in impedance caused by the passage of the cell provides information about RBC number and RBC volume. Haematocrit is calculated from the measured RBC number and volume [29].

These 48 whole blood samples were distributed in two different groups (Fig. 1.d). The first one (group I), composed of 10 samples, was used to calibrate the system, whereas the second one (group II), composed of the other randomly collected 38 whole blood samples, was used to validate the whole system performance.

The samples in group I have been selected to cover the entire possible haematocrit range present in human blood. Therefore, the obtained haematocrit (HCT(%)), haemoglobin (Hb (g/dL)) and anaemia diagnosis for the different blood samples in group I was as shown in Table I:

TABLE I
GROUP I WHOLE BLOOD SAMPLES FOR SYSTEM CALIBRATION.

Sample	HCT (%)	Hb (g/dL)	Anaemia diagnose
Sample 1	21	6.6	Critical
Sample 2	23	7.4	Critical
Sample 3	25	8.2	Severe
Sample 4	27	9.0	Severe
Sample 5	29	9.2	Severe
Sample 6	33	10.1	Moderate
Sample 7	36	11.9	Very Moderate
Sample 8	40	12.7	Absence
Sample 9	45	14.5	Absence
Sample 10	51	16.1	Absence

Obtained haematocrit and haemoglobin for the remaining 38 whole blood samples defined as a validation group (group II) are shown in Table II:

TABLE II
GROUP II WHOLE BLOOD SAMPLES FOR SYSTEM VALIDATION.

Sample	HCT (%)	Hb (g/dL)	Sample	HCT (%)	Hb (g/dL)
1	25	8,2	20	34	11
2	26	8,3	21	34	11,1
3	26	8,5	22	34	11,4
4	27	8,9	23	35	11,5
5	28	9	24	35	11,5
6	28	9	25	36	11,6
1	28	9,1	26	39	12,5
2	29	9,2	27	40	12,7
3	29	9,2	28	41	12,7
4	29	9,3	29	42	13,3
5	30	9,4	30	42	13,3
6	31	9,5	31	43	14,5
13	31	9,6	32	44	14,5
14	31	10,1	33	45	14,5
15	32	10,4	34	45	14,5
16	32	10,5	35	46	14,8
17	33	10,5	36	46	15,5
18	33	10,5	37	47	15,9
19	34	10,8	38	49	16,1

D. System Description

A full custom electronic circuit was specifically designed to carry out the FRA approach with a 3 electrode sensor topology. The device architecture has two modules: a) an Electrodes Biasing and Instrumentation module (EBI in Fig. 2.a) which provides a frequency configurable voltage signal and an instrumentation amplifier based potentiostat; and b) a Signal Digitalization and Post-Processing module (SDPP in Fig. 2.a), which adapts both signals needed for the FRA analysis, Reference Signal (V_{RS} in Fig. 2.a) and Measurement Signal (V_{IS} in Fig.2.a), from a bi-polar single-ended to an uni-polar differential signal to be processed by a 12-bit parallel output analog-to-digital converter. Finally, a digital lock-in amplifier (DLIA) carries out the FRA approach that provides the Bode diagrams for both impedance magnitude and phase.

The first module (EBI), Electrodes Biasing and Instrumentation, is based on a signal generator, OSC in Fig. 2.a (AD9833; Analog Devices, Norwood, USA), and an instrumentation amplifier based potentiostat. The signal generator provides a stable voltage signal with a wide variable frequency range, 0 MHz to 12.5 MHz, which is controlled by an SPI communication protocol. The instrumentation is based on a potentiostat with an instrumentation amplifier current readout stage [30], [31], which consists of an operational amplifier to bias the sensor and an instrumentation amplifier as an electrode current readout. The operational amplifier, OA in Fig. 2.a (AD825; Analog Devices, Norwood, USA), is a dual supply high speed JFET amplifier with low leakage current and low distortion capable of high output driving, which tracks the signal on to the electrodes. The instrumentation amplifier, IA in Fig. 2.a (AD8421; Analog Devices, Norwood, USA), is a dual supply high speed instrumentation amplifier with low noise and ultralow bias current. The instrumentation amplifier converts the current through the electrodes (3) into a voltage signal (V_{IS}) by means of a sensing resistor on the counter electrode (R_{SENSE} in Fig. 2.a) between the amplifier's non-inverting and inverting inputs

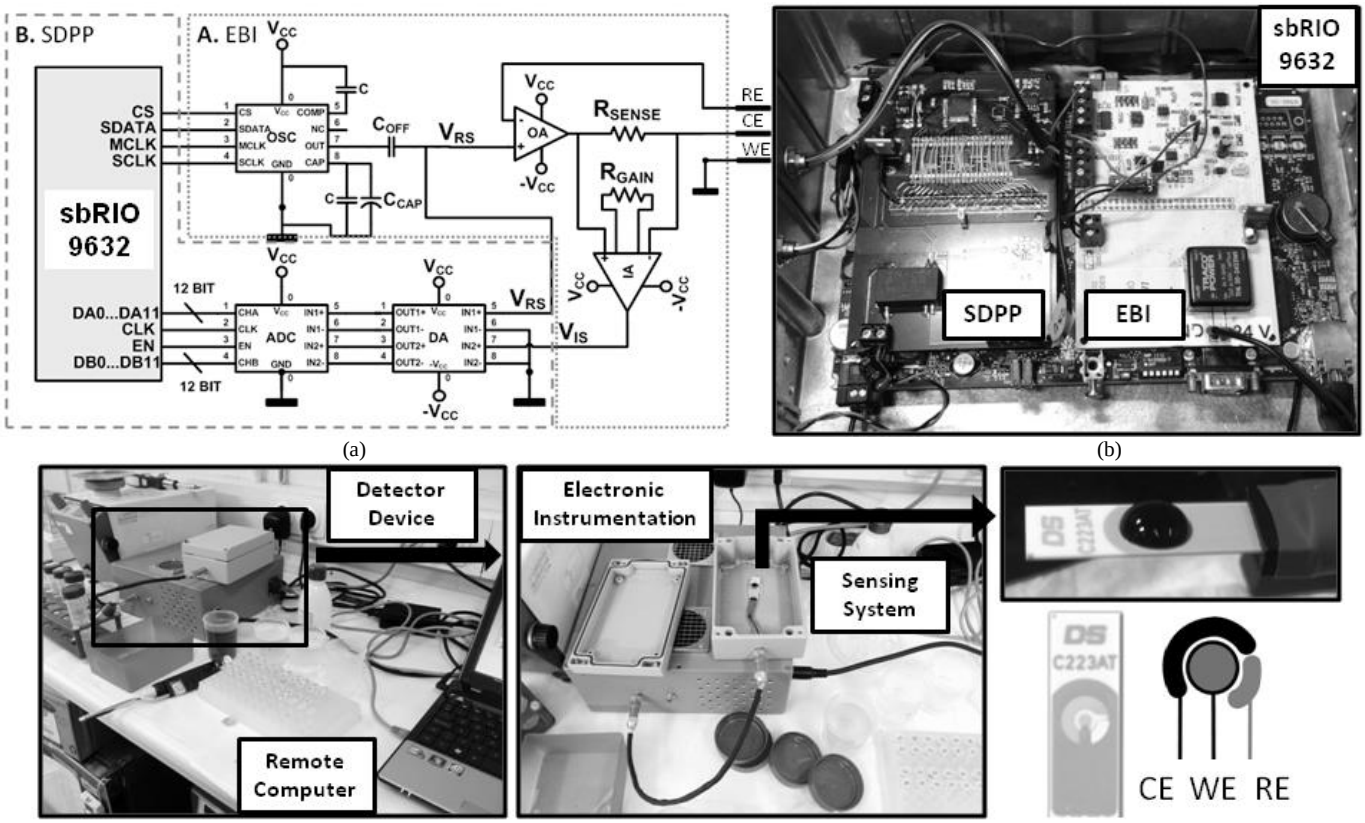

Fig. 2. PoC device prototype and set-up. (a) Prototype electronics schematic, A: Electrodes Biasing Module; B: Signal Digitalization and Post-Processing. (b) Device prototype electronics: Two custom PCB and a sbRIO 9632 board (National Instruments) on a faraday cage (c) Experimental set-up: Disposable sensor; Electronic instrumentation; External computer with control and data displaying software.

(4). The amplifier's gain has been set to 1 in order to optimize the amplifier's Total Harmonic Distortion (THD) [30].

$$I_{CELL} = V_{RS} / Z_{CELL} \quad (3)$$

$$V_{IS} = (V_+ - V_-) = R_{SENSE} I_{CELL} = V_{RS} (R_{SENSE} / Z_{CELL}) \quad (4)$$

$$Z_{CELL} = R_{SENSE} (V_{RS} / V_{IS}) \quad (5)$$

This stage has been designed with 4 different multiplexed sensing resistors (R_{SENSE}) taking into account the expected impedance values shown in the literature between 100Ω and 100kΩ [12], [15], [16], [32], [33], as was subsequently confirmed in the system validation experiments. These resistors are automatically multiplexed with an auto-scale function that will be explained below.

The second module (SDPP), Signal Digitalization and Post-Processing, consists in a 12-bit dual, low power ADC, ADC in Fig. 2.a (ADC12D040; Texas Instruments, Dallas, USA), capable of converting both analogue input signals at 40 MSPS simultaneously. 12-bit resolution does not represent a significant drawback in the final system resolution, as V_{RS} is scaled to the full range ADC analogue input and the system provides a real time gain auto scale for the R_{SENSE} gain factor. The analogue inputs are converted from single ended to differential with a differential amplifier, DA in Fig. 2.a (AD8138; Analog Devices, Norwood, USA), with a high slew rate with low distortion and input noise. Finally, a DLIA based on real-time mathematical processing [30] is embedded on a 400 MHz microprocessor from a real-time platform, sbRIO 9632 in Fig. 2.a (sbRIO9632; National Instruments, Austin, USA). Final impedance bode plot is composed of sample impedance magnitude $|Z_{CELL}|$ (6) and impedance phase φ_{CELL} (7), where V_{REAL} (8) and V_{IM} (9) stand for real part and imaginary part of the measured impedance.

$$|Z_{CELL}| = R_{SENSE} (|V_{RS}|^2 / 2 sqrt(V_{REAL}{}^2 + V_{IM}{}^2)) \quad (6)$$

$$\varphi_{CELL} = \arctan(V_{IM} / V_{REAL}) t(V_{REAL}{}^2 + V_{IM}{}^2)) \quad (7)$$

$$V_{REAL} = V_{RS} V_{IS} \cos(\varphi_{IS}) / 2 \quad (8)$$

$$V_{IM} = V_{RS} V_{IS} \sin(\varphi_{IS}) / 2 \quad (9)$$

In addition, real-time platform sbRIO9632 has a FPGA (Xilinx Spartan-3; Xilinx, San Jose, USA), which allows us to provide steady clock signals as needed on the instrumentation that can be automatically real-time adjusted, allowing complete parallel signal acquisition for all the frequency ranges. Furthermore, embedded hardware control, like R_{SENSE} multiplexed auto-scale and signal generator automatic frequency sweep can be developed. This real-time embedded hardware control represents the basic features for an automated and complete FRA approach.

The real-time platform allows the system configuration and data display, with a user-friendly front-end user panel, by means of an external computer connected to the platform with a standard Ethernet connection. The user panel, depicted in Fig. 3, has two different configurations that can be selected from a menu (A label). Each option allows the system to perform different experiments when the start button (D label) key is pressed. The first one is a complete EIS that provides the Bode diagrams for both impedance magnitude (F label) and phase (G label), where the user could choose the number of points per decade (C label). EIS frequency ranges are fixed to the defined bandwidth on section II.A and R_{SENSE} values are auto-scaled. The second is an automatic haematocrit analyzer, where the blood sample haematocrit is displayed with four significant numbers (B label).

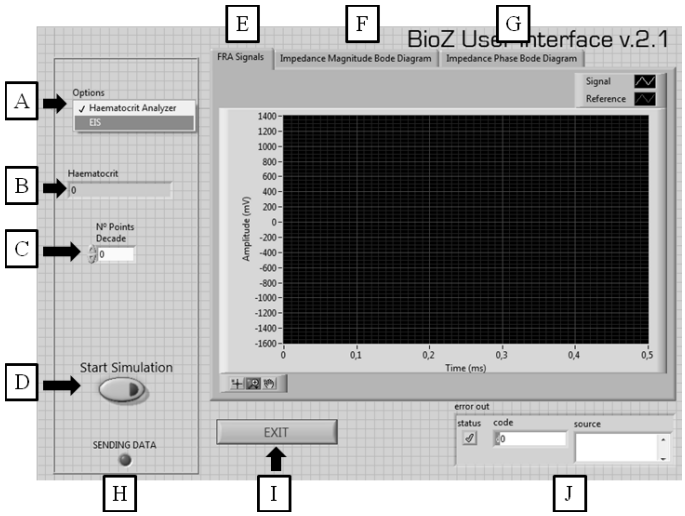

Fig. 3. Software front-panel for experiments control and data displaying.

Moreover, the front panel has several displays for user control and error monitoring. The two signals needed for the FRA analysis, Reference Signal (V_{RS} in Fig. 2.a) and Measurement Signal (V_{IS} in Fig.2.a), are real-time monitored and shown on a graph (E label). Errors in electronics connection with the remote computer are displayed (H label) and generic Labview errors are explained (J label). The whole system and the impedance detection performance has been validated using passive components and ferrocyanide/ferricyanide solution. These preliminary studies have been previously published [34].

III. Results and Discussion

A. System calibration: EIS haematocrit analysis

The designed device was validated through EIS experiences with the specified sensor described in section II.B for each whole blood sample described in section II.C. Experimental set-up is depicted in Fig. 2.c. All the measurements have been performed at clinical laboratory room temperature.

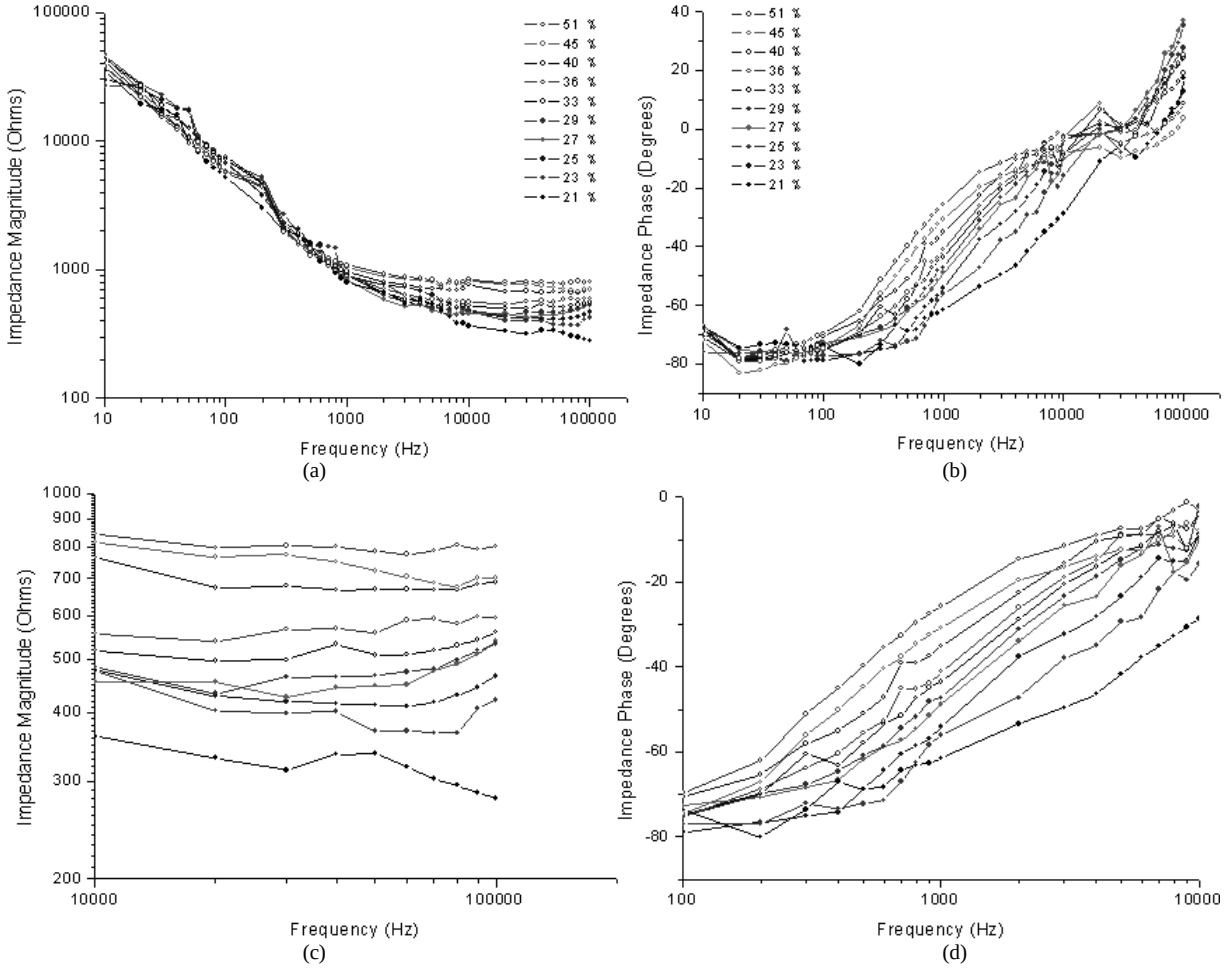

Fig. 4. Whole blood impedance magnitude and phase measurement for group I whole blood samples. (a) Impedance magnitude and (b) impedance phase over full frequency spectra. (c) Impedance magnitude and (d) impedance phase over frequency working range.

First of all, we measured a complete impedance spectrum for the group I whole blood samples. In Fig. 4 shows the obtained impedance magnitude (Fig. 4.a) and phase (Fig. 4.b) bode diagram for whole blood samples. We observed that, both in impedance magnitude and phase, there exists a difference between impedance results for different samples in specific frequency ranges. Furthermore, these differences must be related to whole blood haematocrit, as the response current I_{CELL} flow outside the RBCs, as introduced in section II.A. When haematocrit is higher, the current flow path becomes larger between the reference and working electrodes, which represents an increment on measured Z_{CELL} impedance. Therefore, measured impedance differences must be defined as impedance increments related to haematocrit increments. However, this phenomenon is not present on the whole frequency range defined on the section II.A, 10 Hz to 100 kHz, but on a more specific one. So, we have defined working ranges depending on the correlation between impedance measurement and haematocrit. In terms of impedance magnitude (Fig. 4.c) the frequency working range is in the 10 kHz to 100 kHz range and for impedance phase (Fig. 4.d) it is in the 1 kHz to 5 kHz range.

It is interesting to be able to determine impedance magnitude and phase differences for different haematocrit samples on a wide frequency working range. It gives flexibility and data redundancy to the system as long as it is not single frequency response dependant, which makes simple statistical data analysis techniques, such as linear fit, feasible, turning out to be a more robust and reliable device.

Hence, once we have assumed that measured impedance increments, on the defined frequency working range, are related to blood samples haematocrit increment, we must determine the system's capacity for haematocrit detection, resolution and sensitivity.

B. System calibration: automatic haematocrit detection.

In this section, linear fit technique has been used to study the relation between impedance data collected and whole blood samples haematocrit, as we have assumed a linear dependence between them. With this study we want to determine the system haematocrit detection accuracy, sensitivity and coefficient of variation. We have implemented a software, embedded on the microprocessor from the real-time platform sbRIO 9632, to instantly measure impedance on the previously defined frequency working range. As a first approach to the detection system, only the impedance magnitude measurements will be evaluated. Although impedance phase measurements may be related to haematocrit, as it is shown in Fig.4.d, these values, unlike the impedance magnitude, are strongly frequency dependant, so more complex data analysis is needed, resulting in a more

complex and slower system. To calibrate the system, the impedance magnitude measurements of the whole blood samples from group I will be compared with the haematocrit values (HCT (%)). 5 repetitions have been done for each whole blood sample using different sensors and sub-samples from the original sample. Table III shows the impedance magnitude values, the standard deviation and coefficient of variation for each whole blood sample.

TABLE III
SYSTEM CALIBRATION MEASUREMENTS

HCT (%)	Mean Impedance Magnitude (Ω)	Standard Deviation (Ω)	Coefficient of Variation (%)
21	343,08	11,13	3,24
23	382,24	21,82	5,71
25	396,77	10,76	2,71
27	421,08	7,11	1,69
29	453,37	12,97	2,86
33	511,42	15,26	2,98
36	536,82	18,09	3,37
40	566,05	16,94	2,99
45	606,49	27,28	4,50
51	645,99	16,05	2,49

The relation of impedance magnitude (|Z|) mean value and whole blood samples haematocrit had been analysed as a linear dependence approach (10), where the slope (β_Z) defines the sensitivity, in terms of ohms per haematocrit percentage (Ω/%). Meanwhile the haematocrit detection accuracy (%) is the relation between the linear fit standard deviation and β_Z. Precision can be evaluated with the coefficient of variation: that is, the standard deviation divided by the mean value of the 5 repetitions measurements. In Fig. 5 the impedance magnitude for the different haematocrit (HCT (%)) is depicted.

$$|Z|(\Omega) = \alpha_Z + \beta_Z HCT(\%) \tag{10}$$

The haematocrit detection system has a 10.46 Ω/% sensitivity and a 1.13 % accuracy error with a linear correlation of 0.987. Precision can be evaluated with the coefficient of variation (CV), which is the standard deviation (SD) divided by the mean value of the 5 repetitions. The CV of the system is acceptable as it is normally below 5%.

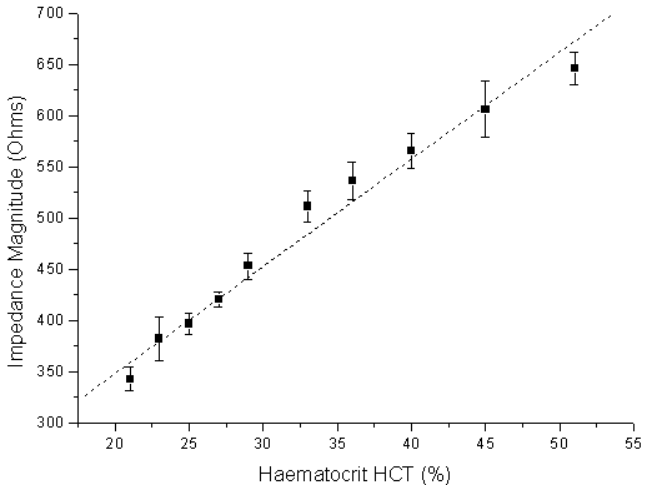

Fig. 5. Measured impedance magnitude as a function of whole blood samples haematocrit (HCT (%)). Calibration curve.

C. Whole blood haematocrit detection

In previous sections, we have analysed the haematocrit (HCT (%)) relation with impedance measurement, in both magnitude and phase, defining the frequency working range. An embedded software has been developed to instantly measure impedance magnitude on the defined working range, and we have studied the sensitivity, accuracy and coefficient of variation of the device. With the data from these previous studies, we have implemented an automatic real-time anaemia detection device that provides instantaneous haematocrit (HCT (%)) measurement. An HCT (%) evaluation algorithm, based on impedance magnitude measurement, has been embedded on the microprocessor from the real-time platform sbRIO 9632. The accuracy, precision and repeatability of the detection device will be evaluated using 38 whole blood samples from the validation group, described in section II.C (group II), which were randomly collected. 5 repetitions have been done for each whole blood sample, using different sensors and sub-samples, to evaluate the precision of the device.

The predicted haematocrit from the detection device (DHCT (%) in Table IV) is the mean value of the 5 measurements performed with each whole blood sample, and it was compared with the haematocrit measurement (CHCT (%) in Table IV) of the complete blood count (CBC) performed with the haematology analyser (Advia 2120, Siemens AG, Madrid, Spain). Haematocrit measurement and its standard deviation (SD) results are depicted in Table IV.

TABLE IV
DEVICE VALIDATION WITH GROUP II WHOLE BLOOD SAMPLES.

CHCT (%)	DHCT (%)	SD (%)	CHCT (%)	DHCT (%)	SD (%)
35	33,82	1,47	34	33,05	1,19
36	32,96	1,28	33	30,08	1,11
33	33,93	1,15	34	35,50	0,62
39	38,71	0,83	42	40,21	1,39
34	35,61	1,64	45	41,14	1,77
49	48,26	1,04	43	40,28	0,94
45	44,40	0,80	31	29,61	1,42
28	27,57	0,77	29	27,90	0,44
32	31,61	1,85	29	28,26	0,41
46	46,72	1,78	41	38,41	1,17
29	28,14	1,27	26	25,42	0,40
31	33,59	1,30	46	42,90	1,21
28	30,33	1,46	42	39,84	1,30
42	39,29	0,84	26	26,39	0,40
28	28,40	1,17	28	26,57	0,54
32	32,48	0,92	47	41,17	1,35
30	32,26	1,04	35	34,35	1,05
34	32,50	1,52	25	24,06	0,30
44	40,44	1,64	31	34,06	1,18

In Fig. 6. a comparison between detected haematocrit and haematocrit calculated with a clinical haematology analyser is shown. The proposed device presented great accuracy in detecting haematocrit, with a linearity of 0.93 and an accuracy error of 1.75% with a correlation of 0.98. The coefficient of variation has a mean value of 3.27% for the whole samples, without any particular case above 5%. In quality control procedures in clinical haematology measurements, coefficient of variation of less than 5% for a test is considered acceptable [29].

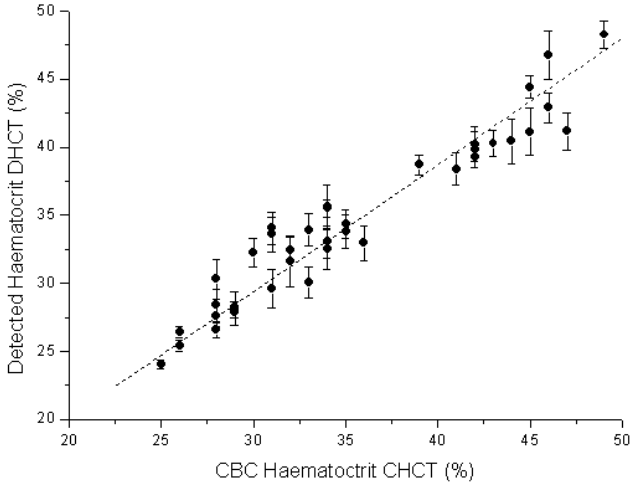

Fig. 6. Whole blood haematocrit measurement (DHCT (%)) compared with haematocrit measurements obtained with a CBC performed by a haematology analyzer (CHCT (%)). Error bars represent the standard deviations across five repetitions.

As a first approach, which only contemplates impedance magnitude to a haematocrit analysis algorithm for anaemia detection, as previously stated, it would be interesting to develop a more complex algorithm involving both impedance magnitude and phase on a wide frequency working range, for more precision and better performance on detection.

IV. Conclusions.

In this work, a first approach to a novel point-of-care (PoC) device has been designed, fabricated and tested for instantaneous anaemia detection based on custom instrumentation electronics, electrical impedance spectroscopy technique and disposable sensor without any microfluidic. The system performs real time instrumentation control, data acquisition and results display by means of an external computer and user-friendly software. The device has been proved to exhibit reliable, robust and effective results using label-free disposable commercial sensors using 50µL whole blood samples. Furthermore, unlike actual clinical equipment for blood analysis, whole blood samples are not destroyed in the measurement process.

48 whole blood samples, randomly collected from hospitalized patients in Hospital Clínic, were used to demonstrate the feasibility of the impedance measurement technique to perform an easy, fast and sensitive haematocrit study using disposable label-free commercial sensors with low voltage biasing. A first approach for a haematocrit evaluation algorithm for anaemia detection, based on whole blood impedance analysis, is presented and validated. The system has been evaluated through comparison with complete blood count (CBC) using a clinical haematology analyser (Advia 2120, Siemens AG, Madrid, Spain). The anaemia detection device has a linearity of 0.93 and an accuracy error of 1.75% with a correlation of 0.98. Coefficient of variation is below 5%, with a worst case resolution of 1.63%. Considering this as a first approach algorithm for anaemia detection, the development of a more complex algorithm and a more accurate clinical assay with higher testing population will lead to more accurate results to assess the device performance. Additionally, as the system is based on straightforward standards on instrumentation electronics and sensing, it represents an economic, portable, safe and reliable system of anaemia detection with a high degree of integration for the clinical environment.

Further development must be considered for future stages: real-time platform sbRIO9632 (National Instruments) has been used for fast software prototype development and versatility, but it is a major drawback in terms of power consumption, size and price. It must be replaced by a low-cost microcontroller for instrumentation control, data acquisition and post-processing. All the future system improvements must push towards the development of a truly autonomous, portable and versatile device relying on the presented work.

Commercial devices for PoC anaemia detection, based on microfluidics devices, such as AnemiaCheck (Express Diagnostics, Blue Earth, Minnesota), or on photometry haemoglobin detection, such as STAT-Site (Stanbio Laboratory, Boerne, Texas) or HemoPoint H2 (Alere, Waltham, Massachusetts), are much slower presenting similar detection performance results, Table V. Moreover, getting digitalised information provides the possibility of remote care, monitoring and implementation of other clinical actuators. Other commercial PoC devices, like the i-STAT analyzer (Abbott Point of Care, Princeton, New Jersey), despite providing lab-quality results for patient point-of-care testing, turn out to be less specific involving a much more expensive and slower device.

TABLE V
COMMERCIAL DEVICES COMPARISON

Device	Test time (sec.)	Range (HCT and Hb)	SD (%)	CV (%)
Proposed Device	< 2	HCT: 0% – 100%	1.17	3.27
Anemia Check	900	HCT: 12% – 42%	0.74	4.10
STAT-Site	120	Hb: 5.6 g/dL – 20.6 g/dL	---	4.20
Hemo Point H2	60	Hb: 0 g/dL – 25.6 g/dL HCT: 36% – 54%	---	1.5

In summary, this paper describes the design, development and test of a novel instantaneous anaemia detection PoC device with low-cost disposable commercial sensors and instrumentation electronics. The device presents reliable, sensitive and robust haematocrit detection, relying on low-cost straightforward electronic equipment and sensing systems.

Acknowledgment

Authors thank investigators of the Department of Hemotherapy and Hemostasis, Hospital Clinic, Biomedical Diagnosis Centre, Institute of Biomedical Research August Pi i Sunyer, University of Barcelona, Barcelona, Spain for helping with experiments.

References

[1] C.A. Northrop-Clewes, and D.I. Thurnham, “Biomarkers for the differentiation of anemia and their clinical usefulness.” *J. Blood Medicine*. no. 4, pp. 11–22, Mar. 2013.

[2] B. de Benoist, E. McLean, I. Egli, and M.E. Cogswell, "Worldwide Prevalence of Anaemia 1993–2005: WHO Global Database on Anaemia", Geneva, Switzerland, 2008.

[3] A. Belardinelli, M. Benni, P.L. Tazzari, and P. Pagliari, "Noninvasive methods for haemoglobin screening in prospective blood donrs." Vox Sang. no.105, pp. 116–120, Apr. 2013.

[4] M. Pinto, M.L. Barjas-Castro, S. Nascimento, M.A. Falconi, R. Zulli, and V. Castro, "The new noninvasive occlusion spectroscopy hemoglobin measurement method: a reliable and easy anemia screening test for blood donors." Transfusion. no 53, pp. 766–769, Apr. 2013.

[5] World Health Organization, "Iron Deficiency Anaemia: Assessment, Prevention and Control; A Guide for Programme Managers." Geneva, Switzerland, 2001.

[6] R. B. Thompson, *A Short Textbook of Haematology*, fourth ed., Pitman Medical Publishing Co., Kent, 1975.

[7] D.J. Ernst, L.O. Ballance, R.R. Calam, R. McCall, D.I. Szamosi, and L. Tyndall, Procedures and Devices for the Collection of Diagnostic Capillary Blood Specimens; Approved Standard, sixth ed. CLSI, Wayne, Pennsylvania, 2008.

[8] S.D. Asha, A.C.F. Chan, E. Walter, P.J. Kelly, R.L. Morton, A. Ajami, R.D. Wilson, and D. Honneyman, "Impact from point-of-care devices on emergency department patient processing times compared with central laboratory testing of blood samples: a randomised controlled trial and cost-effectiveness analysis." J. Emerg. Med. No. 0, pp. 1–6, Jun. 2013.

[9] C.D.H. Jones, J. Howick, N.W. Roberts, C.P. Price, C. Heneghan, A. Plüddemann, and M. Thompson, "Primary care clinicians' attitudes towards point-of-care blood testing: a systematic review of qualitative studies", BMC Family Practice. no. 14, pp. 117. Aug. 2013.

[10] P. Thavendiranathan, A. Bagai, A. Ebidia, A.S. Detsky, and N.K. Choudhry, "Do blood tests cause anemia in hospitalized patients? The effect of diagnostic phlebotomy on hemoglobin and hematocrit levels." J Gen Intern Med. no. 20, pp. 520–524, Jun. 2005.

[11] N. Ramirez, A. Regueiro, O. Arias, and R. Contreras, "Electrochemical impedance spectroscopy: An effective tool for a fast microbiological diagnosis." Biotecnologia Aplicada. no. 26, pp. 72–78, Mar. 2009.

[12] N. Li, A. Brahmendra, A.J. Veloso, A. Prashar, X.R. Cheng, V.W.S. Hung, C. Guyard, M. Terebiznik, and K. Kerman, "Disposable Immunochips for the Detection of Legionella pneumophila Using Electrochemical Impedance Spectroscopy." Anal. Chem. no. 84, pp. 3485–3488, Mar. 2012.

[13] G.A.M. Pop, W.J. Hop, L. Moraru, M. van der Jagt, J. Quak, D. Dekkers, Z. Chang, F.J. Gijsen, D.J. Duncker, and D.J. Slager, "Blood Electrical Impedance Closely Matches Whole Blood Viscosity as Parameter of Hemorheology and Inflammation." Appl. Rheol. no. 13, pp. 305–312, Oct. 2003.

[14] G.A.M. Pop, L.L. Bisschops, B. Iliev, P.C. Struijk, J.G. van der Hoeven, and C.W., Hoedemaekers, "On-line blood viscosity monitoring in vivo with a central venous catheter, using electrical impedance technique." Biosensors and Bioelectronics. no. 41, pp. 595–601, Oct. 2012.

[15] F. Hernández, C. Guerrero, and J. Bernal, "Determinación de las propiedades eléctricas en tejido sangíneo." Ingenierias. no. 29, pp. 7–13, Oct.-Dic. 2005.

[16] R. Pradhan, A. Mitra, and S. Das, "Impedimetric characterization of human blood using three-electrode based ECIS devices." J. of Electrical Bioimpedance. no. 3, pp. 12–19, 2012.

[17] Z. Chang, A.G.M. Pop, and G.C.M. Meijer, "A comparison of two- and four-electrode techniques to characterize blood impedance for the frequency range of 100 Hz to 100 MHz." IEEE Trans. Biomed. Eng. no. 3, pp. 1247–1249, Mar. 2008.

[18] J. Wtorek, and A. Polinski, "The contribution of blood-flow-induced conductivity changes to measured impedance." IEEE Trans. Biomed. Eng. no. 1, pp. 41–49, Jan. 2005.

[19] S. Park, J. Yoo, B. Chang, and E. Ahn, "Novel instrumentation in electrochemical impedance spectroscopy and a full description of an electrochemical system." J. Pure and App. Chem. no. 5, pp. 1069–1080, Aug. 2005.

[20] G. Li, M. Zhou, F. He, and L. Lin, "A novel algorithm combining oversampling and digital lock-in amplifier of high speed and precision." Review of Scientific Instruments. no. 82 (2011).

[21] Y. Zheng, E. Shojaei-Baghini, A. Azad, C. Wang, and Y. Sun, "High-throughput biophysical measurement of human red blood cells." Lab. Chip. no. 12, pp. 2560–2567, Jul. 2012.

[22] B. Ramaswamy, T.Y. Yin-Ting, and Z. Si-Yang, "Microfluidic device and system for point-of-care blood coagulation measurement based on electrical impedance sensing3" Sensors and Actuators B: Chemical. no. 180, pp. 21–27, Apr. 2013.

[23] J.P. Esquivel, J. Colomer-Farrarons, M. Castellarnau, M. Salleras, F.J. del Campo, J. Samitier, P. Miribel-Català, and N. Sabaté, "Fuel cell-powered microfluidic platform for lab-on-a-chip applications: Integration into an autonomous amperometric sensing device." Lab. Chip. no. 12, pp. 4232–4235, Nov. 2012.

[24] L.V. Chernomordik, and Y.A. Chizmadzhev, "Electrical breakdown of lipid bilayer membranes." In *Electroporation and Electrofusion in Cell Biology* E. Neumann, A.E. Sowers, and C.A. Jordan (Eds.), SpringerLink, 1989, pp. 83–95.

[25] R. Patterson, "Bioelectric Impedance Measurements3" in *The Biomedical Engineering Handbook*, 2nd Edition, J.D. Bronzino (Ed.), CRC Press, Boca Raton, 2000, pp. 734–773.

[26] C. Beriet, and D. Pletcher, "A microelectrode study of the mechanism and kinetics of the ferro/ferricyanide couple in aqueous media: The influence of the electrolyte and its concentration." J. Electroanalytical Chemistry. no. 361, pp. 93–101, Dec. 1993.

[27] C. Grosse, and H.P. Schwan, "Cellular membrane potentials induced by alternating fields." J. Biophys. no. 63, pp. 1632–1642, Dec. 1992.

[28] D.W. Hill, and F.D. Thompson, "The effect of haematocrit on the resistivity of human blood at 37ºC and 100 kHz." J. Medical and Biological Engineering. no. 13, pp. 182–186, Mar. 1975.

[29] L. Corash, "Laboratory Hematology: Methods for the Analysis of Blood," in *Blood, Principles and Practice of Hematology*, R.I. Handin, S.E. Lux and T.P. Stossel, Eds. 1st ed. Philadelphia, J.B. Lippincott & Co., 1995, ch. 2, pp. 23–61.

[30] J. Punter-Villagrasa, J. Colomer-Farrarons, and P. Miribel, "Bioelectronics for Amperometric Biosensors," in *State of the Art in Biosensors - General Aspects*, T. Rinken, [Online]. Available: http://www.intechopen.com/books/state-of-the-art-in-biosensors-general-aspects/bioelectronics-for-amperometric-biosensors

[31] A.P. Brokaw, M.P. Timko, "An improved monolithic instrumentation amplifier." J. Solid-State Circuits. no. 10, pp. 417–423, Dec. 1975.

[32] C. Ribaut, K. Reybier, O. Reynes, J. Launay, A. Valentin, P.L. Fabre, and F. Nepveu, "Electrochemical impedance spectroscopy to study physiological changes affecting the red blood cell after invasion by malaria parasites." Biosensors and Bioelectronics. no. 24, pp. 2721–2725, Apr. 2009.

[33] M. Xu, X., Luo, and J.J. Davis, “The label free picomolar detection of insulin in blood serum.” Biosensors and Bioelectronics. no. 39, pp. 21–25, Jan. 2013.
[34] J. Punter-Villagrasa, B. del-Moral, J. Colomer-Farrarons, P. Miribel, I. Rodriguez-Villarreal, J. Cid and B. Prieto-Simon, “Towards a portable point-of-use blood analysis with EIS technique device” in Proc. 11th International Multi-Conference on Systems, Signals and Devices 2014, pp. 1–6.
[35] S.K. Arya, K.C. Lee, D.B. Dah'alan, and A.R. Rahman, “Breast tumor cell detection at single cell resolution using an electrochemical impedance technique.” Lab. Chip. no. 12, pp. 2362–2368, Apr. 2012.

Publication 2.

An Instantaneous low-cost point-of-care anemia detection device.

Punter-Villagrasa, J.; Cid, J.; Páez-Avilés, C.; Colomer-Farrarons, J.; Rodriguez-Villarreal, I.; Juanola-Feliu, E.; Miribel-Catala, P.L.

Sensors, vol. 15, no. 2, pp. 4564-4577, February 2015.

Sensors **2015**, *15*, 4564-4577; doi:10.3390/s150204564

OPEN ACCESS

sensors

ISSN 1424-8220

www.mdpi.com/journal/sensors

Article

An Instantaneous Low-Cost Point-of-Care Anemia Detection Device

Jaime Punter-Villagrasa [1,*], Joan Cid [2], Cristina Páez-Avilés [1], Ivón Rodríguez-Villarreal [3], Esteve Juanola-Feliu [1], Jordi Colomer-Farrarons [1] and Pere Ll. Miribel-Català [1]

[1] Department of Electronics, University of Barcelona, Martí i Franquès 1, Barcelona 08028, Spain; E-Mails: cpaezaviles@el.ub.edu (C.P.-A.); ejuanola@el.ub.edu (E.J.-F.); jcolomer@el.ub.edu (J.C.-F.); pmiribel@el.ub.edu (P.L.M.-C.)

[2] Department of Hemotherapy and Hemostasis, CDB, IDIBAPS, Hospital Clínic, Villarroel 170, Barcelona 08036, Spain; E-Mail: jcid@clinic.ub.es

[3] Centre de Recerca Matemàtica, Campus Bellaterra, UAB, Edifici C, Barcelona 08193, Spain; E-Mail: irodvill@crm.cat

* Author to whom correspondence should be addressed; E-Mail: jpunter@el.ub.es; Tel.: +34-93-4020876.

Academic Editor: Roberto Pilloton

Received: 21 November 2014 / Accepted: 9 February 2015 / Published: 16 February 2015

Abstract: We present a small, compact and portable device for point-of-care instantaneous early detection of anemia. The method used is based on direct hematocrit measurement from whole blood samples by means of impedance analysis. This device consists of a custom electronic instrumentation and a plug-and-play disposable sensor. The designed electronics rely on straightforward standards for low power consumption, resulting in a robust and low consumption device making it completely mobile with a long battery life. Another approach could be powering the system based on other solutions like indoor solar cells, or applying energy-harvesting solutions in order to remove the batteries. The sensing system is based on a disposable low-cost label-free three gold electrode commercial sensor for 50 µL blood samples. The device capability for anemia detection has been validated through 24 blood samples, obtained from four hospitalized patients at Hospital Clínic. As a result, the response, effectiveness and robustness of the portable point-of-care device to detect anemia has been proved with an accuracy error of 2.83% and a mean coefficient of variation of 2.57% without any particular case above 5%.

Keywords: whole blood; hematocrit; impedance analysis; electronics; point-of-care

1. Introduction

According to the World Health Organization (WHO), anemia is defined as a condition in which the number of red blood cells (RBCs) or their oxygen-carrying capacity is insufficient to meet physiological needs [1]. Anemia affects about two billion people, or 30% of the world's population. Pregnant women and children are the most vulnerable segment, and it is considered a worldwide health issue affecting both developed and developing countries [2,3]. The highest prevalence is in Africa (67.6%) and South-East Asia (65.5%). In the Eastern Mediterranean, the prevalence is 46% and around 20% in the other WHO regions, the Americas, Europe and Western Pacific [3]. The major health consequences in severe cases are pregnancy disorders, poor physical and cognitive development, and increased risk of morbidity, while less severe cases provoke weakness, fatigue and dizziness [3,4]. The most common cause of anemia is nutritional deficiencies, especially in developing countries due to severe malnutrition [5], or diseases like colon cancer or gastrointestinal lesions [6,7]. Other conditions causing anemia are inherited hematologic diseases such as sickle cell anemia or thalassemia causing hemolytic anemia [8,9], cancer treatments (chemotherapy and radiation) [10], and indirect causes, such as lower erythropoietin (EPO) production due to kidney disease [11]. Also, frequent blood donations may induce anemia in blood donors, especially females [12].

Evaluation of hemoglobin (Hb) concentration is the most reliable indicator for anemia detection; being a required condition in possible blood donors in most countries of the world, generically the only laboratory control test performed before donation [13]. Hematocrit (HTC) screening is also a reliable indicator for anemia, which is the proportion of blood volume occupied by RBCs, and is determined by cell number and size. HTC numbers below a certain reference range may indicate anemia or abnormal cell development [14]. Automated hematology analyzers provide the necessary information about HTC and Hb with a high degree of precision by means of a complete blood count (CBC), which represents an extremely useful tool for evaluating anemia [4]. However, hematology analyzers are huge and expensive devices which need to be operated by skilled technicians using venous blood sample, requiring a phlebotomy practiced by a specialist. Access to electricity to power the instrumentation is also required [15,16]. These different factors make the access to these devices very limited and often incompatible with the constraints of resource-limited settings [15]. Furthermore, access to this equipment is an issue in developing countries, where less reliable equipment and evaluation techniques are available [17]. These different factors push towards the development of point-of-care (PoC) anemia detecting devices that provide an easy to use, reliable and economic test for patients, the general public and first aid personnel screening for anemia. Detection of anemia with a short response time in a portable PoC device relying on a blood drop (50 μL sample that can be capillary collected [18]), provides reduced disposition decision time [19], improving patient satisfaction [20], and avoids inducing anemia or making it worse (phlebotomy is reported to induce anemia [21]).

Electrical impedance has been reported as an accurate solution for cellular detection, quantification and monitoring in different environments both *in-vivo* and *ex-vivo* [22–26]. Pop *et al*., [24] presented a continuous *in-vivo* hematocrit monitoring in the human right atrium by venous catheter equipped with an impedance-measuring device. On the other hand, Pradhan *et al*., [25] studied the electrical properties of blood and its constituents using Electrochemical Impedance Spectroscopy (EIS). Ramaswamy *et al*., [26] performed a blood coagulation test based on a custom microfluidic device and the electrical impedance detection of whole blood samples. Our group has previously studied this technique and has used it in the design of a novel anemia detection device [27]. The device presented reliable, sensitive and robust hematocrit detection, relying on low-cost straightforward electronic equipment and sensing systems. Moreover, the impedance measurement technique provided an actual hematocrit instantaneous measurement, with a wide measuring range oscillating from 0% to 100%, while other techniques, such as optical photometry, a slower hemoglobin measurement for a subsequent hematocrit indirect calculation. Additionally, considering a truly PoC device, the impedance measurement technique is a much less complex technique that does not require any optical measurement or chemical agent, resulting in a more economic, longer battery life and environmentally safe device.

This work presents an improvement on the previously reported device [27], as a compact, economic and portable PoC solution, for instantaneous detection of hematocrit through whole blood samples. The previously developed device relied on full spectrum analysis of blood samples by means of a Digital Lock-In Amplifier (DLIA) based on a Frequency Response Analyzer (FRA) approach. Full spectrum analysis involved a microprocessor for system control and data processing, and further electronics for signal conditioning, such as an SPI controlled oscillator AD9833 from Analog Devices (Norwood, MA, USA), and a 12-bit dual ADC ADC12D040 from Texas Instruments (Dallas, TX, USA) capable of converting simultaneously two analogue input signals at 40 MSPS. Moreover, a real-time platform sbRIO9632 from National Instruments (Austin, TX, USA) was used for fast software prototype development and versatility. All these electronics were a major drawback in terms of power consumption, size and price, when aiming for a specific PoC device.

The system is composed of an economic and reusable low-cost electronic device and a plug-and-play disposable commercial sensor. This sensor is based on three screen-printed electrodes for an envisaged sample of 50 μL. In order to validate the instantaneous hematocrit detection system, different blood samples, which came from the manipulation and dilution of whole blood samples extracted from 4 healthy donors, have been studied. These samples were randomly obtained from hospitalized patients of Hospital Clínic located in Barcelona, Spain.

2. Materials and Methods

2.1. Hematocrit, Electrodes, Impedance Measurement and Sensing System

A typical cellular electrical model for dilute cell suspensions can be described as a network of electrical passive components, so the biological electrical impedance is the response to applying an electrical stimulus to a biological material through a sensing system and measuring its electrical response as defined by Ohm's law [28] (Equation (1)):

$$Z_{CELL} = \frac{V_{CELL}}{I_{CELL}} \quad (1)$$

In this work we have adopted a configuration of three electrodes, which are defined as follows: the *working electrode* (WE), where electrical response of the object under investigation is measured; the *reference electrode* (RE), which tracks the electric signal and the *counter or auxiliary electrode* (CE), which supplies the current required. With this electrode configuration, the problematic behavior of the simpler two electrodes topology is avoided [27]. This configuration is defined by the WE, where the sample is placed and the electrical signal is applied, and the CE, which tracks the solution potential and supplies the current required for experience, creating a polarization effect causing a distortion of the applied electrical signal. With this sensing system topology, the electrical stimulus applied is an ac voltage (V_{CELL}), while the electrical response is the current flow through the WE electrode (I_{CELL}).

Hence, electrical properties can be described as a passive electrical components network [29] (Figure 1a), so the current related to the electrical stimulus (I_{CELL}) can flow through an external cellular path (R_E) or across the cell membrane ($RM \| CM$) and go through the intra-cellular medium (R_I). Hill and Thompson [30] confirmed the close relation between hematocrit and impedance at low frequencies (up to 100 kHz), where I_{CELL} flow path is located outside the RBCs across RE impedance. This phenomenon implies a correlation of impedance and hematocrit, so that an increment in RBCs makes the current flow path larger between the reference and working electrodes, becoming an increment on Z_{CELL} impedance due to an increment of R_E impedance (Figure 1b).

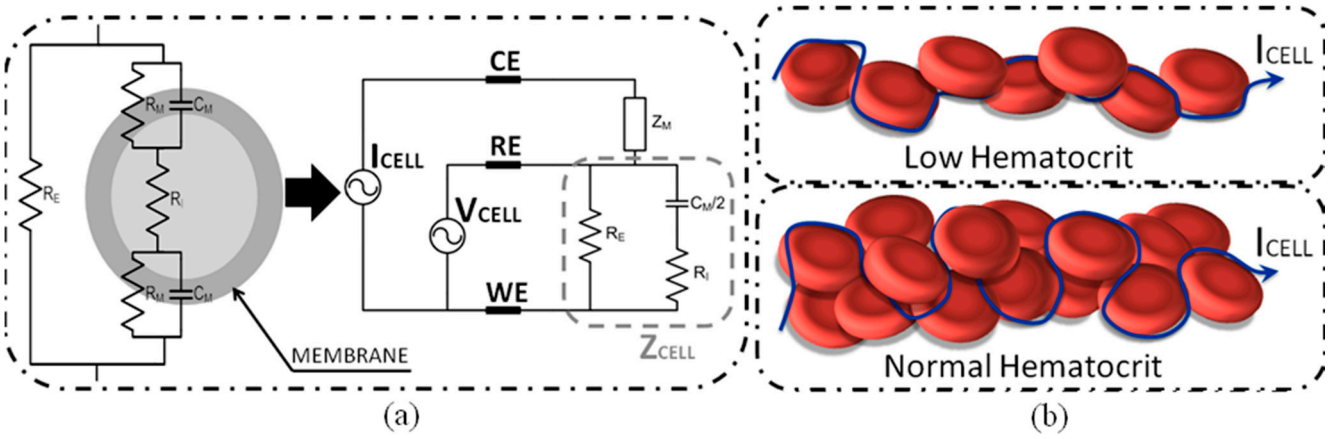

Figure 1. (**a**) Red Blood Cell (RBC) electrical model. Three electrodes topology for RBC sample; (**b**) Current flow path through different blood samples with different hematocrit. (Reproduced from [27] with kind permission from IEEE Publishers).

This phenomenon has been studied previously [27], demonstrating the feasibility of the impedance measurement technique to perform an easy, fast and sensitive hematocrit detection, evaluated through comparison with complete blood count (CBC) by using a clinical hematology analyzer, the Advia 2120 from Siemens AG (Munich, Germany). This sensing system is a low-cost disposable three-electrode sensor that works with 50 μL blood samples. This is the standard volume for a whole blood drop, which is easy to manipulate by clinical laboratory technicians using standard clinical laboratory tools. Furthermore, the sensor electrodes must be made of gold, an acknowledged bio-compatible material. Different commercial sensors have been evaluated, such as AC1 sensor from BVT Technologies

(Brno, Czech Republic), or the G-AUG sensor series from Bio-Logic SAS (Claix, France). The commercial sensor that best reaches the defined specifications is the C223AT from Dropsens (Llanera, Spain). This sensor is specifically designed to work with 50 µL drop samples and has gold screen-printed electrodes of 1.6 mm diameter. Blood samples were easily put on top of the sensor electrodes with an automatic pipette.

2.2. Blood Samples

Four blood samples were obtained in 4-mL tubes containing ethylenediaminetetraacetic acid (EDTA 7.2 mg from BD Vacutainer, (Franklin Lakes, NJ, USA) from four random hospitalized patients in Hospital Clinic. To obtain a larger sample collection, the initial four whole blood samples were centrifuged (Jouan CR412 from DJB Labcare, Newport Pagnell, UK) at 2200 rpm for 15 min in order to separate blood plasma from RBCs. Finally, 24 blood samples were obtained diluting obtained RBCs in different volumes of blood plasma using a Labopette Manual 10–100 µL automatic pipette from Hirschmann Laborgeräte (Louisville, KY, USA). We performed a complete blood count (CBC) of the 24 blood samples with an ABX Micros 60 haematology analyzer (Horiba, Kyoto, Japan) which reported the hemoglobin and hematocrit results as g/dL and percentage (%), respectively. This analyzer used electrical impedance technology to perform the CBC. With this methodology, whole blood is aspirated into the system, the sample stream is split, one portion is used for hemoglobinometry and one portion is used for RBC counting and size. Hemoglobinometry is based on RBC analysis and measurement of hemoglobin concentration by absorbance of spectrophotometry. RBC counting and size analyses are performed by passing the RBCs singly through a small direct current. The temporary increase in impedance caused by the passage of the cell provides information about RBC number and RBC volume. Hematocrit is calculated from the measured hemoglobin, RBC number and RBC volume [31]. Therefore, the obtained hematocrit (HCT (%)) and hemoglobin (Hb (g/dL)) for the different blood samples are shown in Table 1.

Table 1. Twenty four blood samples obtained in Hospital Clínic from four random hospitalized patients. Blood samples were obtained diluting RBCs in different volumes of blood plasma. Hematocrit (HCT (%)) and hemoglobin (Hb (g/dL)) values for the different blood samples were obtained by means of a complete blood count (CBC).

HCT (%)	Hb (g/dL)	HCT (%)	Hb (g/dL)	HCT (%)	Hb (g/dL)
14.2	5.0	25.5	9.0	34.7	12.4
18.5	6.7	28.4	9.7	37.8	12.5
18.9	6.6	29.0	9.8	40.0	12.8
19.3	7.0	29.2	9.7	40.4	14.0
20.4	6.9	30.0	10.5	40.8	14.0
23.2	7.8	33.7	11.5	44.5	14.9
23.4	8.1	33.9	11.8	45.0	15.2
24.0	8.1	34.5	11.5	50.6	18.0

2.3. System Description

A full custom electronic circuit was specifically designed to carry out impedance measurements using a disposable three-electrode C223AT sensor. The electronic system was designed based on the specifications found in the study previously reported [27]. The architecture of the device is divided in three parts: an oscillator that provides the ac voltage signal (V_{CELL}), a sensor driving instrumentation and a rms-to-dc converter (Figure 2a). The oscillator is a Wien bridge oscillator, a stable output amplitude with low distortion. The operational amplifier (OSC in Figure 2a) is the AD8066 from Analog Devices, which is a low-cost, high speed Junction Gate Field Effect Transistor (JFET) amplifier dual supply with low leakage current and distortion, in order to provide a stable sinus voltage signal with low offset (V_{OSC}).

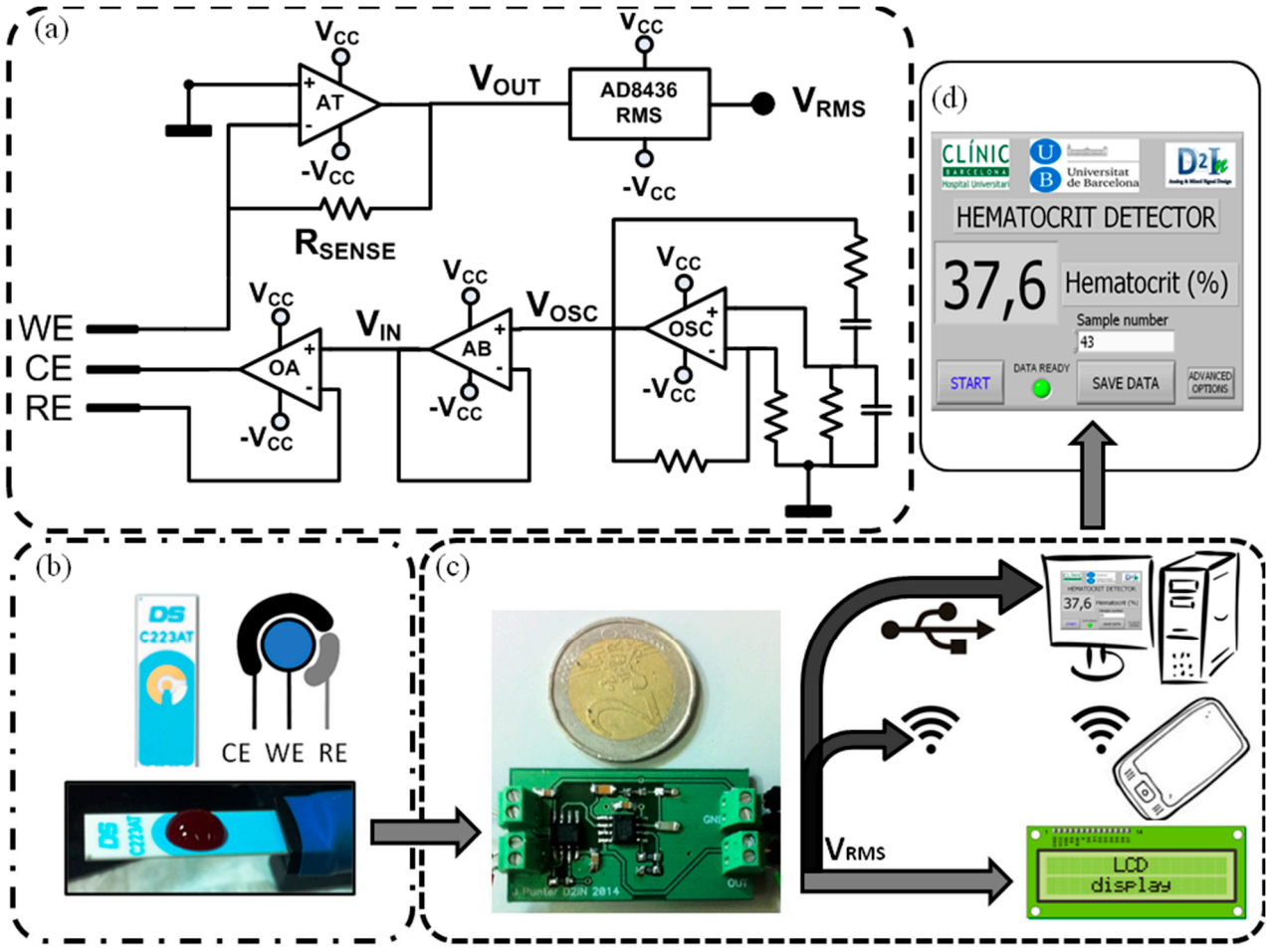

Figure 2. (**a**) Custom electronic instrumentation; (**b**) Commercial C223AT disposable sensor with a 50 µL whole blood drop; (**c**) Device prototype electronics and different suitable and functional user readout interfaces (the reference coin has a diameter of 25.75 mm); (**d**) Actual user-friendly front-end user interface develop with Labview©. (Reproduced from [27] with kind permission from IEEE Publishers).

The oscillator has been configured to provide a voltage sinus signal of 33 kHz, a well-suited frequency for hematocrit detection using the C223AT [28]. Moreover, as the AD8066 commercial integrated circuit provides two isolated amplifiers, the second amplifier has been used as a voltage

follower (AB in Figure 2a), due to its high speed and low distortion specifications for isolating the oscillator from the potentiostat. The sensor driving instrumentation is based on a potentiostat with a transimpedance amplifier current readout stage [32], composed of an operational amplifier to bias the sensor and an operational amplifier in transimpedance configuration as a sensing system current readout. The operational amplifier (OA in Figure 2a) is the AD8066 from Analog Devices, which is perfectly designed for singly driving the electrodes and track the voltage-biasing signal (V_{IN}) to the electrodes (2).

The JFET high input impedance avoids RE electrode voltage distortion, considering the low load impedance on the sensing system [27], and the high bandwidth and slew-rate provides stability to the system. The second amplifier included on the integrated circuit package has been configured as the transimpedance amplifier (AT in Figure 2a). The transimpedance amplifier converts the current through the electrodes (3) into a voltage signal (V_{OUT}) by means of a sensing resistor (R_{SENSE} in Figure 2a). The main drawback of this configuration, an amplifier with low input impedance [capitol intech antic], is avoided with the JFET input of the AD8066:

$$Z_{CELL} = \frac{V_{IN}}{I_{CELL}} \tag{2}$$

$$V_{OUT} = -R_{SENSE} \cdot I_{CELL} = -R_{SENSE} \frac{V_{IN}}{Z_{CELL}} \tag{3}$$

Finally, the rms-to-dc converter is the AD8436 from Analog Devices, which computes a precise dc equivalent (V_{RMS}) of the transimpedance amplifier ac signal (V_{OUT}). It is a low cost, low power device, with wide dynamic input range and wide bandwidth that provides low distortion with a Zero subthreshold swing Field Effect Transistor (ZFET) input buffer for electronic isolation from the instrumentation stage. Considering that the electrodes voltage biasing signal (V_{IN}) and the sensing resistor (R_{SENSE}) are stable and well known, the rms dc variations of V_{OUT} are only related to the variations of Z_{CELL}. The device dc output voltage (V_{RMS}) is inverse compared to the hematocrit values, so as the hematocrit increases, V_{RMS} decreases. The device usage is very simple not requiring any qualified users. A blood sample is placed on top of the sensor electrodes and, once the power supply is connected, the device dc output voltage (V_{RMS}) is ready for reading on the output pin. On the presented manuscript, a software interface on an external computer with Labview©, from National Instruments, controlled an electric switch to enable the power supply (an external source at ±5 V), and presents the resultant data on a user-friendly user interface (Figure 2d). The electronics and the computer were connected by means of a NI USB-6361 data acquisition (DAQ) device from National Instruments. However, the presented device readout stage can be greatly improved to address different applications and user skills (Figure 2c), such as an integrated Liquid Crystal Display (LCD) for an untrained user self-screening, a remote computer connected to the electronics by means of an standardized protocol (USB, ethernet, *etc*.), or a wireless communication protocol for self-monitoring device in telemedicine applications. Additionally, the presence of an electrical signal directly correlated to hematocrit allows the device implementation as a controller of other clinical actuators in different environments and situations increasing functionality.

The overall low cost and low power system composed of optimized straightforward standards for instrumentation electronics, results in a reusable, robust and low consumption device (300 mWh)

making it completely mobile with a long battery life time. Moreover, it is important to highlight that it is an easy to manipulate and economic electronics (less than 10 € per device), providing an instantaneous impedance measurement.

3. Results

A small, compact and portable device for point-of-care early instantaneous detection of anemia was prototyped. For its validation, we analysed 24 consecutive blood samples from patients hospitalized at Hospital Clínic in Barcelona. We performed a complete blood count (CBC) of the blood samples with a haematology analyser, the Advia 2120 from Siemens AG, which reported the hemoglobin and hematocrit results as g/dL and percentage (%), respectively. We tested all samples with the prototype within 2 h of blood collection and CBC. As it is an instantaneous detector with a time response of several milliseconds, to evaluate system precision and accuracy, every whole blood sample was tested 5 times consecutively using fresh sensors and fresh sub-samples. Figure 3 depicts the output dc voltage (V_{RMS}) of the device and compares it with the different whole blood samples hematocrit (Hematocrit (%)).

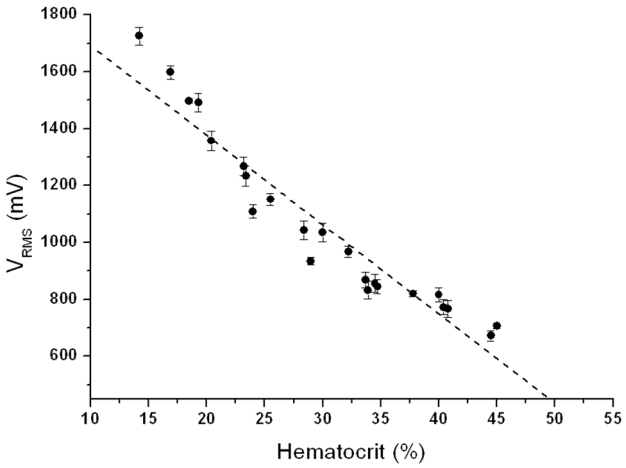

Figure 3. Measured output dc voltage (V_{RMS} (mV)) mean value (n = 5) as a function of blood samples hematocrit (Hematocrit (%)).

We used the Linear Regression (LR) analysis to measure the Pearson's correlation coefficient (r) and coefficient of determination (r^2) between the reference method (CBC method) and the custom electronic device method, where the output voltage (V_{RMS}) mean value (n = 5) has been compared with whole blood samples CBC hematocrit. The LR slope (β) defines the sensitivity, in terms of mV per hematocrit percentage (mV/%). Meanwhile the hematocrit detection accuracy (%) is the relation (4) between r^2 and β:

$$V_{RMS}(mV) = \alpha + \beta \cdot Hematocrit(\%) \quad (4)$$

In Table 2 the experimental results of whole blood samples hematocrit (HCT (%)), the output voltage mean value (V_{RMS} (mV)) of the five measurements performed with each whole blood sample and its standard deviation (SD (mV)) are shown. Precision was evaluated with the coefficient of variation: the standard deviation (SD (mV)) divided by the mean value (V_{RMS} (mV).

Table 2. Device validation with whole blood samples.

HCT (%)	V_{RMS} (mV)	SD (mV)	HCT (%)	V_{RMS} (mV)	SD (mV)	HCT (%)	V_{RMS} (mV)	SD (mV)
14.2	1725.92337	31.28	25.5	1152.10028	21.24	34.7	845.70887	25.20
16.9	1598.31218	24.08	28.4	1043.23605	32.28	37.8	820.04855	10.32
18.5	1498.75603	8.12	29.0	934.82407	13.08	40.0	816.04674	25.08
19.3	1491.64678	32.4	30.0	1035.4325	33.88	40.4	773.16798	25.20
20.4	1358.14206	34.56	32.2	968.69188	20.04	40.8	766.09567	30.36
23.2	1268.13432	33.00	33.7	869.14198	26.44	44.5	671.69091	18.52
23.4	1233.56278	34.16	33.9	832.33453	31.32	45.0	707.49377	8.76
24.0	1109.21312	23.28	34.5	856.91271	30.12	50.6	490.1229	6.32

The proposed anemia detector device presented great accuracy at detecting hematocrit, with a Pearson's correlation coefficient of −0.96, an accuracy error of 2.83% hematocrit, and a coefficient of determination of 92.72%. The mean coefficient of variation is 2.57% without any particular case above 5%. Acceptable values in quality control procedures in clinical haematology measurements show a coefficient of variation less than 5% [30]. The device presents reliable, sensitive and robust anemia detection compared with other commercial PoC devices for anemia detection, such as AnemiaCheck from Express Diagnostics (Blue Earth, MN, USA), STAT-Site from Stanbio Laboratory (Boerne, TX, USA), or HemoPoint H2 from Alere (Waltham, MA, USA), where its detection performance is similar to the proposed prototype but with much slower response.

Recently, other PoC anemia devices have been published, such as a color-based diagnostic test for self-screening/self-monitoring of anemia presented by Tybursky *et al*., [33], a novel PoC diagnostic test for self-screening, self-monitoring of anemia. The device measures hemoglobin (Hgb) levels, which are estimated via visual interpretation by the user using a color scale. This system presents several performance drawbacks when compared with our device. First of all, the readout stage, based on a color scale, relies on the visual interpretation of the user, which could introduce errors on the Hgb levels data interpretation, and reduces considerably the system resolution. Furthermore, the principle of operation of the color-based POC device is based on biochemical reactions, where the blood comes into contact with a reagent solution initiating a redox reaction, which is a slow and destructive procedure.

4. Market and Technology Transfer Challenges

Commercialization of biosensors technology is still delayed compared with research in academia. This reduced technology transfer activity could be attributed to technical barriers or cost considerations. Therefore, devices must be versatile to allow automation at a competitive cost [34]. Additionally, to ensure success in the development, innovation and technology transfer, it is necessary to foster a particular scenario typified by the convergence of technologies and disciplines [35]. In this context, one of the main characteristics of the proposed device is its multidisciplinarity: in an effort to integrate knowledge from various dimensions, main actors and activities. The cross-disciplinary interaction must be examined in the way scientific knowledge flows between engineers, researchers and physicians. Currently, there are huge opportunities to be exploited by researchers and innovation managers in the development of high-tech products, above all in the field of medical devices. As such,

the University–Hospital–Industry–Administration (plus Citizens) system should emerge as an essential five-helix leading to a successful technology transfer and commercialization of public-funded medical devices [36].

In biomedical research, there is a great need for multipurpose and reliable telemetric tools. By using sensor inputs, such devices allow the automated gathering of information on physiological parameters minimizing adverse effects for the patients [35]. In this context the proposed device could improve the diagnosis especially in countries where clinics are often many miles away from villages, where there is absence of laboratory facilities and trained staff, or there are hostile environmental conditions [15]. Additionally, this device could overcome some of the complications related to blood extractions used in conventional methods, including hematoma formations, nerve damage, pain, hemoconcentration, extra-vasation, iatrogenic anemia, arterial puncture, petechiaes, allergies, infection, syncope and fainting, excessive bleeding, edema or thrombus [37].

PoC testing promotes a shift away from traditional diagnostic tests in the clinical laboratory setting to near-patient situations, improving the timely diagnostic information so as to make informed decisions regarding diagnosis and treatment. Rapid advances are already being achieved at remarkably low cost with modest investments; therefore there is a high growth rate market [38]. PoC devices represent 31% of the diagnostics market, 18% glucose testing, 11% professional PoC products, and 2% over-the-counter [39]. It is expected that the global market will increase to US$16.5 billion by 2016 and $34.6 billion by 2021 [40]. Additionally, the total LoC-based biochip market was US$2.4 billion in 2009 and was projected to increase to US$5.9 billion in 2014. This should be a powerful incentive for commercial efforts to move toward true global health solutions [15].

5. Conclusions

In this work, a novel point-of-care (PoC) device for instantaneous anemia detection based on custom instrumentation electronics, impedance measurement technique and a disposable low-cost sensor has been designed, fabricated and tested. The device has been proved to exhibit reliable, robust and effective results using disposable commercial sensors with 50 μL whole blood samples. Advantages of the proposed device include: (i) the facility of use; (ii) compactness and small size; (iii) portability; (iv) less invasive and less quantity of blood; (v) rapidity and accuracy of results; and (vi) low-cost accessibility. These characteristics are valuable for anemia-risk patients, especially for pregnant women, neo-nates, pediatric patients and elderly, but also for chronically anemic patients, such as cancer patients receiving chemotherapy, patients with renal failure, patients with chronic inflammatory/immunologic disorders, or patients with primary hematologic disorders. Low manufacturing cost and the accessible price are important advantages, especially in disadvantaged regions where the health domain is undervalued. Commercial devices for PoC anemia detection, based on microfluidic manipulator devices, such as AnemiaCheck from Express Diagnostics, or on photometry hemoglobin detection, such as STAT-Site from Stanbio Laboratory, or HemoPoint H2 from Alere, relay on slower hemoglobin measurement for a subsequent hematocrit indirect calculation, with results open to user interpretation as the readout stages are optically represented. The presented device outputs instantaneous reliable results based on electric voltage data directly correlated to hematocrit, the system have further versatility in terms of applications compared with other

commercial devices, such as a point-of-care hematocrit detector, a monitoring device for telemedicine applications, or as a controller of other clinical actuators. Furthermore, unlike actual clinical equipment for blood analysis, whole blood samples are not destroyed in the measurement process and the adverse effects for patients and blood samples are being mitigated.

PoC anemia diagnostic devices recently published, such as a color-based diagnostic test by Tybursky *et al.*, [40], present severalby of the user, which could introduce errors on the data interpretation, and reduces the system resolution, being a slower and destructive technique, with less functionalities in Point-of-Care and Lab-on-a-Chip devices for medical and research applications.

Twenty four blood samples, obtained from four patients hospitalized at Hospital Clínic, were used to demonstrate the feasibility of the impedance measurement technique to perform an easy, fast and low-cost hematocrit study using disposable commercial sensors. The system has been evaluated through comparison with complete blood count (CBC) using a clinical haematology analyser. The anemia detection device has a Pearson's correlation coefficient of −0.96 and a coefficient of determination of 92.72% hematocrit. Coefficient of variation is below 5%, with a worst-case accuracy error of 2.83%. Additionally, as the system is based on straightforward low cost and low power standards on instrumentation electronics and sensing, it represents an economic, portable, safe and reliable system of anemia detection with a high degree of integration for the clinical environment, driving the development of a truly autonomous, portable and versatile device relying on the presented work. In Table 3 is presented a performance comparison table with different commercial and published anemia PoC diagnostic test.

Table 3. Comparison table with different commercial and published anemia PoC diagnostic test.

Device	Test Time (s)	Range (HCT (%) and Hb (g/dL))	Standard Deviation (%)	Coefficient Variation (%)
Presented device.	Instantaneous	HCT: 0%–100%	2.83%	2.57%
STAT-Site.	900	HCT: 12%–42%	0.74%	4.10%
Alere HemoPoint H2 System.	120	Hb: 5.6 g/dL–20.6 g/dL	NA	4.20%
Anemia Check.	60	Hb: 0 g/dL–25.6 g/dL HCT: 36%–54%	NA	1.5%
Tybursky *et al*., (2014) [40]	60	Hb: <9 g/dL–>12 g/dL	NA	NA

Once again, this demonstrates the importance of a multidisciplinary team that integrates the clinical research with the university, in an effort to obtain a cross-fertilization development that aims to satisfy medical but also social needs through R + D + i. With this combined effort and symbiosis, it is possible to obtain innovative products and also reduce the time-to-market in medical research settings.

In summary, this paper describes the design, development and test of a novel instantaneous anemia detection PoC device with low cost disposable commercial sensors and instrumentation electronics. The device presents reliable, sensitive and robust anemia detection, relying on low power straightforward electronic equipment and sensing systems for hematocrit monitoring.

Author Contributions

Jaime Punter-Villagrasa (J.P.-V.) developed and tested the Point-of-Care (PoC) electronic device and acquisition software, did the experimental study with blood samples, analyzed and interpreted the acquired data. He wrote the manuscript and approved the final version of the manuscript. Joan Cid (J.C.) and Ivón Rodríguez-Villareal (I.R.-V.) have contributed in the experiments design and protocols, and sample manipulation supervision. They have contributed to write the manuscript as well as approved the final version for its publication. Besides, J.C. was in charge of the experimental study and provided the blood samples for its posterior use in the study. Pere Ll. Miribel-Català (P.L.M.-C.) and Jordi Colomer-Farrarons (J.C.-F.) supervised the development of the PoC device and the acquisition software. They have discussed the resultant data, contributed in the manuscript and approved the final version for its publication. Esteve Juanola-Feliu (E.J.-F.) and Cristina Páez-Avilés (C.P.-A.) have contributed with the analysis of the innovative scenario typified by the convergence of technologies, the multidisciplinarity and the cross-fertilization of technologies, as well as the commercialization and technology transfer challenges, especially for public funded medical devices and the situation of PoCs testing devices in the current diagnostics market.

Conflicts of Interest

The authors declare no conflict of interest.

References

1. World Health Organization (WHO). Anaemia. Available online: http://www.who.int/nutrition/topics/anaemia/ (accessed on 2 November 2014).
2. World Health Organization (WHO). Micronutrient deficiencies. Available online: http://www.who.int/nutrition/topics/ida/en/ (accessed on 2 November 2014).
3. De Benoist, B.; McLean, E.; Egli, I.; Cogswell, M.E. *Worldwide Prevalence of Anaemia 1993–2005: WHO Global Database on Anaemia*; WHO: Geneva, Switzerland, 2008.
4. World Health Organization (WHO). *Iron Deficiency Anaemia: Assessment, Prevention and Control. A Guide for Programme Managers*; WHO: Geneva, Switzerland, 2001.
5. Thakur, N.; Chandra, J.; Pemde, H.; Singh, V. Anemia in severe acute malnutrition. *Nutrition* **2014**, *30*, 440–442.
6. Rottoli, M.; Sabharwal, T.; Schizas, A.M.; George, M.L. Bleeding pseudoaneurysm of the internal iliac artery after extended resection for advanced rectal cancer: Report of two cases. *Int. J. Colorectal Dis.* **2014**, doi:10.1007/s0038401419534.
7. Ong, B.; Rockey, D.C. The syndrome of a large drop in hematocrit in hospitalized patients: Clinical features and gastrointestinal bleeding outcomes. *J. Investig. Med.* **2014**, doi:10.1097/JIM.0000000000000109.
8. National Heart, Lung, and Blood Institute. What Is Sickle Cell Anemia? Available online: http://www.nhlbi.nih.gov/health/health-topics/topics/sca/ (accessed on 10 November 2014).
9. Medline Plus. Thalassemia. Available online: http://www.nlm.nih.gov/medlineplus/ency/article/000587.htm (accessed on 10 November 2014).

10. American Cancer Society. Anemia in People with Cancer. Available online: http://www.cancer.org/treatment/treatmentsandsideeffects/physicalsideeffects/anemia/anemia-in-people-with-cancer (accessed on 10 November 2014).
11. Portolés, J.; Gorriz, J.L.; Rubio, E.; de Alvaro, F.; García, F.; Alvarez-Chivas, V.; Aranda, P.; Martinez-Castelao, A. The development of anemia is associated to poor prognosis in NKF/KDOQI stage 3 chronic kidney disease. *BMC Nephrol.* **2013**, *14*, doi:10.1186/1471-2369-14-2.
12. Pinto, M.; Barjas-Castro, M.L.; Nascimento, S.; Falconi, M.A.; Zulli, R.; Castro, V. The new noninvasive occlusion spectroscopy hemoglobin measurement method: A reliable and easy anemia screening test for blood donors. *Transfusion* **2013**, *53*, 766–769.
13. Belardinelli, A.; Benni, M.; Tazzari, P.L.; Pagliari, P. Noninvasive methods for haemoglobin screening in prospective blood donros. *Vox Sang*. **2013***, 105*, 116–120.
14. Northrop-Clewes, C.A.; Thurnham, D.I. Biomarkers for the differentiation of anemia and their clinical usefulness. *J. Blood Med.* **2013**, *4*, 11–22.
15. Fu, B.E.; Yager, P.; Floriano, P.N.; Christodoulides, N.; Mcdevitt, J.T. Perspective on Diagnostics for Global Health. *IEEE Pulse* **2011**, *6*, 40–50.
16. Brown, J.; Theis, L.; Kerr, L.; Zakhidova, N.; O'Connor, K.; Uthman, M.; Richards-Kortum, R. A hand-powered, portable, low-cost centrifuge for diagnosing anemia in low-resource settings. *Am. J. Trop. Med. Hyg.* **2011**, *85*, 327–332.
17. Thompson, R.B. *Short Textbook of Haematology*, 4th ed.; Pitman Publishing, Kent, UK, 1975.
18. Ernst, D.J.; Ballance, L.O.; Calam, R.R.; McCall, R.; Szamosi, D.I.; Tyndall, L. *Procedures and Devices for the Collection of Diagnostic Capillary Blood Specimens; Approved Standard, 6th ed.*; H04-A6; Clinical and Laboratory Standard Institute: Wayne, PA, USA, 2008.
19. Asha, S.D.; Chan, A.C.F.; Walter, E.; Kelly, P.J.; Morton, R.L.; Ajami, A.R.D. Wilson, A.; Honneyman, D. Impact from point-of-care devices on emergency department patient processing times compared with central laboratory testing of blood samples: A randomised controlled trial and cost-effectiveness analysis. *J. Emerg. Med.* **2013**, *31*, 1–6.
20. Jones, C.D.H.; Howick, J.; Roberts, N.W.; Price, C.P.; Heneghan, C.; Plüddemann, A.; Thompson, M. Primary care clinicians' attitudes towards point-of-care blood testing: A systematic review of qualitative studies. *BMC Fam. Pract.* **2013**, *14*, 117.
21. Thavendiranathan, P.; Bagai, A.; Ebidia, A.; Detsky, A.S.; Choudhry, N.K. Do blood tests cause nemia in hospitalized patients? The effect of diagnostic phlebotomy on hemoglobin and hematocrit levels. *J. Gen. Intern. Med.* **2005**, *20*, 520–524.
22. Ramirez, N.; Regueiro, A.; Arias, O.; Contreras, R. Electrochemical impedance spectroscopy: An effective tool for a fast microbiological diagnosis. *Biotechnol. Apl.* **2008**, *26*, 72–78.
23. Pop, G.A.; Bisschops, L.L.; Iliev, B.; Struijk, P.C.; van der Hoeven, J.G.; Hoedemaekers, C.W. On-line blood viscosity monitoring *in vivo* with a central venous catheter, using electrical impedance technique. *Biosens. Bioelectron.* **2013**, *41*, 595–601.
24. Hernández, F.; Guerrero, C.; Bernal, J. Determinación de las propiedades eléctricas en tejido sangíneo. *Ciencia UANL* **2011**, *8*, 7–13.
25. Pradhan, R.; Mitra, A.; Das, S. Impedimetric characterization of human blood using three-electrode based ECIS devices. *J. Electr. Bioimpedance* **2012**, *3*, 12–19.

26. Ramaswamy, B.; Yin-Ting, T.Y.; Si-Yang, Z. Microfluidic device and system for point-of-care blood coagulation measurement based on electrical impedance sensing. *Sens. Actuators B Chem.* **2013**, *180*, 21–27.
27. Punter-Villagrasa, J.; Cid, J.; Colomer-Farrarons, J.; Rodriguez-Villarreal, I.; Miribel-Catala, P.Ll. Towards an Anaemia Early Detection Device Based on 50 μL Whole Blood Sample. *IEEE Trans. Biomed. Eng.* **2014**, doi:10.1109/TBME.2014.2364139.
28. Patterson, R. Bioelectric Impedance Measurements. In *The Biomedical Engineering Handbook*, 2nd ed.; Bronzino, J.D., Ed.; CRC Press: Boca Raton, FL, USA, 2000; pp. 734–773.
29. Beriet, C.; Pletcher, D. A microelectrode study of the mechanism and kinetics of the ferro/ferricyanide couple in aqueous media: The influence of the electrolyte and its concentration. *J. Electroanal. Chem.* **1993**, *361*, 93–101.
30. Hill, D.W.; Thompson, F.D. The effect of hematocrit on the resistivity of human blood at 37 °C and 100 kHz. *J. Med. Biol. Eng.* **1975**, *13*, 182–186.
31. Corash, L. Laboratory Hematology: Methods for the Analysis of Blood. In *Blood: Principles and Practice of Hematology,* 1st ed.; Handin, R.I., Lux, S.E., Stossel, T.P., Eds.; Lippincott Williams & Wilkins: Philadelphia, PA, USA, 1995; pp. 23–61.
32. Punter-Villagrasa, J.; Colomer-Farrarons, J.; Miribel, P.Ll. Bioelectronics for Amperometric Biosensors. In *State of the Art in Biosensors—General Aspects*, 1st ed.; Rinken, T., Ed.; InTech: Rijeka, Croatia, 2013.
33. Tyburski, E.A.; Gillespie, S.E.; Stoy, W.A.; Mannino, R.G.; Weiss, A.J.; Siu, A.F.; Bulloch, R.H.; Thota, K.; Cardenas, A.; Session, W.; *et al*. Disposable platform provides visual and color-based point-of-care anemia self-testing. *J. Clin. Investig.* **2014**, 4387–4394.
34. Luong, J.H.T.; Male, K.B.; Glennon, J.D. Biosensor technology: Technology push *versus* market pull. *Biotechnol. Adv.* **2008**, *26*, 492–500.
35. Juanola-Feliu, E.; Miribel-Català, P.L.; Páez-Avilés, C.; Colomer-Farrarons, J.; González-Piñero, M.; Samitier, J. Design of a customized multipurpose nano-enabled implantable system for *in-vivo* theranostics. *Sensors* **2014**, *14*, 19275–306.
36. Juanola-Feliu, E.; Colomer-Farrarons, J.; Miribel-Català, P.; Samitier, J.; Valls-Pasola, J. Market challenges facing academic research in commercializing nano-enabled implantable devices for *in-vivo* biomedical analysis. *Technovation* **2012**, *32*, 193–204.
37. Buowari, O. Complications of venepuncture. *Adv. Biosci. Biotechnol.* **2013**, *4*, 126–128.
38. Sachs, J.D. Primary health care in low-income countries: Building on recent achievements. *J. Am. Med. Assoc.* **2012**, *307*, 2031–2032.
39. Chin, C.D.; Linder, V.; Sia, S.K. Commercialization of microfluidic point-of-care diagnostic devices. *Lab Chip* **2012**, *12*, 2118–2134.
40. Gomez, F. The future of microfluidic point-of-care diagnostic devices. *Bioanalysis* **2013**, *5*, 1–3.

Publication 3.

Combined dielectrophoretic and impedance system for on-chip controlled bacteria concentration: Application to Escherichia coli.

Del Moral-Zamora, B.; Punter-Villagrasa, J.; Oliva-Brañas, A.M.; Álvarez-Azpeitia, J.M.; Colomer-Farrarons, J.; Samitier, J.; Homs-Corbera, A.; Miribel-Catala, P.L.

Electrophoresis, vol. 36, no. 9-10, pp. 1130-1141, April 2015.

APTARA | ELPS | elps201400446 | Dispatch: March 26, 2015 | CE:
Journal | MSP No. | No. of pages: 12 | PE: XXXXX

Q1
Beatriz del Moral-Zamora[1]
Jaime Punter-Villagrassa[1]
Ana M. Oliva-Brañas[2]
Juan Manuel Álvarez-Azpeitia[2]
Jordi Colomer-Farrarons[1]
Josep Samitier[1,2,3]
Antoni Homs-Corbera[1,2,3]
Pere LI Miribel-Català[1]

[1]Department of Electronics, University of Barcelona, Barcelona, Spain
[2]Nanobioengineering Group, Institute for Bioengineering of Catalonia (IBEC), Barcelona, Spain
Q2
[3]Centro de Investigación Biomédica en Red en Bioingeniería, Biomateriales y Nanomedicina (CIBER-BBN), Spain

Received September 19, 2014
Revised February 4, 2015
Accepted March 9, 2015

Research Paper

Combined dielectrophoretic and impedance system for on-chip controlled bacteria concentration: Application to *Escherichia coli*

The present paper reports a bacteria autonomous controlled concentrator prototype with a user-friendly interface for bench-top applications. It is based on a microfluidic lab-on-a-chip and its associated custom instrumentation, which consists of a dielectrophoretic actuator, to preconcentrate the sample, and an impedance analyzer, to measure concentrated bacteria levels. The system is composed of a single microfluidic chamber with interdigitated electrodes and an instrumentation with custom electronics. The prototype is supported by a real-time platform connected to a remote computer, which automatically controls the system and displays impedance data used to monitor the status of bacteria accumulation on-chip. The system automates the whole concentrating operation. Performance has been studied for controlled volumes of *Escherichia coli* samples injected into the microfluidic chip at constant flow rate of 10 μL/min. A media conductivity correcting protocol has been developed, as the preliminary results showed distortion of the impedance analyzer measurement produced by bacterial media conductivity variations through time. With the correcting protocol, the measured impedance values were related to the quantity of bacteria concentrated with a correlation of 0.988 and a coefficient of variation of 3.1%. Feasibility of *E. coli* on-chip automated concentration, using the miniaturized system, has been demonstrated. Furthermore, the impedance monitoring protocol had been adjusted and optimized, to handle changes in the electrical properties of the bacteria media over time.

Q4

Keywords:
Autonomous device / Bacteria concentrator / Dielectrophoresis / *Escherichia coli* / Impedance analysis
DOI 10.1002/elps.201400446

1 Introduction

In the last few years, the electrical properties of cells and pathogens have been used to explore new methods of manipulation and characterization, such as dielectrophoresis (DEP) [1] or impedance analysis (IA) [2, 3]. For instance, DEP has been recently used to control stem cells to form embryonic bodies in shorter time [4] and Fatoyinbo et al. [5] have measured biophysical parameters of cells (cytoplasmic conductivity, membrane conductivity, and cell-wall conductivity) by analyzing its cells' DEP behavior. Moreover, IA was also advantageous to detect ovarian cancer cells SKV3 [6] or to detect insulin levels in blood serum [7] so as to diagnose diabetes or trauma. We present a miniaturized and compact specific solution to concentrate bacteria in a controlled manner using a fully automated instrument combining DEP and IA.

Bacteria concentration is a time-consuming procedure in regular microbiology laboratory practices that involves cell-culturing processes [8, 9] to obtain a significant sample. This could be improved by using DEP as a means of concentration in tiny fluidic spaces. DEP refers to the force experienced by a particle inside a nonuniform electric field [10, 11] and is a convenient, rather selective, handling method that has been applied in many biological fields and in lab-on-a-chip (LoC) devices [12–14]. An example of this is the work reported by Lapizco-Encinas et al. [15], where several types of bacteria in water were concentrated and separated by DEP induced by insulator-based structures (iDEP), or in the paper presented by Braff et al. [16], where bacteria were successfully DEP trapped in PMMA constructs. DEP selectivity has also been repeatedly reported as a benefit for sample preparation, since it allows isolation of the desired cell or pathogen based on their electric and geometric properties [17–19]. As

Q3
Correspondence: Jaime Punter-Villagrasa, Department of Electronics, University of Barcelona, Martí i Franquès 1, 08028 Barcelona, Spain
E-mail: jpunter@el.ub.edu

Abbreviations: ADC, analog-to-digital converter; **DEP**, dielectrophoresis; **FRA**, frequency response analyzer; **IA**, impedance analysis; **IDE**, interdigitated electrode; **LoC**, lab-on-a-chip

Colour Online: See the article online to view Figs. 1, 2,4 and 5 in colour.

an example, Moon et al. [19] used DEP to separate and detect circulating tumor cells, whose size and resistance to filtering shear stress presented significant differentiating properties, from regular blood cells. This also becomes an advantage in the case of environmental samples, where soil particles with the same bacteria size are also present and could not be eliminated by filtration or centrifugation. This has also been solved by using DEP [20], taking advantage of its selectivity by cell electrical properties. Hence, we used DEP here for concentration purposes.

On the other hand, current bacteria-detection protocols are expensive in terms of equipment and time, typically requiring several days to obtain results [21, 22]. Techniques such as pathogenic-specific antibody-coated magnetic beads [23, 24] or hybridization of DNA fragments of bacteria [25] have shown to improve the analysis time down to several hours, but they still need complex equipment. This could be improved by using IA. Impedance frequency dependence, which is related to the electrical conductivity and permittivity properties of the material, was reported as an effective solution to characterize cells and their behavior, also in LoC devices [26]. Some publications have reported the use of IA technique to control bacterial growth or to detect its presence [27]. One example of such work is the paper presented by Dweik et al. [28], where bacterial presence was rapidly detected by measuring the antibody/antigen bonding using IA in the 100 Hz to 10 MHz range. Another example is the work of Grossi et al. [29], where the quantity of bacteria during a culture process was detected by impedance measured at 200 Hz using a sinusoidal signal with a 50 mV amplitude.

The combination of DEP and IA [3, 30] in a single equipment based on LoC and microfluidic technologies allows to develop a practical bench-top device. In recent years several biosensors and applications aiming for the successful combination of both techniques have been presented. Hamada et al. [3] presented a bacterial detection device combining both positive DEP and negative DEP with dielectrophoretic impedance measurement. The biosensor relied on a pair of interdigitated electrodes (IDEs) for separate DEP concentration and dielectrophoretic impedance measurement, while using commercial devices to operate the application. The cellular solution conductivity varies through time, which affects the impedance measurement, which has not been considered, and measurement instability produced by the magnitude of DEP voltage has been reported. Dastider et al. [30] have designed an impedance biosensor for the specific detection of *Esherichia coli* O157:H7 combining DEP and IA techniques at 2μL/min flow rate, which is relatively low. This work used different IDEs for cellular separation and detection purposes. The detection IDE was functionalized with polyclonal anti-*E. coli* antibodies for specific detection of *E. coli* O150:H7, removing versatility of the device. Moreover, the presented results for cells' concentration detection, based on impedance measurements, did not consider the solution conductivity variations, as well as the influence of DEP voltages on the impedance measurement.

Our work presents a completely customized equipment for a quick and easy way to concentrate bacteria with DEP technique at relatively high flow rates [31, 32], while monitoring its concentration by means of IA technique in a real-time scenario. It addresses the issues associated with the combination of these techniques by simplifying the equipment but also by trying to solving some issues generally avoided, to the best of our knowledge in other scientific works.

The device, with its main components, is presented in Fig. 1. It is composed of a customized electronic module and an LoC. The flowing bacteria sample is preconcentrated through the generated DEP generation and concentration is measured through IA monitoring, with a four-electrode sensor topology, embedded on a single microfluidic chamber. The electronic module is supported by a real-time platform for continuous concentration monitoring, connected to a remote computer through a standard Ethernet connection, which enables the system configuration and data display. First, it allows automated functionalities, such as multiplexing signals between the DEP generator and the IA analyzer in the microfluidic chip, in order to avoid DEP voltages disturbance of IA measurement, and auto-scale of the electronic instrumentation gains when necessary, for better signal acquisition. Second, it is connected to a remote computer with a user-friendly front-end user panel, where the system user can configure the experiment variables, such as measurement time for signal multiplexing, signal operation frequency, and output gain, while displaying the impedance measurements related to actual bacteria concentration level.

The solution presented controls, in an automated way, the bacteria concentration, and monitoring process and has been validated for *E. coli*, which presents pathogenic variants that cause morbidity and mortality worldwide [33]; therefore being a topic of interest. *E. coli* is one of the main antimicrobial-resistant pathogens for healthcare-associated infections reported to the National Healthcare Safety Network [34], being the primary cause of widespread pathologies such as significant diarrheal and extraintestinal diseases [33] or urinary tract infections [35]. Furthermore, *E. coli* can be found as a bacterial food contamination [21] and causes avian colibacillosis, one of the major bacterial diseases in the poultry industry and the most common avian disease communicable to humans [36].

The aims of our study are (i) to prove the feasibility of DEP generator and IA analysis combination for controlled concentration using a single equipment together with a single microfluidic chip; (ii) to establish a protocol for autonomous concentration procedure; and (iii) to develop a complete electronic equipment with an electronic instrumentation, embedded software control, and user interface for a complete autonomous and reliable bacteria concentrator device, based on DEP generator and IA technique.

This novel, specific device has been proven as a robust and reliable automated system and protocol for bacteria controlled concentration. It will provide the scientific community with a rapid tool for bacteria presence detection, by avoiding

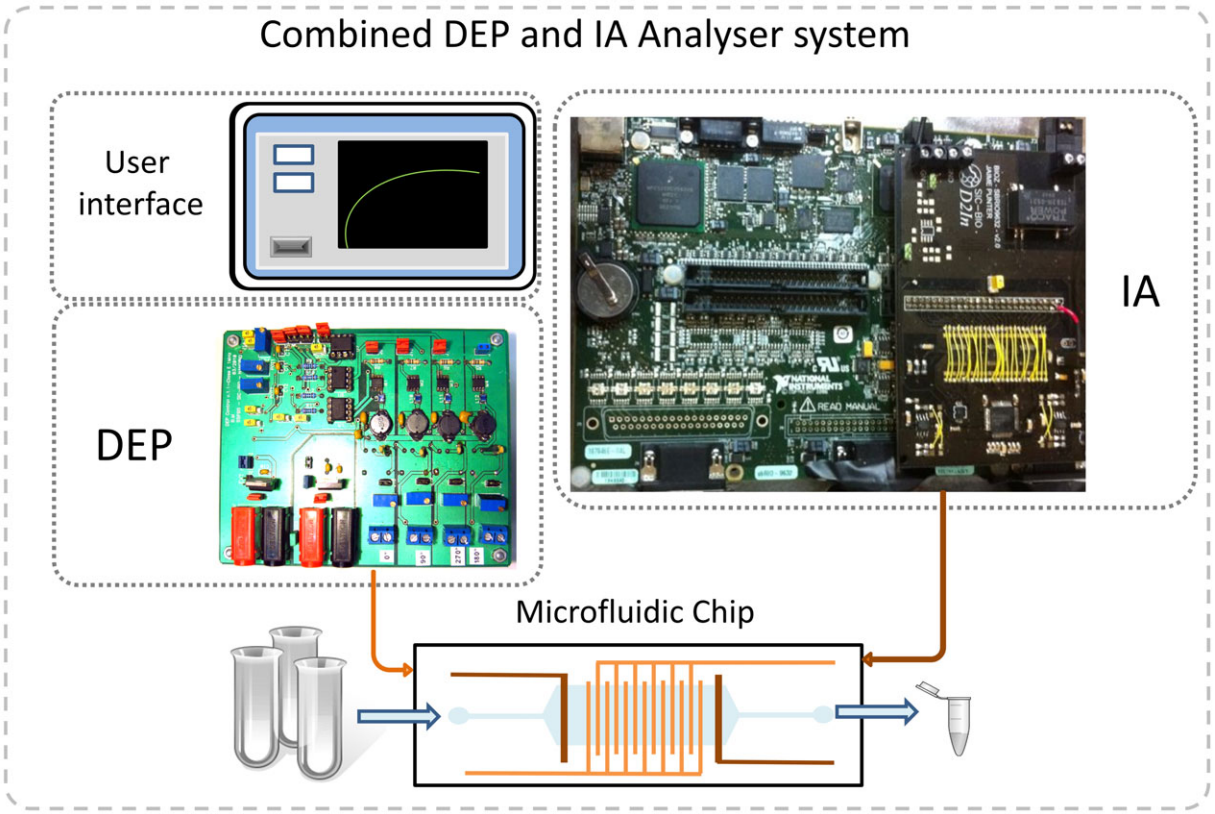

Figure 1. Combined system overview.

previous slow preparations in preconcentration and culture processes, reducing procedure times for a faster diagnosis and treatment.

2 Theory

2.1 The dielectrophoretic effect

DEP [11] defines the movement of an electrically neutral particle when a nonuniform electric field is applied. If the particle is considered homogeneous and isotropic and is polarized linearly, then the dielectrophoretic force is defined by Eq. (1) [37, 38]—where V is the volume of the particle; E is the electric field; and α is the effective polarizability, which is defined by the expression (2):

$$F_{\mathrm{DEP}} = \frac{1}{2} V \cdot Re\left[\alpha^*(\omega)\right] \nabla |\vec{E}|^2 \tag{1}$$

$$\alpha = 3\varepsilon_0 \varepsilon_m F_{\mathrm{CM}}, \tag{2}$$

where ε_0 and ε_m are the vacuum permittivity and the medium permittivity, respectively, and F_{CM} is the Clausius–Mosotti factor. The F_{CM} sign describes the force direction: if F_{CM} is positive, the particle is attracted to an electrical field maximum (which is called positive DEP or p-DEP) and if negative, to an electrical field minimum (negative DEP or n-DEP).

Hence, the DEP force allows control of the movement of a particle by varying the applied signal, changing the electrode shape, placing dielectric structures, or modifying media properties. Here we used a pair of interdigitated gold electrodes to preconcentrate *E. coli* cells. In order to define the suitable trapping frequency, an *E. coli* geometry model is considered. This bacterium is approximated to an ellipsoid shape with two dielectric layers [10], which modifies the Clausius–Mosotti factor expression:

$$F_{\mathrm{CM_i}}(\omega) = \frac{1}{2} \left(\frac{\varepsilon_p^* - \varepsilon_m^*}{\varepsilon_m^* + A_i\left(\varepsilon_p^* - \varepsilon_m^*\right)} \right), \tag{3}$$

where ε_m is the medium permittivity; ε_p is the particle permittivity; and A_i is the depolarization factor of an individual ellipsoid axe ($i = x, y, z$), where e is the eccentricity that involves the ellipsoid dimensions (where "b" is the height and "a" the width):

$$A_x = \frac{(1-e^2)}{(2e^3)} \log\left(1 + \frac{e}{(1-e) - 2e}\right) \tag{4}$$

$$A_z = A_y = \frac{(1 - A_x)}{2} \tag{5}$$

$$e = \sqrt{1 - \left(\frac{b}{a}\right)^2}. \tag{6}$$

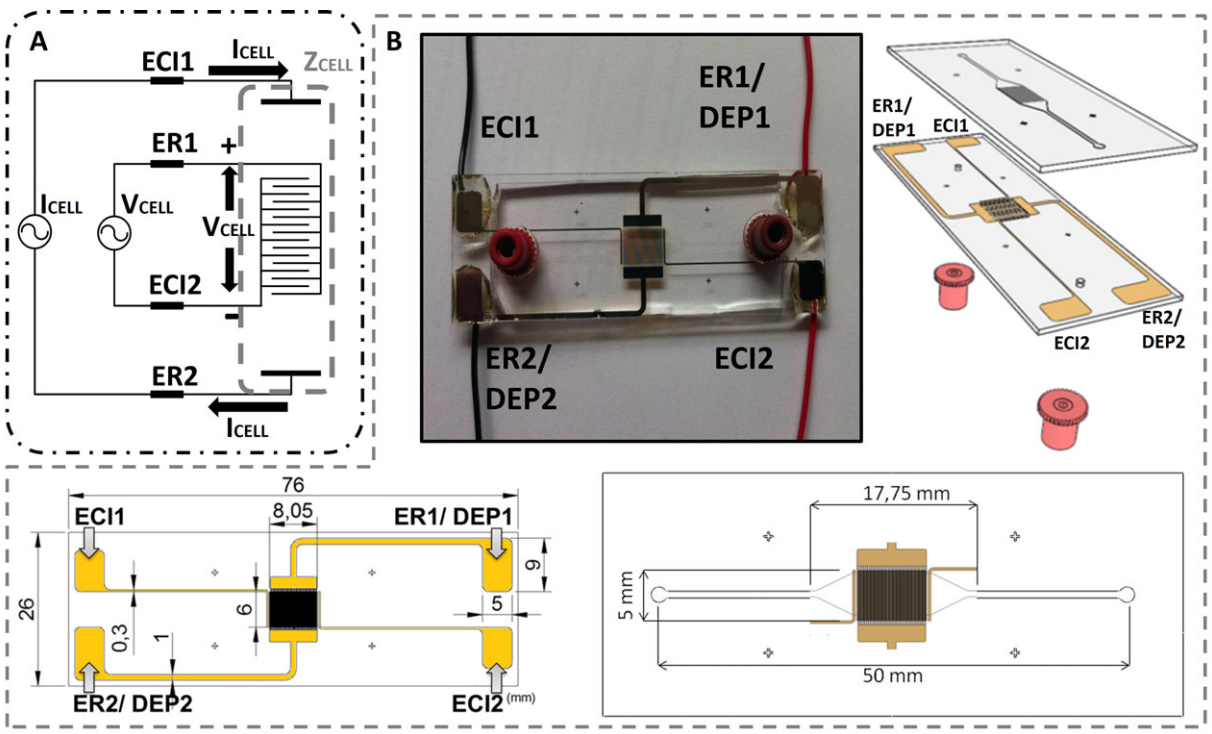

Figure 2. (A) Four-electrode impedance measurement method. (B) Designed microfluidic chip. ECI1–ECI2 are the current injection electrodes, ER1–ER2 are the reading electrodes, and DEP1–DEP2 are referred to electrodes where DEP is applied.

The representation of expression (3) showed that the optimal frequency to manipulate *E. coli* cells by p-DEP is 1 MHz as we know from previous studies of the group [39,40]. This frequency was therefore chosen for the preconcentrating stage.

2.2 Impedance and available measurement methods

The bioimpedance [41, 42] can be measured as the voltage response of a biological material to the application of a current bias signal, and is defined by the Ohm's law. The methods of impedance measurement are classified by the number of electrodes used: two-, three-, and four-electrode methods. The difference among methods resides in how bias current signal is applied and how the sensor voltage signal response is read.

A two-electrode configuration is the basic topology, defined by the working electrode, where bias signal is applied, and the reference electrode, which tracks the bias current signal and provides a reference for the voltage measurement. However, as the current bias signal flows through the reference electrode, this topology entails some problematic behavior as the voltage reference is distorted due to electrode polarization. In order to avoid this effect, the three-electrode topology adds a third electrode to supply the bias current signal, while the reference electrode remains as a voltage reference.

Although this is an improvement, the impedance measurement with this topology can be distorted due to the working electrode impedance polarization, as the current bias signal is directly applied where the single-ended voltage measurement signal is read. In this paper, the four-electrode method was used (Fig. 2A, electrodes ER1, ER2, ECI1, ECI2), which was composed of two current injection electrodes and two voltage reading electrodes, as this electrode topology avoids electrode polarization distortion in impedance measurement due to a complete differential voltage measurement [43].

3 Materials and methods

3.1 Microfluidic chip design and fabrication

The designed microfluidic chip design is showed in Fig. 2B. This had two IDEs, which were shared between the DEP generator and impedance analyzer readout electronics, and two lateral electrodes, which were used to inject the necessary current so as to obtain the impedance measure. The IDEs were formed by 40 pairs of 6 mm × 50 μm electrodes separated by 50 μm. The lateral electrodes (6 mm x 300 μm) were separated by 200 μm from the interdigitated ones. These electrodes were attached to a PDMS microfluidic chamber with a volume of 4.8 μL. The fabrication of the microfluidic chips followed a protocol based on three main steps: microchannel molding, electrode fabrication, and microfluidic chip bonding.

First, SU8 50 (MicroChem) masters were fabricated over glass slides (Deltalab) and PDMS replicas were created. In order to do this, the glass slide was cleaned and activated by Piranha attack for 15 min. Then a 50-μm-high

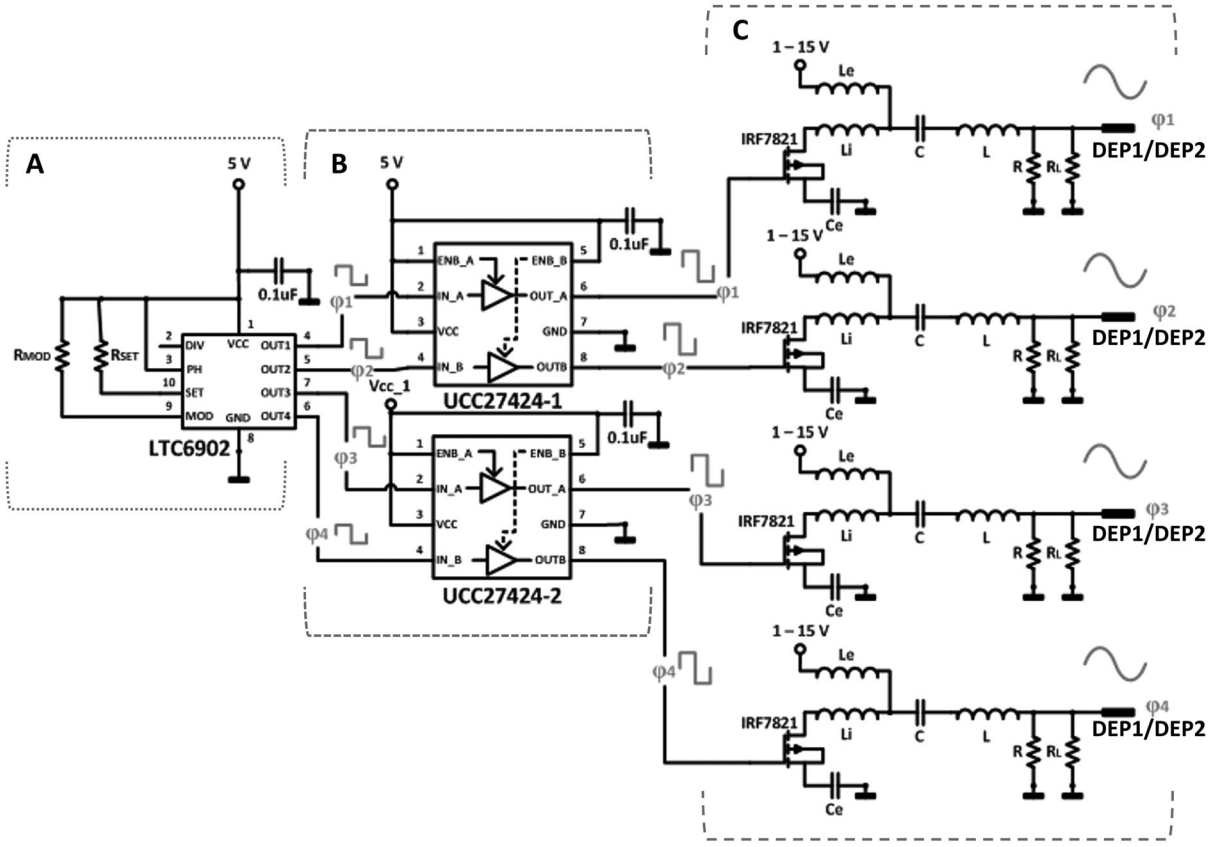

Figure 3. Schematic of the DEP module. (A) Square signal generator. (B) Power driver. (C) Class E amplifier.

SU-8 50 (MicroChem) was spun over the slides. They were later exposed and developed so as to obtain the desired microchannels. Afterward, a 10:1 ratio of PDMS prepolymeric solution (Dow Corning Sylgard184) was mixed, degassed, and poured into the mould to replicate the microchannels. Finally, the PDMS was cured at 70°C for 1 h and peeled from the master.

Second, in order to fabricate the microelectrodes over a set of the LoC sealing glass slides (Deltalab), a lift-off soft lithographic process was used. AZ 1512 (AZ Electronic Materials) photoresist was chosen as a sacrificial layer in this process. First, a Piranha cleaning procedure was performed over the glass slides. Later, AZ 1512 was spun on these slides, exposed, and developed. Then, two metal layers, 20 nm of Ti and 80 nm of gold, were vapor-deposited sequentially. The electrode structures were finally obtained by removing the AZ photoresist.

As a final microfluidic chip fabrication step, once the PDMS replica and the microelectrodes were finished, both parts were assembled to create a sealed structure. First, the surfaces were cleaned using an oxygen plasma process. Hereinafter, the PDMS channels were aligned and attached to the glass substrate. Later, cables were welded to each electrode pad using conductive silver paint and mechanically strengthened using an epoxy glue mix, later cured at room temperature for 60 min. Finally, two NanoPort Assemblies were attached in order to set the inlet and outlet fluidic connections.

3.2 Combined DEP and IA device

3.2.1 Dielectrophoretic signal generator electronics

The designed dielectrophoretic signal generator module is presented in Fig. 3. Four channels with different phases (0°, 90°, 180°, 270°), which could be connected in different ways to the electrodes DEP1 and DEP2, were defined so as to add versatility to the board in dielectrophoretic terms. Each channel generates a sinusoidal signal at 1 MHz with variable output voltage from 1 to 15 Vpp (peak to peak) to control the DEP force intensity, and is composed of three modules: (i) A square signal generator that provides four shifted and frequency stable signals (A); (ii) a power driver that boosts the signal from the previous module so as to activate the following stage (B); (iii) a class E amplifier, which generated the DEP sinusoidal signal (C).

The first module, the square signal generator, is based on the LTC6902 (Linear Technology). The synchronized outputs are shifted $\varphi 1 = 0°$, $\varphi 2 = 90°$, $\varphi 3 = 180°$, and

$\varphi 4 = 270°$, respectively. Their output frequency is selectable by an external resistor (R_{SET}), following the Eq. (7) where ($N = 10$ is related to frequency working range and $M = 4$ is the number of active outputs),

$$f_{out} = \frac{10\ \text{MHz}}{N \cdot M} \left(\frac{20\text{k}\Omega}{R_{set}}\right). \quad (7)$$

LTC6902 outputs have a supplying limit of 400 μA. Hence, a power driver is used to increase the current capabilities. An UCC27424 (Texas Instruments) is chosen for this purpose. This device boosts the current levels of the input signal up to 4 A, which is sufficient current to drive the final module. This module is a class E amplifier that generates the necessary sinusoidal signals to apply DEP. This amplifier configuration generates high-frequency signals with stable output voltages [44– 46] by injecting a square high current control signal.

The class E amplifier is composed of an inductor Le, a capacitor Ce, and a resonance tank formed by the inductor L and the capacitor C. The L–C tank generates a 1 MHz sinusoidal signal by using the 1 MHz square signal from the previous modules. The circuit parameters (Le, Ce, C, L) were configured in function of the necessary output frequency, the output impedance, and the equivalent resistance of the microfluidic chip. Thus, four independent channels perfectly synchronized at φ1, φ2, φ3, and φ4 are obtained.

3.2.2 Impedance analyzer electronics

A fully customized electronic circuit was specifically designed to carry out the IA experiments. As previously stated, the microfluidic device impedance measurement is based on the four-electrode topology. A four-electrode method is composed of two current injection (ECI1 and ECI2) electrodes and two voltage reading (ER1 and ER2) electrodes. The main advantage of this system is that electrode impedances are cancelled, obtaining a more reliable measure. The circuit specifications were defined taking into account the sample media impedance, and considering the microfluidic device characteristics and the frequency ranges where bacterium could be discriminated [47, 48].

The impedance analyzer architecture consists of two modules: the current injection module (CI in Fig. 4B) that provides a frequency configurable voltage sinus signal (V_{RS}) that is converted to a current signal (voltage-to-current converter circuit) to bias/drive the current injection electrodes ECI1 and ECI2. An instrumentation amplifier (IA) senses the differential voltage between the reading electrodes ER1 and ER2 (V_{IS}).

The second module, signal digitalization and post-processing (SDPP in Fig. 4A), calculates the impedance measurement through the voltage signals provided by the previous stage, and automatically controls the hardware configuration. This module is composed of a real-time platform sbRIO9632 (National Instruments) with an embedded software for data processing and hardware control. A signal conditioning stage converts voltage signals from a bipolar single-ended signal to a unipolar differential signal to be processed by an analog-to-digital converter (ADC).

The first module (CI), current Injection, is based on a signal generator AD9833 (Analog Devices) and a voltage-to-current converter. The signal generator AD9833 provides a stable voltage signal with a wide variable frequency range, 0 to 12.5 MHz, which is controlled by an SPI communication protocol. The voltage-to-current converter is a modified Howland cell based on AD8066 (Analog Devices) operational amplifiers (OA1 and OA2) that guarantee a wide bandwidth and a high slew rate while maintaining a low spectral noise and a low offset performance. The Howland cell uses R_{SET} and the reference signal (V_{RS}) amplitude to define a stable current signal (I_{OUT}) at the output of the circuit (8) regardless of the connected load.

$$I_{OUT} = \left(\frac{1}{R_{SET}}\right) V_{RS} \quad (8)$$

The differential voltage between ER1 and ER2 electrodes is acquired by means of the instrumentation amplifier (IA) INA163 (Texas Instruments), which allows a wide bandwidth with a low spectral noise and low total harmonic distortion. The measured voltage (signal V_{IS}) is related to the differential voltage between the reading electrodes (ER1 and ER2), G being the instrumentation amplifier gain. This V_{IS} signal is then adapted and processed by the SDPPM module in order to extract the impedance of the media.

$$V_{IS} = G \cdot (V_{ER1} - V_{ER2}) \quad (9)$$

The second module (SDPP), signal digitalization and post-processing, consists of a 12-bit, dual, low-power ADC ADC12D040 (Texas Instruments), capable of converting both analog input signals at 40 MSPS simultaneously. Twelve-bit resolution does not represent a significant drawback in the final system resolution, as V_{RS} is scaled to the full-range ADC analog input and the system provides a real-time gain auto-scale for the instrumentation amplifier gain G. The analog inputs are converted from single ended to differential with a differential amplifier (DA) AD8138 (Analog Devices), with a high slew rate with low distortion and input noise. The impedance measurement is carried out with a digital lock-in based on the frequency response analyzer (FRA) approach [49]. The FRA is a real-time mathematical processing system, embedded in the 400 MHz microprocessor from the real-time platform sbRIO9632, which adopts sine and cosine signals related to V_{RS}, and by means of two multipliers and a filter stage, the real (V_{REAL}) and imaginary (V_{IM}) components values (10) of the measured signal V_{IS} are obtained (Fig. 4C). The key measurement in our work is the impedance magnitude ($|Z_{CELL}|$) (Eq. (11)). This value is calculated based on the V_{REAL} and V_{IM} components.

$$V_{REAL} = \frac{1}{2V_{RS}} \cdot V_{IS} \cdot \cos(\varphi_{IS})\ ;\ V_{IM} = \frac{1}{2V_{RS}} \cdot V_{IS} \cdot \sin(\varphi_{IS}) \quad (10)$$

$$|Z_{CELL}| = \left(\frac{2\sqrt{{V_{REAL}}^2 + {V_{IM}}^2}}{|V_{RS}|^2}\right) \cdot R_{SET} \quad (11)$$

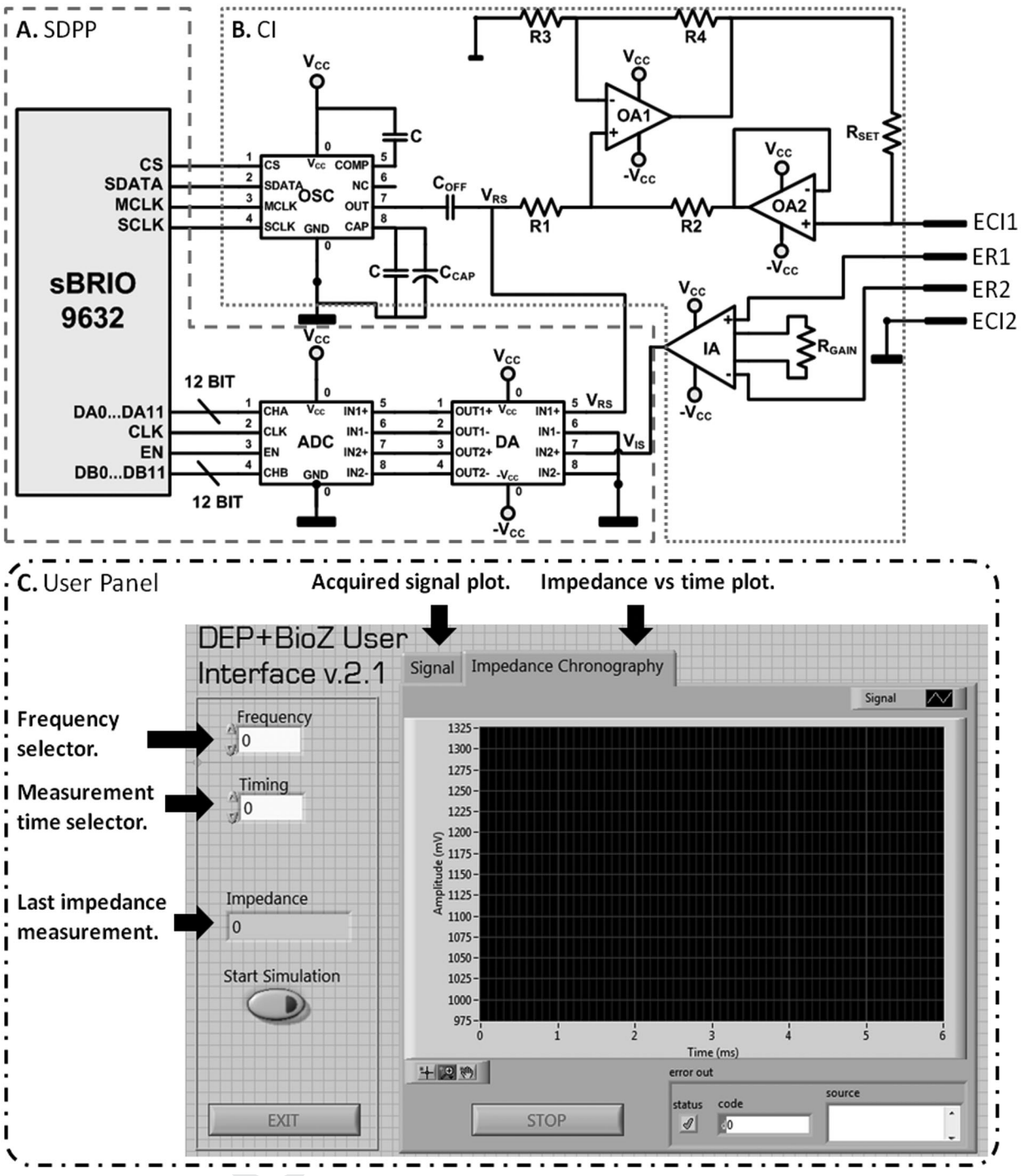

Figure 4. Schematic of the IA module. (A) Signal digitalization and postprocessing module (SDPP). (B) Current injection module (CI). (C) Front-end user panel for experiments control and data displaying.

For accurate hardware control, the real-time platform sbRIO9632 has a FPGA Spartan-3 (Xilinx), which allows us to provide steady clock signals, needed on the instrumentation, which can be automatically adjusted, allowing complete real-time control of the chip electrodes multiplexing. As stated in Section 2.1, the microfluidic chip had two IDEs, which were shared between the DEP generator and the IA readout electronics. When an IA measurement was done the DEP generator was disconnected, suspending the trapping process. If this process was not properly timed, bacteria already trapped would be lost in the process, so the real-time control allowed an optimized timing process minimizing the bacteria loss. Moreover, the disconnection of DEP voltage signals contributes to a better bacterial concentration monitoring

avoiding distortion and instability on the IA measurement. The IA process had been programmed and tested to last for a period of the applied current signal, plus 1 ms for multiplexor switching times and stabilization. In addition, real-time platform allows complete parallel signal acquisition for all the frequency ranges, and the development of an embedded hardware control, such as R_{SET} multiplexed auto-scale, instrumentation amplifier gain G auto-scale, and signal generator automatic frequency sweep. This real-time embedded hardware control represents the basic features of an automated and complete FRA approach. The real-time platform allows the system configuration and data display, with a user-friendly front-end user panel (Fig. 4C), by means of an external computer connected to the platform with a standard Ethernet connection.

3.3 Bacteria culture

A laboratory sample formed by *E. coli* 5K strains (genotypes: F^-, hdsR, hdsM, thr, thi, leu, lacZ) was grown overnight in 10 mL of Luria–Bertani broth at 37°C. The achieved cell concentration (estimated by performing viable cell counts in LB agar) was 10^9 cells/mL. Then, the *E. coli* culture was pelleted by centrifugation at 5000 rpm for 5 min. Bacteria were then resuspended in 10 mL of DI water. Finally, the samples were diluted (final concentration of $2{\cdot}10^7$ cells/mL) and frozen in 1 mL collecting tubes for storage purposes.

3.4 Conductivity measurements

As *E. coli* concentration was measured by means of IA, bacteria samples' conductivity was monitored while in vitro a major factor in IA reliability, using a commercial bench-top conductivity meter Corning 441. Prior to the experiments, bacteria samples were diluted in DI water with a conductivity of $8.2{\cdot}10^{-5}$ S/m, but the conductivity of the samples at the time of the experiment, after the process of storage and thawing, was subject to variations. A sample conductivity analysis had to be done at the beginning of the experiment. The conductivity meter probe was calibrated and introduced into the 1 mL collecting tubes until it was totally covered by the bacteria sample.

3.5 Experimental setup

The microfluidic chip was placed over an inverted microscope stage (Olympus IX71) connected to a digital camera (Hamamatsu Orca R2). Moreover, the microfluidic chip was connected to a six-port manual valve (Valco). This valve was also connected to a 5 mL syringe filled with DI water ($8.2{\cdot}10^{-5}$ S/m) and placed on an infusion micropump (Cetoni NEMESYS) so as to obtain a continuous flow rate. The microfluidic chip's gold electrodes were connected to the custom combined DEP and IA device.

4 Results and discussion

The designed combined device was validated by a series of *E. coli* concentration and impedance measurement tests. First of all, so as to validate the system as an autonomous bacteria concentrator, and study the effect of real-time monitoring by means of IA measurement, *E. coli* was continuously injected through the valve to the microfluidic chip at a 5 μL/min flow rate, and preconcentrated by DEP by two counter-phased signals of 15 Vpp. In addition, the impedance module was programmed to proceed with a 3-ms impedance measurement every 30 s meanwhile DEP module was continuously trapping bacteria. As a first approach, the conductivity of the solution has not been corrected to study the effect its variations over time on the IA measurement. Different tests for different applied current signal frequencies were done. Taking into consideration the electronics and microfluidic chip design, impedance measurement was performed at continuous alternating current of 10 μA in the 500 Hz to 5 kHz frequency range, where bacterium could be discriminated [47, 48] and evaluated using 100 Hz spaced sampling intervals.

The measured bioimpedance ($|Z|$), depicted in Fig. 5A, clearly shows a decreased impedance as the trapped bacteria concentration increases, regardless of the frequency. This behavior was clearly explained by the conductivity changes taking place in bacteria samples over time. Measured conductivity was recorded periodically in-tube during the experiments showing a rise from $0.5{\cdot}10^{-3}$ to $2.5{\cdot}10^{-3}$ S/m until it stabilized. This conductivity change, related to the original sample prior to the trapping process, may be translated into a theoretical variation in impedance. This estimated impedance, related to measured bacteria sample in-tube conductivity, was calculated considering the microfluidic chip electrodes' geometric characteristics. In Fig. 5B impedance variation ($\Delta|Z|$) through time for the measured on-chip impedance, during the trapping process, and for the estimated on-tube impedance are shown.

Results show a very similar behavior through time of both measurements. Acquired data variations through time for the first 40 min, before conductivity stabilization, were $-52.41\ \Omega$/min for measured impedance and $-54.79\ \Omega$/min for conductivity related impedance, which confirms that the first impedance measurements are related to bacteria sample conductivity rather than trapped bacteria concentration, underlining the need for a media conductivity correcting protocol.

A 2D finite element method based study with Multiphysics software (Comsol) further shows the dominating effect of sample conductivity changes on the bioimpedance measurements when left uncontrolled. *E. coli* 5K physical and electrical properties were defined for the different model layers ($\sigma_{wall} = 0.68$ S/m, $\varepsilon_{r\_wall} = 74$, $\sigma_{membrane} = 5 \times 10^{-8}$ S/m, $\varepsilon_{r\_membrane} = 9.5$, $\sigma_{cytoplasm} = 0.19$ S/m, $\varepsilon_{r\_cytoplam} = 49.8$). Then different medium conductivities were defined, as well as the applied potential to the external lateral electrodes. Current conservation and an initial state of potential 0 were applied for all the layers. Afterward, an adaptive physical controlled

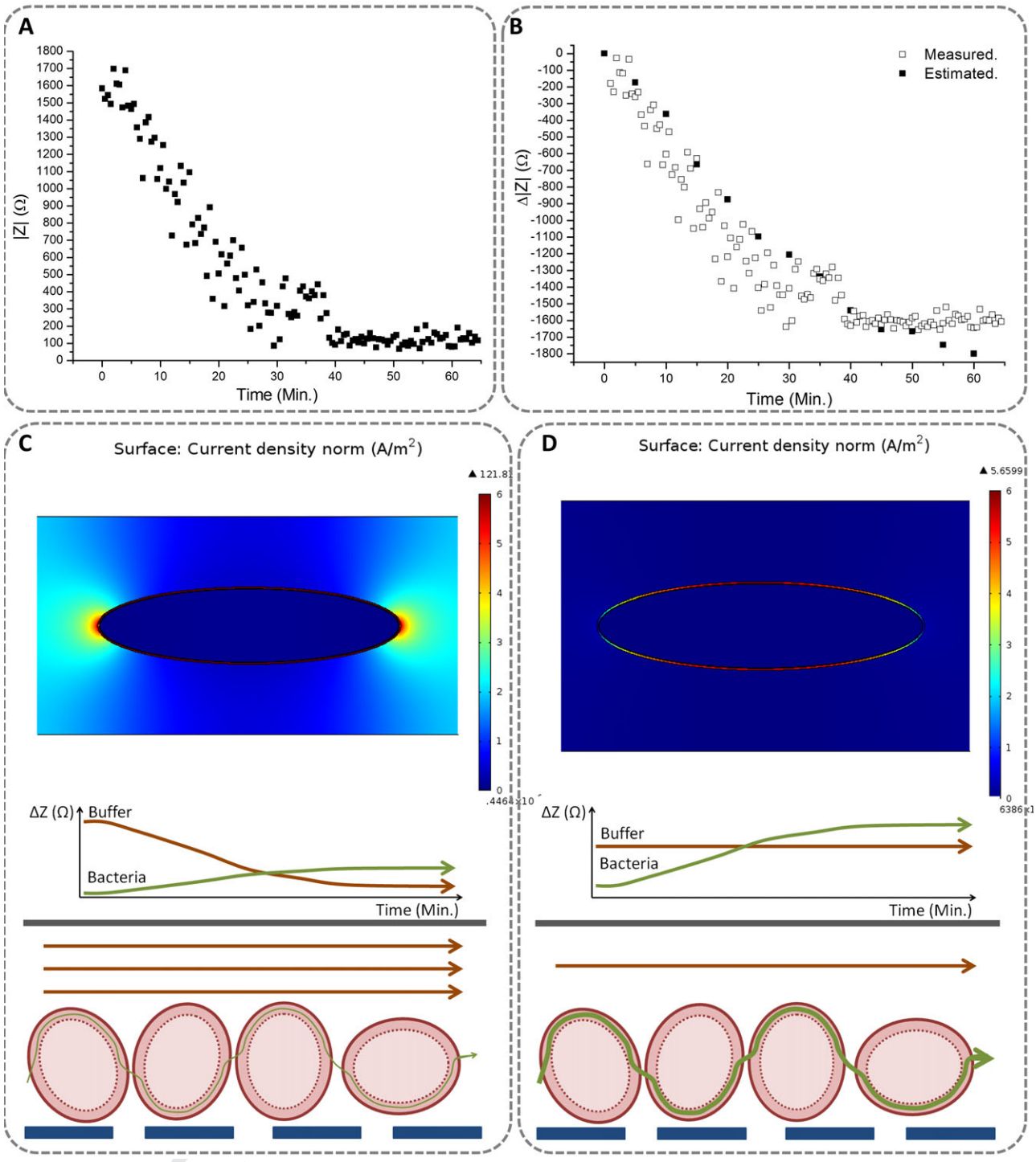

Figure 5. (A) Impedance magnitude measured during the trapping operation. (B) Experimental versus estimated impedance magnitude relative incremental changes. (C) Comsol multiphysics simulation of a single diluted cell on high-conductivity buffer ($0.5{\cdot}10^{-3}$–$2.5\ 10^{-3}$ S/m). Schematic modelization of current flow path and contribution to impedance measurement of both buffer and trapped bacteria. (D) Comsol multiphysics simulation of a single diluted cell on low-conductivity steady buffer (Milli-Q water, $8.2\ 10^{-5}$ S/m). Schematic modelization of current flow path and contribution to impedance measurement of both buffer conductivity and trapped bacteria.

and extra fine mesh was applied. Finally, a frequency domain analysis at 1.7 kHz was performed. Thus, surface current density (ec.normJ) of bacteria was obtained (Fig. 5C andD). From the analysis of the obtained simulations, we could assure that in case of a single bacteria diluted on a buffer with a conductivity which varies from $0.5{\cdot}10^{-3}$ to $2.5{\cdot}10^{-3}$ S/m, current density is 99.9% located outside the bacteria. Hence, measured impedance is totally related to sample buffer conductivity

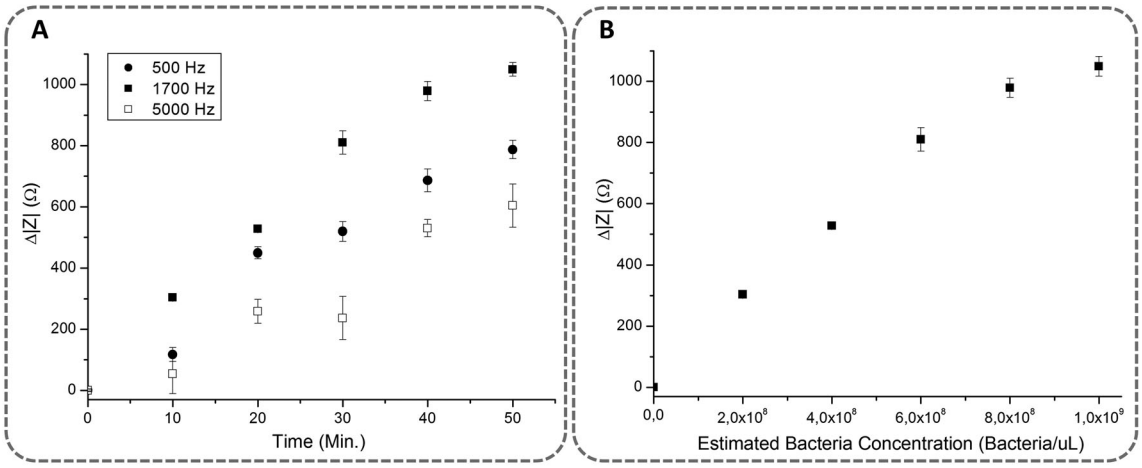

Figure 6. (A) Impedance magnitude measured changes during bacterial sample on-chip concentration at several given times. Medium cleaning procedure was performed before each measurement. (B) Impedance magnitude measurements at 1700 Hz related to estimated bacteria concentrations.

rather than bacteria concentration (Fig. 5C). Controlling buffer conductivity to be stable and at the levels of Milli-Q water, around $8.2{\cdot}10^{-5}$ S/m, current density is mainly located in the cell membrane (Fig. 5D) and impedance variation related to the quantity of trapped bacteria.

Hence, when the cells' media is not controlled by cleaning processes, impedance variations are strongly related to changes in the conductivity of the media due to bacteria [50, 51]. To solve this issue, which is not confronted in other works to the best of our knowledge, an automated periodic cleaning process was implemented as part of the device working protocol assuring a reliable impedance measurement.

In the resulting protocol, the microfluidic chip was first filled with Milli-Q water media to obtain the threshold impedance measurement. Afterward, a 50 μL sample of *E. coli* was injected through a controlled valve to the microfluidic chip and trapped by DEP forces while flowing continuously at 10 μL/min, higher flow rate compared with other solutions for DEP and IA combination, such as 2–4 uL/min [30]. After each 50 μL sample of bacteria was injected into the channel, 50 μL of Milli-Q water, with a specified conductivity of $8.2{\cdot}10^{-5}$ S/m, was automatically injected at 10 μL/min to ensure a steady media conductivity for the impedance measurement. Once the Milli-Q water was injected, the impedance electronic module was activated and the DEP generator deactivated by means of multiplexor. Four contiguous impedance measurements were performed each time in order to evaluate precision. Afterward, another 50 μL sample of *E. coli* was injected and the process repeated until all the samples were injected. So, the impedance measurement is always performed after each 50 μL bacteria sample was injected, trapped, and cleaned. The whole process was performed to scan the 500 Hz to 5 kHz IA frequency range each 100 Hz. The DEP was generated by applying two 15 Vpp counter-phased signals through the IDEs. The results of the experimental impedance measurements for three frequencies (500, 1700, and 5000 Hz) are depicted in Fig. 6.

Results are depicted as the increment ($\Delta|Z| = |Z| - |Z_0|$) between the different impedance magnitude measurements for every bacteria sample injected ($|Z|$) and the initial media impedance magnitude measurement ($|Z_0|$). Figure 6A depicts $\Delta|Z|$ measurements through time for the initial and final frequency value, 500 Hz and 5 kHz, respectively, as well as the 1.7 kHz frequency $\Delta|Z|$ measurements, which seem to be more sensitive and reliable with an accuracy error of less than 2% of bacteria concentration with a correlation of 0.988. Precision can be evaluated with the coefficient of variation, which is the SD of the four experiment repetitions divided by the mean value of the four repetitions' measurement. The mean value of the coefficient of variation is 3.1% on the whole range, although the device is more precise for lower bacteria concentration levels where the coefficient of variation is below 3%.

Thus, steady and sensitive $\Delta|Z|$ measurement at different frequencies, which is bacteria dependent, was observed. Furthermore, bioimpedance control of the achieved sample concentration showed a reliable sensitivity for the protocol including a bacteria-cleaning step. The controlled and steady low media conductivity microenvironment solves issues regarding overall system viability.

The DEP module had a proven trapping efficiency of 85.65 ± 1.07%, for a single 50 μL bacteria sample injected at continuous flow of 10 μL/min, by measuring the escaped and the collected bacteria of a single load by cytometric analysis [40]. Although the whole process trapping efficiency had not been tested, each sample load was estimated to increment the bacteria concentration $2{\cdot}10^8$ bacteria/mL inside the microfluidic chip. Figure 6B depicts the $\Delta|Z|$ measurements for each bacteria concentration increment (bacteria/μL) when 1.7 kHz frequency is applied. However, our main goal was

to verify that the process of bacterial concentration while monitoring the concentration is feasible, as it has been proved. The measured impedance values were related to the quantity of bacteria concentrated with a correlation of 0.988 and a coefficient of variation of 3.1%, avoiding distortion and instability related to undesired effects such as media conductivity variations and DEP voltage interferences.

5 Concluding remarks

Here we describe a novel device and automated protocol, based on DEP and IA, to concentrate bacteria in benchtop setups in a controlled manner. The system consists of a microfluidic chip, with integrated electrodes, and its associated custom instrumentation electronics. It performs bacteria injection, trapping, cleaning, and continuous short-time impedance measuring while achieving the desired levels of concentration. As a proof of concept, it has been applied to concentrate *E. coli* and to automatically monitor its concentration. The electronic apparatus was validated using a microfluidic chip with four integrated gold electrodes specifically designed for the application. The automated system was tested by trapping and measuring samples of *E. coli* 5K at a concentration of $2{\cdot}10^7$ cells/mL. Concentration and real-time detection of the trapped bacteria inside the microfluidic chip were proven, working a high flow injection rate, up to 10 μL/min, for different buffer conductivities [31, 32]. Bacteria media conductivity, and its variability, was demonstrated to be a challenging issue when monitoring concentration by means of IA. An automated protocol integrated in the overall system was proposed to solve this problem, strengthening the system versatility and robustness. Before each measurement, the designed system cleans the bacteria samples periodically, while trapped on the microfluidic chip, with Milli-Q water at a controlled conductivity of $8.2{\cdot}10^{-5}$ S/m. To our best knowledge, this proposed system is a useful tool to solve some current microbiology laboratories shortcomings. Bacteria can be concentrated to given specifications while performing analytical procedures. The development of LoC-based equipment, removing the need of huge and expensive devices, is an important research field aiming for smaller systems with better functionalities, such as the integrated application specific integrated system stimulator for electrokinetically driven microfluidic devices presented by Gomez-Quiñones et al. [52]. Nowadays, electronic technology allows further miniaturization of devices such as our concentrator. A SOI technology such as XTO18 from XFAB would be suitable to combine digital instrumentation and class E amplifiers inside a unique chip. However, some drawbacks must be considered when integrating the full system into the LoC device, as it would either increase disposable cost or reduce applicability due to possible contaminations. Still, the simplicity of the presented microfluidic device and the development of the custom electronics on a single application specific integrated system, along with an automated procedure protocol, pushes toward the development of robust and reliable LoC automated bacterial concentrator relying on DEP concentration and IA monitoring.

This work was financially supported by the THERAEDGE project (FP7-ICT-2007-216027), funded by the "Information and Communication Technologies" programme under the 7th Research Framework Programme of the European Union. The Nanobioengineering group is supported by the Commission for Universities and Research of the Department of Innovation, Universities, and Enterprise of the Generalitat de Catalunya (2009 SGR 505). This work was supported by Obra Social "La Caixa." CIBER-BBN is an initiative funded by the VI National R&D&i Plan 2008–2011, Iniciativa Ingenio 2010, Consolider Program, CIBER Actions, and financed by the Instituto de Salud Carlos III with assistance from the European Regional Development Fund. This material is based upon work supported by the Botín Foundation, Santander, Spain.

The authors have declared no conflict of interest. Q5

6 References

[1] Pethig, R., *Biomicrofluidics* 2010, *4*, 22811.

[2] Sun, T., Morgan, H., *Microfluid. Nanofluidics* 2010, *8*, 423–443.

[3] Hamada, R., Takayama, H., Shonishi, Y., Mao, L., Nakano, M., Suehiro, J., *Sens. Actuators B Chem.* 2013. Q6

[4] Agarwal, S., Sebastian, A., Forrester, L. M., Markx, G. H., *Biomicrofluidics* 2012, *6*, 24101–2410111.

[5] Fatoyinbo, H. O., Hoettges, K. F., Hughes, M. P., *Electrophoresis* 2008, *29*, 3–10.

[6] Venkatanarayanan, A., Keyes, T. E., Forster, R. J., *Anal. Chem.* 2013, *85*, 2216–2222.

[7] Xu, M., Luo, X., Davis, J. J., *Biosens. Bioelectron.* 2013, *39*, 21–25.

[8] Feldsine, P. T., Falbo-Nelson, M. T., Hustead, D. L., *J. AOAC Int.* 1994, *77*, 58–63.

[9] Pouch Downes, F., Ito, K., *Compendium of Methods for the Microbiological Examination of Foods*, 4th edition, American Public Health Association, 2001, p. 676. Q7

[10] Morgan, H., Green, N. G., *AC Electrokinetics: Colloids and Nanoparticles*, Research Studies Press, 2003.

[11] Pohl, H. A., *J. Appl. Phys.* 1951, *22*, 869.

[12] Chin, C. D., Linder, V., Sia, S. K., *Lab Chip* 2007, *7*, 41–57.

[13] Figeys, D., Pinto, D., *Anal. Chem.* 2000, *72*, 330 A–335 A.

[14] Stone, H. A., Stroock, A. D., Ajdari, A., *Annu. Mech.* 2004, *36*, 381–411.

[15] Lapizco-Encinas, B. H., Simmons, B. A., Cummings, E. B., Fintschenko, Y., *Anal. Chem.* 2004, *76*, 1571–1579.

[16] Braff, W. A., Pignier, A., Buie, C. R., *Lab Chip* 2012, *12*, 1327–1331.

[17] Gascoyne, P. R. C., Noshari, J., Anderson, T. J., Becker, F. F., *Electrophoresis* 2009, *30*, 1388–1398.

[18] Gascoyne, P., Mahidol, C., Ruchirawat, M., Satayavivad, J., Watcharasit, P., Becker, F. F., *Lab Chip* 2002, *2*, 70–75.

[19] Moon, H. S., Kwon, K., Kim, S. I., Han, H., Sohn, J., Lee, S., Jung, H. I., *Lab Chip* 2011, *11*, 1118–1125.

[20] Fatoyinbo, H. O., McDonnell, M. C., Hughes, M. P., *Biomicrofluidics* 2014, *8*, 044115.

[21] Zordan, M. D., Grafton, M. M. G., Acharya, G., Reece, L. M., Cooper, C. L., Aronson, A. I., Park, K., Leary, J. F., *Cytometry A* 2009, *75*, 155–162.

[22] Deisingh, A. K., Thompson, M., *Analyst* 2002, *127*, 567–581.

[23] Hahm, B.-K., Bhunia, A. K., *J. Appl. Microbiol.* 2006, *100*, 1017–1027.

[24] Bohaychuk, V. M., Gensler, G. E., King, R. K., Wu, J. T., McMullen, L. M., *J. Food Protoc.* 2005, *68*, 2637–2647.

[25] Hong, B.-X., Jiang, L.-F., Hu, Y.-S., Fang, D.-Y., Guo, H.-Y., *J. Microbiol. Methods* 2004, *58*, 403–411.

[26] Foudeh, A. M., Fatanat Didar, T., Veres, T., Tabrizian, M., *Lab Chip* 2012, *12*, 3249–3266.

[27] Ramírez, N., Regueiro, A., Arias, O., Contreras, R., 1989, *31*.

[28] Dweik, M., Stringer, R. C., Dastider, S. G., Wu, Y., Almasri, M., Barizuddin, S., *Talanta* 2012, *94*, 84–89.

[29] Grossi, M., Lanzoni, M., Pompei, a, Lazzarini, R., Matteuzzi, D., Riccò, B., *Biosens. Bioelectron.* 2010, *26*, 983–990.

[30] Dastider, S. G., Barizuddin, S., Dweik, M., Almasri, M., *RSC Adv.* 2013, *3*, 26297–26306.

[31] Park, S., Zhang, Y., Wang, T.-H., Yang, S., *Lab Chip* 2011, *11*, 2893–2900.

[32] Rozitsky, L., Fine, A., Dado, D., Nussbaum-Ben-Shaul, S., Levenberg, S., Yossifon, G., *Biomed. Microdevices* 2013, *15*, 859–865.

[33] Croxen, M. A., Law, R. J., Scholz, R., Keeney, K. M., Wlodarska, M., Finlay, B. B., *Clin. Microbiol. Rev.* 2013, *26*, 822–880.

[34] Sievert, D. M., Ricks, P., Edwards, J. R., Schneider, A., Patel, J., Srinivasan, A., Kallen, A., Limbago, B., Fridkin, S., *Infect. Control Hosp. Epidemiol.* 2013, *34*, 1–14.

[35] Ulett, G. C., Totsika, M., Schaale, K., Carey, A. J., Sweet, M. J., Schembri, M. A., *Curr. Opin. Microbiol.* 2013, *16*, 100–107.

[36] Dhama, K., Chakraborty, S., Tiwari, R., Verma, A. K., Saminathan, M., Amarpal, Y. S. M., Nikousefat, Z., Javdani, M., Khan, R. U.

[37] Sabounchi, P., Morales, A. M., Ponce, P., Lee, L. P., Simmons, B. A., Davalos, R. V, *Biomed. Microdevices* 2008, *10*, 661–670.

[38] Jones, T. B., *Electromechanics of Particles*, Cambridge University Press, 2005.

[39] Castellarnau, M., Errachid, A., Madrid, C., Juárez, A., Samitier, J., *Biophys. J.* 2006, *91*, 3937–3945.

[40] Moral Zamora, B. del, *Micro Nanosyst.* 2014, *6*.

[41] Fairooz, T., Istya, S., *Int. J. Biol. Life Sci.* 2011.

[42] Patterson, R., in: Bronzino, J. D. (Ed.), *Biomedical Engineering Handbook*, 2000.

[43] Martinson, O. G., Grimnes, S., *Bioimpedance and Bioelectricity Basics*, 2008.

[44] Lenaerts, B., Puers, R., *Omnidirectional Inductive Powering for Biomedical Implants*, Springer, 2009.

[45] Rasid, M. H., González, M. H. R. V., Fernández, P. A. S., *Electrónica de potencia: Circuitos, dispositivos y aplicaciones*, Pearson Educación, 2004.

[46] Sokal, N. O., *QEX Commun. Quart.* 2001, 9–20.

[47] Cheng, M. S., Ho, J. S., Lau, S. H., Chow, V. T. K., Toh, C.-S., *Biosens. Bioelectron.* 2013, *47*, 340–344.

[48] Yang, L., *Talanta* 2008, *74*, 1621–1629.

[49] Punter-Villagrasa, J., Colomer-Farrarons, J., Miribel, P. L., Rinken, T. (Ed.), *Bioelectronics for Amperometric Biosensors*, Intech 2013. Available at: http://www.intechopen.com/books/state-of-the-art-in-biosensors-general-aspects/bioelectronics-for-amperometric-biosensors.

[50] Varshney, M., Li, Y., *Biosens. Bioelectron.* 2009, *24*, 2951–2960.

[51] Li, M., Li, S., Cao, W., Li, W., Wen, W., Alici, G., *Microfluid. Nanofluidics* 2013, *14*, 527–539.

[52] Gomez-Quiñones, J., Moncada-Hernández, H., Rossetto, O., Martinez-Duarte, R., Lapizco-Encinas, B.H., Madou, M., Martinez-Chapa, S.O. *New Circuits and Systems Conference (NEWCAS)* 2011, 350–353.

